



EX LIBRIS
UNIVERSITATIS
ALBERTENSIS

The Bruce Peel
Special Collections
Library



Digitized by the Internet Archive
in 2025 with funding from
University of Alberta Library

<https://archive.org/details/0162018299592>

University of Alberta

Library Release Form

Name of Author: Anne Marie Hearn

Title of Thesis: Gas-Phase Ethylene Polymerization with the Polyphenoxide
Ligand Tris(2,6-dihydroxyphenyl)ethene: Development of a New
Silica-Supported Ti-Mg Catalyst

Degree: Master of Science

Year this Degree Granted: 2003

Permission is hereby granted to the University of Alberta Library to reproduce single copies of this thesis and to lend or sell such copies for private, scholarly or scientific research purposes only.

The author reserves all other publication and other rights in association with the copyright in the thesis, and except as herein before provided, neither the thesis nor any substantial portion thereof may be printed or otherwise reproduced in any material form whatever without the author's prior written permission.

University of Alberta

Gas-Phase Ethylene Polymerization with the Polyphenoxide Ligand
Tris(2,6-dihydroxyphenyl)ethene: Development of a New Silica-Supported
Ti-Mg Catalyst

by

Anne Marie Hearn



A thesis submitted to the Faculty of Graduate Studies and Research in partial
fulfillment of the requirements for the degree of
Master of Science
in
Chemical Engineering

Department of Chemical and Materials Engineering

Edmonton, Alberta

Fall 2003

University of Alberta

Faculty of Graduate Studies and Research

The undersigned certify that they have read, and recommend to the Faculty of Graduate Studies and Research for acceptance, a thesis entitled **Gas-Phase Ethylene Polymerization with the Polyphenoxide Ligand Tris(2,6-dihydroxyphenyl)ethene: Development of a New Silica-Supported Ti-Mg Catalyst** submitted by **Anne Marie Hearn** in partial fulfillment of the requirements for the degree of **Master of Science in Chemical Engineering**.

ABSTRACT

Silica-supported polymerization catalysts were prepared with the polyphenoxide ligand 1,1,2-tris(2,6-dihydroxyphenyl)ethene. The effect of catalyst preparation conditions on gas-phase activity profiles for ethylene homopolymerization and ethylene/1-hexene copolymerization were studied. Reactor conditions such as co-catalyst concentration, temperature, pressure, hydrogen concentration, and comonomer concentration were varied to examine the effect on activity and polymer properties. The bimetallic (Ti-Mg) polyphenoxide catalyst had significantly higher polymerization activities than catalysts prepared without the ligand.

Catalyst and polymer characteristics were examined with various techniques. Particle size distributions and surface areas were measured, and elemental analysis was performed for titanium and magnesium contents. Molar masses were measured with size exclusion chromatography (SEC), and temperature rising elution fractionation (TREF) was used to assess comonomer incorporation. Surface and internal structures of polymer particles were explored with scanning electron microscopy (SEM). Characterization studies showed the Ti-Mg polyphenoxide catalyst had low 1-hexene incorporation and that molar masses can be controlled with hydrogen.

ACKNOWLEDGEMENTS

My many acknowledgements begin with a Haiku-styled poem:

“Polyethylene, produced full-scale in Joffre, white and dense as hail.”

I would like to convey my gratitude to my supervisors Sieghard Wanke and Jeffrey Stryker. I was fortunate to have their insight and guidance, which was invaluable for the success of my research. In addition, I appreciated their sense of humour because it made my graduate studies thoroughly enjoyable.

There are many people in the Department of Chemical and Materials Engineering who were especially helpful. Naiyu Bu diligently completed the GPC analysis on my polymer samples. Long Wu patiently and thoroughly explained the operation of the polymerization equipment. I thank Ah-Dong Leu for performing the BET measurements, and Jim Skwarok for his assistance with the particle size distributions. The SEM images were collected with the expertise of Tina Barker. The Machine Shop and Instruments staff kept the polymerization and characterization equipment in excellent working condition. In addition, John Duke in the SLOWPOKE Nuclear Reactor Facility at the University of Alberta performed the INAA on the polymerization catalysts.

NOVA Chemicals Corporation, the Natural Science and Engineering Research Council, and the Alberta Ingenuity Fund provided generous financial support to both the Polymerization Group and me, personally.

I am also very grateful to my parents and sisters for putting up with me while I was on the path to completing this degree. Their encouragement was priceless. And for everything else, there was MasterCard®.

TABLE OF CONTENTS

1.0	INTRODUCTION	1
2.0	LITERATURE REVIEW	4
2.1	Gas-Phase Olefin Polymerization	4
2.1.1	Global Polyethylene Business	4
2.1.2	Commercial Gas-Phase Reactors	5
2.1.3	Stability and Dynamics of Gas-Phase Reactors	6
2.1.4	Limitations of Gas-Phase Processes	7
2.1.5	Laboratory Gas-Phase Reactors	8
2.2	Silica	9
2.2.1	Surface Chemistry of Silica	10
2.2.2	Silica as a Catalyst Support in Olefin Polymerization	12
2.3	Olefin Polymerization Catalysts	13
2.3.1	Ziegler-Natta (Z-N) Catalysts	13
2.3.1.1	Features of Heterogeneous Z-N Catalysts	15
2.3.1.2	Trends in Patented Ti-Mg Silica Catalysts	16
2.3.1.3	Kinetic Characteristics of Z-N Catalysts	19
2.3.2	Aryloxide Complexes	20
2.3.2.1	Sterically Hindered Magnesium Aryloxides	21
2.3.2.2	Chelated or Bridged Aryloxide Complexes	22
2.3.2.3	Ancillary Aryloxide Ligation	27
2.4	Ligand Effects in Olefin Polymerization	29
2.5	Catalyst Activity Profiles in Olefin Polymerization	30
3.0	EXPERIMENTAL PROCEDURES	32
3.1	Catalyst Preparation	32
3.1.1	Support Treatment	33

3.1.2	Ligand Anchoring	34
3.1.3	Magnesium Incorporation	36
3.1.4	Titanium Addition	37
3.2	Polymerization Experiments	39
3.2.1	Description of the Polymerization Reactor	39
3.2.2	Operating Procedure for the Polymerization Reactor	43
3.3	GC Analysis of Reactor Gas Composition	47
3.3.1	Hydrogen Concentration	48
3.3.2	1-Hexene Concentration	48
3.4	Characterization Techniques	53
3.4.1	Nitrogen Adsorption	53
3.4.2	Elemental Analysis	57
3.4.3	Particle Size Distribution	58
3.4.4	Size Exclusion Chromatography (SEC)	58
3.4.5	Temperature Rising Elution Fractionation (TREF)	60
3.4.6	Scanning Electron Microscopy (SEM)	62
4.0	POLYMERIZATION RESULTS AND DISCUSSION	66
4.1	Reproducibility of Gas-Phase Activity Profiles	70
4.2	Effect of Co-Catalyst Concentration on Activity	74
4.3	Activity Profiles for Different Catalysts	77
4.4	Effect of Titanium Addition Method on Activity	79
4.5	Effect of Catalyst Drying Temperature on Activity	82
4.6	Effect of Ethylene Pressure on Activity	86
4.7	Effect of Temperature on Activity	94
4.8	Effect of Hydrogen	99
4.8.1	Effect of Hydrogen Concentration on Activity	99
4.8.2	Effect of Hydrogen Concentration on Molar Mass	104
4.8.3	Hydrogen Consumption During Polymerization	114

4.9	Effect of 1-Hexene	115
4.9.1	Effect of 1-Hexene Concentration on Activity	115
4.9.2	Effect of 1-Hexene Concentration on Molar Mass	118
4.9.3	1-Hexene Consumption During Polymerization	122
4.9.4	1-Hexene Incorporation	123
4.10	SEM of Polymer Samples	133
5.0	CATALYST CHARACTERIZATION	137
5.1	Surface Areas and Pore Size Distributions	137
5.2	Particle Size Distributions	138
5.3	Titanium and Magnesium Elemental Analysis	144
6.0	CONCLUSIONS AND RECOMMENDATIONS	150
	REFERENCES	158
	APPENDIX A: Catalyst Preparation Conditions	165
	APPENDIX B: Summary of Polymerization Results	172
	APPENDIX C: Hydrogen Consumption Calculations	261
	APPENDIX D: TREF Profiles	265

LIST OF TABLES

Table 3.1	Thermal Treatment Conditions for Silica.	34
Table 3.2	Summary of Catalyst Preparation Conditions.	38
Table 3.3	SEC Results Comparing Heating Times.	59
Table 4.1	SEC Results Comparing TiCl_4 Addition Methods.	107
Table 4.2	SEC Results Comparing Ligand Loadings on Silica.	107
Table 4.3	Molar Masses for Homopolymers Produced with Hydrogen.	108
Table 4.4	Hydrogen Concentration during Polymerization.	114
Table 4.5	Molar Masses for Copolymers Produced with Hydrogen.	121
Table 4.6	Molar Masses for Ethylene/1-Hexene Copolymers.	122
Table 4.7	Methylene Branching in Copolymers with Hydrogen.	131
Table 4.8	Methylene Branching in Ethylene/1-Hexene Copolymers.	132
Table 5.1	Surface Areas for Silica and Catalysts.	138
Table 5.2	Particle Size Statistics for Silica.	142
Table 5.3	Particle Size Statistics for Catalysts.	144
Table 5.4	Ti and Mg Contents for the Polymerization Catalysts	145
Table 5.5	Cl Contents for the Polymerization Catalysts	146
Table 5.6	Catalyst Preparation Conditions versus Ti/Mg	147

Table A.1	Thermal Treatment Conditions for Silica.	165
Table A.2	Batches of Catalyst Precursor Mg/Ligand/Silica.	166
Table A.3	Summary of Catalyst Preparation Conditions.	167
Table A.4	Colorimetric Results for Ti Content.	170
Table B.1	Summary of Polymerization Conditions and Yields.	173
Table C.1	Polymerization Data for Hydrogen Consumption.	261
Table C.2	GC Data for Hydrogen Consumption.	262
Table C.3	Calculated Values for Hydrogen Mole Fractions.	262
Table C.4	Comparison of Hydrogen Peak Areas.	263

LIST OF FIGURES

Figure 2.1	Siloxane and silanol groups on the surface of silica particles.	10
Figure 2.2	Titration of silanol groups with hydride ions (e.g. LiAlH_4).	11
Figure 2.3	Condensation of silanols to form siloxane groups.	11
Figure 2.4	Ligands for studying polynuclear Mg and Ti-Mg species (Sobota et al., 2000b).	15
Figure 2.5	Surface reaction between silica and a Grignard reagent.	17
Figure 2.6	Sterically hindered magnesium phenoxide dimers (Calabrese et al., 1988).	22
Figure 2.7	Molecular structure of calix[4]arene.	23
Figure 2.8	Ti complexes of p-tert-butylcalix[4]arene (Ozerov et al., 1999).	24
Figure 2.9	Bridged Ti polyphenoxide species (van der Linden et al., 1995).	25
Figure 2.10	Chelated Ti polyphenoxide species (van der Linden et al., 1995).	25
Figure 2.11	Chelated Ti aryloxide complex (Matilainen et al., 1996).	26
Figure 2.12	Bis(phenoxy-imine) titanium complexes (Furuyama et al., 2003).	27
Figure 2.13	Examples of ancillary aryloxide complexes.	28
Figure 2.14	Types of catalyst activity profiles (Kissin, 1985).	31
Figure 3.1	Molecular structure of tris(2,6-dihydroxyphenyl)ethene.	32
Figure 3.2	Synthetic route for tris(2,6-dihydroxyphenyl)ethene.	33

Figure 3.3	Proposed mechanism for anchoring the ligand to silica.	35
Figure 3.4	Schematic diagram of the polymerization reactor.	40
Figure 3.5	Schematic diagram of the gas purification trains.	41
Figure 3.6	Activity profiles showing catalyst deactivation due to the amount of catalyst injected into the reactor.	42
Figure 3.7	Activity profiles illustrating ethylene flow restriction.	44
Figure 3.8	GC calibration for hydrogen/ethylene separation.	49
Figure 3.9	Vapour pressure of 1-hexene as a function of temperature.	51
Figure 3.10	Maximum volume of liquid 1-hexene for saturation.	52
Figure 3.11	GC calibration for ethylene/1-hexene separation.	54
Figure 3.12	GC calibration for ethylene/1-hexene separation at low 1-hexene concentrations.	55
Figure 3.13	Response factor for ethylene/1-hexene separation.	56
Figure 3.14	Programmed temperature cycle for TREF oven.	63
Figure 3.15	TREF profile for a polymer sample with high molar mass.	64
Figure 3.16	TREF profile for a polymer sample with low molar mass.	65
Figure 4.1	Comparison of TEA and TIBA as co-catalysts.	68
Figure 4.2	Activity profiles for silica- and HEMA PS-DVB-supported catalysts.	69
Figure 4.3	Reproducibility of gas-phase activity profiles.	71

Figure 4.4	Reproducibility of gas-phase activity profiles.	72
Figure 4.5	Reproducibility of gas-phase activity profiles.	73
Figure 4.6	Activity profiles for different TIBA concentrations.	75
Figure 4.7	Temperature profiles for different TIBA concentrations.	76
Figure 4.8	Activity profiles for different catalysts.	78
Figure 4.9	Activity profiles for ethylene homopolymerization comparing methods of titanium (IV) chloride addition.	80
Figure 4.10	Activity profiles for ethylene/1-hexene copolymerization comparing methods of titanium (IV) chloride addition.	81
Figure 4.11	Activity profiles comparing catalyst drying temperatures (50°C TC Bath, TIBA evacuated).	83
Figure 4.12	Activity profiles comparing catalyst drying temperatures (50°C TC Bath, TIBA kept in reactor).	84
Figure 4.13	Activity profiles comparing catalyst drying temperatures (70°C TC Bath, TIBA evacuated).	85
Figure 4.14	Activity profile for AH-20-04.	87
Figure 4.15	Activity profiles for CAT-27 at different ethylene pressures.	88
Figure 4.16	Temperature profiles for CAT-27 at different ethylene pressures.	89
Figure 4.17	Activity profiles for CAT-27 at different TC bath temperatures.	90
Figure 4.18	Activity profiles for CAT-30 at different ethylene pressures.	91
Figure 4.19	Temperature profiles for CAT-30 at different ethylene pressures.	92

Figure 4.20	Activity profiles for CAT-30 at different TC bath temperatures.	93
Figure 4.21	Temperature profiles for CAT-27 at different TC bath temperatures.	95
Figure 4.22	Temperature profiles for CAT-30 at different TC bath temperatures.	96
Figure 4.23	Temperature profiles showing effect of mixing and heat transfer.	97
Figure 4.24	Activity profiles showing the effect of mixing and heat transfer.	98
Figure 4.25	Activity profiles with hydrogen at different TC bath temperatures.	100
Figure 4.26	Temperature profiles with hydrogen at different TC bath temperatures.	101
Figure 4.27	Activity profiles showing effect of hydrogen.	102
Figure 4.28	Temperature profiles for polymerization experiments performed with and without hydrogen.	103
Figure 4.29	Activity profiles for the Ti-Mg polyphenoxide catalyst at different hydrogen concentrations.	105
Figure 4.30	Activity profiles for the Ti-Mg silica catalyst at different hydrogen concentrations.	106
Figure 4.31	Fitting of hydrogen termination kinetics for the Ti-Mg polyphenoxide catalyst.	110
Figure 4.33	Fitting of hydrogen termination kinetics for the Ti-Mg silica catalyst.	111
Figure 4.33	Molar mass distributions for the Ti-Mg polyphenoxide catalyst.	112

Figure 4.34	Molar mass distributions for the Ti-Mg silica catalyst.	113
Figure 4.35	Activity profiles showing effect of 1-hexene without hydrogen.	116
Figure 4.36	Activity profiles showing effect of 1-hexene with hydrogen.	117
Figure 4.37	Activity profiles for the Ti-Mg polyphenoxide catalyst at different hydrogen concentrations.	119
Figure 4.38	Activity profiles for the T-Mg silica catalyst at different hydrogen concentrations.	120
Figure 4.39	1-Hexene concentration during polymerization for AH-29-07.	124
Figure 4.40	1-Hexene concentration during polymerization for AH-30-07.	125
Figure 4.41	TREF profiles for the Ti-Mg polyphenoxide catalyst at different hydrogen concentrations.	127
Figure 4.42	TREF profiles for the Ti-Mg polyphenoxide catalyst at different 1-hexene concentrations.	128
Figure 4.43	TREF profiles for the Ti-Mg silica catalyst at different 1-hexene concentrations.	129
Figure 4.44	SEM picture showing view of many particles.	134
Figure 4.45	SEM picture showing outer surface of one particle.	134
Figure 4.46	SEM picture showing inner structure of one particle.	135
Figure 4.47	SEM picture showing view of many particles.	135
Figure 4.48	SEM picture showing partially dissolved salt crystal.	136
Figure 4.49	SEM picture showing polymer growth on a salt crystal.	136

Figure 5.1	Pore size distributions for thermally treated silica.	139
Figure 5.2	Pore size distributions for silica and catalysts.	140
Figure 5.3	Particle size distributions for silica.	141
Figure 5.4	Particle size distributions for silica and catalysts.	143
Figure A.1	Glassware used to dry catalyst precursor before TiCl_4 addition.	168
Figure A.2	Calibration for Ti content with the colorimetric method.	171
Figure C.1	Calibration plot for final hydrogen concentration.	264

1.0 INTRODUCTION

Polyethylene (PE) has the highest annual production among the synthetic commodity polymers with over 51 million metric tons produced worldwide in 2001 (Chemical Economics Handbook, 2002). Several processes exist for commercial polyolefin production with a large portion produced in gas-phase reactors. In addition to process development, many families of catalysts have been discovered for the production of high-density polyethylene (HDPE) and linear low-density polyethylene (LLDPE).

Reactor operation in commercial gas-phase olefin polymerization processes is challenging due to unstable behaviour. The low heat transfer efficiency in gas-phase operations combined with high catalytic activity causes temperature control problems that may result in polymer particle agglomeration. Although there have been improvements in gas-phase reactor operation due to process modifications, most advances have been through catalyst development.

The discovery of transition metal catalysts for olefin polymerization, particularly Ziegler-Natta catalysts, has lead to extensive exploration into the activity of new catalyst families. In general, conventional Ziegler-Natta catalysts are heterogeneous systems consisting of transition metal halides (e.g. TiCl_4 , Ti(OR)_4), magnesium compounds (e.g. MgCl_2 , CH_3MgCl), and aluminum alkyls or halides (Huang and Rempel, 1995; Soga and Shiono, 1997). For example, most LLDPE is produced with Ziegler-Natta catalysts (McAuley et al., 1995), specifically MgCl_2 -supported TiCl_4 . More recently, organometallic coordination complexes (i.e. homogeneous Ziegler-type catalysts) have been developed to produce new polymer resins (Soares and Hamielec, 1995; Hlatky, 2000). The active site environment of the transition metal influences the activity and stereospecificity of polymerization catalysts, consequently, studies have focused on altering the ligand functionality of coordination catalysts.

The objectives of this work were to prepare silica-supported, titanium (IV) chloride-based polymerization catalysts with the new polyphenoxide ligand 1,1,2-tris(2,6-dihydroxyphenyl)ethene, and evaluate the activity and polymer properties of the catalysts as a function of reactor conditions in gas-phase ethylene homopolymerization and ethylene/1-hexene copolymerization. This research exemplifies the usefulness of laboratory-scale gas-phase reactors in the development of new catalysts and will expand our understanding of the influence that ligand functionality has on the activity of heterogeneous catalysts in olefin polymerization.

The initial focus was to determine suitable catalyst preparation conditions to attain high activity in gas-phase polymerization. Incorporation of magnesium onto the supported polyphenoxide ligand was necessary for high activity. The conditions for titanium (IV) chloride addition were also identified as a critical factor affecting activity. In addition to achieving high productivities with the bimetallic (Ti-Mg) polyphenoxide catalyst, the shapes of the activity profiles were different than for conventional Ziegler-Natta catalysts.

Several catalysts were prepared to evaluate different active site environments. The activity and polymer properties of the Ti-Mg polyphenoxide catalyst were compared to that of a conventional Ziegler-Natta catalyst, which was a Ti-Mg silyloxide complex prepared by incorporation of magnesium onto silica with a Grignard reagent and subsequent addition of titanium (IV) chloride. The Ti-Mg polyphenoxide catalyst was much more active than the Ti-Mg silica catalyst. The presence of multiple active sites was evident in the molar mass distributions for both catalysts, but the distributions were unusually narrow for the Ti-Mg polyphenoxide catalyst compared to conventional Ziegler-Natta catalysts.

The reproducibility of the activity profiles was examined because gas-phase olefin polymerization is known to be very sensitive to variations in operating conditions.

Reactor conditions such as co-catalyst concentration, pressure, temperature, hydrogen concentration, and 1-hexene concentration were varied to determine the effect on activity and polymer properties. The high activities caused temperature control problems that produced activity profiles with unusual shapes. Hydrogen suppressed the activity and it reduced the molar masses of the polymer products. The activity was drastically higher in the presence of 1-hexene, but the molar masses were affected less by 1-hexene than hydrogen.

Catalyst and polymer properties were evaluated with several techniques. Molar masses were determined with size exclusion chromatography (SEC). The trends in molar masses as a function of hydrogen concentration showed there were differences in active sites for the Ti-Mg polyphenoxide and Ti-Mg silica catalysts. There was limited comonomer (1-hexene) incorporation as indicated by the temperature rising elution fractionation (TREF) profiles. Elemental analysis determined that the catalysts had high titanium content, but it was possible that some titanium (IV) chloride was not active in polymerization. Physical characterizations of catalyst and silica particles revealed differences in pore size distributions.

2.0 LITERATURE REVIEW

2.1 Gas-Phase Olefin Polymerization

Gas-phase olefin polymerization involves a heterogeneous system of gaseous monomers and solid catalysts; the polymerization zone does not have a liquid phase. During polymerization, the gas phase supplies monomers to the catalyst particles, mixes polymer particles, and removes heat from the reaction zone. Unlike conventional high-pressure processes, gas-phase polymerization is carried out at moderate temperatures and pressures with the use of coordination catalysts (Choi and Ray, 1985; Xie et al., 1994).

Commercial gas-phase polymerization processes utilize fluidized or stirred bed reactors (Choi and Ray, 1985; Xie et al., 1994). Despite the existence of unstable behaviour (Gorbach et al., 2000; Hutchinson and Ray, 1987; McAuley et al., 1995), there are many advantages to gas-phase polymerization over other existing technology. Laboratory-scale gas-phase reactors have been designed to facilitate catalyst testing and modeling; their use has been invaluable in studying the catalyzed production of polyethylene (Bu et al., 1995; Wu et al., 1999).

2.1.1 Global Polyethylene Business

The polyethylene business experiences cyclical profit variability due to global competition. In addition to plant capacity and low feedstock cost position, commercial success of the polyethylene business is attributed to proprietary catalysts and process technology (Chemical Industries Newsletter, 2000). Major improvements in commercial polyethylene production have been achieved through catalyst development (Xie et al., 1994); the success of the Union Carbide gas-phase

process for the production of LLDPE exemplifies the importance of catalyst development (Choi and Ray, 1985). The estimated sales value of LLDPE was \$13.6 billion in 2001 with worldwide production of 13.5 million metric tons (Chemical Economics Handbook, 2002); a large portion was produced in gas-phase reactors with Ziegler-Natta catalysts (McAuley et al., 1995).

2.1.2 Commercial Gas-Phase Reactors

Continuous processes are utilized in commercial polyethylene production. Gas-phase polymerization is the most recently developed process with the other process categories including conventional high-pressure, solution, and slurry polymerization (Xie et al., 1994). The type of reactor, operating conditions, and polymerization mechanism characterize the process categories.

Many patents have been filed on process technology for commercial gas-phase polymerization (Xie et al., 1994). Union Carbide constructed the first commercial gas-phase polymerization plant in 1968, and their UNIPOL gas-phase process has been licensed worldwide for the production of HDPE and LLDPE (Xie et al., 1994). The UNIPOL process consists of a fluidized bed reactor with a disengagement zone to collect the polymer product; the success of the technology is attributed to the proprietary catalysts that perform well under gas-phase conditions (Choi and Ray, 1985). The BASF gas-phase process uses a continuous stirred-bed reactor, and their first commercial-scale reactor was built in 1976 for the production of HDPE (Xie et al., 1994). In the mid-1970s, other commercial-scale gas-phase polymerization processes were developed with distinguishing features. For example, the AMOCO process utilizes a compartmentalized horizontal stirred bed reactor with a post-polymerization zone for adiabatic polymerization to melt the polymer for pelletizing (Choi and Ray 1985). In general, gas-phase polymerization reactors are operated at

relatively low pressures of 30-35 atmospheres, and reactor temperatures of 80-110°C are maintained to keep the gas-phase temperature above the dew point of the monomers but below the melting point of the polymer to prevent polymer particle agglomeration (Xie et al., 1994).

To some extent, the gas-phase processes were designed to accommodate the nature of the coordination catalysts used for olefin polymerization (Xie et al., 1994). Fine particles coat reactor surfaces and these particles can fuse into sheets as polymerization proceeds, thus reducing the heat transfer efficiency. Also, solid chunks of polymer can impede gas flow and obstruct the reaction zone. The ethylene feed systems, heat exchangers, cooling systems, and the reactor and disengagement zones are designed to minimize polymer particle agglomeration. BP Chemicals developed a major technology improvement for gas-phase polymerization by including a pre-polymerization stage in the process (Xie et al., 1994). The initial period of polymerization has the greatest potential to cause polymer particle agglomeration because the maximum rate is reached soon after catalyst injection, which can lead to the formation of hot spots in the reactor and fracturing of polymer grains into fine particles. Better control of the catalyst activity and polymer particle morphology was achieved with the two-stage polymerization process.

2.1.3 Stability and Dynamics of Gas-Phase Reactors

Unstable behaviour is commonly encountered in gas-phase reactors; temperature oscillations are prone to affect reactor stability and dynamics (Gorbach et al., 2000). Heat removal is critical in the process design for catalyzed olefin polymerization (Hutchinson and Ray, 1987), and proper temperature control is necessary to avoid problems of multiple steady states, limit cycles, and temperature excursions (McAuley et al., 1995). Poor heat transfer can lead to the formation of hot spots in

the reaction zone and result in polymer particle agglomeration on internal reactor surfaces.

Multiple steady states have been predicted for individual polymer particles and for the macroscopic reactor. The rates of heat generation and dissipation can lead to overheating and result in a high temperature steady state within individual polymer particles (Hutchinson and Ray, 1987). Mechanistic models have also predicted multiple steady states within fluidized bed reactors (Choi and Ray, 1985b) and stirred bed reactors (Gorbach et al., 2000); two-phase models have been used to account for heat and mass transfer resistances. McAuley et al. (1995) showed that multiple types of catalyst sites and catalyst deactivation significantly influenced reactor stability. For a well-mixed reactor with a two-site Ziegler-Natta catalyst, the model predictions demonstrated that an unstable steady state existed and limit cycle behaviour occurred in the reactor when catalyst sites had different activation energies for the propagation reaction as well as for the case of a deactivating catalyst. The dynamic analysis of steady state multiplicity has been useful in understanding the transient behaviour of commercial gas-phase reactors and in designing control systems to avoid unstable reactor behaviour. Catalyst design has also proven invaluable to enhance gas-phase reactor stability; the catalyst particle size and morphology are important factors that affect gas-phase polymerization (McAuley et al., 1995).

2.1.4 Limitations of Gas-Phase Processes

Gas-phase polymerization has technological and economic incentives over other processes. Gas-phase reactors can produce polyethylene with a full range of densities and melt indexes because there are no solubility or viscosity constraints (Xie et al., 1994). Moderate temperatures and pressures are used in gas-phase processes so there are lower energy requirements than other processes, and lower capital costs are

involved because no separation equipment is needed to recover solvents (Choi and Ray, 1985). As well, smaller quantities of aluminum alkyls are needed as co-catalysts and impurity scavengers, which has safety and environmental benefits because these compounds are hazardous.

Although gas-phase polymerization processes are commercially successful, some disadvantages persist in the technology. The productivity of gas-phase reactors is limited because low reactor operating temperatures must be maintained to prevent polymer particle agglomeration (Choi and Ray, 1985; Xie et al., 1994). Temperature instability problems exist because the gas phase has poor heat transfer efficiency (Gorbach et al., 2000; Hutchinson and Ray, 1987). It is also common for fine particles to deposit on heat transfer surfaces, which can lead to fouling (Xie et al., 1994). In addition, gas-phase processes are difficult to operate because they are sensitive to variations in catalyst and monomer feed rates and product discharge (McAuley et al., 1995).

2.1.5 Laboratory Gas-Phase Reactors

Slurry reactors are typically used in laboratory studies of polyolefin production and modeling because it is easier to operate semibatch slurry reactors than gas-phase reactors (Jejelowo et al., 1991). Despite challenges, the gas-phase polymerization process has been successfully scaled down for academic research with laboratory-scale reactors (Lynch et al., 1991; Han-Adebekun et al., 1997).

Laboratory- and commercial-scale gas-phase reactors have different dynamics because of the disparity in volume to surface area ratios; temperature oscillations are dampened in laboratory-scale reactors because the heat capacity of the reactor walls, hence the rate of heat loss to the surrounding medium, is large (McAuley et al.,

1995). Unfortunately, temperature control problems exist in certain instances for laboratory-scale reactors (Xie et al., 1994). Heat transfer is an issue with high activity catalysts because the initial polymerization rates are too high for oil or water bath cooling systems to efficiently remove heat from the reaction zone. Besides affecting the shape of the activity profiles, inadequate heat removal could lead to polymer particle agglomeration. The gas-phase reactor design must also ensure proper particle suspension (i.e. stirring) and reproducible catalyst injection (Jejelowo et al., 1991). These concerns can be alleviated with the use of appropriate operating conditions and procedures. Only small amounts of catalyst are required (10-100 mg for a 1-L reactor), and adequate mixing of the reactor contents is assisted by the use of inert seedbeds such as glass beads, polyethylene powder, or salt (NaCl).

2.2 Silica

Silica (SiO_2 or $\text{SiO}_2 \cdot \text{H}_2\text{O}$) is an amorphous solid with a random structure of polymerized silicate particles, which are called micelles (Ullmann's Encyclopedia of Industrial Chemistry, 1993). The state of aggregation of the silica micelles determines physical characteristics such as particle size, porosity, and surface area. The material has an amorphous structure, as determined by x-ray diffraction, with a framework of interconnected pores (Pullukat and Hoff, 1999). The high surface areas (ca. 300-1000 m^2/g silica) and surface chemistry of silica account for its numerous uses including adsorbents, abrasives, chromatographic material, and catalyst supports in olefin polymerization (Pullukat and Hoff, 1999; Ullmann's Encyclopedia of Industrial Chemistry, 1993).

2.2.1 Surface Chemistry of Silica

Silica is composed of silanol (Si-OH) and siloxane (Si-O-Si) groups (see Figure 2.1). The surface of silica particles contains silanols that can be isolated, bridged, or geminal (Ullmann's Encyclopedia of Industrial Chemistry, 1993). The silanol groups are hydrophilic, thus silica gel is wettable and water molecules adsorb through hydrogen bonding to all types of silanols. The silanol concentration on the surface of fully hydroxylated silica varies between 4-5 SiOH/nm² (Pullukat and Hoff, 1999; Ullmann's Encyclopedia of Industrial Chemistry, 1993), and is determined by the quantity of hydrogen formed in the titration with lithium aluminum hydride (see Figure 2.2). The silanols are also reactive towards various organometallic complexes (Nait Ajjou and Scott, 1997; Rice and Scott, 1997; Muñoz-Escalona, 1990).

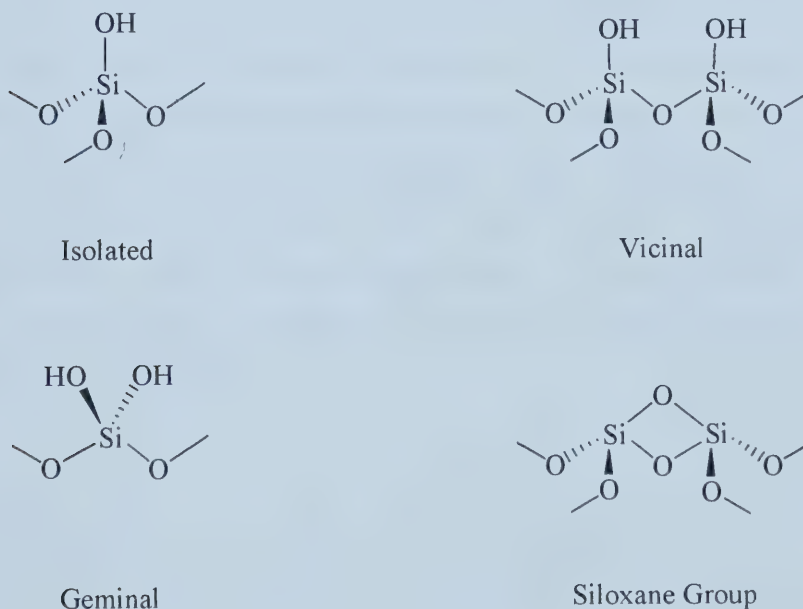


Figure 2.1. Siloxane and silanol groups on the surface of silica particles.



Figure 2.2. Titration of silanol groups with hydride ions (e.g. LiAlH_4).

Most siloxane bonds in the silica matrix are chemically stable, but strained dimer rings are created on the surface of the particles upon heating silica below its melting point. The ring strain increases the reactivity of the siloxane dimers; ring opening occurs in the presence of coupling agents such as organosiloxanes (e.g. hexamethyldisiloxane) (Grabbe et al., 1995).

Adsorbed water is easily removed from silica at temperatures between 100-200°C, but condensation of silanols to form siloxane groups (see Figure 2.3) requires higher temperatures. All vicinal silanols condense before 450-500°C and only isolated silanols remain after 800°C; sintering occurs above 500°C, which results in loss of surface area (Ullmann's Encyclopedia of Industrial Chemistry, 1993). Strained siloxane bridges are formed during the thermally induced condensation up to 500°C, and they are converted into stable siloxane bridges at higher temperatures. For dehydroxylation at 500°C, the siloxane concentration is about 3 SiOSi/nm^2 and the silanol content is about 2 SiOH/nm^2 on average (Ullmann's Encyclopedia of Industrial Chemistry, 1993).

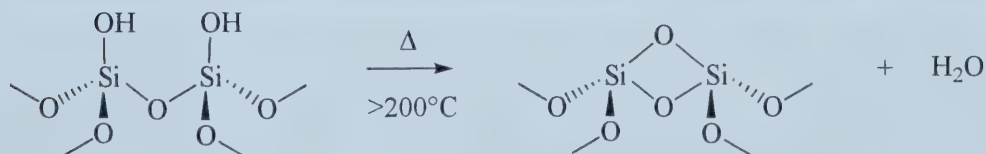


Figure 2.3. Condensation of silanols to form siloxane groups.

2.2.2 Silica as a Catalyst Support in Olefin Polymerization

Catalyst design has scientific interest and economic importance for olefin polymerization processes. Silica is frequently used as a catalyst support because the porous particles have high specific surface areas with potentially reactive hydroxyl and oxide groups on the surface (Ullmann's Encyclopedia of Industrial Chemistry, 1993). Through understanding the chemical reactivity and physical properties of silica, new polyethylene resins have been developed (Pullukat and Hoff, 1999).

Other granular materials such as alumina (Czaja et al., 1999), styrene-divinylbenzene resins (Fuhrmann and Pohl, 1993), and various magnesium compounds (Hlatky, 2000; Smith et al., 1993) have been used as supports for heterogeneous catalysts, but silica-supported catalysts have certain advantages. As opposed to magnesium chloride (MgCl_2) supports, there is less chloride residue in the polymer to discolour the polymer resin and corrode processing equipment (Soga and Shiono, 1997). In addition, silica-supported Ziegler-Natta catalysts have more uniform polymerization rates than other supports, which removes the need for a pre-polymerization stage and lower quantities of aluminum alkyl are required to achieve maximum activity (Pullukat and Hoff, 1999). The chemical reactivity of the surface groups makes silica a suitable support for many types of catalysts. Various ligands can be anchored to the surface or stabilized by chemical interaction with the hydroxyl or oxide groups (e.g. Phillips' hexavalent chromium species forms silyl chromates with surface hydroxyls during the high temperature activation stage) (Vollmert, 1973). The high surface areas of porous silica facilitate the distribution of active sites, which has led to high catalyst productivities with low catalyst residues in the polyethylene resin (Pullukat and Hoff, 1999). Steric accessibility of the pores affects monomer diffusion, thus influencing polymerization activities (Muñoz-Escalona et al., 1990). Also, the production of fines and reactor fouling can be minimized through the selection of particle sizes with suitable pore structure because particle fragmentation

is controlled by the mechanical strength of the network of interconnected pores (McAuley et al., 1995). Unfortunately, the amorphous structure of silica limits morphology control of the polymer particles; spherical MgCl_2 -supported TiCl_4 catalysts are capable of replicating their shape during polymerization to produce morphology-controlled polymer granules (Wu et al., 1999).

2.3 Olefin Polymerization Catalysts

Although gas-phase reactor operation has been improved through process modifications, most advances have been a result of catalyst development (Xie et al., 1994). Catalyst properties have been manipulated to improve gas-phase reactor stability; the problem of polymer particle overheating can be resolved through catalyst design (McAuley et al., 1995). It is important to control the particle size distribution because it affects fluidization of polymer particles in the reactor and influences heat transfer between polymer particles and the gas phase (Choi and Ray, 1985). In addition, the ligand environment of transition metal catalysts has great potential for modifying polymerization performance (Karol and Kao, 1994).

The following discussion describes the history, development, and general kinetic characteristics of Ziegler-Natta catalysts for olefin polymerization. A brief review of patented Ti-Mg silica catalysts is given as well as a summary of polymerization results for aryloxide-based polymerization catalysts that are reported in the literature.

2.3.1 Ziegler-Natta (Z-N) Catalysts

The discovery of Ziegler-Natta catalysts has lead to extensive academic and industrial research into the synthesis of new catalysts for olefin polymerization (Vollmert,

1973). Novel organometallic complexes have produced new types of polyolefins (Huang and Rempel, 1995), and Ziegler-Natta catalysts evolved through several generations to improve commercial polyolefin production.

In 1954, Karl Ziegler demonstrated that a mixture of transition metal salts and metal alkyls would yield high-density polyethylene at low pressures (O dian, 1970). Giulio Natta showed that isotactic polypropylene was produced with the same type of catalyst system; the first-generation Ziegler-Natta catalyst system consisted of a binary mixture of $3\text{TiCl}_3\cdot\text{AlCl}_3$ and $\text{Al}(\text{C}_2\text{H}_5)_2\text{Cl}$ (Soga and Shiono, 1997). Although the discovery was instrumental in advancing olefin polymerization, the first-generation catalyst system had low productivity and poor stereoregularity. Further research yielded the second-generation Ziegler-Natta catalysts, which were more active and stereospecific due to the incorporation of a Lewis base as an electron donor (Huang and Rempel, 1995). Unfortunately, the polymer had to be treated to remove the transition metal because the catalyst contained high levels of inactive titanium salt. A better system consisted of TiCl_4 supported on spherical MgCl_2 with a Lewis base, and these third-generation heterogeneous Ziegler-Natta catalysts required trialkylaluminum compounds as co-catalysts (Soga and Shiono, 1997).

Commercial polyolefin production with third-generation heterogeneous Ziegler-Natta catalysts has been successful because the catalysts have high productivity and stereoregularity with good molar mass control (Soga and Shiono, 1997). Supporting titanium halides on solid carriers enhanced the activity of conventional Ziegler-Natta catalysts; many silica-supported Ti-Mg catalysts have been patented, but the highest activity was obtained using MgCl_2 as the solid support (Soga and Shiono, 1997). In addition to high activity, the morphology of MgCl_2 -supported catalysts is replicated to produce spherical polymer particles with controlled particle size distributions (Wu et al., 1999).

The role of the coordination site created by MgCl_2 on polymerization activity has been explored through characterization of polynuclear magnesium and magnesium-titanium compounds (Sobota et al., 2000b); the active catalyst component $\text{MgCl}_2(\text{THF})_{1.5}$ has been studied with magnesium (II) species involving bidentate chelating aryloxy ligands (Figure 2.4). Similarly, the interaction of catalyst components and silica surface groups, specifically silanols, has been investigated through the preparation of alkoxo magnesium and aluminum compounds that resemble Ziegler-Natta catalyst intermediates (Sobota et al., 2000).

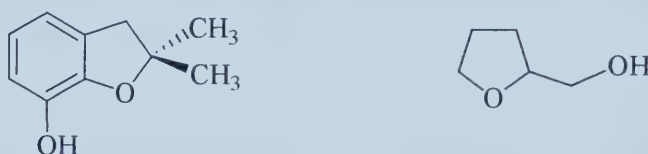


Figure 2.4. Ligands for studying polynuclear Mg and Ti-Mg species (Sobota et al., 2000b).

2.3.1.1 Features of Heterogeneous Z-N Catalysts

Academic and industrial research efforts have lead to improved Ziegler-Natta catalysts; however, the complexity of the catalyst system has limited the understanding of the mechanisms controlling the activity and stereospecificity (Huang and Rempel, 1995). Polymerization processes have been simplified by the introduction of MgCl_2 -supported catalysts that utilize Lewis bases as internal donors (Soga and Shiono, 1997).

Supporting titanium halides on solid carriers enhanced the activity of conventional Ziegler-Natta catalysts; the highest activity was obtained using MgCl_2 as the solid support (Soga and Shiono, 1997). Galli et al. (1981) proposed that MgCl_2 had similar crystal structures and ionic radii to TiCl_4 , and the higher activity was attributed to a

greater number of active sites due to dispersion of the active titanium species on MgCl_2 . Soga and Shiono (1997) investigated the effect of various metal chlorides (MCl_x e.g. MnCl_2 , CoCl_2 , NiCl_2 , FeCl_2 , TiCl_3 , GaCl_4 , TaCl_5 , etc.) on polymerization rate; electron donation from the metal chloride to the active titanium species enhanced the polymerization rate.

Numerous additives, which are commonly referred to as internal donors, were incorporated into the solid matrix during catalyst preparation (O dian, 1970); the activity and stereospecificity of the catalysts varied considerably for some donors (Soga and Shiono, 1997). Internal donors play important roles in the polymerization mechanism by: (1) enhancing the effective surface area to prevent coagulation of MgCl_2 particles during catalyst preparation (ball milling); (2) participating in the formation of highly isospecific sites; and (3) preventing the formation of non-stereospecific sites from TiCl_4 attachment to the MgCl_2 surface (Soga and Shiono, 1997). Many internal donors were explored including alcohols, amines, inorganic halides (KCl , NaF), organic halides, phenols, ethers, and aromatic esters (O dian, 1970). Specifically, Lewis bases such as ethyl benzoate (EB), dibutyl phthalate (DBP), and phenyltriethoxysilane (PES) have been recently investigated (Soga and Shiono, 1997).

2.3.1.2 Trends in Patented Ti-Mg Silica Catalysts

Mobil Oil Company, Exxon, Union Carbide, and Chemplex/Quantum Chemical Company hold patents on titanium-magnesium silica (Ti-Mg silica) catalysts for polyethylene resins, as reviewed by Pullukat and Hoff (1999). Although the role of silica in the catalyst formulation varied to favour the perspective of the inventors, unique features were present in the proprietary catalyst preparation procedures. The

following discussion provides brief details about the evolution of Ti-Mg silica catalysts for ethylene polymerization.

In the 1970s, Grignard reagents (e.g. ethyl magnesium chloride) in ether were the most readily available organomagnesium compounds; the probable surface reaction between magnesium compounds and porous silica, as described in the Chemplex/Quantum patents, is illustrated in Figure 2.5 (Pullukat and Hoff, 1999). During catalyst preparation, porous silica was thermally pretreated at 280°C for 16 hours prior to the addition of ethyl magnesium chloride in ether at room temperature. Next, the magnesiated support was filtered, washed and dried before adding neat titanium (IV) chloride with heating to temperatures of 40-180°C for 1 hour. Finally, the catalyst was repeatedly washed with hexane. The procedure was later improved by using a hydrocarbon solvent to eliminate the drying step before titanium (IV) chloride addition. Although the surface area of the silica was not reported, the catalyst consisted of 2.44 mmol Mg, 1.2 mmol Ti, and 7.4 mmol Cl per gram of silica (Pullukat and Hoff, 1999). Higher melt indexes for HDPE were obtained through catalyst modification, specifically, the addition of alcohols (e.g. butyl alcohols, cyclohexanol, and benzyl alcohol) to silica either before or after reaction with the organomagnesium compound (Pullukat and Hoff, 1999). Further, polyethylene resins with different molecular weight distributions (MWD) and melt indexes (MI) were produced as a result of silica surface modification, specifically, the use of higher heating temperatures (600°C), incorporation of sodium or magnesium ions, and surface reactions with silyl compounds (Pullukat and Hoff, 1999).



Figure 2.5. Surface reaction between silica and a Grignard reagent.

The patents for Mobil Oil reflect the goal of modifying the Ti-Mg silica catalysts for MWD tuning and LLDPE production; thus the surface properties and reactivity of silica were explored (Pullukat and Hoff, 1999). The preparation procedure was similar to that for the Chemplex/Quantum catalysts except excess organomagnesium compound to surface hydroxyl groups ($\text{Mg/SiOH} = 1.1\text{-}3.5$) was used with silica possessing reduced initial surface hydroxyl contents of 0.3-0.7 mmol SiOH/g, which was achieved by thermally treating the silica for 12 hours at 800°C. The Mobil researchers proposed that some of the magnesium was chemically bound to the silanols and some magnesium was physically bonded to the surface by precipitation during solvent evaporation (Pullukat and Hoff, 1999). Further, the average pore diameter of the support was identified as a factor that affected activity, comonomer incorporation, and MI. Overall, the catalysts showed superior 1-butene incorporation compared to anhydrous $\text{MgCl}_2\text{-TiCl}_4\text{-THF}$ complexes that were deposited on silica (Pullukat and Hoff, 1999), and reagents such as chlorinated alcohols (e.g. trichloroethanol) and silicon alkoxides (Si(OR)_4) were used to modify the catalyst.

To differ from the Chemplex/Quantum and Mobil patents, Exxon took the viewpoint that silica and other oxide supports were inert. Although it was conceded that hydroxyl groups are reactive, the Exxon patents stated that hydroxyl groups are removed upon heating to temperatures of 300-800°C, thus silica is rendered inert during the thermal treatment (Pullukat and Hoff, 1999). The unique feature in their catalyst preparation was treatment of the reaction products of dialkyl magnesium compounds and transition metal halides on the inert silica support with a halogenating reagent (e.g. benzoyl chloride) (Pullukat and Hoff, 1999); other Exxon catalysts were prepared with dialkoxymagnesium compounds, titanium alkoxides, and trialkylaluminum compounds.

BP Chemicals developed a two-stage polymerization process for gas-phase polymerization in which the catalyst was exposed to low olefin concentrations prior

to charging the catalyst into the main reactor (Xie et al., 1994). Better control of the catalyst activity and polymer particle morphology was achieved by including this pre-polymerization stage in the process. The proprietary BP catalyst was prepared from the reaction of dibutyl magnesium with porous silica having controlled surface hydroxyl concentrations of 0.5-3 mmol SiOH/g (Pullukat and Hoff, 1999). A monochloroorganic compound (e.g. t-butyl chloride) was also added; the presence of a certain amount of chloride reagent provided no reducing capability for titanium (IV) chloride. Similarly, the Union Carbide patents related their proprietary catalysts to their fluidized bed gas-phase process; the silica-supported catalysts consisted of a titanium chloride compound and magnesium dihalide with electron donors such as THF participating as liquids to dissolve the components (Pullukat and Hoff, 1999). Two methods were used to prepare the supported magnesium precursor. In one method, the support was impregnated with the magnesium compound in THF solution followed by removal of excess THF, and the other method involved the additional step of incorporating aluminum alkyl to partially activate the catalyst. According to the Union Carbide patents, silica acted as a template to control polymer particle size and bulk density for their fluidized bed process (Pullukat and Hoff, 1999).

2.3.1.3 Kinetic Characteristics of Z-N Catalysts

Kissin et al. (1999) describe general kinetic features for ethylene homopolymerization and ethylene/1-hexene copolymerization with heterogeneous Ti-based Ziegler-Natta catalysts. Only a few kinetic studies for catalytic olefin polymerization in gas-phase reactors are reported in the literature for SiO₂/MgCl₂-supported (Bu et al., 1995) and MgCl₂-supported (Wu et al., 1999) TiCl₄ catalysts.

The kinetic features of Ti-based Ziegler-Natta catalysts are explained by the presence of multiple active sites (Huang and Rempel, 1995). The polymer molar masses as

well as the catalytic responses to α -olefins and hydrogen are the result of differences in stability and formation of the active sites for polymerization; sites deactivate at different rates and each site produces polymer molecules with different molar masses (Kissin et al., 1999; Soares and Hamielec, 1995). Ethylene is the most reactive α -olefin for homopolymerization; however, introduction of another α -olefin (e.g. 1-butene or 1-hexene) for copolymerization may result in a large increase in the reaction rate; diffusion or kinetic effects have been proposed to explain the activation effect in copolymerization (Kissin et al., 1999). Conversely, hydrogen suppresses the reaction rate by controlling the rate of chain termination, but the effect is reversible upon the removal of hydrogen. The reaction order with respect to ethylene concentration for Ziegler-Natta catalysts in gas-phase polymerization has been reported to vary from <1 to 1.7 (Bu et al., 1995; Wu et al., 1999).

2.3.2 Aryloxide Complexes

The polyphenoxide ligand tris(2,6-dihydroxyphenyl)ethene was designed to function as a template for the construction of polymetallic coordination complexes (Fujita, 2001). Phenoxide-based ligands have an affinity for early transition metals; hence they have the potential to model bimetallic, heterogeneous Ziegler-Natta catalysts involving titanium (IV) and magnesium (II). Based on the number of articles published in the open literature, research on metallocene catalysts seems to be currently fashionable. Insight into Ziegler-Natta (Ti-Mg) catalyst systems might be gained through contributions of this work with the polyphenoxide ligand.

In addition to a few sterically hindered magnesium aryloxide complexes, a number of Ti(IV) and Zr(IV) aryloxide complexes for olefin polymerization are described in the literature; there are bridged or chelated ligand species as well as complexes with ancillary aryloxide ligation environments at the metal center. The average activities

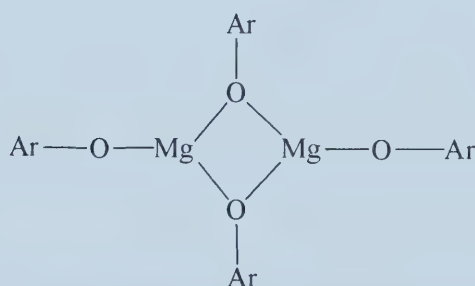
(kg PE/(mol metal·h)) for most of the complexes were reported for ethylene homopolymerization and ethylene/1-hexene copolymerization in slurry (Ozerov et al., 1999; van der Linden et al., 1995; Matilainen et al., 1996). Because activity profiles were not included, it is difficult to adequately compare catalysts, particularly for the different polymerization conditions. In addition, direct comparisons of gas-phase and slurry polymerization activities are not possible for high activity catalysts because of differences in activation and deactivation processes (Jejelowo et al., 1991).

2.3.2.1 Sterically Hindered Magnesium Aryloxides

For the most part, the organometallic aryloxide complexes described in the literature did not contain magnesium (II); presumably, the goal of the researchers was to prepare single-site catalysts for olefin polymerization. Ziegler-Natta catalysts have been prepared using magnesium aryloxides ($\text{Mg}(\text{OR})_2$) as supports, but only a few $\text{Mg}(\text{OR})_2$ complexes have been well characterized. Typically, sterically hindered ligands are used to increase solubility and prevent the formation of oligomeric complexes (Zechmann et al., 2000).

Investigations of high activity MgCl_2 -supported catalysts lead Calabrese et al. (1988) to use sterically hindered phenoxide ligands such as 2,6-di-tert-butyl-4-methylphenol as Lewis base electron donors to synthesize magnesium compounds for olefin polymerization; the resulting dimers were characterized and found to be composed of terminal and bridged phenoxides (see Figure 2.6). Similarly, the researchers prepared sterically hindered aryloxide-substituted aluminum alkyl compounds as part of their program initiative to understand the influence of hindered phenols in Ziegler-Natta catalyst systems (Shreve et al., 1988). More recently, Zechmann et al. (2001) characterized a series of sterically and electronically diverse magnesium aryloxide complexes (OR = 2,6-di-isopropyl phenoxy, 2,4,6-trichlorophenoxy, and

2,6-dimethyl phenoxy) in a variety of solvents (THF and pyridine). Interestingly, soluble polynuclear complexes were obtained in the absence of donor solvents; Henderson et al. (2003) found similar oligomeric behaviour and solubility findings for other magnesium aryloxy complexes. Unfortunately, polymerization data were not included for Ti(IV) complexes of these sterically hindered magnesium aryloxides. As well, no supported aryloxy complexes were found in the literature to compare to the silica-supported, bimetallic (Ti-Mg) polyphenoxide ligand that was used in this gas-phase polymerization study.



Ar = 2,6-di-tert-butyl-4-methylphenoxy or 2,6-di-tert-butylphenoxy

Figure 2.6. Sterically hindered magnesium phenoxide dimers (Calabrese et al., 1988).

2.3.2.2 Chelated or Bridged Aryloxy Complexes

Recently, transition metal complexes containing calixarene ligands have been explored for their potential to catalyze ethylene polymerization. Calixarenes (e.g. Figure 2.7) are macrocyclic ligand systems consisting of four or more aryloxy rings joined by methylene bridges, which are prepared by the condensation of phenols with formaldehyde (Chen et al., 2001). Ozerov et al. (1999) synthesized various Ti(IV) complexes of p-tert-butylcalix[4]arene with the calixarene ligand imposing different stereochemical environments at the metal center (Figure 2.8). The slurry

polymerization activities for these Ti(IV) calixarene complexes with methylaluminoxane (MAO) in toluene at 25°C and 0.1 MPa (14.7 psi) ethylene ranged from 9 to 70 kg PE/(mol Ti·h). Rare earth (Y, Nd, Sm, and Dy) calix[4]arene and (Y, La, Nd, Sm, and Dy) calix[6]arene complexes were prepared by Chen et al. (2001), and activities of 2-56 kg PE/(mol metal·h) were obtained for slurry polymerization experiments in toluene at 60-120°C and 1.2 MPa (174 psi) ethylene.

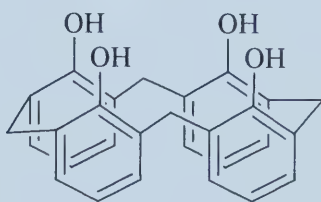


Figure 2.7. Molecular structure of calix[4]arene.

In addition to several bridged titanium phenoxide complexes (e.g. Figure 2.9), a series of chelated phenoxides of the form (O—O)MX₂ (O—O = chelated phenoxide ligand; M = Ti, Zr; X = Cl, Me, CH₂SiMe₃, CH₂Ph) was prepared by van der Linden et al. (1995) for olefin polymerization. The chelated phenoxide complexes are analogous to bridged Group IV metallocenes with the distinction of possessing sterically hindered ligands. The phenoxide ligands were designed to be stereochemically rigid to inhibit disproportionation reactions and allow control over the degree of electronic shielding; the influence of the ligand environment at the metal center on the polymerization activity was studied. Low activities were obtained for most of the complexes with the exception of one ligand (Figure 2.10) in which activities of about 100 kg PE/(g M·h) (M = Ti, Zr) were obtained for polymerization in toluene at 20°C and 0.3 MPa (43.5 psi) ethylene with MAO as co-catalyst. The weight average molar masses (M_w) ranged from 2×10⁵ to 4.2×10⁵ with number average molar masses (M_n) of 8300 to 50000; the polymer samples had broad distributions with polydispersities of 7 to 24 (van der Linden et al., 1995).

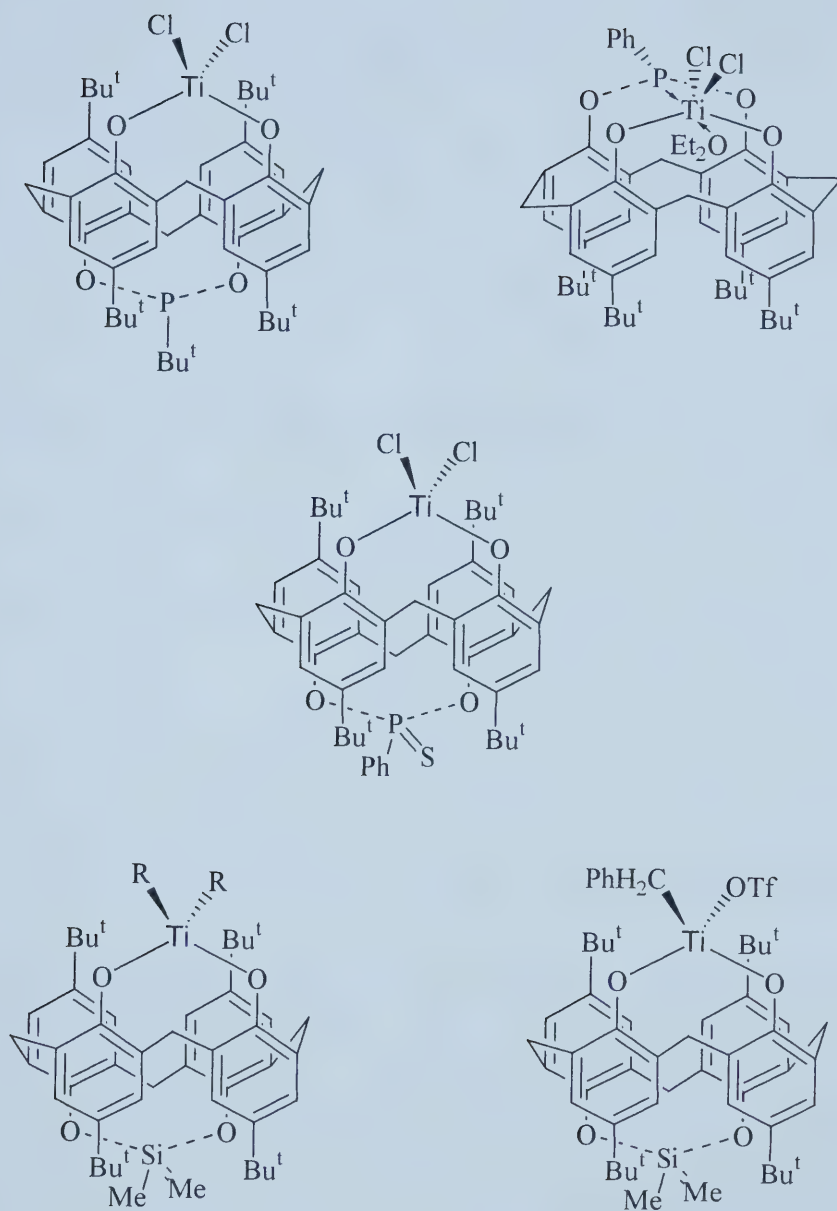


Figure 2.8. Ti complexes of p-tert-butylcalix[4]arene (Ozerov et al., 1999).

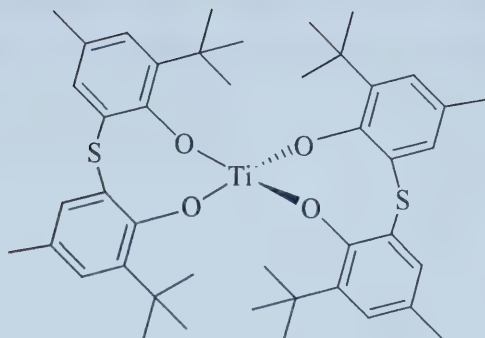


Figure 2.9. Bridged Ti polyphenoxide species (van der Linden et al., 1995).

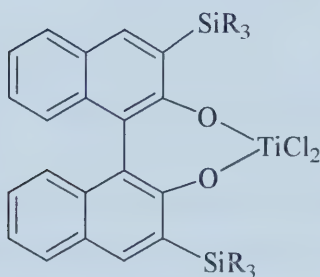
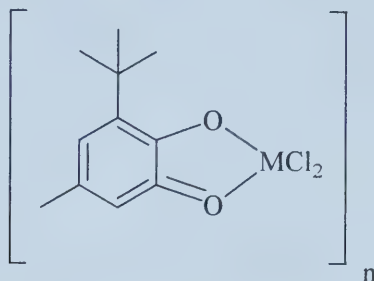


Figure 2.10. Chelated Ti polyphenoxide species (van der Linden et al., 1995).

Matilainen et al. (1996) synthesized Group IV transition-metal (Ti, Zr) aryloxy complexes for olefin polymerization. The complexes (e.g. Figure 2.11) were designed to possess favourable characteristics of catalytically active systems. Coordinative and electronic unsaturation at the metal center is the main feature of catalytically active complexes, and selectivity is controlled by chiral and structural rigidity. In addition, mononuclear complexes containing sterically hindered ligands are protected against deactivation reactions. Activities of 8-80 kg PE/(g M·h) (M = Ti, Zr) were obtained for ethylene homopolymerization and ethylene/1-hexene copolymerization, which were performed in heptane at 80°C and 1 MPa ethylene. The homopolymer samples had broad molar mass distributions with polydispersities

of about 16; Mw ranged from 6×10^5 to 9×10^5 with Mn of 37000 to 54000 (Matilainen et al., 1995). Higher molar masses and broader distributions were obtained for copolymer samples.



M = Ti or Zr

n = 1 or 2

Figure 2.11. Chelated Ti aryloxide complex (Matilainen et al., 1996).

Researchers at Mitsui Chemicals Inc. (Furuyama et al., 2003) prepared a series of bis(phenoxy-imine) titanium complexes for ethylene and propylene polymerization (see Figure 2.12). They claim to have the highest reported polymerization activity of 3240 kg PE/(mol cat·h) for titanium complexes without cyclopentadienyl ligands. Ligand effects were determined to play an important role in the polymerization behaviour; the steric bulk of the ortho substituent (R^1) to the phenoxy oxygen was shown to significantly affect the polymerization activity and molar mass distribution. The polymerization experiments were performed in toluene at 25°C with atmospheric ethylene pressures. Molar masses exceeding 1×10^6 were measured for some polymer samples, and it was of interest that the molar mass distributions were unusually narrow with polydispersities of 1.29 to 3.13. Given their findings, the sterically hindered environment for the ortho-substituted phenols in the polyphenoxide ligand tris(2,6-dihydroxyphenyl)ethene could be a favourable design feature.

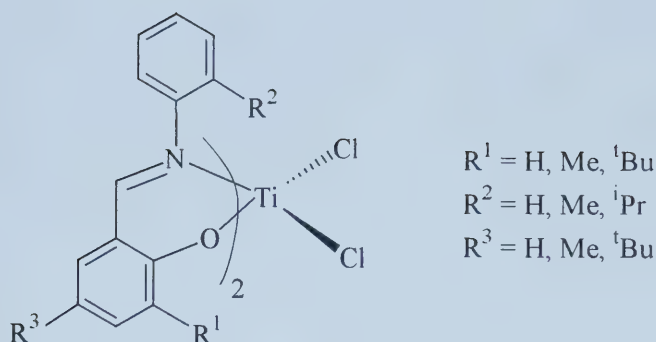
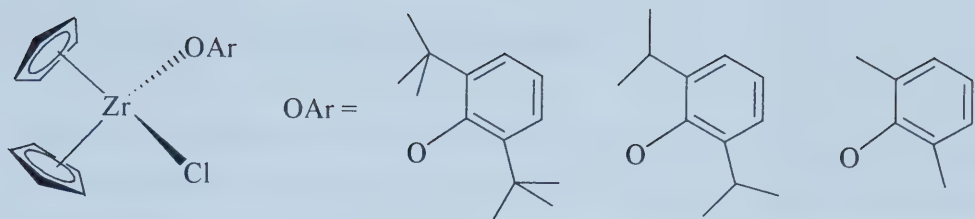


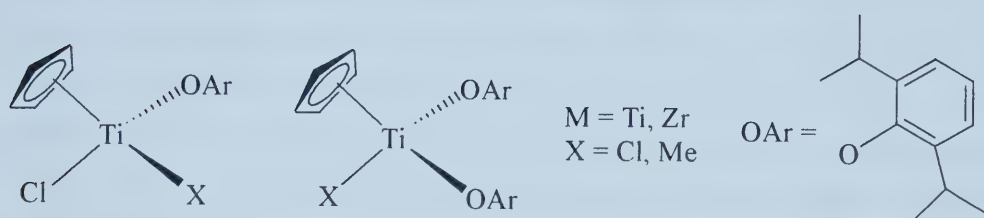
Figure 2.12. Bis(phenoxy-imine) titanium complexes (Furuyama et al., 2003).

2.3.2.3 Ancillary Aryloxyde Ligation

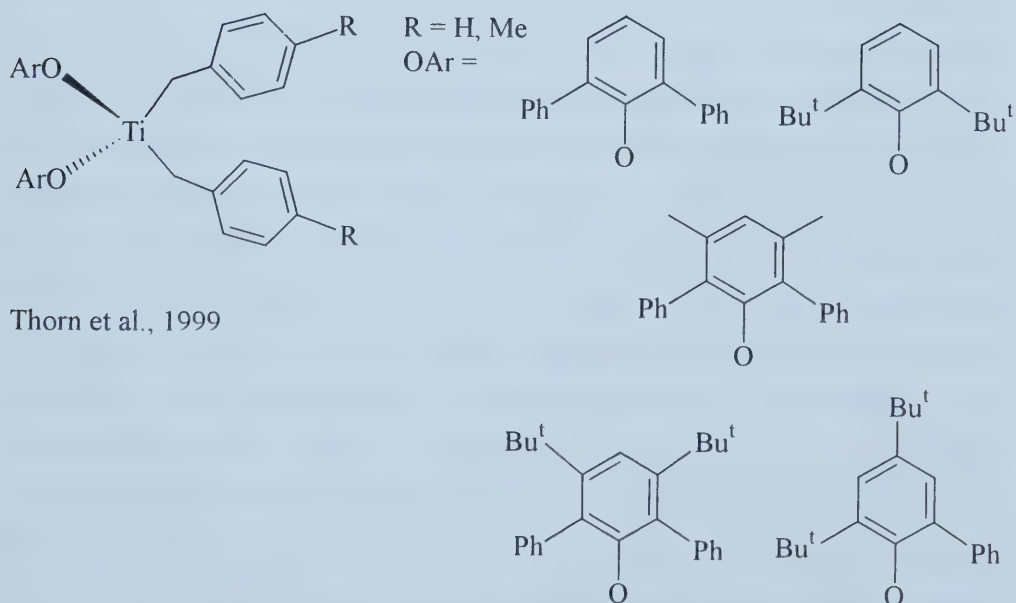
With the discovery of methylaluminoxane (MAO) as an activator for Group IV metallocene complexes, much interest has focused on the development of new catalysts with different ligation at the metal center (Hlatky, 2000). A series of phenoxy substituted metallocene complexes have been prepared and characterized (Repo et al., 1997; Firth et al., 1999). In some instances, incorporation of the aryloxyde ligands resulted in higher polymerization activities than the parent metallocene complexes (Firth et al., 1999). Structurally, the ancillary aryloxyde complexes (see Figure 2.13) are based on half-sandwich complexes with the ligand imposing less steric hindrance at the metal center than the bridged or chelated aryloxyde complexes. In addition, interest into non-cyclopentadienyl ligation has initiated studies of compounds containing aryloxydes. Thorn et al. (1999) synthesized a series of bis(alkyl) substituted titanium and zirconium complexes with various 2,6-di-substituted phenoxides (see Figure 2.13).



Repo et al., 1997



Firth et al., 1999



Thorn et al., 1999

Figure 2.13. Examples of ancillary aryloxy complexes.

2.4 Ligand Effects in Olefin Polymerization

Polymerization performance can be altered through control of the ligand environment at the transition metal center; the ligand functionality of olefin polymerization catalysts influences activity, comonomer incorporation, and hydrogen response (Karol and Kao, 1994). In addition, polymer properties such as molar mass and comonomer incorporation are affected by the chemical nature of the active sites (Soares and Hamielec, 1995). From the point of view of process design, the industrial application of catalysts with different ligand functionalities may lead to technological developments that will enhance gas-phase reactor performance (Karol and Kao, 1994). Laboratory-scale empirical studies of catalyst families for olefin polymerization will expand our understanding of the influence that ligand functionality has on reactor performance.

Modification of active site environments is one route to alter the mechanisms of olefin polymerization. The activity of Ziegler-Natta catalysts was greatly improved through the interaction of titanium halides with magnesium compounds, and electron donor compounds are thought to interact with the active sites and the aluminum alkyl co-catalysts (Soga and Shiono, 1997). The reactivity and selectivity of unsaturated sites are thought to control olefin polymerization for coordination transition metal compounds (Huang and Rempel, 1995). For example, the $\text{CrO}_3/\text{SiO}_2$ catalyst has little hydrogen response as a chain transfer agent, but the molar masses for polymer produced with silica-supported bis(cyclopentadienyl)-, bis(indenyl)-, and bis(fluorenyl)-chromium catalysts decrease in the order of the ligands cyclopentadienyl > indenyl > fluorenyl, likely due to lower electron density at the chromium center (Karol and Kao, 1994). Consideration of steric and electronic effects in the design of ligand environments has proven invaluable to the success of zirconocene catalysts. It was observed that zirconocene catalysts with more structural rigidity (cf indenyl versus cyclopentadienyl ancillary ligands) produced

polymer with higher molar masses, and ligands with greater electron donating ability had the effect of increasing the polymerization activity and comonomer incorporation (Karol and Kao, 1994). In summary, the active site environment has great potential for altering polymerization behaviour, and ligand functionality is an important factor to be considered in catalyst design.

2.5 Catalyst Activity Profiles in Olefin Polymerization

When temperature and monomer concentrations are held constant over time, catalyst activity profiles are reaction rate curves for the production of polyethylene. The activity profiles are convenient for interpreting and presenting polymerization results, specifically in studying the kinetics of olefin polymerization (Bu et al., 1995; Wu et al., 1999). Figure 2.14 illustrates the four types of observed rate behaviour; the shape of the activity profile is determined by reaction mechanisms for activation and deactivation (Kissin, 1985). Curves of Types 1 and 2 are observed for low activity catalysts, whereas Types 3 and 4 are typical for high activity catalysts. Many catalysts have profiles similar to Type 4 with the activity reaching a maximum rate followed by decay in the rate to a somewhat steady-state level (Odian, 1970).

Catalyst preparation and polymerization conditions affect the shape of the activity profile (Kissin, 1985), and the shape of activity profiles has important implications for catalyzed systems because they reflect the coupling between mass and energy balances for the exothermic polymerization reactions (Wells and Ray, 2001). Ziegler-Natta catalysts exhibit complicated kinetic behaviour; activity profiles resembling Type 4 are typically observed (Odian, 1970; Kissin, 1985). The shape of the activity profile suggests different types of active sites are present in the Ziegler-Natta catalyst. Some sites become deactivated during the initial period of high activity and, over time, the steady-state rate is attained or a continuous decay in the

rate occurs, possibly due to catalyst destruction at the high polymerization temperatures or restricted monomer diffusion to active sites through the layer of polyethylene (Czaja et al., 1999).

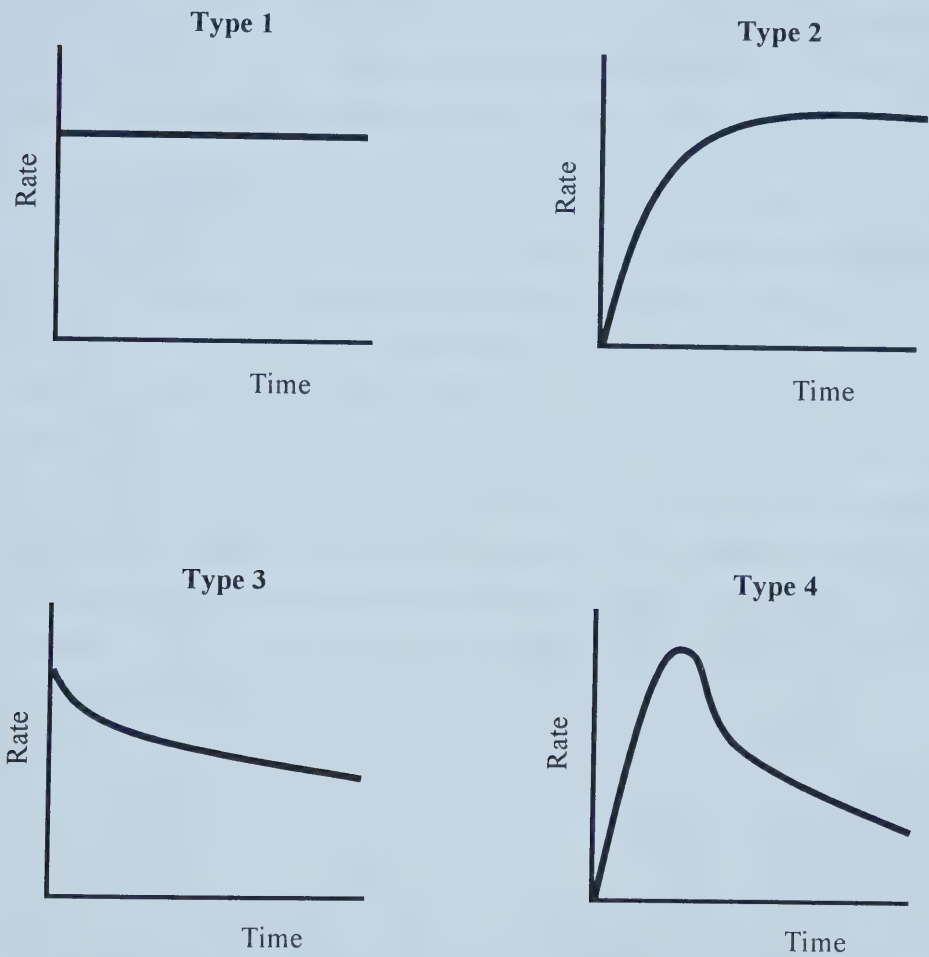


Figure 2.14. Types of catalyst activity profiles (Kissin, 1985).

3.0 EXPERIMENTAL PROCEDURES

3.1 Catalyst Preparation

Professor Stryker's group in the Department of Chemistry at the University of Alberta developed the polyphenoxide ligand used in this work. Yasuda (2000) described the synthesis of 1,1,2-tris(2,6-dihydroxyphenyl)ethene (see Figure 3.1). The synthetic route was later modified by Dzwiniel (2000) to improve yields (see Figure 3.2).

The supported, bimetallic (Ti-Mg) polyphenoxide catalyst was prepared in four steps: (1) thermal treatment of the support; (2) chemical anchoring of the polyphenoxide ligand on the support; (3) incorporation of magnesium onto the supported ligand; and (4) metallation with titanium (IV) chloride. Silica was selected as the support because it contains the appropriate surface functional group to chemically bind the polyphenoxide ligand. Other catalysts were prepared with various combinations of the above steps to evaluate the effect of different active site environments on polymerization activity and polymer properties. The different silica-supported catalysts will be identified with reference to the constituent components used in their preparation: Ti for titanium (IV) chloride; Mg for methyl magnesium chloride; and Ligand for tris(2,6-dihydroxyphenyl)ethene.

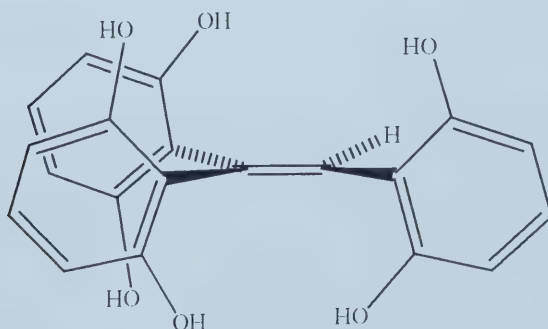
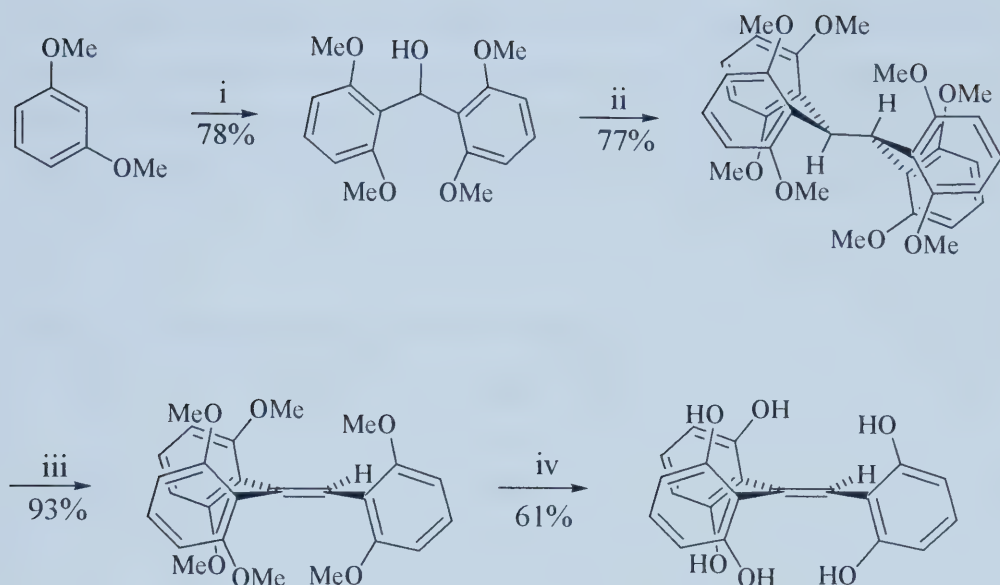


Figure 3.1. Molecular structure of tris(2,6-dihydroxyphenyl)ethene.



- (i) $n\text{-BuLi}$, TMEDA, -78°C ; then HCO_2Et .
(ii) CrCl_2 , HCl , acetone.
(iii) $\text{C}_7\text{H}_7^+ \text{BF}_4^-$, $\text{ClCH}_2\text{CH}_2\text{Cl}$.
(iv) BBr_3 , -78°C to RT.

Figure 3.2. Synthetic route for tris(2,6-dihydroxyphenyl)ethene.

3.1.1 Support Treatment

The support used to prepare all the catalysts was a commercially available silica gel (Lot #6403) provided by NOVA Chemicals Corporation. The silica was thermally treated to prepare the surface for anchoring the polyphenoxide ligand. It was placed in a Vycor U-tube that was attached at both ends with fittings to a detachable holder. Ultratorr o-rings sealed the ends of the U-tube at the fittings. The U-tube section was heated to about 500°C in a temperature controlled furnace. Moisture was removed by

passing nitrogen through the silica at a rate of 60 mL/min. The heating period varied for different batches of silica with a minimum time of 6 hours; details for the treatment of different batches are listed in Table 3.1. The heating temperature of 500°C was chosen to maximize the concentration of surface siloxanes without loss of surface area.

Table 3.1: Thermal Treatment Conditions for Silica.

Silica Batch Number	Heating Temperature (°C)	Heating Time (hours)
1	500	8.5
2	500	6.0
3	500	9.0
4	500	16.5
5	520	11.0
6	500	16.0

3.1.2 Ligand Anchoring

The polyphenoxide ligand was anchored to silica by mixing the slurry of the two components. Tris(2,6-dihydroxyphenyl)ethene is soluble in polar solvents such as acetone but fairly insoluble in nonpolar solvents like toluene. It was desirable to use toluene because subsequent preparative steps involved use of a Grignard reagent and titanium (IV) chloride, which would decompose in the presence of residual acetone. Chemical binding of the polyphenoxide ligand to the partially dehydroxylated silica was accomplished by stirring the toluene slurry at room temperature for a minimum of 24 hours in the glove box. The slurry was stirred for long times before evaporating the solvent because the ligand was slow to dissolve.

The ligand was anchored to silica through its hydroxyl groups. The siloxane ring structure has a bond angle of approximately 90° , which makes the strained siloxane group susceptible to hydrolysis reactions (Grabbe et al., 1995). The siloxane groups on the silica surface that were created during the thermal treatment are reactive towards the hydroxyl groups on the ligand; the proposed mechanism is given in Figure 3.3. For a heating temperature of 500°C , the concentration of surface siloxanes is approximately $3 \text{ Si-O-Si}/\text{nm}^2$ (Ullmann's Encyclopedia of Industrial Chemistry, 1993). This information was used as a guide to calculate an acceptable ligand loading on silica, and catalysts were prepared with several different ligand loadings. It was difficult to choose loading values because there were six hydroxyl groups on the ligand that could enable multiple attachments to silica for one ligand molecule. The extent of siloxane homogeneity on the surface was not known, which would affect the number of attachments. Likely, there would only be attachments through one face of the ligand molecule. The surface area of the silica was determined to be about $300 \text{ m}^2/\text{g}$ by the BET method. Assuming attachment occurred through three hydroxyl groups per ligand molecule, the maximum loading was calculated to be $175 \text{ mg ligand/g silica}$, but the catalysts were prepared with lower ligand loadings.

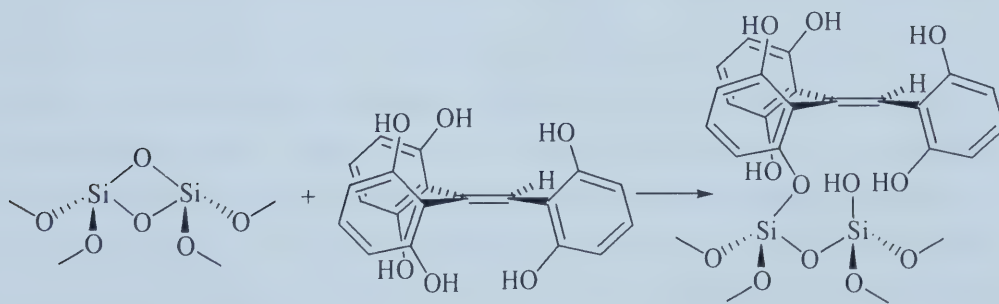


Figure 3.3. Proposed mechanism for anchoring the ligand to silica.

3.1.3 Magnesium Incorporation

Magnesium was incorporated onto the supported ligand with a Grignard reagent. Methyl magnesium chloride (3M in THF, Aldrich) was slowly added dropwise, while stirring, to the supported ligand suspended in tetrahydrofuran (THF). The slurry was stirred for an additional 30 minutes following the addition. Reaction with the Grignard reagent resulted in the formation of magnesium aryloxides with the polyphenoxide ligand and magnesium siloxides with the residual silica silanols. Excess quantities of the Grignard reagent were used because the concentration of ligand hydroxyls and residual silanols was unknown, and it was desirable to ensure that magnesium was incorporated onto all the ligand hydroxyls. Many surface species could be present with magnesium bridging multiple oxygen, and it was also likely THF was coordinated to magnesium.

After reaction with the Grignard reagent, the catalyst was filtered and repeatedly washed with THF with a total volume of 50-100 mL, depending on the amount of magnesiated catalyst precursor. The washing removed excess, unbound Grignard reagent from the catalyst. Solvent was removed from the magnesiated catalyst precursor using the Schlenk vacuum line in the glove box then the high vacuum line (10^{-5} Torr) in the laboratory. The drying temperature of the magnesiated catalyst precursor was one of the preparation conditions varied. Higher activities were obtained when longer drying times were used so the temperature was varied to accelerate the drying process and establish more consistent drying conditions. A cylindrical resistance heater was constructed to fit around the Schlenk flask containing the magnesiated catalyst precursor, and the temperature was adjusted to the desired value within 2°C . Typically, the magnesiated catalyst precursors were dried under vacuum for 5 days at the elevated temperature, and the final pressure was usually $<0.05\text{ Pa}$ (4×10^{-4} Torr).

3.1.4 Titanium Addition

Once the magnesiated catalyst precursors had been thoroughly dried to remove residual THF, the final step in the preparation was the addition of titanium (IV) chloride. Two methods were used to prepare the catalysts. A summary of catalyst preparation conditions is given in Table 3.2, and more details are described in Appendix A.

In two cases (CAT-17 and CAT-22), titanium was incorporated into the magnesiated catalyst precursors using a slurry method. This method allows better control of the titanium content of the catalysts. The addition was performed at room temperature with hexane or toluene used as the solvent. The catalysts were suspended and stirred in the selected solvent and a dilute solution of titanium (IV) chloride was added dropwise. After the addition, the solvent was evaporated with the Schlenk line in the glove box.

The other method involved the vapour deposition of titanium (IV) chloride. Once degassed, the vapour pressure of titanium (IV) chloride was sufficient to enable the deposition within a reasonable time. Unfortunately, there was poor control over the amount of titanium deposited onto the magnesiated catalyst precursor with this method. The contact time was varied to determine whether there were diffusion or reaction time limitations. One catalyst was prepared with a very short contact time to observe the colour change resulting from the incorporation of titanium (IV) chloride; longer contact times were also tested. Except for one catalyst (CAT-31), the addition was performed with the catalysts maintained at room temperature. At the end of the addition, excess titanium (IV) chloride was condensed into its Schlenk flask and the catalyst holder was evacuated until the pressure was below atmospheric.

Table 3.2: Summary of Catalyst Preparation Conditions.

Catalyst Name	Silica Batch ^a	Ligand ^b (mg [mmol])	Ligand Loading (mg/g)	Grignard ^c (mmol)	Drying Temp ^d (°C)	TiCl ₄ Addition ^e
CAT-12	1	18.1 [0.051]	7.1	None	RT	V (45 min)
CAT-13	2	None	N/A	None	RT	V (1.5 h)
CAT-14	2	56.4 [0.160]	55.7	3.8	RT + heat	V (5.5 h)
CAT-15	3	None	N/A	4.0	RT + heat	V (5.5 h)
CAT-16 ^f	N/A	21.4 [0.061]	42.1	7.3	RT + heat	V (75 min)
CAT-17	3	51.2 [0.145]	51.4	2.4	60	S (toluene)
CAT-18 ^g	3	51.2 [0.145]	51.4	2.4	60	V (15 min)
CAT-19	3	58.3 [0.165]	47.8	3.8	RT	V (10 min)
CAT-20	3	58.3 [0.165]	47.8	3.8	RT	V (5.5 h)
CAT-21	3	58.3 [0.165]	47.8	3.8	RT	V (5.5 h)
CAT-22	3	58.3 [0.165]	47.8	3.8	RT	S (hexane)
CAT-23	3	58.3 [0.165]	47.8	3.8	RT	V (5.5 h)
CAT-24 ^g	4	77.7 [0.220]	38.8	4.1	RT + 50	V (7.5 h)
CAT-25	4	77.7 [0.220]	38.8	4.1	RT + 50	V (6 h)
CAT-26	4	77.7 [0.220]	38.8	None	RT	V (10 h)
CAT-27	4	84.6 [0.240]	38.9	5.9	90	V (6 h)
CAT-28 ^g	4	84.6 [0.240]	38.9	5.9	70	V (6 h)
CAT-29	4	84.6 [0.240]	38.9	5.9	80	V (6 h)
CAT-30	4	84.6 [0.240]	38.9	5.9	60	V (6 h)
CAT-31	5	99.0 [0.281]	39.0	5.3	60	V (8.5 h) ^h
CAT-32	5	99.0 [0.281]	39.0	5.3	70	V (7 h)
CAT-33	5	None	N/A	3.1	70	V (6 h)
CAT-34	5	63.2 [0.179]	39.6	3.1	70	V (8, 15 h) ⁱ

a Refer to Table 3.1 for details

b MW of 1,1,2-tris(2,6-dihydroxyphenyl)ethene = 352.34 g/mol

c Used 3M solution of CH₃MgCl in THF (density = 1.013 g/mL)

d Temperature for resistance heater, RT for room temperature, or heat for heat gun

e S (solvent) for slurry method or V (contact time) for vapour deposition method

f Used HEMA PS-DVB as support

g Catalyst discoloured after drying (some exposure to air)

h Catalyst heated at 60°C during vapour deposition of TiCl₄

i Vapour deposition performed in two stages

3.2 Polymerization Experiments

3.2.1 Description of the Polymerization Reactor

A schematic diagram of the polymerization reactor system is given in Figure 3.4. The cylindrical-shaped, stainless steel reactor had an internal volume of about one litre. The removable bottom section was sealed to the stationary top flange with a Viton o-ring. The reactor was submerged in a 26-L silicone oil bath (50 CST, Dow Corning 200® Fluid) with a constant temperature immersion circulator (Lauda, Model MS) for temperature control (TC).

In the polymerization experiments, a continuous supply of polymer grade ethylene (Praxair) was fed into the reactor and the total pressure was set with a pressure regulator (0 to 3.4 MPa, Tescom, Model 26). The pressure was monitored with two pressure transducers, which were positioned before the inlet to the magnetic stirrer. One pressure transducer was a low-precision load cell and the other transducer (Omega, Model PX621) had a higher precision. The feed gases were passed through purification vessels (Figure 3.5) to remove trace impurities, and the feed rates were measured with Matheson mass flow meters. The mass flow meters had maximum flow rates of 1072 cm³/min and 2128 cm³/min, which were exceeded in some polymerization experiments as seen by a flat section in the activity profiles (e.g. Figure 3.6). The liquid comonomer 1-hexene (NOVA Chemicals Corporation) was fed to the reactor with a syringe pump (ISCO, Model 500D), and the catalyst and co-catalyst were injected with a dry catalyst holder and syringe port, respectively. The reactor contents were mixed with a variable speed magnetic drive stirrer (Autoclave Engineers Ltd., Magnedrive Model 1.5-1-5K) with paddle-type blades. Type J thermocouples were positioned at various radial positions along the sides of the reactor to monitor the gas-phase temperatures in the reaction zone. The gas composition in the reactor could be sampled and analyzed with a gas chromatograph

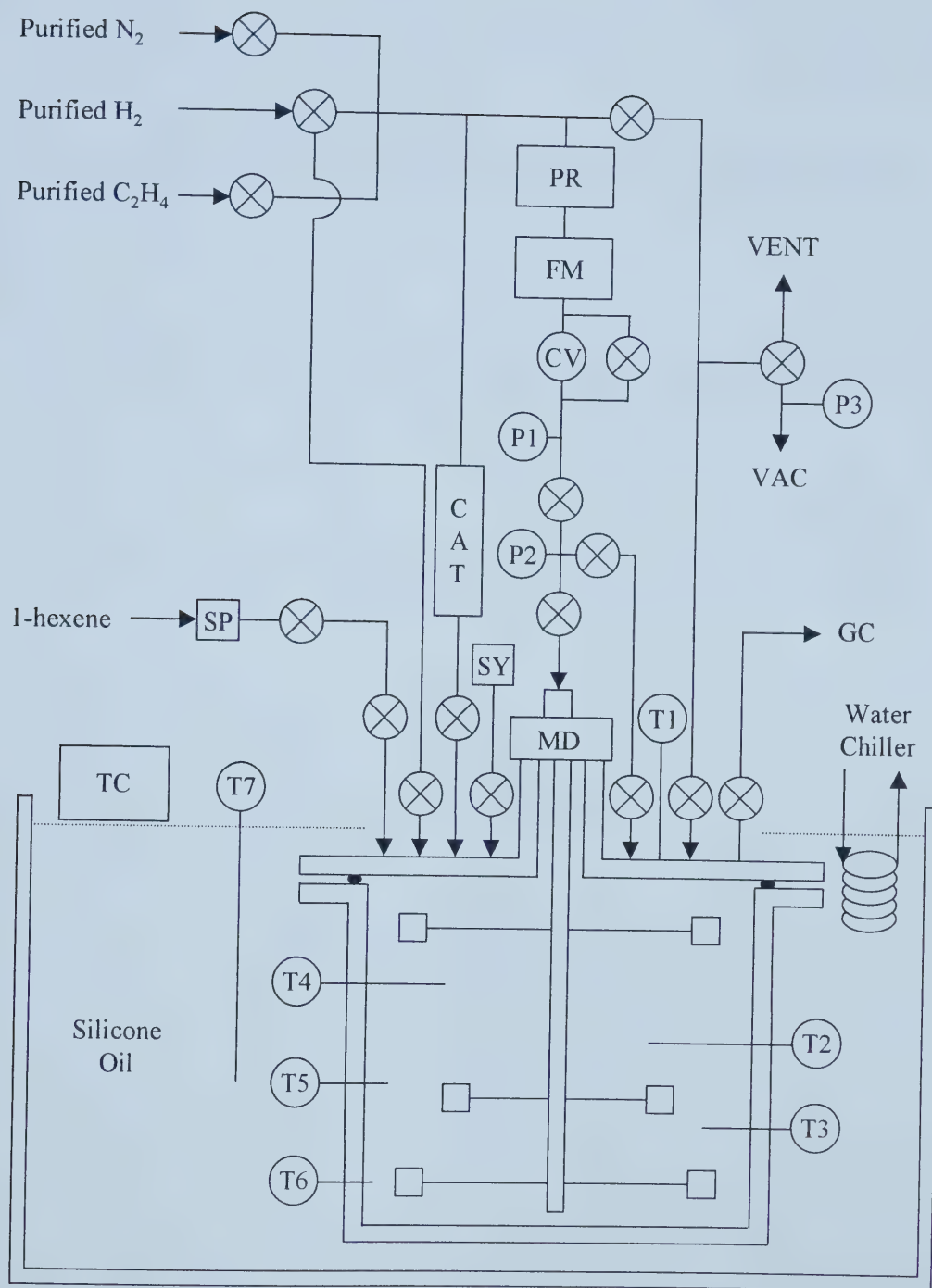
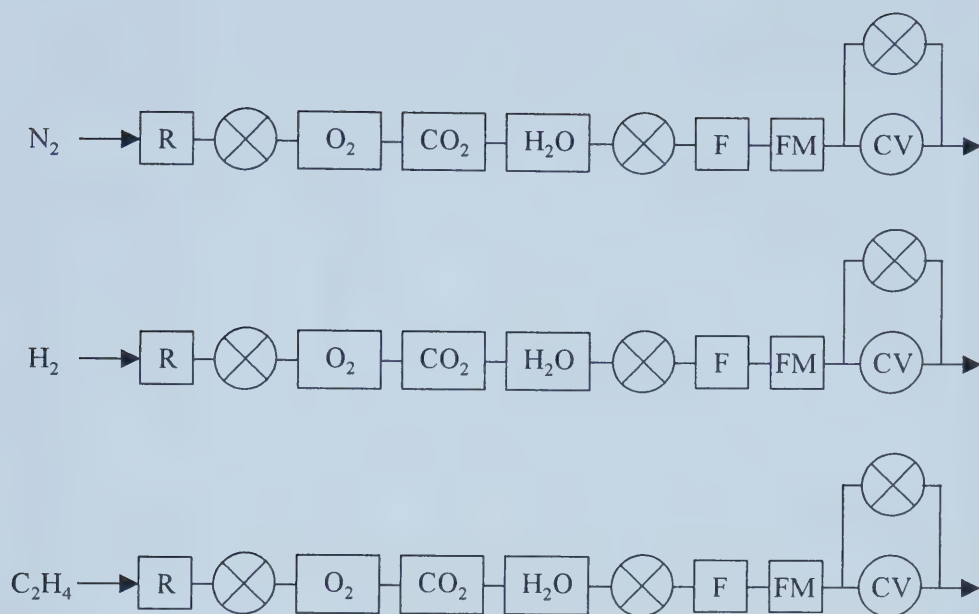


Figure 3.4. Schematic diagram of the polymerization reactor.




	: ball valve
CAT	: dry catalyst holder
CV	: control valve
F	: filter
FM	: mass flow meter
MD	: magnetic drive stirrer
O ₂ , CO ₂ , H ₂ O	: gas purification vessels
P#	: pressure gauge
PR	: pressure regulator
R	: gas cylinder regulator
SP	: syringe pump
SY	: syringe port
T#	: thermocouple
TC	: temperature controller

Figure 3.5. Schematic diagram of the gas purification trains.

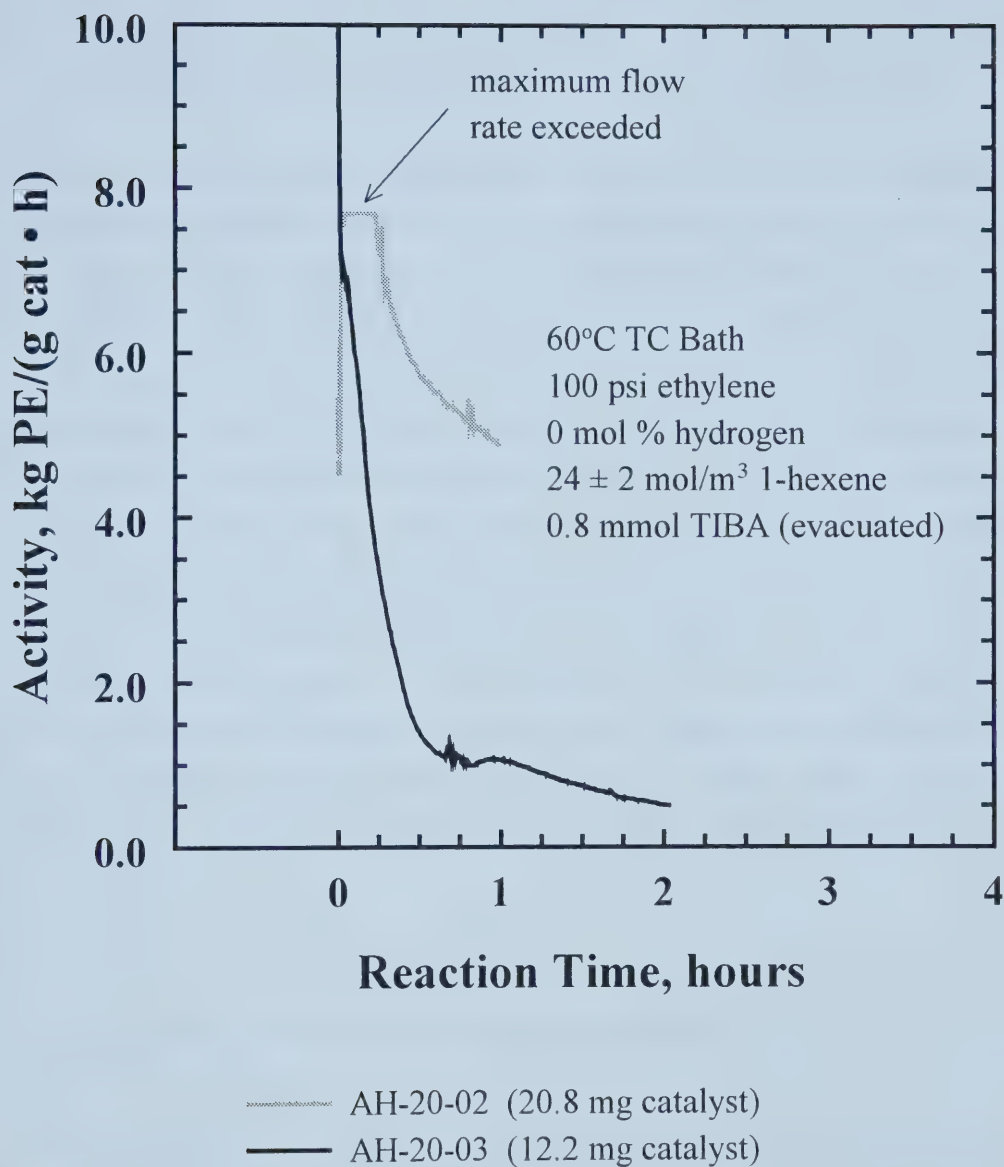


Figure 3.6. Activity profiles showing catalyst deactivation due to the amount of catalyst injected into the reactor.

(Hewlett-Packard, 5890A series II). The pressure, temperatures, and mass flow rates were recorded every 10 seconds with a data acquisition program on a PC. Lynch and Wanke (1991) describe additional details about the polymerization reactor system.

A recent modification to the reactor system was the addition of a by-pass line to admit ethylene into the reactor. The by-pass line was teed into the tubing at the top of the magnetic stirrer and connected to a port on the top flange. Previously, ethylene was only fed through the hollow magnetic stirrer shaft, but the shaft became partially plugged with polymer during the experiments due to the high productivities. Over successive experiments, it was noticed that there was an increase in the time required to fill the reactor, which indicated the ethylene flow into the reactor was restricted. Although the magnetic stirrer was periodically disassembled and cleaned, it still seemed that there was a flow restriction in some experiments because the flow rate oscillated. It was thought the orifice at the top of the magnetic stirrer was too small to accommodate the high ethylene flow rates required in some experiments. The flow restriction affected the magnitude of the activity and the shape of the activity profile, as seen in Figure 3.7, because the reactor pressure was likely much lower than indicated on the pressure transducer. Installation of the by-pass line alleviated the flow restriction.

3.2.2 Operating Procedure for the Polymerization Reactor

Lynch and Wanke (1991) established the operating procedure for the polymerization reactor. One important variable affecting the success of the polymerization experiments was the amount of catalyst injected into the reactor. It was noticed that the rate of catalyst deactivation was affected by the amount of catalyst (Figure 3.6).

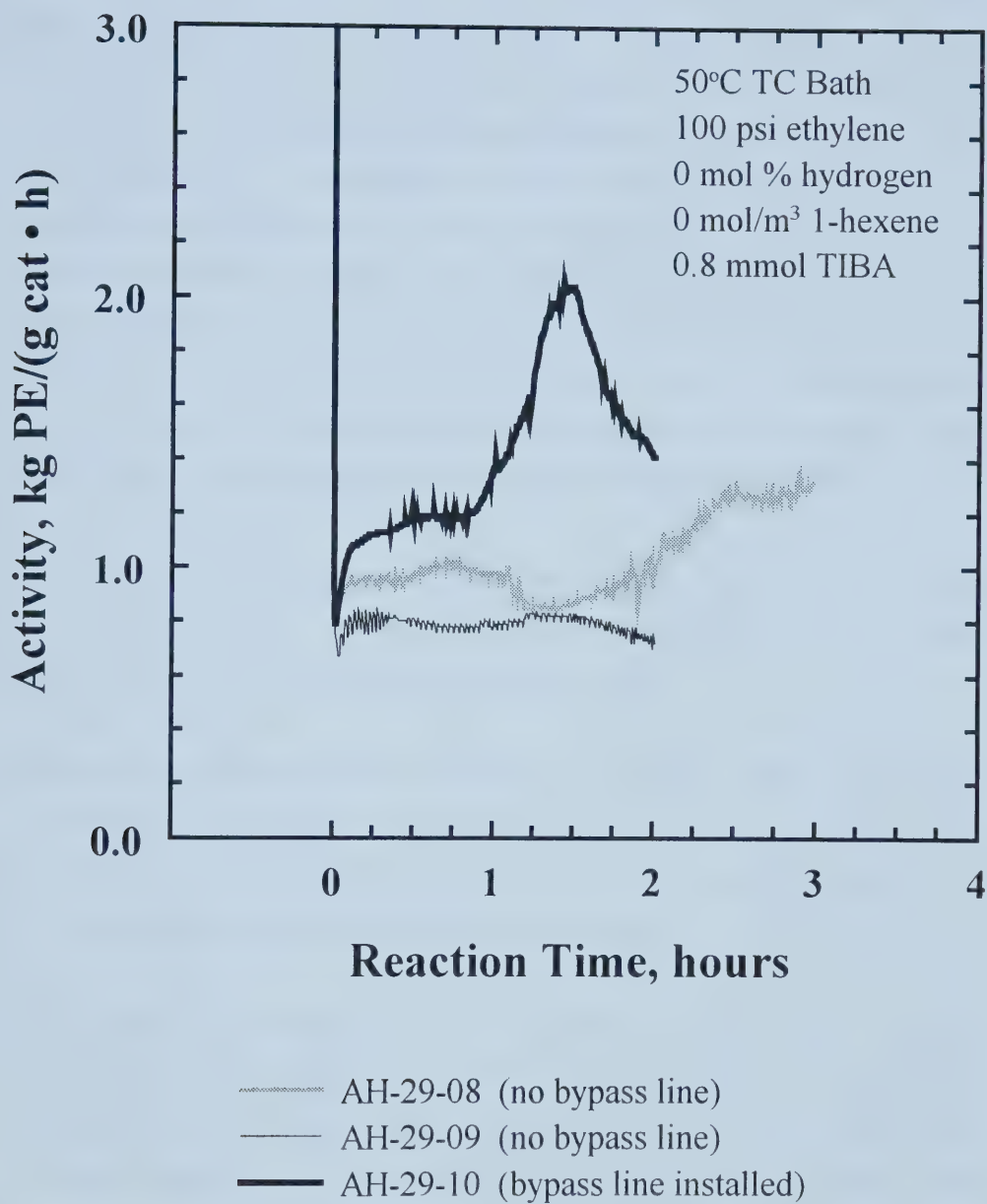


Figure 3.7. Activity profiles illustrating ethylene flow restriction.

Because the ethylene flow rate decreased more rapidly with lower quantities of catalyst, it seemed there was a minimum amount of catalyst required to sustain the activity. The concentration of reactor impurities should be similar in all polymerization experiments so catalyst deactivation was likely not the cause of the rapid deactivation. Considering microscopic and macroscopic aspects of polymerization in the reactor system, use of small quantities of catalyst might not be sufficient to sustain polymerization. Microscopically, heat generation in the growing polymer particles would promote higher polymerization rates thus contributing to the shape of the activity profile in the macroscopic reactor system. To maintain adequate polymerization rates with good reproducibility, a minimum of 0.02 g catalyst with a loading of about 40 mg ligand/g silica was used in all subsequent experiments.

The gas-phase polymerization experiments were performed using sodium chloride (99.0%, particle size 0.5 mm, Fisher Scientific) as a seedbed to disperse catalyst particles, and the following operating procedure was used:

1. Reactor pretreatment consisted of cleaning the internal surfaces with solvent, adding 80 g sodium chloride, and testing for leaks at 250 psi with nitrogen. The reactor was fully submerged in the silicone oil bath and heated overnight at 90°C under dynamic vacuum with an Edwards vacuum pump.
2. The catalyst and aluminum alkyl were handled in the glove box (Vacuum Atmospheres Ltd., Model HE-493). The catalyst holder, which consisted of stainless steel quick-connect fittings and plug valves separated by 6 cm of ¼ inch Swagelok fittings, was filled with salt and 0.02 to 0.05 g \pm 0.001 g catalyst. First, about 0.4 g sodium chloride was added into the base of the holder. The catalyst was weighed in a plugged funnel, and about 0.4 g salt was mixed into the catalyst. After loading the catalyst, the holder was filled to the top with salt (about 0.4 g) and the top section of the holder was attached. A gas-tight syringe was filled with

the desired amount of aluminum alkyl (neat, Aldrich) and the end of the needle was sealed with a septum.

3. After reactor pretreatment, the oil bath was cooled to the desired temperature with the water chiller. The reactor was isolated from the vacuum and nitrogen was admitted to about 40 psi. The valve on the top flange for the catalyst injection port was removed and the end of the catalyst holder was purged with nitrogen before securing the connection to the port. The other end of the catalyst holder was connected to the flex hose line after being purged with high-pressure (400 psi) nitrogen. Next, the reactor and all tubing leading to the reactor from the exit of the purification vessels were evacuated until the reading on the vacuum pressure gauge was <20 Pa (0.15 Torr). Data acquisition commenced prior to filling the reactor with ethylene. Ethylene was admitted into the reactor to 20-30 psi, and the aluminum alkyl was injected through the syringe port. The reactor contents were stirred at 150 rpm for 15 minutes to scavenge impurities. Unless otherwise specified, the reactor was evacuated for 2 minutes to remove some aluminum alkyl after scavenging impurities. If hydrogen and 1-hexene were required, they were added to the reactor followed by 20-30 psi ethylene. The reactor contents were stirred for about 2 minutes then the stirrer was stopped and valves were closed to isolate the reactor from the feed lines. High-pressure (400 psi) ethylene on the upstream side of the catalyst holder was used to inject the catalyst into the reactor. The mixer was set to 330 rpm and the pressure regulator was adjusted to the desired total pressure. Finally, the valves at the stirrer and by-pass line were opened to feed ethylene into the reactor.
4. At the end of the polymerization experiment, the ethylene flow into the reactor and data acquisition were stopped. After turning off the magnetic stirrer, the reactor was vented to atmospheric pressure and low-pressure air was blown through the syringe port to deactivate the catalyst.

5. The product was placed in a cellulose extraction thimble (90 mm × 200 mm, Whatman®) and rinsed with warm water to remove the salt. The polymer was dried overnight in the oven at 70°C, and weighed to determine the yield. Some of the yields were higher than the integrated values from the ethylene flow rate data. Scanning electron microscopy (SEM) images of the washed product revealed that polymer grew on and around some salt crystals (i.e. the washing did not remove all the salt).

Appendix B contains the pressure, ethylene flow rate, and temperature profiles for all the polymerization experiments discussed in Chapter 4.0. As well, there is a table summarizing the polymerization conditions and yields for all the experiments performed with CAT-12 through CAT-33. The polymerization experiments were named with the notation AH-XX-YY, where XX refers to the catalyst number and YY gives the run number. Blank-1 and Blank-2 were collected with the same procedure as described above except no catalyst or co-catalyst was injected into the reactor. In the blank runs, the pressure in the reactor reached the set point shortly after admitting ethylene into the reactor, as evidenced by the ethylene flow rate rapidly dropping to zero. It took approximately 90 seconds to fill the empty reactor regardless of the pressure set point.

3.3 GC Analysis of Reactor Gas Composition

The gas composition in the reactor was measured by gas chromatography. The separations were achieved with Alltech Porapak Q (80/100 mesh) packing that was contained in an 85-cm stainless steel column with an inner diameter of 0.08 inches. The oven and detector temperatures were set according to the desired separation, and Argon (60 psi) was the column carrier gas.

3.3.1 Hydrogen Concentration

The hydrogen concentration in the reactor was measured to determine hydrogen consumption during the course of the polymerization experiments. The thermal conductivity detector (TCD), which was maintained at 200°C, was used for measuring hydrogen and ethylene concentrations.

Calibration data were collected to determine sensitivity limits for the hydrogen/ethylene analysis. Hydrogen was admitted into the reactor to specific pressures and the reactor was filled with ethylene to about 100 psi. The reactor gas was sampled through Teflon tubing with an outside diameter of $1/16$ -inch at a flow rate of 15 mL/min; a Swagelok metering valve (SS2-A) was used to control the flow rate. The calibration data showed sufficient sensitivity and reproducibility to detect concentration changes of about 1 mole % hydrogen. Figure 3.8 gives the calibration plot for the hydrogen/ethylene separation. An excellent linear relationship was obtained between mole % hydrogen and peak area for hydrogen in the chromatogram.

3.3.2 1-Hexene Concentration

The 1-hexene concentrations were also monitored during polymerization for some experiments to assess consumption. The GC analysis was performed using the flame ionization detector (FID). For the ethylene/1-hexene separation, the oven temperature was maintained at 185°C and the detector was set to 200°C. The detector flame was ignited with a hydrogen and air mixture with supply pressures of 20 psi and 80 psi, respectively. The gas composition was calculated with the response factor determined from calibration data.

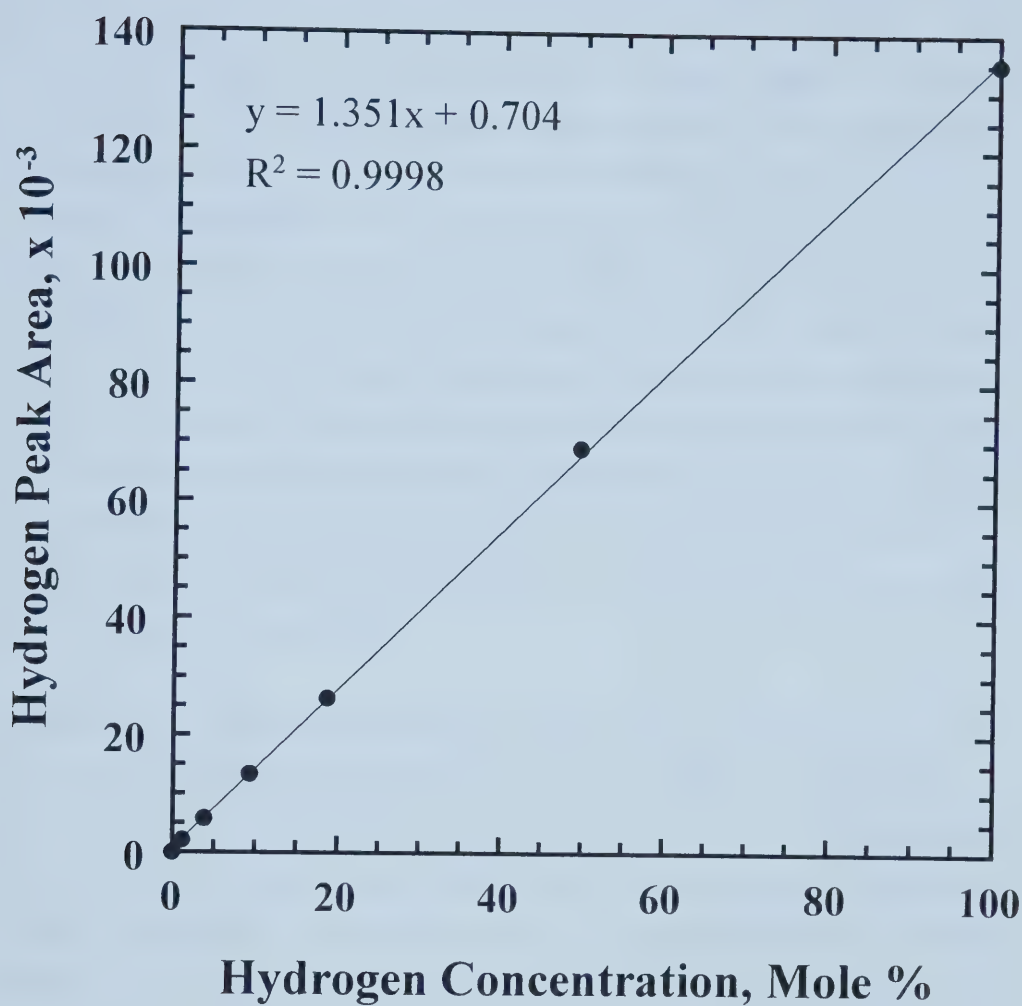


Figure 3.8. GC calibration for hydrogen/ethylene separation.

The amount of liquid 1-hexene added to the reactor was chosen to ensure it would all be in the gas-phase. The GC and activity results would be inaccurate if liquid 1-hexene was present in the reactor because the liquid would be continually evaporating as it was consumed and some catalyst particles could be enveloped in a liquid droplet, which would affect the diffusion of ethylene to active sites. Figure 3.9 gives the saturation pressure for 1-hexene as a function of temperature. The vapour pressures were retrieved from the Aspen Plus database. The ideal gas law was used to calculate the maximum volume of 1-hexene allowed for a specific reactor temperature. Liu (2002) showed 1-hexene vapour pressure determined with the ideal gas law was adequate compared to that calculated from the Redlich-Kwong-Soave (RKS) and Peng-Robinson (PR) equations. Because the liquid 1-hexene was metered from the pump reservoir at room temperature, the density of 0.6731 g/mL (20°C) was used to calculate the maximum liquid 1-hexene that could be added to the reactor at a given temperature (Figure 3.10).

There was some error in the GC analysis of the 1-hexene concentrations. It was likely some 1-hexene condensed in the valve or tubing leading to the GC injector port because of the pressure drop involved in sampling the reactor gas. The pressure drop occurred inside the sampling valve, which was at a lower temperature outside the reactor. This problem was resolved in the new 2-L polymerization reactor with the installation of a modified sampling valve that allowed the pressure drop to occur inside the reactor (Mannan et al., 2003). Also, some 1-hexene could condense on cooler internal reactor surfaces. The temperature of the top flange was always a few degrees cooler than the rest of the reactor because it was only covered by a few centimeters of silicone oil, and 1-hexene could condense in the mixer shaft, which was not submerged in the oil bath.

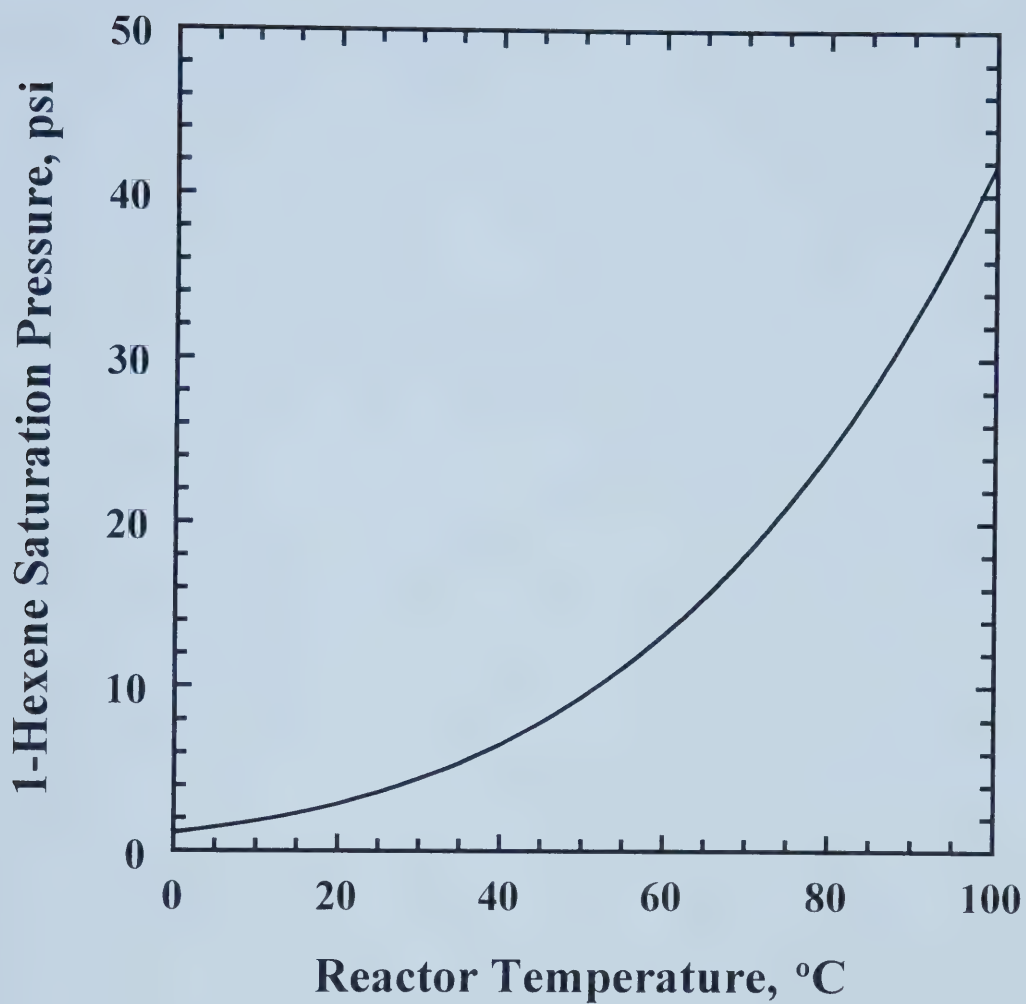


Figure 3.9. Vapour pressure of 1-hexene as a function of temperature.

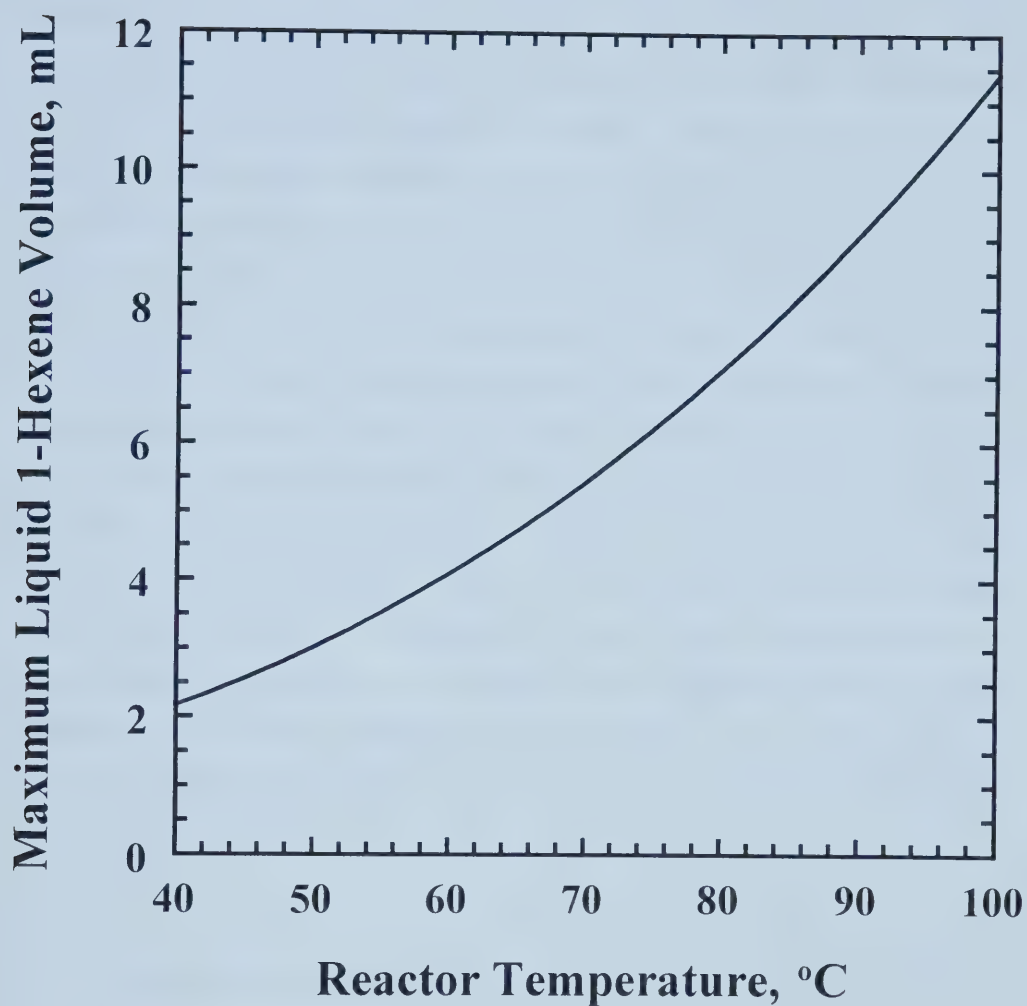


Figure 3.10. Maximum volume of liquid 1-hexene for saturation.

Calibration data were collected to determine the response factor for the ethylene/1-hexene separation so that the 1-hexene concentration in the reactor during the polymerization experiments could be calculated. The calibration was performed at 80°C to permit use of larger volumes of 1-hexene. Various amounts of 1-hexene ranging between 0.7-6 mL were added to the reactor then ethylene was admitted to about 100 psi. After mixing the reactor contents for a few minutes to vaporize all the 1-hexene, the reactor gas was sampled at a flow rate of about 28 mL/min. The calibration plot for the ethylene/1-hexene separation is given in Figure 3.11. The peak areas for 1-hexene in the chromatograms reflected the change in 1-hexene concentration until about 10 mole %. For higher 1-hexene concentrations, the peak areas for 1-hexene remained constant regardless of the amount of 1-hexene added to the reactor. It was likely that 1-hexene condensed in the valve or Teflon tubing leading to the GC injection port for these data points because the valve and tubing were at room temperature. When only the lower 1-hexene concentrations were plotted (Figure 3.12), there was an excellent linear relationship between mole % 1-hexene and peak area for 1-hexene in the chromatogram. The response factor for 1-hexene concentration was determined to be 4.3 from the ratio of 1-hexene peaks areas to ethylene peak areas (Figure 3.13).

3.4 Characterization Techniques

3.4.1 Nitrogen Adsorption

Nitrogen adsorption was used to determine the surface area (BET method) and pore size distribution (BJH method) for the silica support and catalyst particles (Gregg and Sing, 1982). About 100 mg sample was used for the analysis with an accurate weight determined after degassing. The samples were degassed at 350°C for several hours before collecting the adsorption and desorption isotherms.

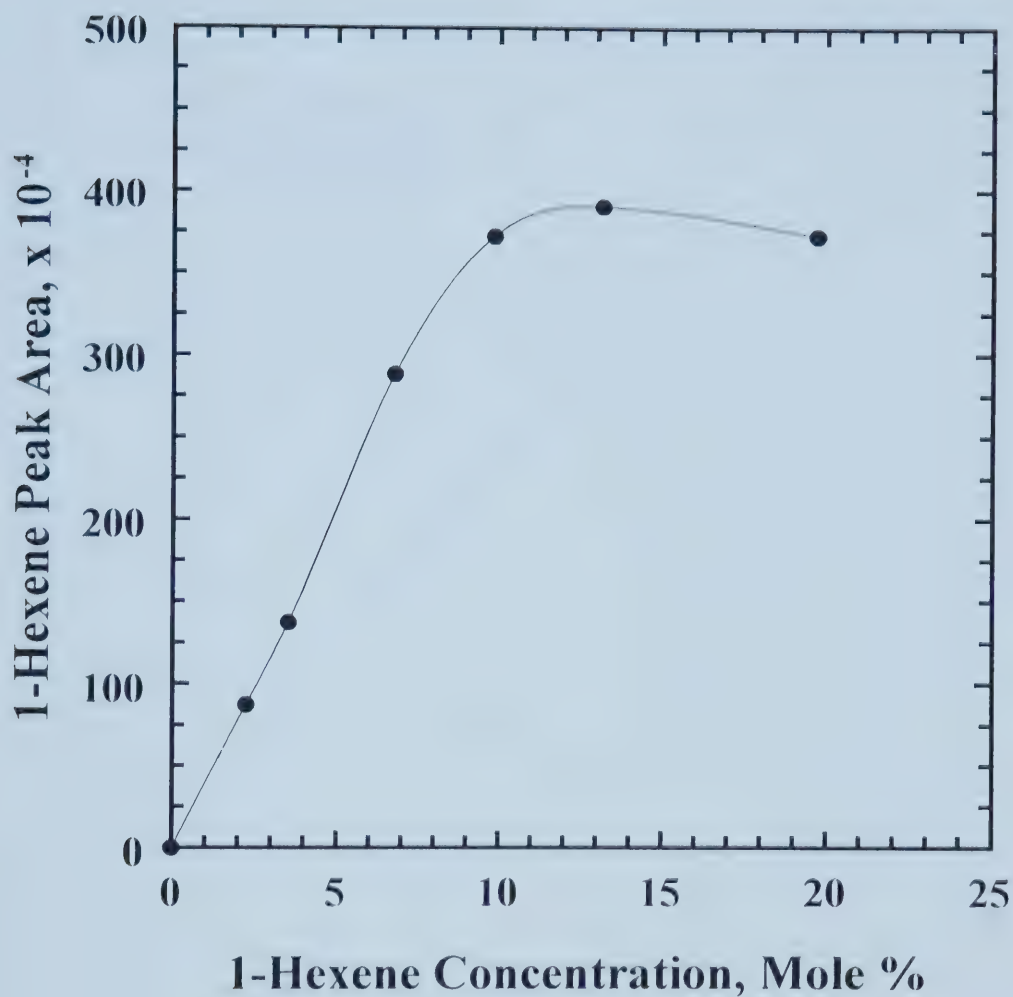


Figure 3.11. GC calibration for ethylene/1-hexene separation.

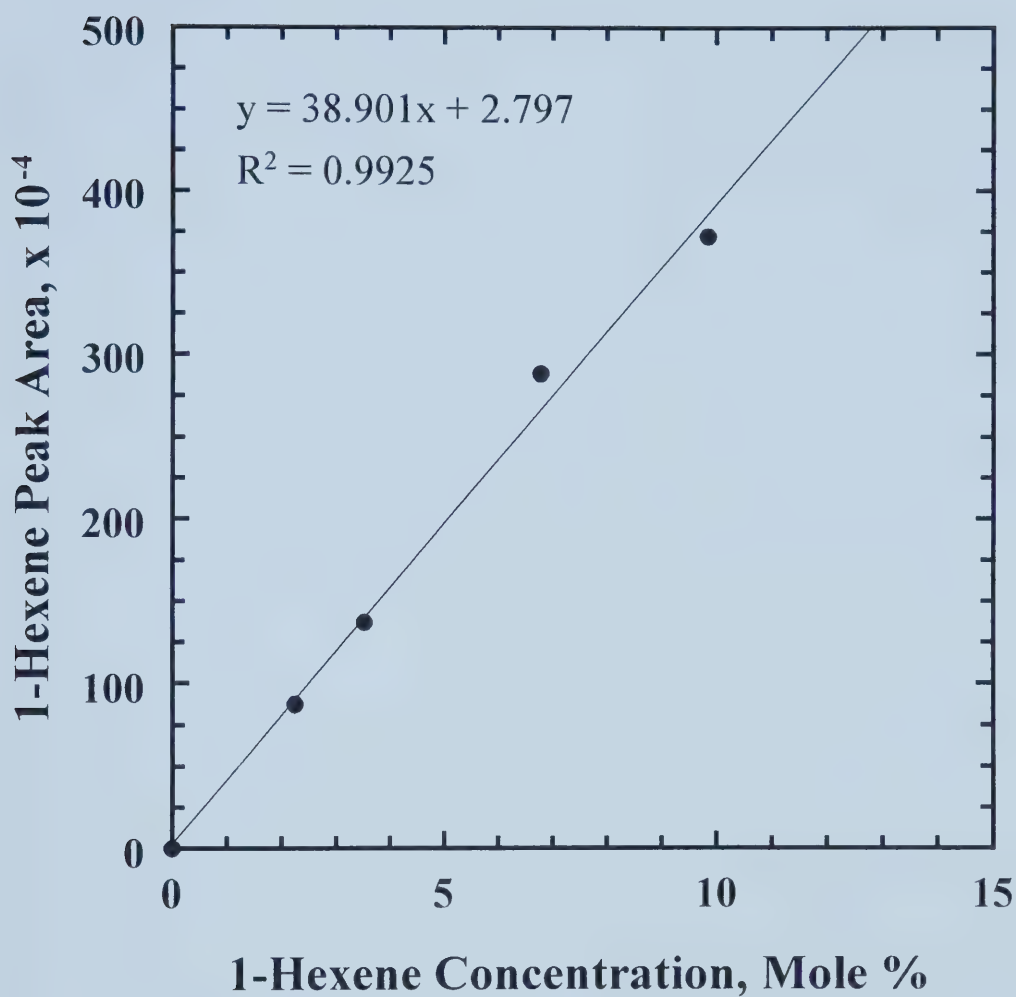


Figure 3.12. GC calibration for ethylene/1-hexene separation at low 1-hexene concentrations.

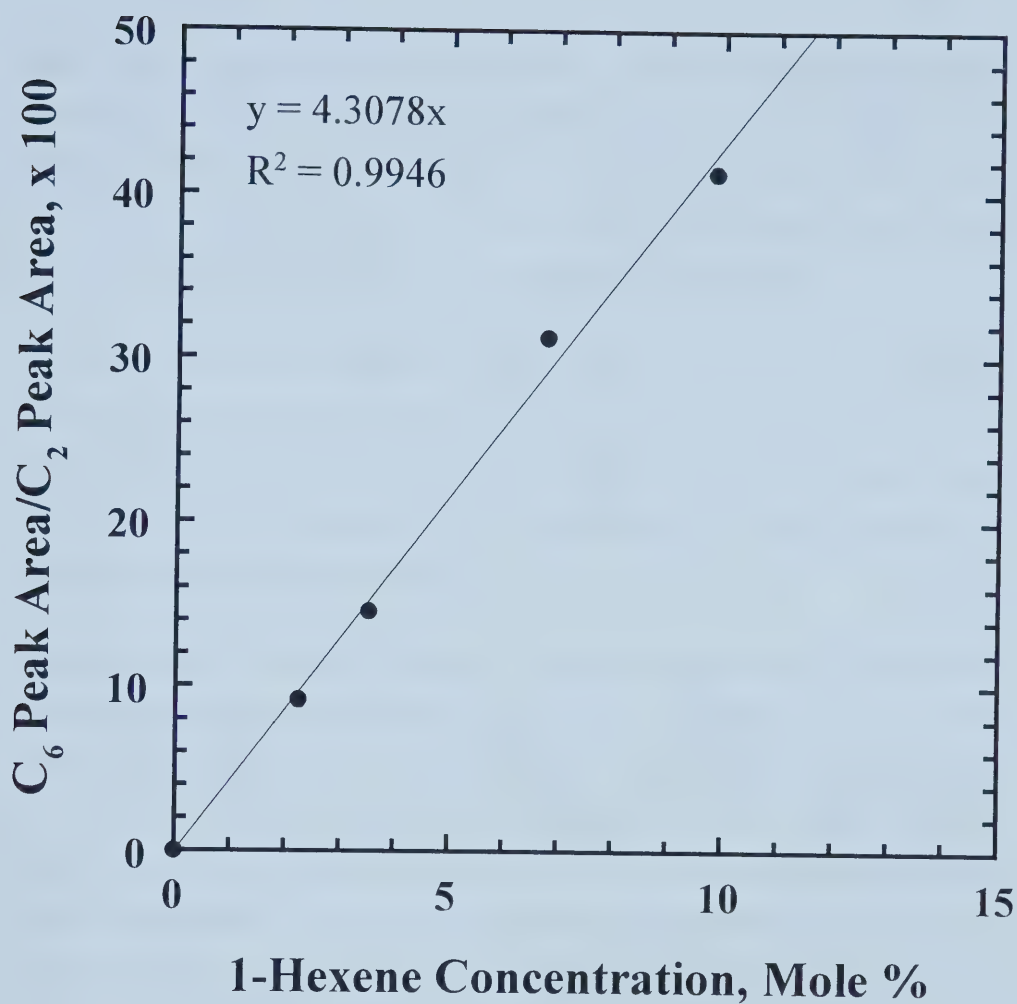


Figure 3.13. Response factor for ethylene/1-hexene separation.

3.4.2 Elemental Analysis

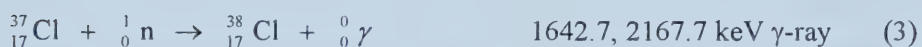
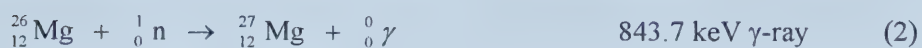
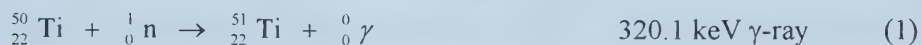
Highly active Ziegler-Natta catalysts for olefin polymerization contain titanium, magnesium, and chlorine; the active ingredients usually include transition metal halides (e.g. TiCl_4 , Ti(OR)_4) and magnesium compounds (e.g. MgCl_2 , RMgCl) (Soga and Shiono, 1997). Nowlin et al. (1988) showed that the activity and polymer properties are affected by the catalyst composition (i.e. Ti/Mg ratio).

Dr. John Duke in the SLOWPOKE Nuclear Reactor Facility at the University of Alberta determined titanium, magnesium, and chlorine contents of the polymerization catalysts with instrumental neutron activation analysis (INAA). The results proved useful in proposing explanations for the observed activity profiles, especially for different catalyst preparation conditions.

Neutron activation is a reliable and sensitive method for quantitative, multi-elemental analysis of major and trace elements (Lyon, 1964). In principle, the NAA method involves subjecting a sample to nuclear reactions then measurement of the subsequent radioactivity allows for identification and quantification of the constituent elements. Nuclear reactors are the source of neutrons for the neutron capture reactions (n,γ); a neutron collides with the target nucleus to form an excited-state nucleus, and the excited-state nucleus returns to its stable configuration through the emission of gamma radiation (Kruger, 1971). Each radioactive nucleus decays at a rate characterized by its unique half-life, and sample composition is determined from γ -ray detection.

In the INAA procedure, 11-67 mg catalyst was accurately weighed into sample vials in the glove box to prevent oxidation. Each sample was individually irradiated for 300s inside the SLOWPOKE II Nuclear Reactor at a nominal thermal neutron flux of $1 \times 10^{11} \text{ n cm}^{-2} \text{ s}^{-1}$. Upon removal from the reactor, there was a 360 second decay

period prior to γ -ray detection with the hyper-pure Ge detector. The samples were counted for 300 seconds at a sample-to-detector distance of 6 cm. The relevant neutron capture reactions with the corresponding γ -ray energies are given below with Ti, Mg, and Cl half-lives of 5.10, 9.462, and 37.24 minutes minutes, respectively.



3.4.3 Particle Size Distribution

The particle size distributions of the silica and catalyst particles were measured with the Mastersizer 2000 optical unit (Malvern Instruments, Hydro 2000SM). The instrument used a He-Ne laser and a blue LED light source to measure the scattering pattern for the particles dispersed in a water suspension. The scattering information produced a particle size distribution from the average of two scans that were calculated using a refractive index of 1.544 for silica.

3.4.4 Size Exclusion Chromatography (SEC)

The molar mass distributions of polymer samples were measured with Waters Alliance 2000 GPCV using Millennium 2000 data acquisition software. The separation was achieved with three Waters Styrag HT6E columns and a guard column. The columns and detector were enclosed in the oven, which was maintained

at 145°C. Polymer solutions were prepared with concentrations varying between 0.4-0.7 g/L, and these solutions were heated for 2 hours at 160-175°C to dissolve the polymer. The samples were eluted through the columns with 1,2,4-trichlorobenzene (HPLC Grade, Aldrich) containing 0.25 g/L of the antioxidant 2,6-di-tert-butyl-methylphenol. The solvent was pumped through the column at a rate of 1.0 cm³/min. Linear polystyrene paraffins (C₂₀, C₄₀, and C₆₀ from Fluka) and polyethylene calibration standards (1475, 1482, 1483, and 1484 from NIST) with narrow polydispersities were used to determine the molar mass distributions of the samples.

There were problems measuring molar masses for some samples. The high molar masses caused erratic pressure and flow rate variations, typically as the polymer solution entered each of the columns. Although the sharp flow deviations affected the accuracy, the results were sufficient to make relative comparisons. Because it was difficult to dissolve polymer with high molar masses, all the solutions were heated at higher temperatures (160-175°C) than usual (150-160°C), and a longer heating time was examined. Unfortunately, degradation occurred when the polymer solution was heated longer as indicated by the lower molar masses after longer heating times (Table 3.3). Subsequent polymerization experiments were performed with hydrogen to reduce the molar masses.

Table 3.3: SEC Results Comparing Heating Times.

Run ID	GPC Solution Heating Time	Averaged SEC Results		
		Mn (x 10 ⁻³)	Mw (x 10 ⁻³)	PD
AH-24-01-a	6 h	317	876	2.8
AH-24-01-b	6 h	293	898	3.1
AH-24-01-c	2 h	411	1124	2.7

a,b,c are different solutions

3.4.5 Temperature Rising Elution Fractionation (TREF)

TREF is a useful technique for assessing the extent of comonomer incorporation in polyolefins because the polymer chains are fractionated based on differences in crystallizability due to short chain branching (Kelusky et al., 1987). The TREF profile shows the short chain branching distribution for the polymer.

In brief, the custom-built TREF system consisted of a stainless steel column contained inside a programmable temperature oven (Thermotron, Model S-1.2C-B). Solvent from the reservoir was pumped through the column with a HPLC pump (DuPont Instruments, Model 860). There was a pressure transducer at the exit of the pump to monitor the pressure. The concentration of polymer in the solvent was measured with an IR detector (DuPont Instruments, Model 7850) using the $\text{CH}_2\text{-CH}_2$ stretching frequency of 2960 cm^{-1} . Several thermocouples were positioned inside the oven and IR cell to monitor the temperatures. A data acquisition program collected the temperature, IR signal, and pressure data. The TREF apparatus was fully described by Chakravarty (1993) and Lacombe (1995).

Prior to being loaded into the column, the polymer sample was crystallized onto glass beads in a controlled manner; the following procedure was used:

1. About 5-6 mg polymer was weighed into a 10-mL glass hypovial with about 1.5 g glass beads (80/100 mesh, Chromatographic Specialties), a disposable magnetic stir bar (12 x 4 mm, Fisher), and 6 mL o-xylene (Reagent Grade, Fisher).
2. The sealed hypovials were heated in a silicone oil bath at about 125°C on a heating mantle, and the solutions were stirred to completely dissolve the polymer.

3. After 2-3 hours on the heating mantle, the hypovials were fully submerged in a temperature controlled silicone oil bath. The solutions were cooled at a rate of 1.5°C/h from 125°C to -8°C without stirring. After the controlled crystallization step, the hypovials were stored in the freezer.

Once the crystallized polymer samples were prepared, they were loaded into the column for the TREF analysis. The procedure for loading the column and the TREF parameters are described below:

1. The column was removed from the oven, and the oven was cooled to 0°C. The column, which consisted of $\frac{7}{8}$ -inch stainless steel tubing and Swagelok fittings, was cleaned. A new 5 micron stainless steel filter (Swagelok) was placed on the inlet side of the column. About 0.2 g glass beads were poured into the column to cover the filter. The column was placed onto a vacuum flask to load the crystallized polymer sample. After rinsing the column with cold acetone, the solution was poured into the column. The sides of the hypovial were scraped and washed with cold acetone several times to transfer as much of the polymer as possible. The column was filled to the top with glass beads and a new 10 micron filter was placed on the outlet side.
2. The column was installed inside the oven and it was allowed to cool to 0°C over 15-20 minutes. With the oven temperature maintained at 0°C, the HPLC pump was turned on to flush residual acetone from the sample with the elution solvent. The solvent reservoir contained 1,2-dichlorobenzene (99%, Aldrich) with 1g/L of the antioxidant 2,6-di-tert-butyl-4-methylphenol (99+%, Aldrich), and the pump flow rate was 1.0 mL/min. The data acquisition program was initiated to monitor the IR signal while establishing the baseline signal. Once the IR signal stabilized, the sample was ready to start the programmed temperature rise.

3. Data acquisition was restarted for sample analysis. The programmed temperature rise (Figure 3.14) consisted of 10 minutes at 0°C, elution at a heating rate of 1°C/min until the oven temperature reached 125°C, then 5 minutes at 125°C to flush residual polymer from the column. The oven was programmed to cool to 20°C at the end of the heating phase.

The IR signal intensity, which was proportional to the concentration of polymer chains having a certain degree of short chain branching, was plotted as a function of elution temperature through the column. It was not possible to collect high quality TREF profiles for polymer samples produced without hydrogen because the molar masses were too high. The pressure readings for these samples indicated the solvent merely swelled the polymer, and the solution could not pass through the column until the temperature exceeded 100°C (see Figure 3.15). In 1,2-dichlorobenzene, all polyethylene should be eluted below about 105°C. No such difficulties with TREF profiles were encountered for polymer samples with low molar masses (Figure 3.16).

3.4.6 Scanning Electron Microscopy (SEM)

Polymer particles were examined with SEM to view particle morphology. The samples were coated in the carbon evaporator (Hitachi, HUS-4) to enable them to conduct electrons, and the imaging was performed with a Hitachi S-2700 microscope using PGT software for data acquisition. Because polymer surfaces can accumulate electrons with the use of high electron energies, a low probe voltage of 10 kV was used to reduce charging of the particles. Poor images are obtained from charged surfaces because the probing electrons are reflected. Several particles were scanned to ensure the images were representative of all particles. The SEM images were collected at various magnifications to inspect features of interest.

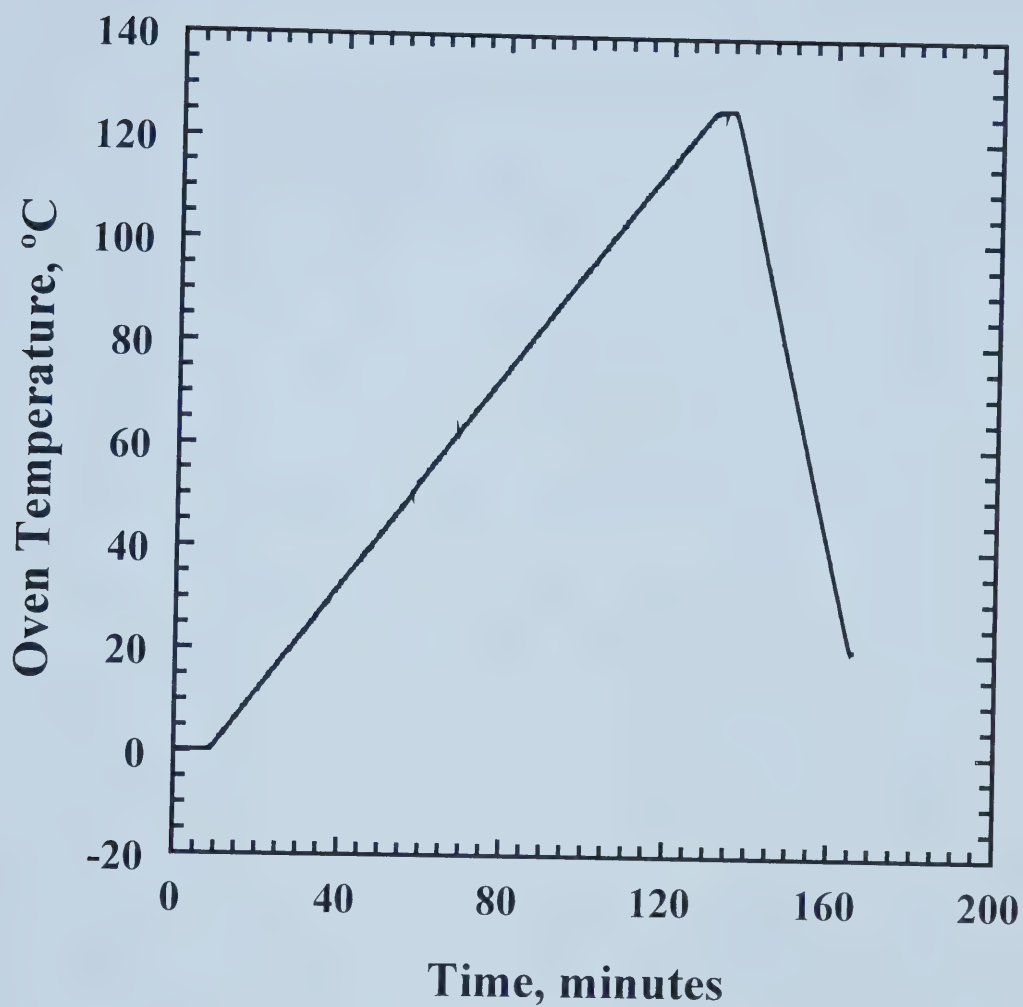


Figure 3.14. Programmed temperature cycle for TREF oven.

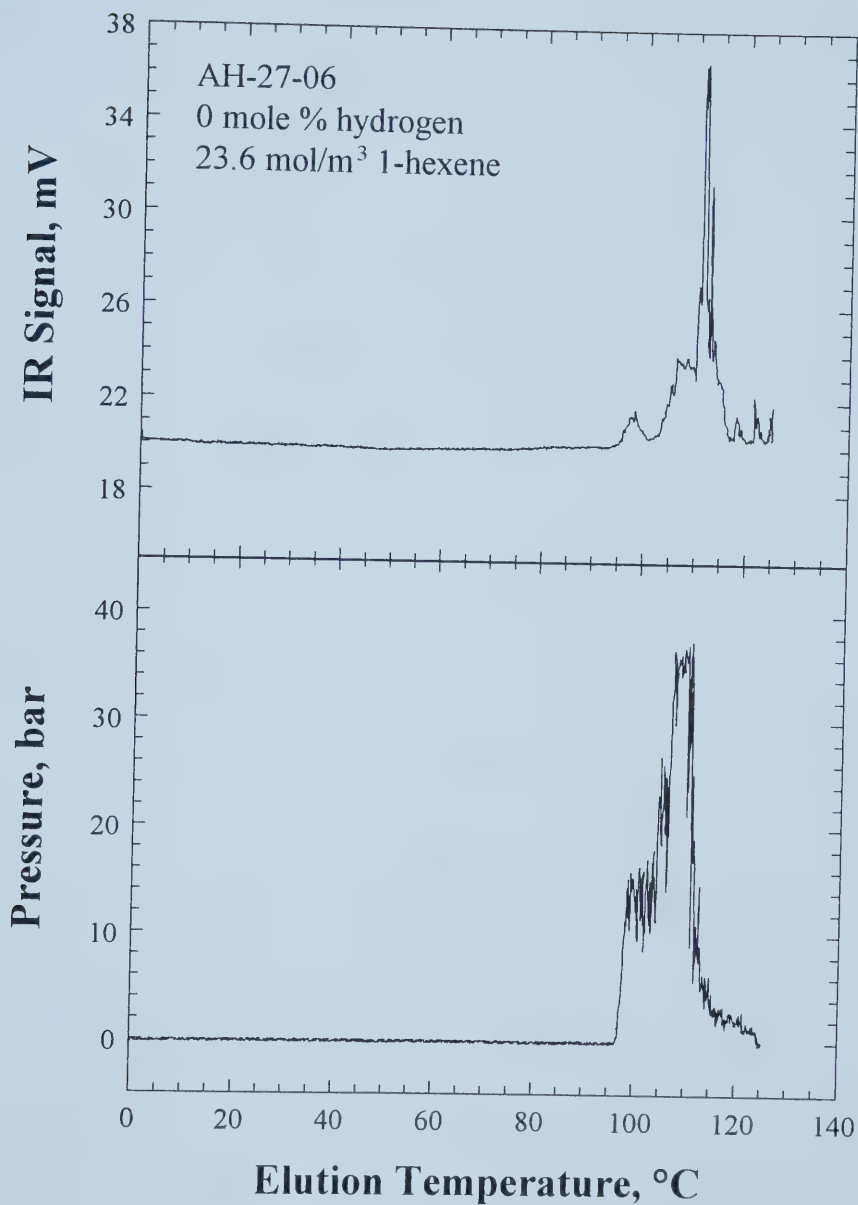


Figure 3.15. TREF profile for a polymer sample with high molar mass.

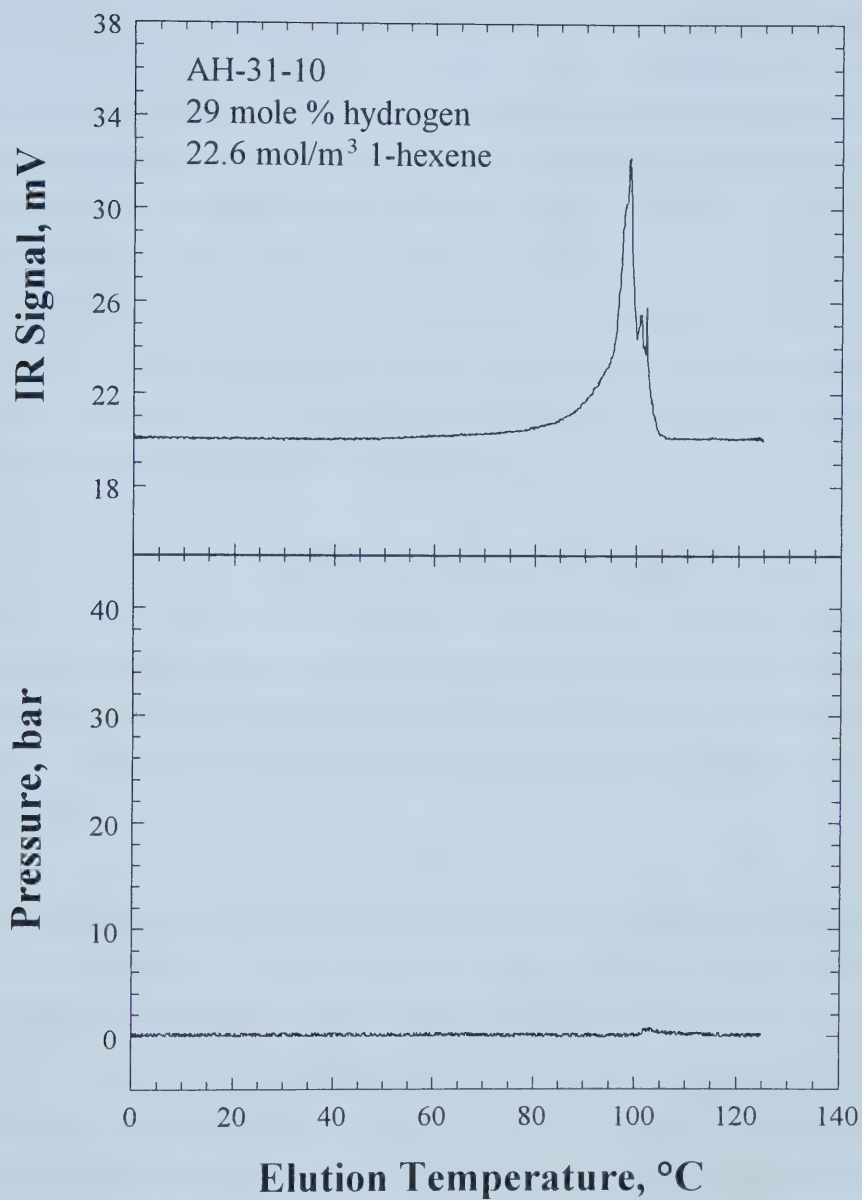


Figure 3.16. TREF profile for a polymer sample with low molar mass.

4.0 POLYMERIZATION RESULTS AND DISCUSSION

The objectives of this work were to prepare silica-supported, titanium (IV) chloride-based polymerization catalysts with the new polyphenoxide ligand tris(2,6-dihydroxyphenyl)ethene; catalyst preparation conditions were varied to attain high activity in gas-phase polymerization. Activity profiles were used to evaluate the catalyst preparation conditions under different reactor conditions, and various analytical techniques were utilized to measure polymer properties. The ethylene homopolymerization and ethylene/1-hexene copolymerization results were categorized to discuss reproducibility, catalyst preparation conditions, and reactor operating conditions such as co-catalyst concentration, temperature, pressure, hydrogen response, and comonomer concentration.

Appendix B contains the polymerization data (pressure, ethylene flow rate, and temperature profiles) for all the experiments discussed in this chapter; Table B.1 summarizes the polymerization conditions and yields. Some runs were excluded from the discussion because problems were encountered during the polymerization experiments. There were numerous experiments with catalyst injection port plugging or ethylene flow rate restrictions.

Catalyst preparation was discussed in the previous chapter, and additional details are given in Appendix A. The numbering system for the catalysts with the tris(2,6-dihydroxyphenyl)ethene ligand starts with CAT-12 because CAT-1 through CAT-11 were prepared with a different ligand. The polymerization experiments for some catalysts are not discussed because the preparation technique was deemed poor or the catalyst was exposed to air and/or moisture. The supported, magnesiated ligand was white in colour before the addition of titanium (IV) chloride; a change in colour to light brown was an indication that the catalyst precursor had been exposed to air and/or moisture.

Most of the polymerization results for CAT-14 are not discussed in this chapter because poor preparative technique was used in this first attempt at preparing the supported, bimetallic (Ti-Mg) polyphenoxide catalyst. Improvements were made in the preparation procedure for subsequent catalysts (CAT-17), specifically, the use of glassware that would reduce the likelihood of exposure to air during the drying step on the high vacuum line in the laboratory (see Appendix A). A majority of the polymerization experiments with CAT-14 were performed with neat triethylaluminum (TEA) (Aldrich) as co-catalyst, and tri-isobutylaluminum (TIBA) (neat, Aldrich) was used in the last few experiments. Although there were ethylene flow rate restrictions, the activity profile for the TEA experiment showed steady deactivation while the TIBA profile exhibited a period of activation and polymerization at a somewhat steady rate (Figure 4.1). The activity was lower with TEA likely because it is a stronger Lewis acid. From a safety perspective, it was easier to use TIBA as the co-catalyst in subsequent experiments because it is less reactive in air; residual TEA left in the syringe needle after co-catalyst injection ignited when exposed to oxygen.

Catalyst preparation was repeated for CAT-12 and CAT-15 to confirm polymerization results. Despite use of the glassware with the vacuum side arm for catalyst preparation, the polymerization results for CAT-13 (Ti/Silica) were thought to be accurate because the catalyst was not dried on the high vacuum line as long as the other catalysts (see Appendix A). CAT-16 was prepared with a functionalized polymer support, 2-hydroxyethylmethacrylate polystyrene divinylbenzene (HEMA PS-DVB), to compare its activity to the silica-supported catalyst. It was hoped the spherical PS-DVB beads would improve polymer particle morphology. The activity for CAT-16 was low compared to the silica-supported catalyst with a similar ligand loading of approximately 40 mg ligand/g support (Figure 4.2). The 2-hydroxyethylmethacrylate (HEMA) functional group was probably not suitable to chemically bind the polyphenoxide ligand.

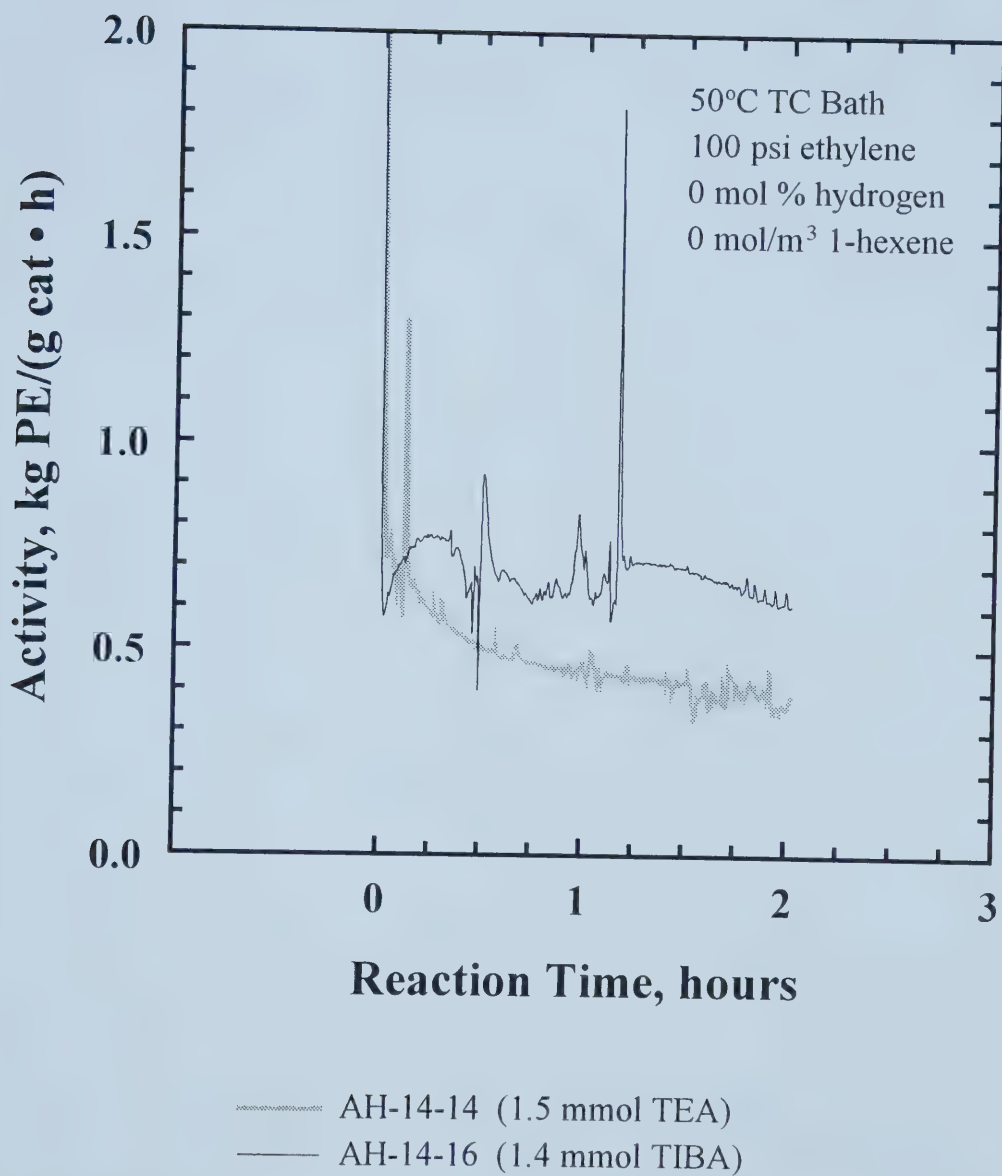


Figure 4.1. Comparison of TEA and TIBA as co-catalysts.

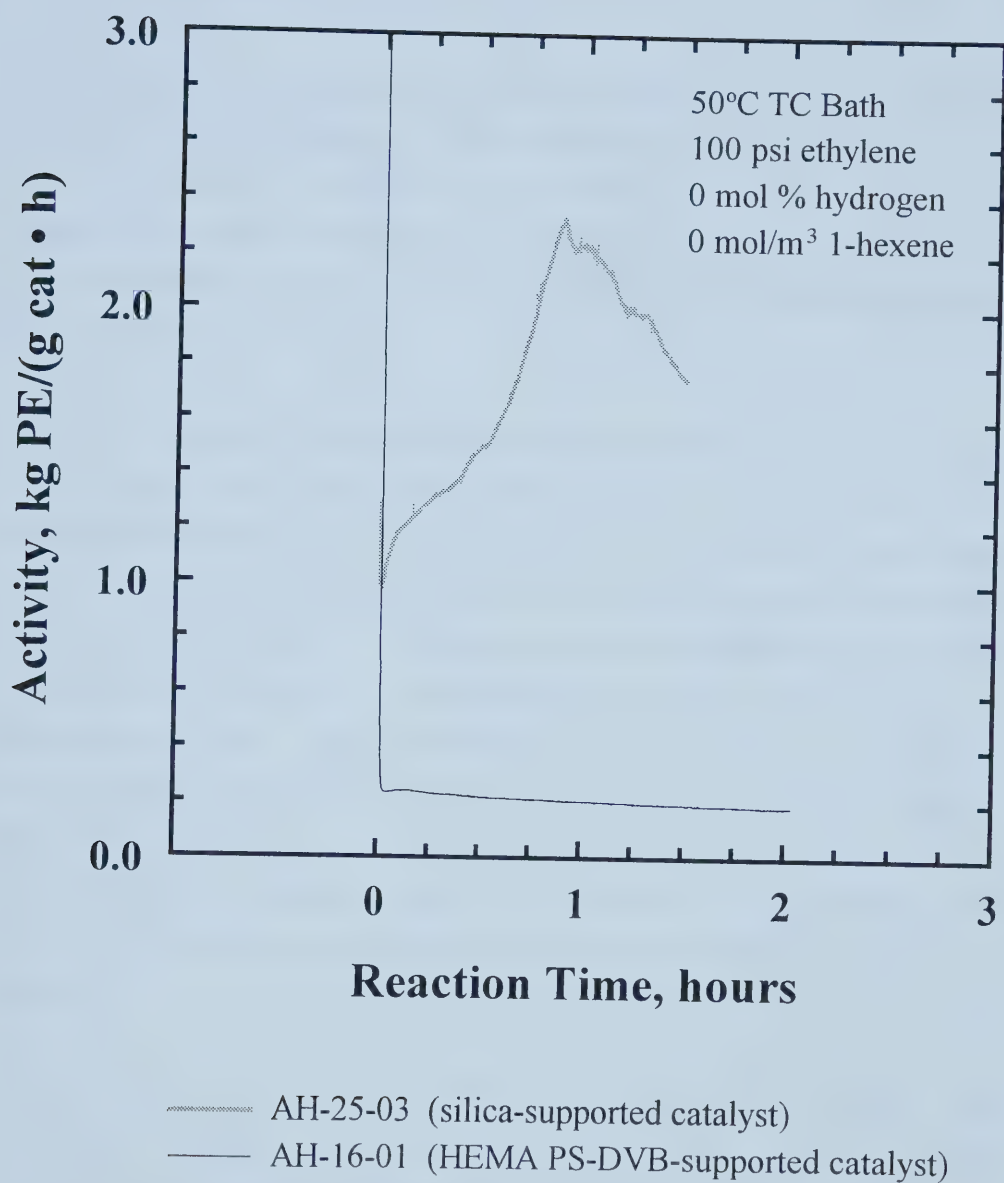


Figure 4.2. Activity profiles for silica- and HEMA PS-DVB-supported catalysts.

4.1 Reproducibility of Gas-Phase Activity Profiles

Gas-phase ethylene polymerization is known to be particularly sensitive to variations in reactor conditions (Jiang et al., 1997; McAuley et al. 1995). Three experiments (AH-32-10, AH-32-11, AH-32-12) were performed at similar polymerization conditions to assess the reproducibility of gas-phase activity profiles (Figure 4.3). Other experiments were also repeated to confirm the polymerization results were accurate (Figures 4.4 and 4.5).

About 15% variability was observed between experiments AH-32-10, AH-31-11, and AH-32-12 likely due to irreproducible catalyst injection. The catalyst injection port was usually found plugged with polymer at the end of the experiments; some catalyst particles adhered to the walls of the catalyst holder and top flange during and after injection possibly because the particles had acquired static charge from being handled in the glove box. The variation in catalyst injection was likely the main contributor to irreproducibility with a minor contribution due to co-catalyst concentration. Although reactor operation was performed consistently, it was likely not possible to achieve the same co-catalyst concentration by evacuating the reactor for a certain length of time after scavenging impurities. Consequently, there was possibly some variation in activity because slightly different amounts of co-catalyst were present in the reactor.

For the most part, the activity profiles had the same rates of activation and deactivation, as indicated by the similar shapes of the profiles. It was encouraging that the activity profiles were reproducible despite poor temperature control in some experiments (cf AH-30-02 and AH-30-06 in Figure 4.4). Overall, the observed reproducibility in activity profiles for gas-phase ethylene polymerization was good.

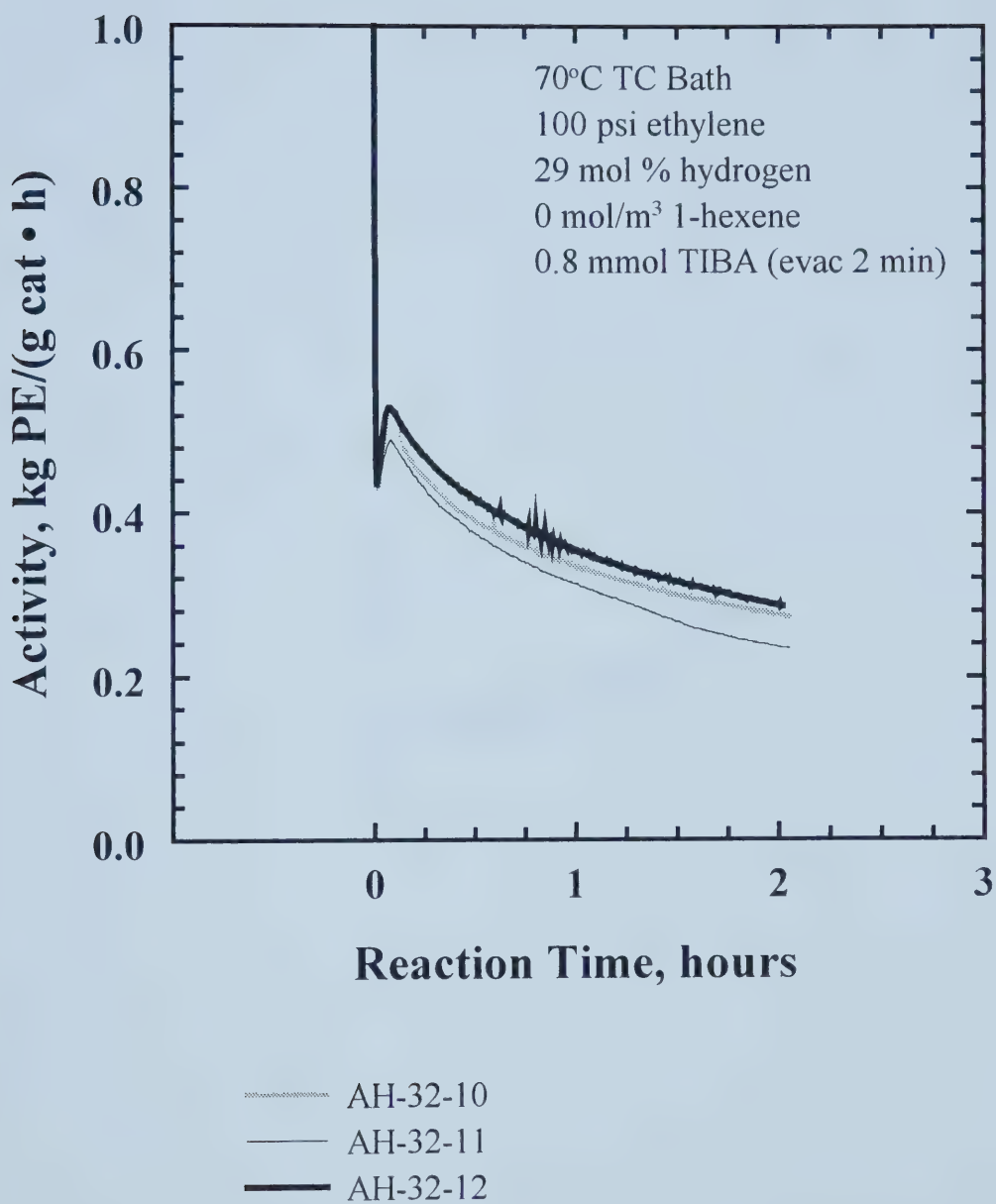


Figure 4.3. Reproducibility of gas-phase activity profiles.

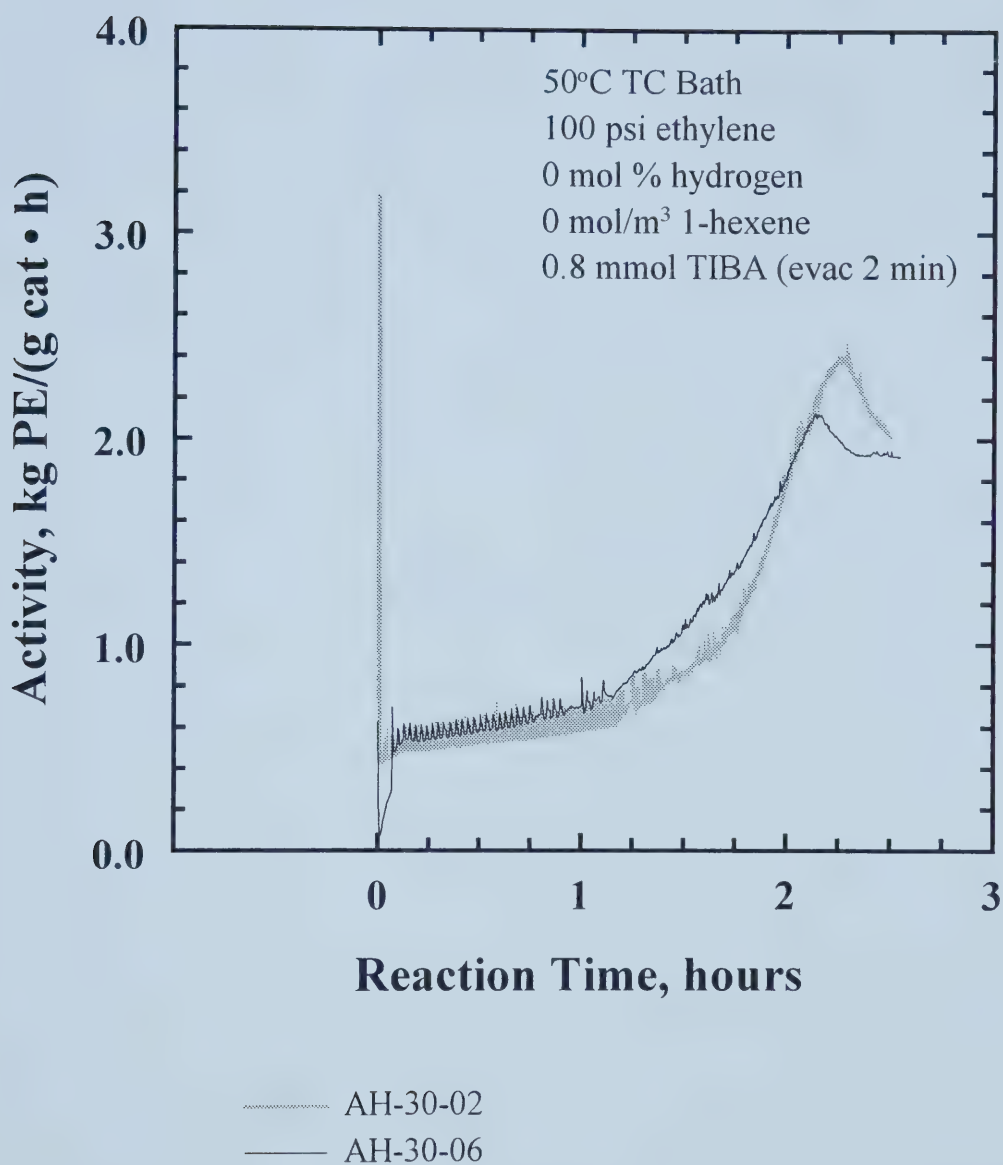


Figure 4.4. Reproducibility of gas-phase activity profiles.

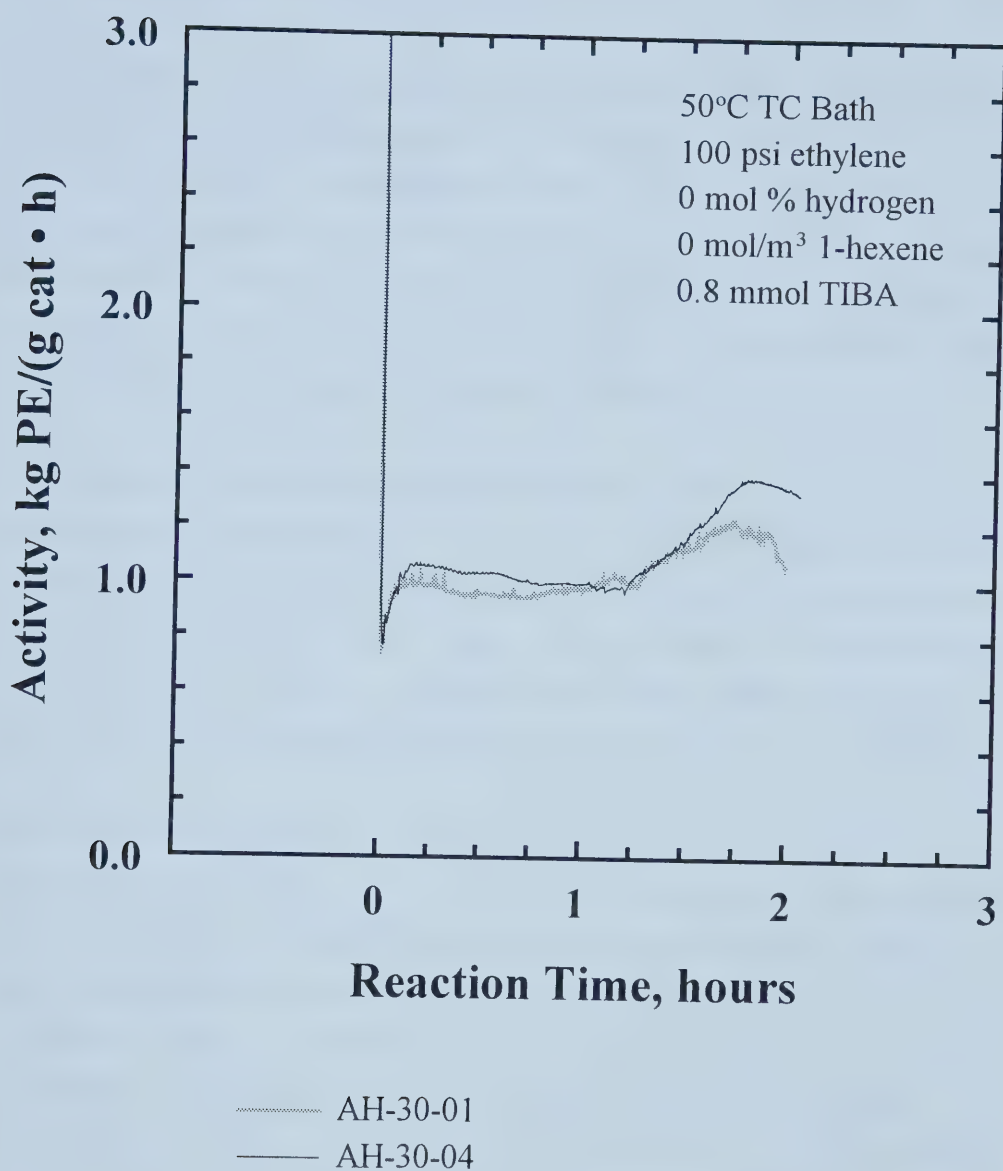


Figure 4.5. Reproducibility of gas-phase activity profiles.

4.2 Effect of Co-Catalyst Concentration on Activity

Prior to catalyst injection, aluminum alkyl (TIBA) was added to the reactor to scavenge impurities and participate as a co-catalyst. Three experiments were performed with different concentrations of TIBA. In all three experiments, 0.20 mL (0.8 mmol) neat TIBA was injected into the reactor and allowed to scavenge impurities for 15 minutes. The various TIBA concentrations were established by evacuating the reactor for different lengths of time before catalyst injection. The activity profiles for these experiments are given in Figure 4.6.

The experiment with the lowest TIBA concentration (AH-25-05) had the lowest average activity. A higher maximum activity was obtained in the experiment with an intermediate TIBA concentration (AH-25-04), but there was a long induction period before this maximum activity was reached. When the entire 0.8 mmol TIBA was kept in the reactor (AH-25-03), the activity was initially higher than that for an intermediate TIBA concentration; however, a lower maximum activity was attained.

The shape of activity profiles is affected by reaction mechanisms for activation and deactivation (Wells and Ray, 2001). The TIBA concentration affected the magnitude of the initial activity indicating TIBA was needed as a co-catalyst to activate the catalytic sites for polymerization. Higher TIBA concentrations promoted activation of more sites at the start of polymerization to give higher initial activities. Because the gas-phase temperature did not remain constant throughout the experiments, it is not possible to speculate on the effect TIBA concentration had on activity at longer reaction times because the shape of the activity profiles could be a result of the elevated gas-phase temperatures. Figure 4.7 shows the large excursions and variations in the gas-phase temperatures at different locations within the reactor for the three experiments with different TIBA concentrations.

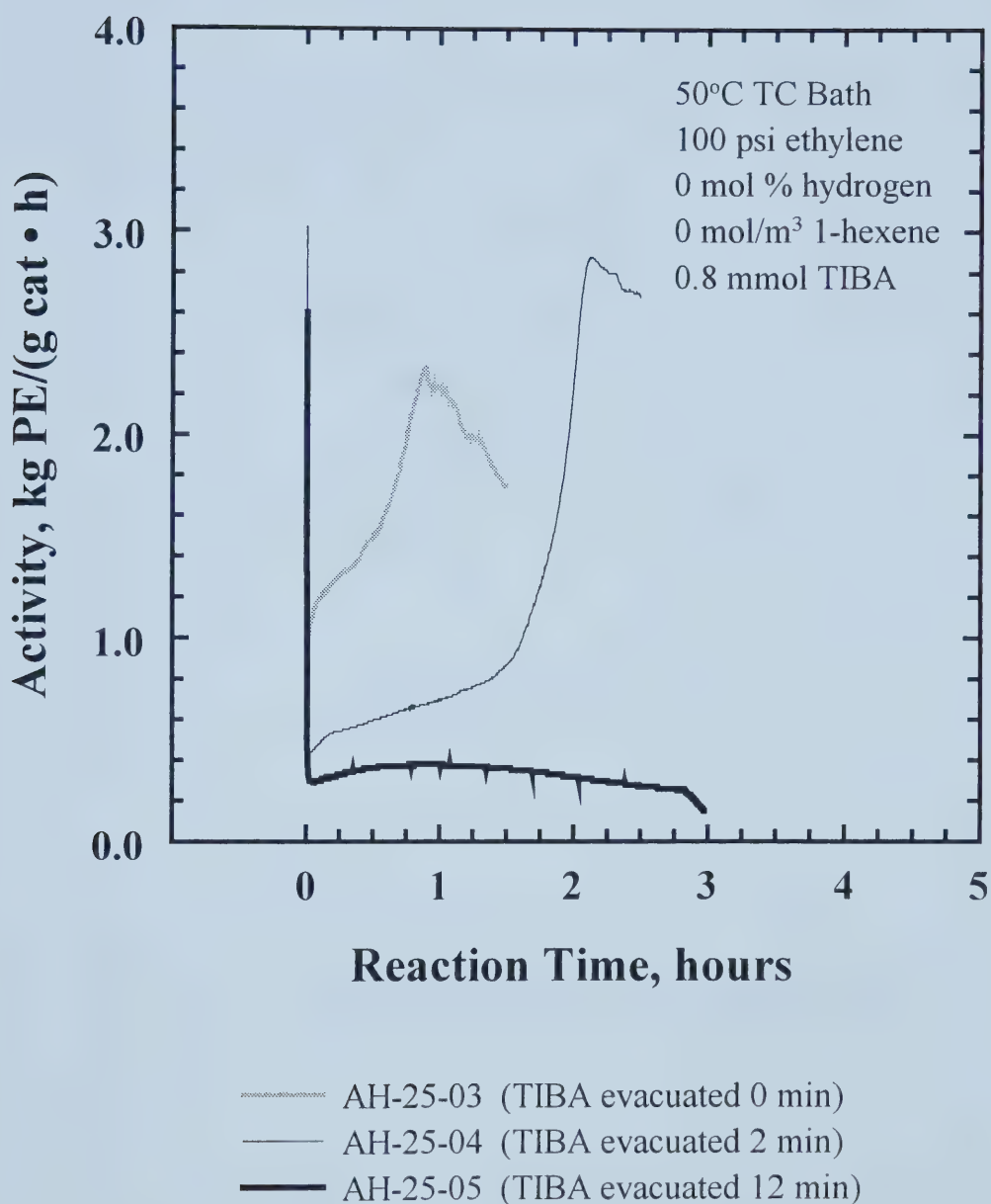


Figure 4.6. Activity profiles for different TIBA concentrations.

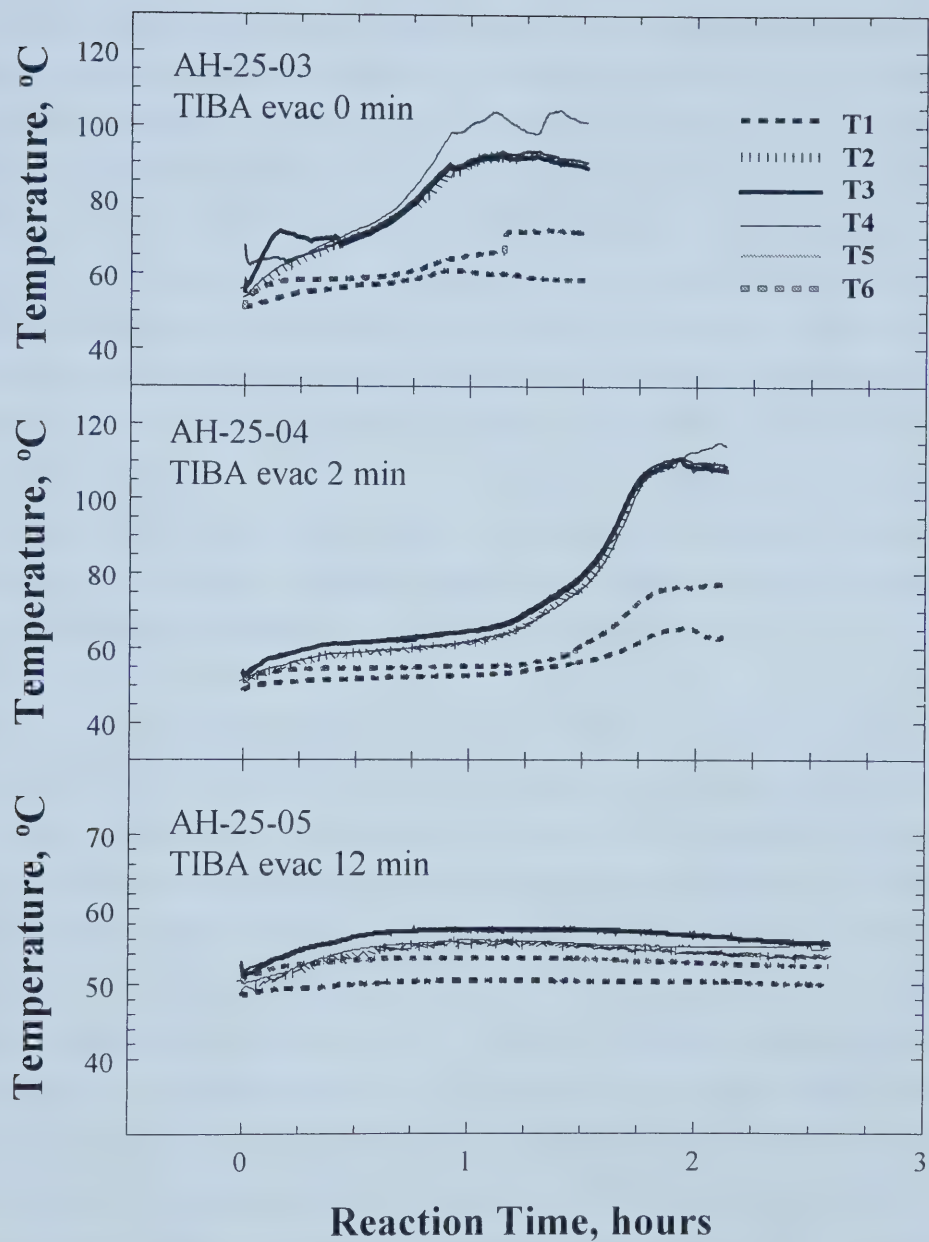


Figure 4.7. Temperature profiles for different TIBA concentrations.

4.3 Activity Profiles for Different Catalysts

Four silica-supported catalysts were prepared under similar conditions with different combinations of the constituent components. The silica-supported catalysts include: (1) Ti/Mg/Ligand/Silica (CAT-25); (2) Ti/Mg/Silica (CAT-33); (3) Ti/Silica (CAT-13); and (4) Ti/Ligand/Silica (CAT-26). Figure 4.8 gives the activity profiles for ethylene homopolymerization with the different catalysts. It can be seen that magnesium was necessary to attain high activity with the polyphenoxide ligand (cf Ti/Mg/Ligand/Silica to Ti/Ligand/Silica). The Ti/Mg/Silica catalyst, which was a Ti-Mg silyloxy complex prepared by incorporation of magnesium onto silica with a Grignard reagent and subsequent addition of titanium (IV) chloride, was expected to have high activity, but overall, the bimetallic polyphenoxide catalyst (Ti/Mg/Ligand/Silica) had a much higher activity than this conventional Ziegler-Natta catalyst. In addition, the activity profile for the Ti-Mg polyphenoxide catalyst had an unusual shape possibly due to elevated gas-phase temperatures.

Initially, it was thought the higher activity of the Ti-Mg polyphenoxide catalyst as compared to the Ti-Mg silica catalyst could be due to the presence of more active sites because there are more hydroxyl groups. However, the concentration of ligand hydroxyl groups is small compared to the concentration of surface silanols. For silica dehydroxylated at 500°C, the concentration of surface silanols is about 2 OH/nm² (Ullmann's Encyclopedia of Industrial Chemistry, 1993). Consequently, silica with a surface area of 300 m²/g has about 6×10²⁰ mol OH/g whereas the polyphenoxide ligand would only contribute about 3.4×10⁻⁴ mol OH/g for a ligand loading of 40 mg/g. As a result, ligand functionality could be controlling catalyst behaviour during polymerization. The propagation rates for magnesium aryloxy sites and magnesium silyloxy sites could be substantially different. Polymer properties will give indications whether the activity was the result of ligand functionality or surface modification of silica.

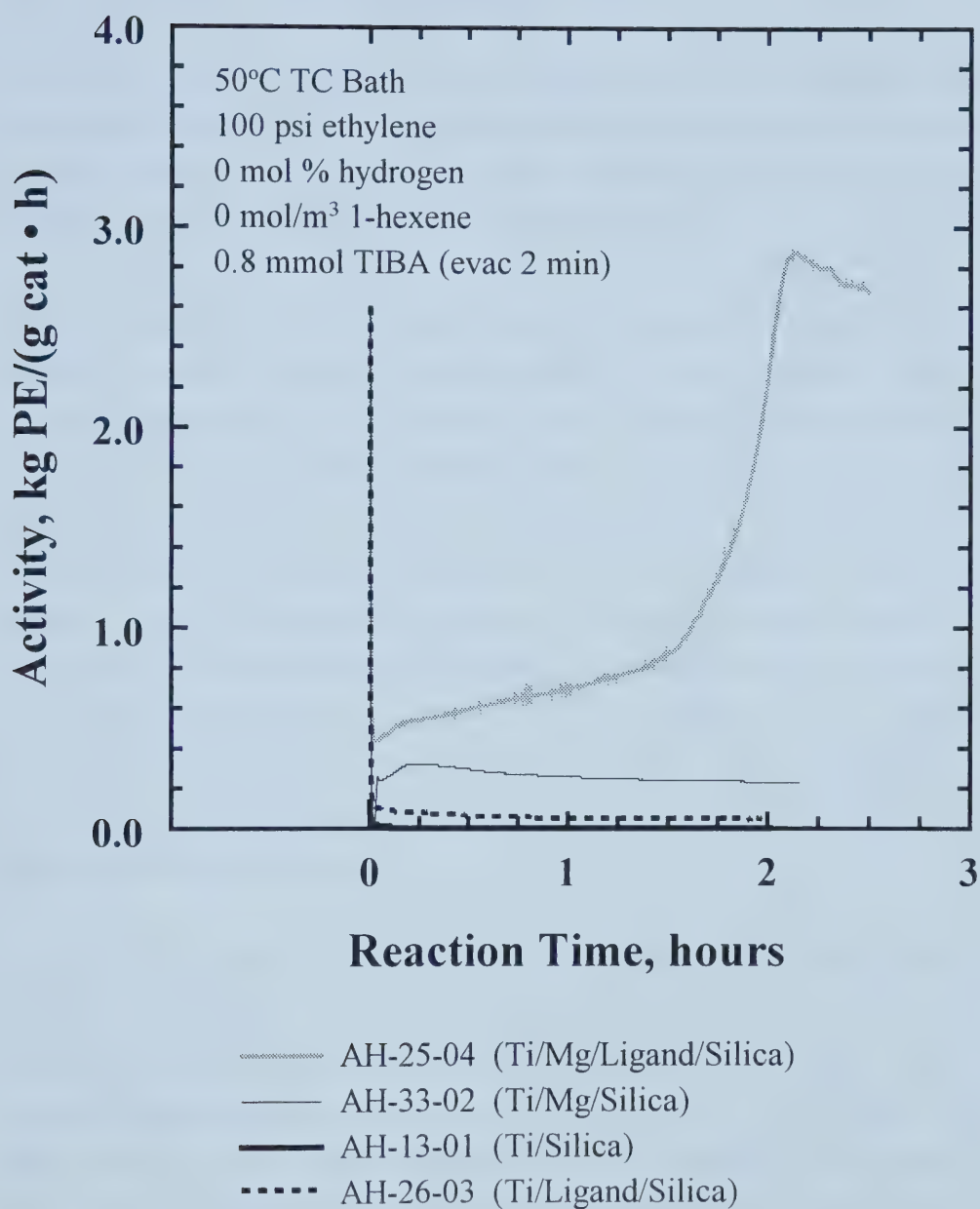


Figure 4.8. Activity profiles for different catalysts.

4.4 Effect of Titanium Addition Method on Activity

The final step in catalyst preparation was the addition of titanium (IV) chloride, and this was done using the slurry or vapour deposition methods. The effectiveness of the addition methods in producing active catalysts was evaluated for both ethylene homopolymerization and ethylene/1-hexene copolymerization.

The activity profiles in Figure 4.9 show the effect of titanium (IV) chloride addition method on activity for ethylene homopolymerization. The two catalysts prepared with the slurry method (CAT-17 and CAT-22) had much lower activities than those prepared by the vapour deposition method (CAT-19 and CAT-20). This result was unusual because the patent literature for commercial catalysts (Pullukat and Hoff, 1999) reported use of the slurry method to prepare very active catalysts; however, the difference could be the result of heating the commercial catalysts above room temperature. It is also possible that the Ti-Mg polyphenoxide complex is only active for a short period of time in solution. Fujita (2001) prepared Ti-Mg aryloxide complexes in situ prior to the introduction of ethylene in solution polymerization experiments; the activity varied with the mixing time for titanium (IV) chloride and the magnesium aryloxide complexes.

Longer contact times for vapour deposition produced a more active catalyst (CAT-20). Qualitatively, the addition of titanium (IV) chloride produced a colour change in the supported catalyst precursor. The magnesium polyphenoxide complex was white when supported on silica, whereas the Ti-Mg polyphenoxide complex was orange-brown in colour; a deeper shade of brown was obtained for longer contact times. Diffusion limitations or slow reaction could explain the lower activities for the shorter contact time (CAT-19). The same trends were observed for ethylene/1-hexene copolymerization (Figure 4.10). Given these results, subsequent catalysts were prepared using the vapour deposition method with long contact times.

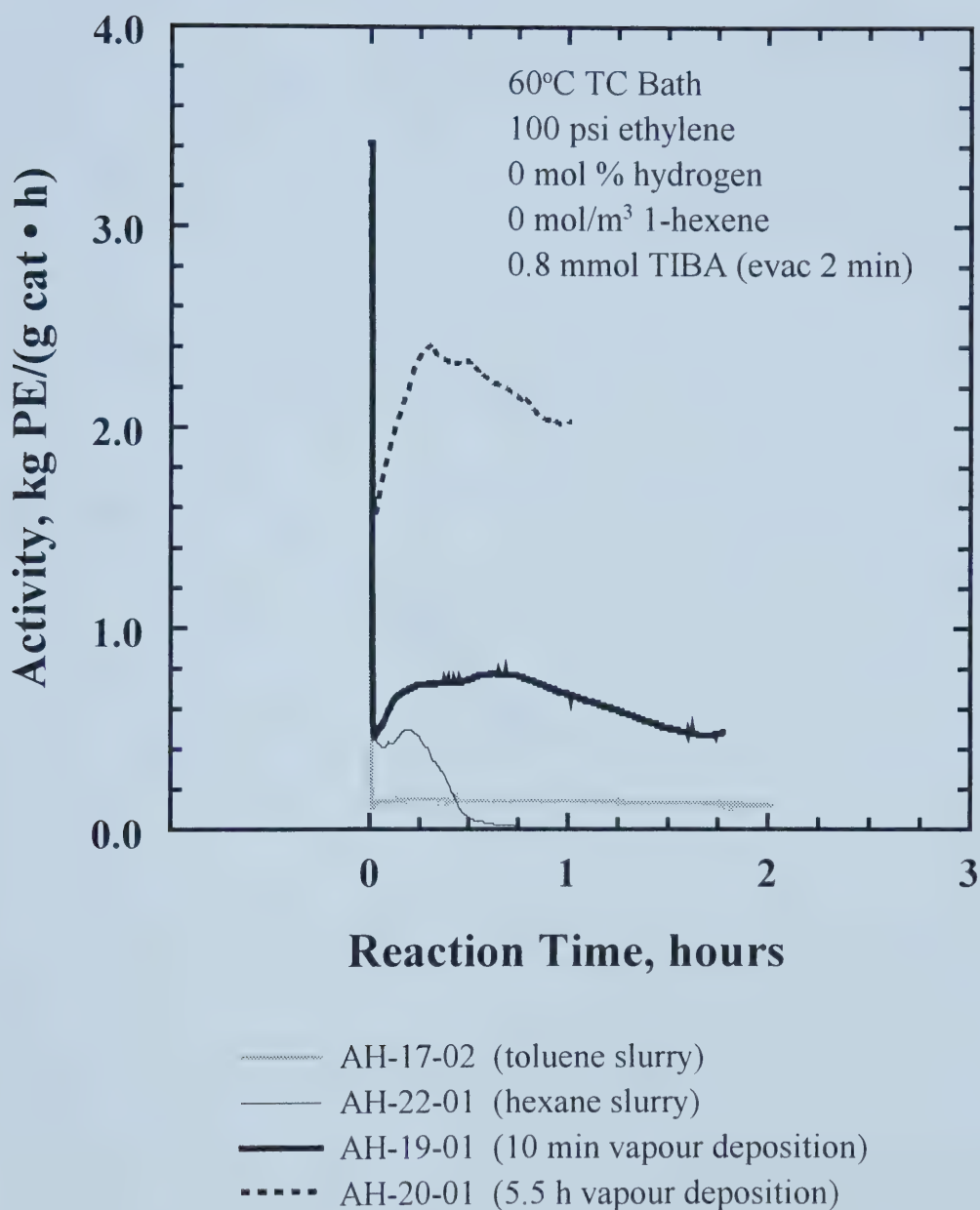


Figure 4.9. Activity profiles for ethylene homopolymerization comparing methods of titanium (IV) chloride addition.

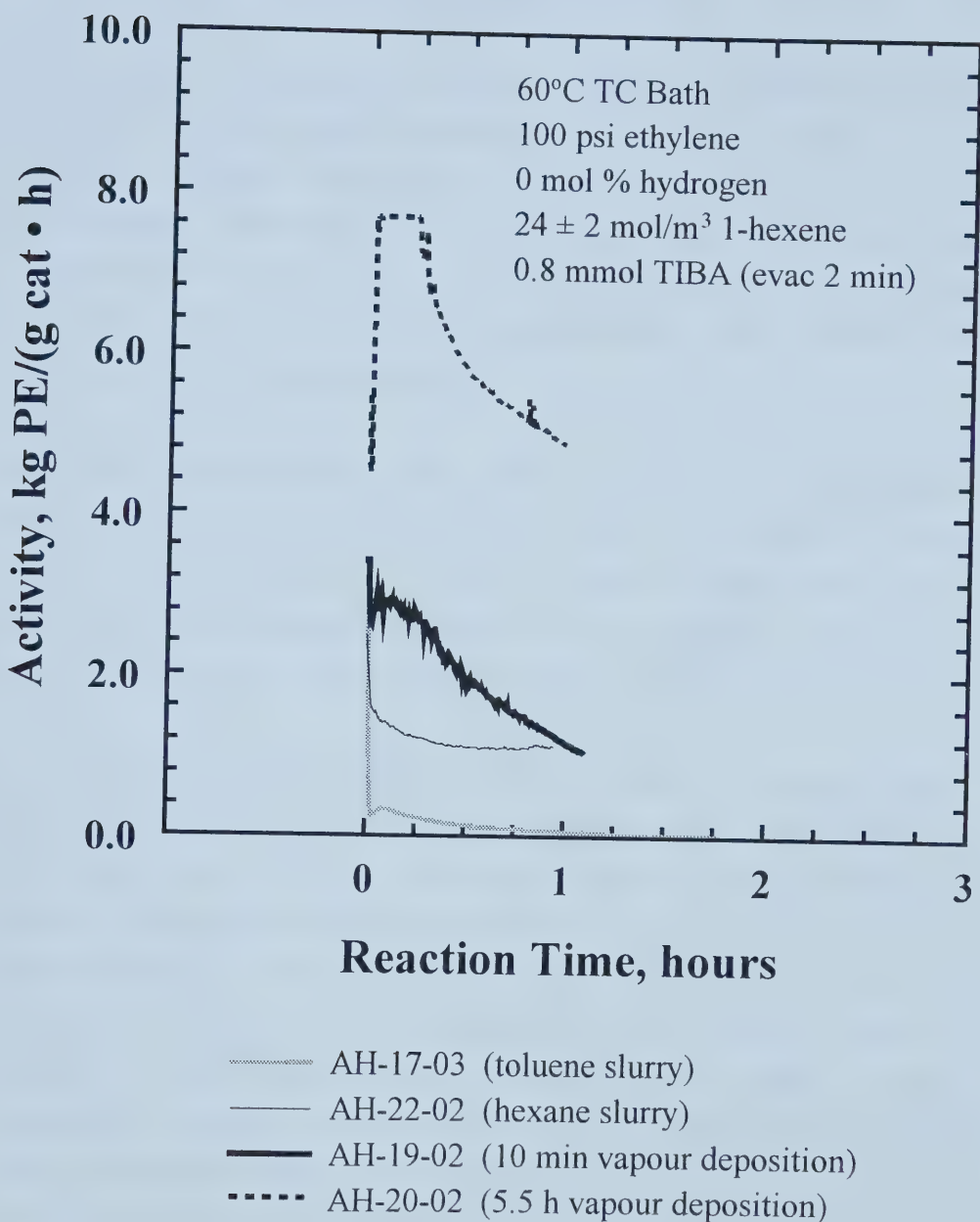


Figure 4.10. Activity profiles for ethylene/1-hexene copolymerization comparing methods of titanium (IV) chloride addition.

4.5 Effect of Catalyst Drying Temperature on Activity

Prior to addition of titanium (IV) chloride, the magnesiated catalyst precursor was dried under vacuum to remove uncoordinated THF because it would deactivate titanium (IV) chloride. Various drying temperatures were examined to observe the effect on activity, and three sets of experiments were performed to determine whether a trend existed in the activity profiles. The activity profiles in Figures 4.11, 4.12, and 4.13 were collected for ethylene homopolymerization with different TIBA concentrations and TC bath temperatures.

Examination of the three sets of activity profiles revealed that there were differences in the magnitude of the initial activity and/or variations in the induction periods before the maximum activity was attained. Overall, the catalyst dried at 90°C (CAT-27) had the lowest activity and the activity profiles were fairly flat for all three sets of reactor conditions. There was no discernable trend for the other catalysts.

It was thought the gas-phase temperature affected the activity and induction period. Polymer sheets formed on the reactor walls reducing the heat transfer efficiency to the circulating silicone oil bath so the gas-phase temperature slowly increased with time, and consequently, the activity also increased. Examination of the temperature profiles revealed the rapid increase in activity occurred when the gas-phase temperature reached about 70°C. Because isothermal reactor conditions could not be maintained, it was difficult to make conclusions about the effect of drying temperature on activity. The polymer samples were not analyzed because the high molar masses caused erratic pressure and flow rate variations in the SEC analysis. An optimal drying temperature may exist because there were differences in the initial activity when the gas-phase temperatures were similar for all catalysts.

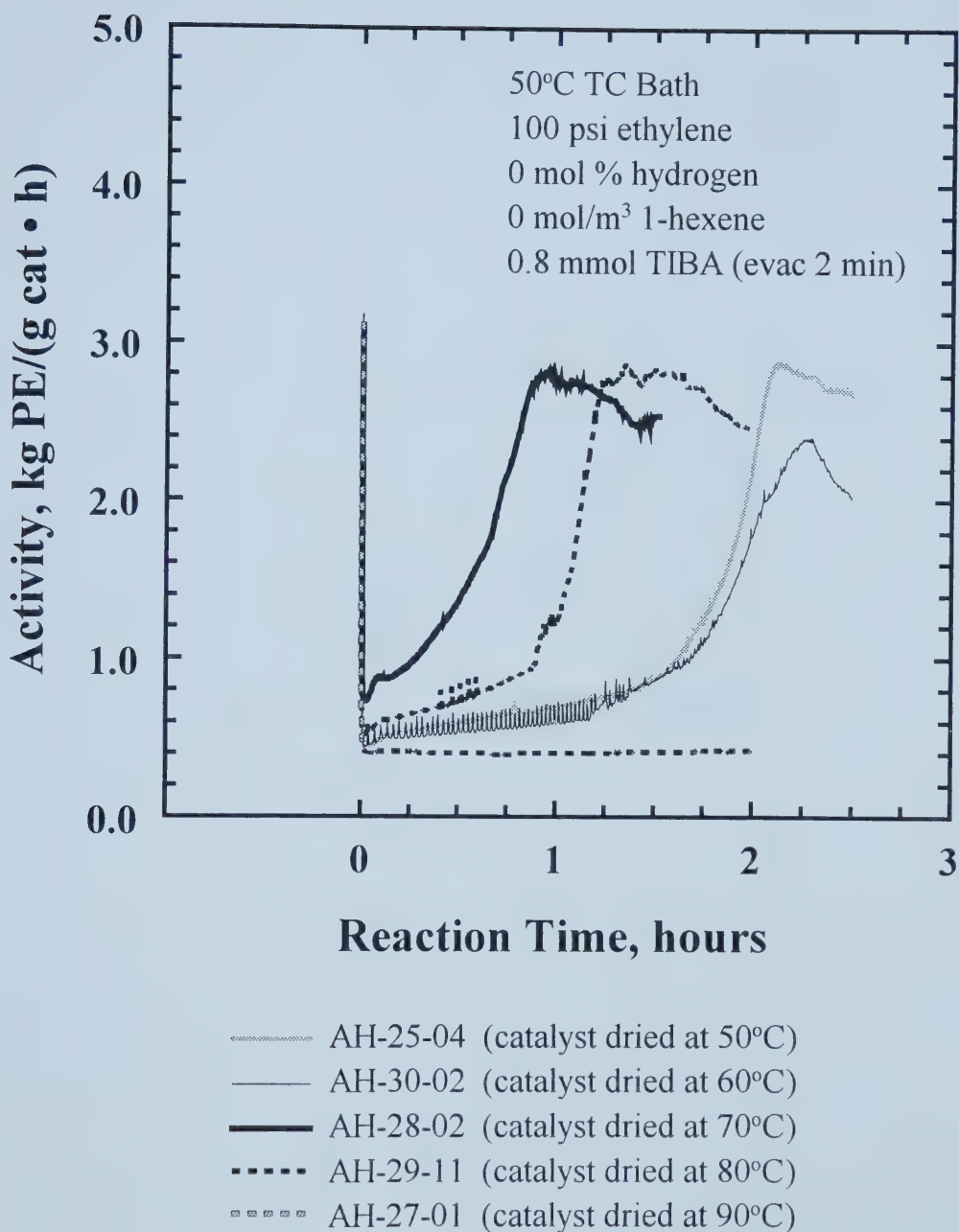


Figure 4.11. Activity profiles comparing catalyst drying temperatures (50°C TC Bath, TIBA evacuated).

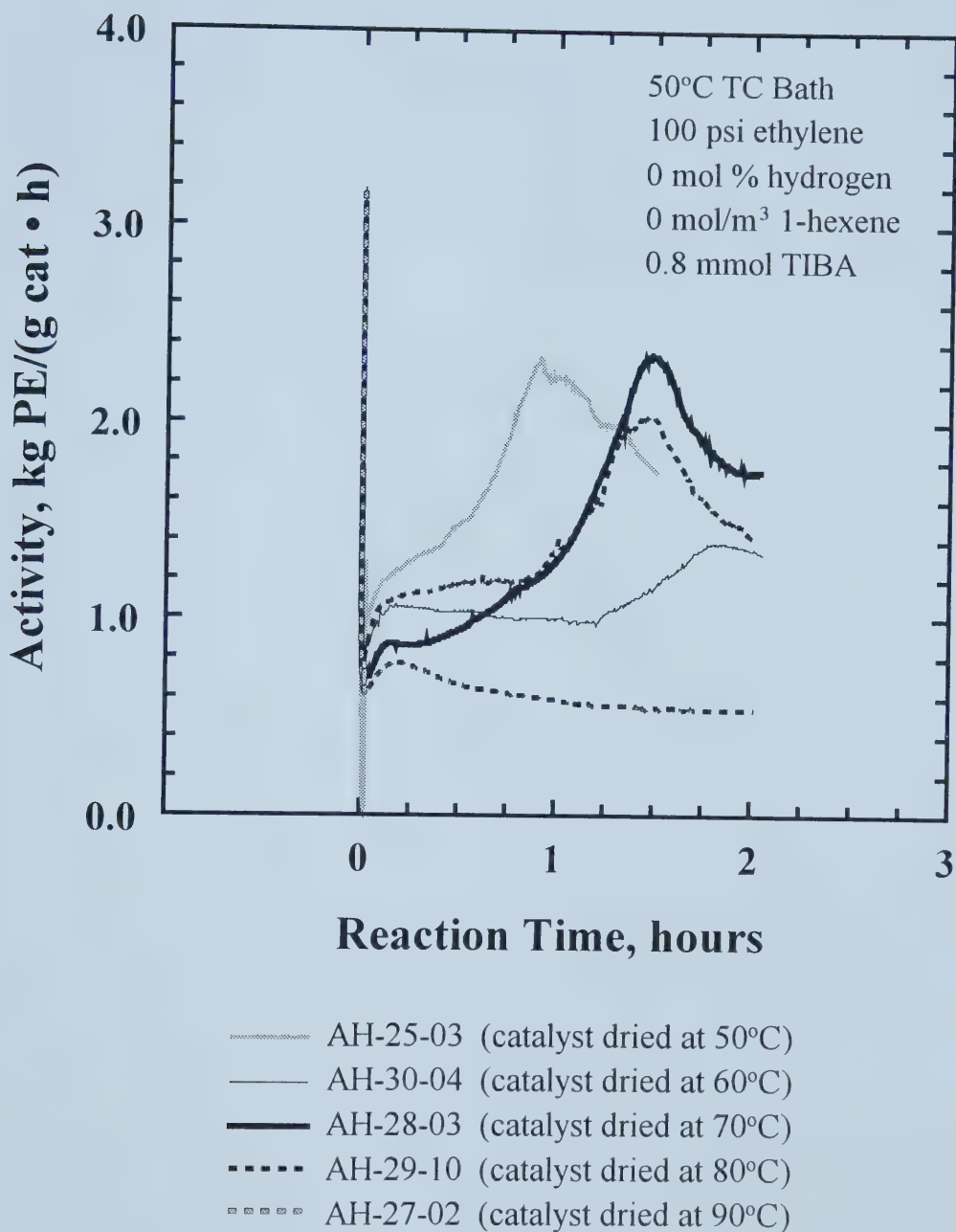


Figure 4.12. Activity profiles comparing catalyst drying temperatures (50°C TC Bath, TIBA kept in reactor).

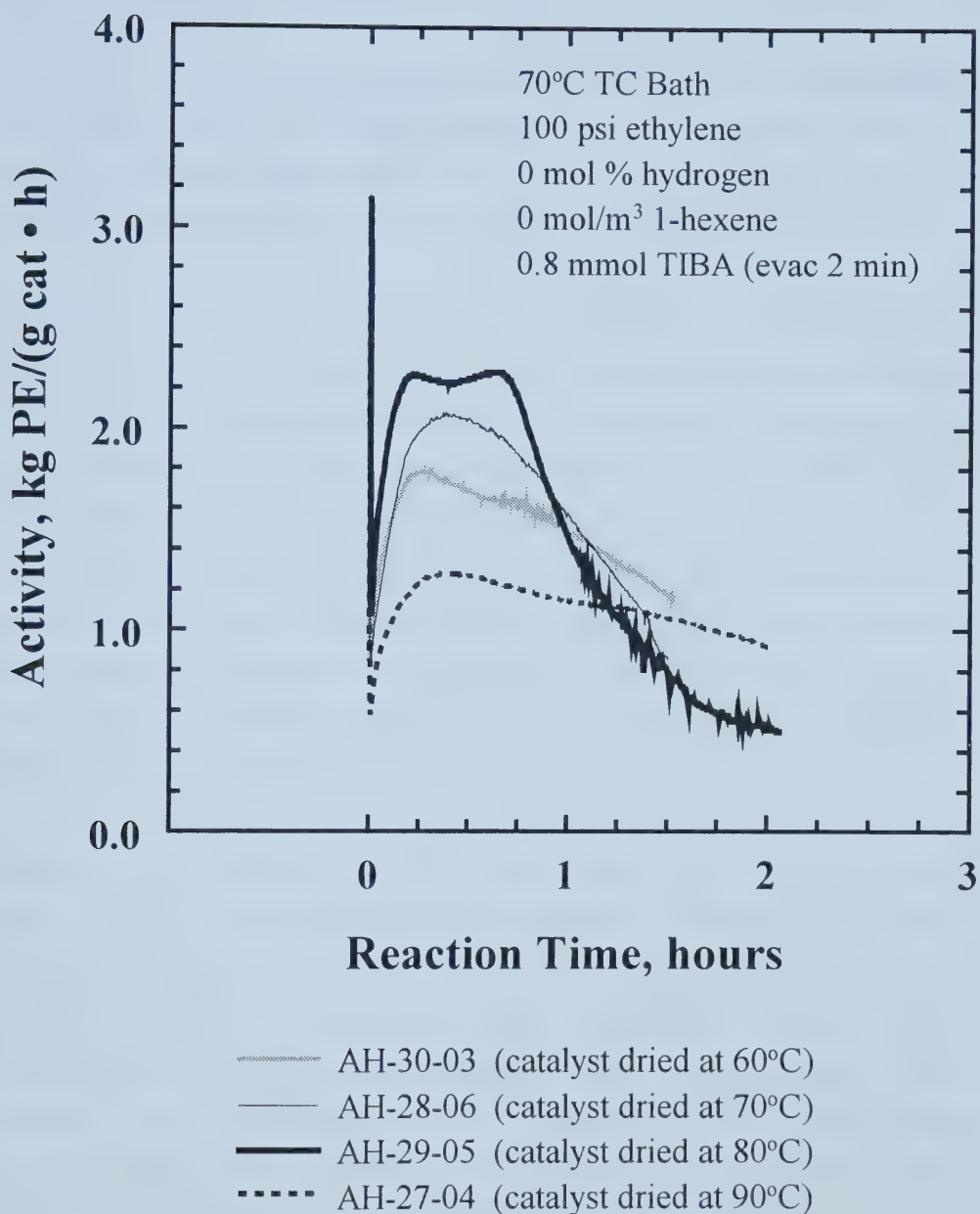


Figure 4.13. Activity profiles comparing catalyst drying temperatures (70°C TC Bath, TIBA evacuated).

4.6 Effect of Ethylene Pressure on Activity

Most of the polymerization experiments were performed with 100 psi ethylene because the focus was to evaluate catalyst preparation conditions under similar reactor conditions. Higher pressures were used in several experiments (AH-20-04, AH-27-03, and AH-30-08) to examine the effect of ethylene pressure on activity.

In AH-20-04, the ethylene pressure was increased from 100 psi to 200 psi in the middle of the experiment (Figure 4.14). Before the ethylene pressure was changed, the activity profile showed slow deactivation and the gas-phase temperatures were slowly decreasing. The activity approximately doubled when the ethylene pressure was doubled, but the change in activity cannot be solely attributed to the increase in ethylene pressure because there was a 25°C temperature rise that accompanied the pressure set point change. The polymerization activity exhibits Arrhenius behaviour with changes in temperature; an increase in activity results from an increase in temperature. It would be necessary to maintain isothermal reactor conditions to determine the effect of ethylene pressure on activity.

Because the activity profiles for CAT-27 were relatively flat in contrast to the other catalysts at a TC bath temperature of 50°C (Figures 4.11 and 4.12), an additional experiment (AH-27-03) was performed at 200 psi to determine whether the same behaviour persisted at a higher ethylene pressure. There was a dramatic increase in activity (Figure 4.15) and gas-phase temperatures (Figure 4.16) at the higher ethylene pressure. Figure 4.17 compares the activity profiles for CAT-27 at two TC bath temperatures; the activity was higher at the higher reactor temperature. Similar results were obtained for CAT-30 (Figures 4.18, 4.19, and 4.20). The effect of ethylene pressure on activity could not be determined because it was not possible to control reactor temperature at the high polymerization rates.

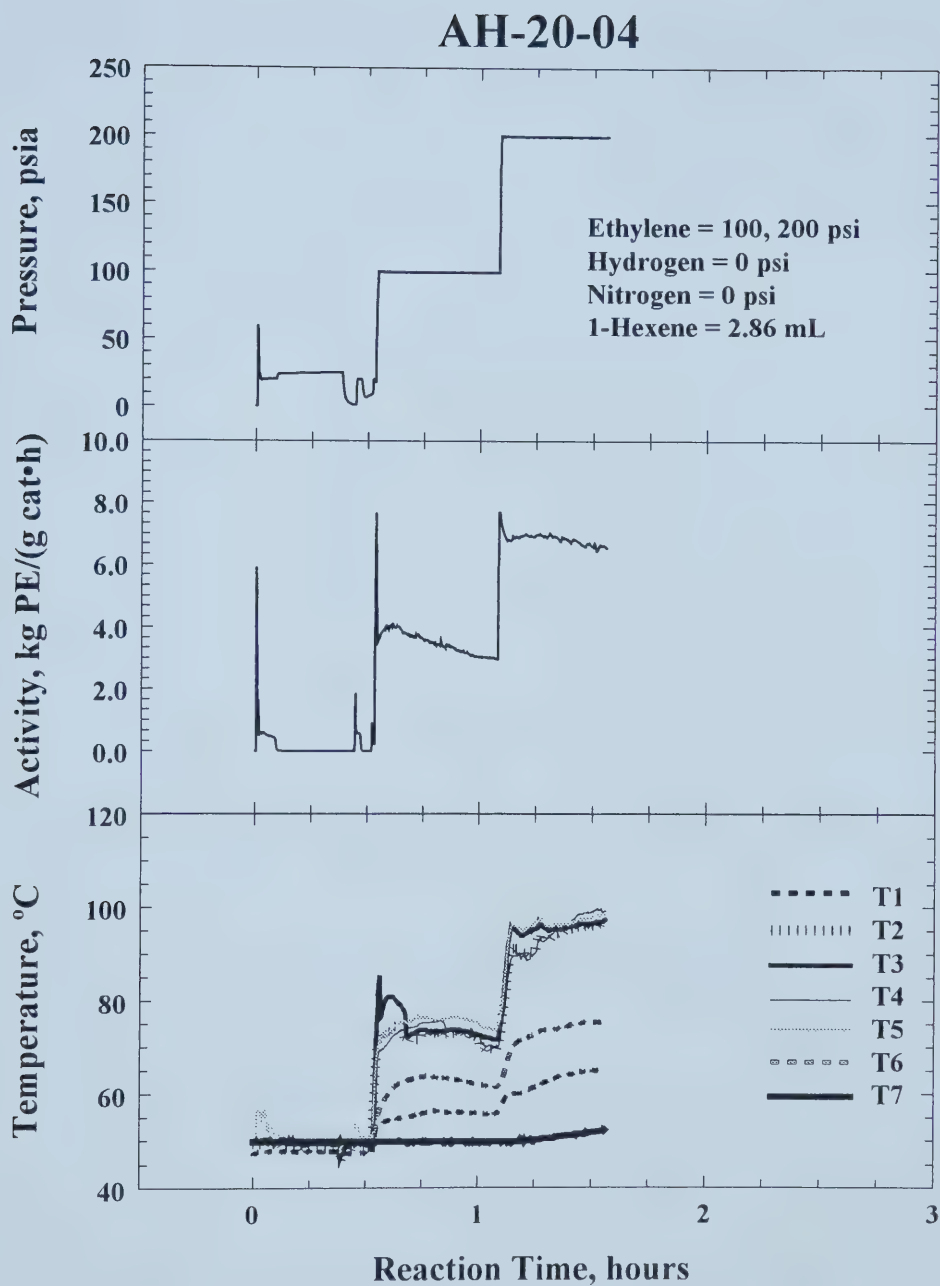


Figure 4.14. Activity profile for AH-20-04.

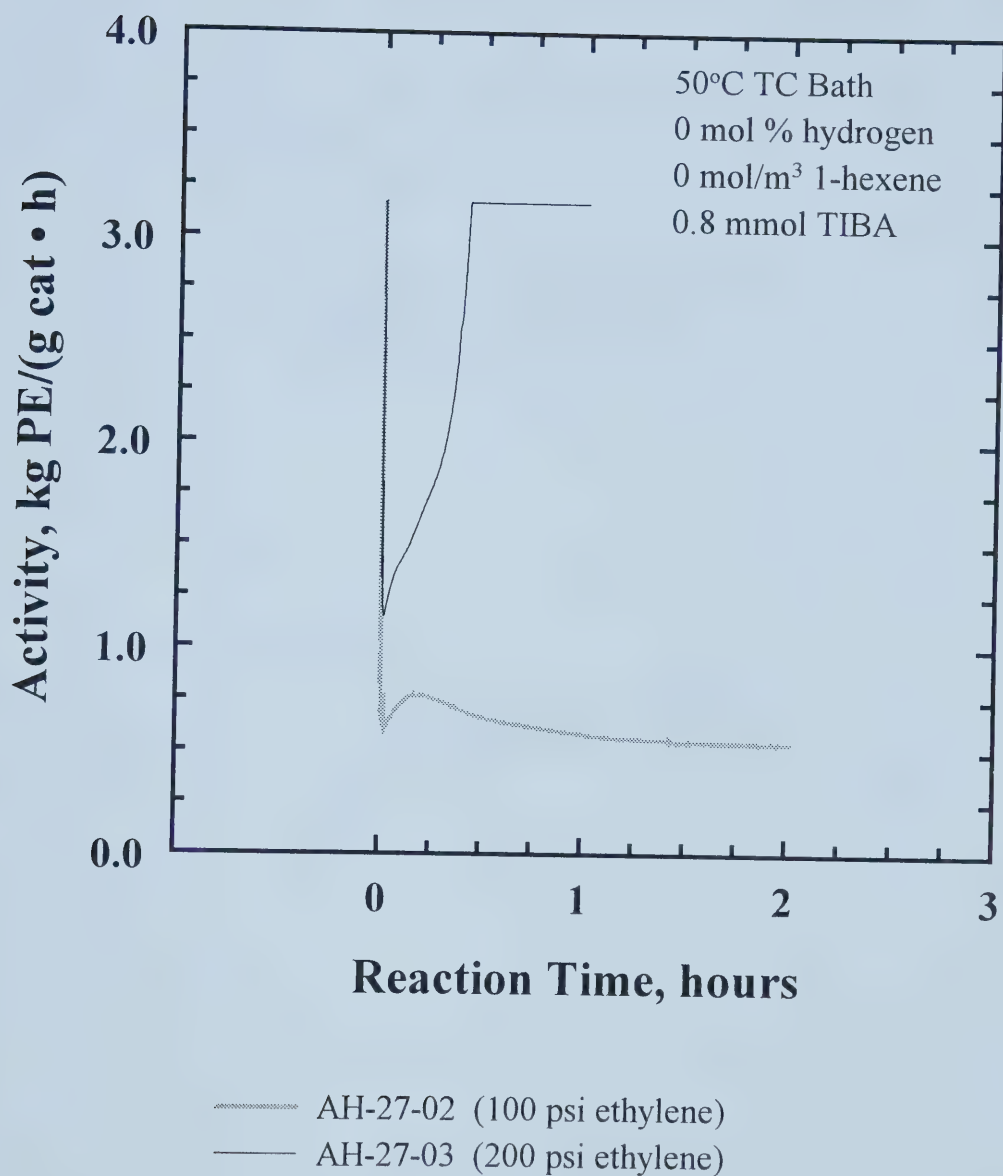


Figure 4.15. Activity profiles for CAT-27 at different ethylene pressures.

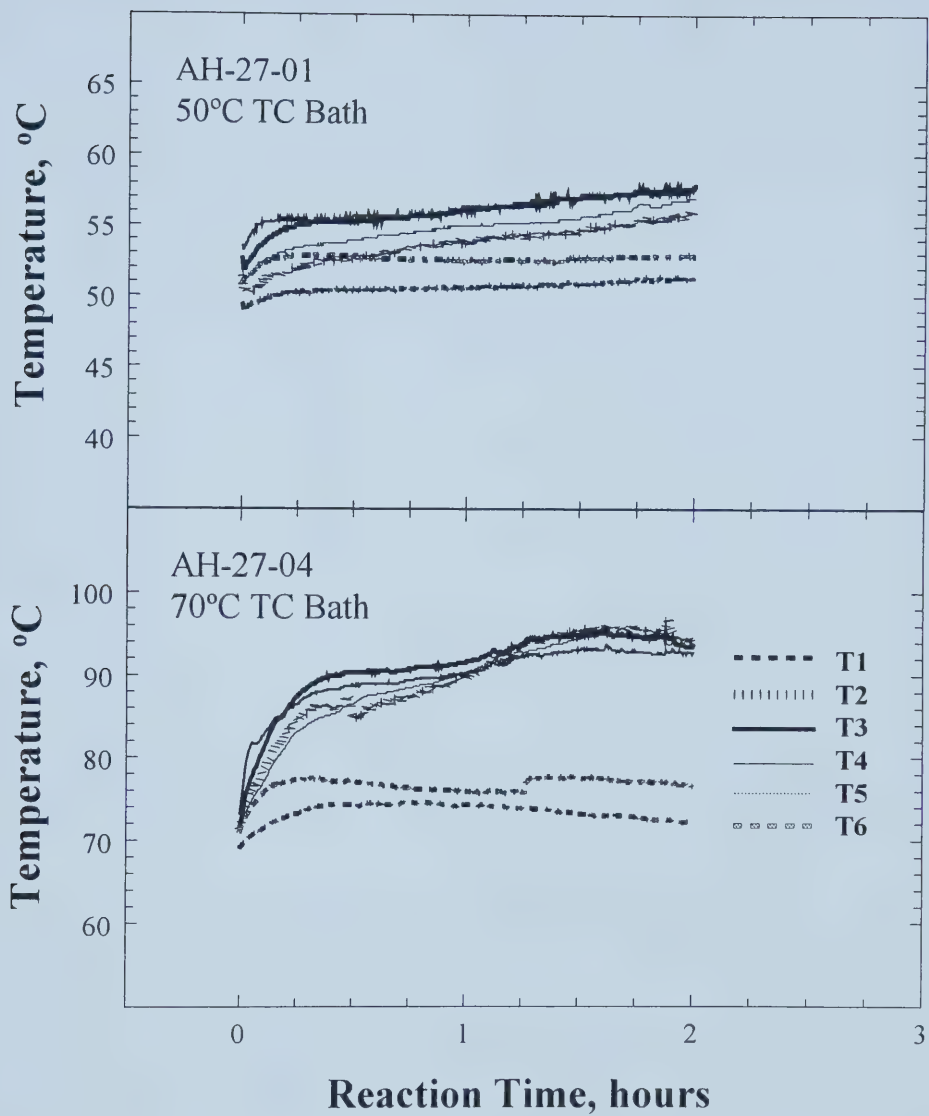


Figure 4.16. Temperature profiles for CAT-27 at different ethylene pressures.

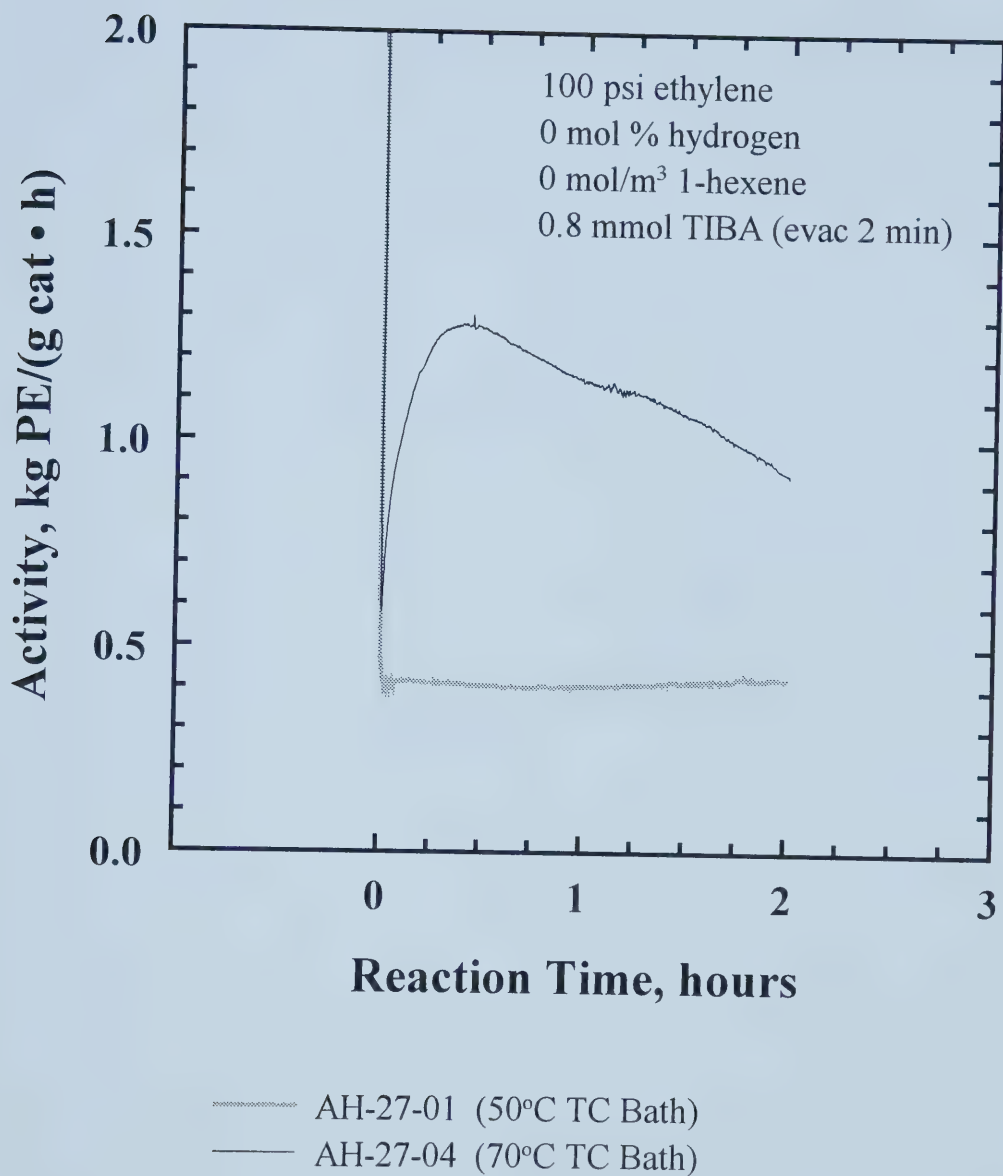


Figure 4.17. Activity profiles for CAT-27 at different TC bath temperatures.

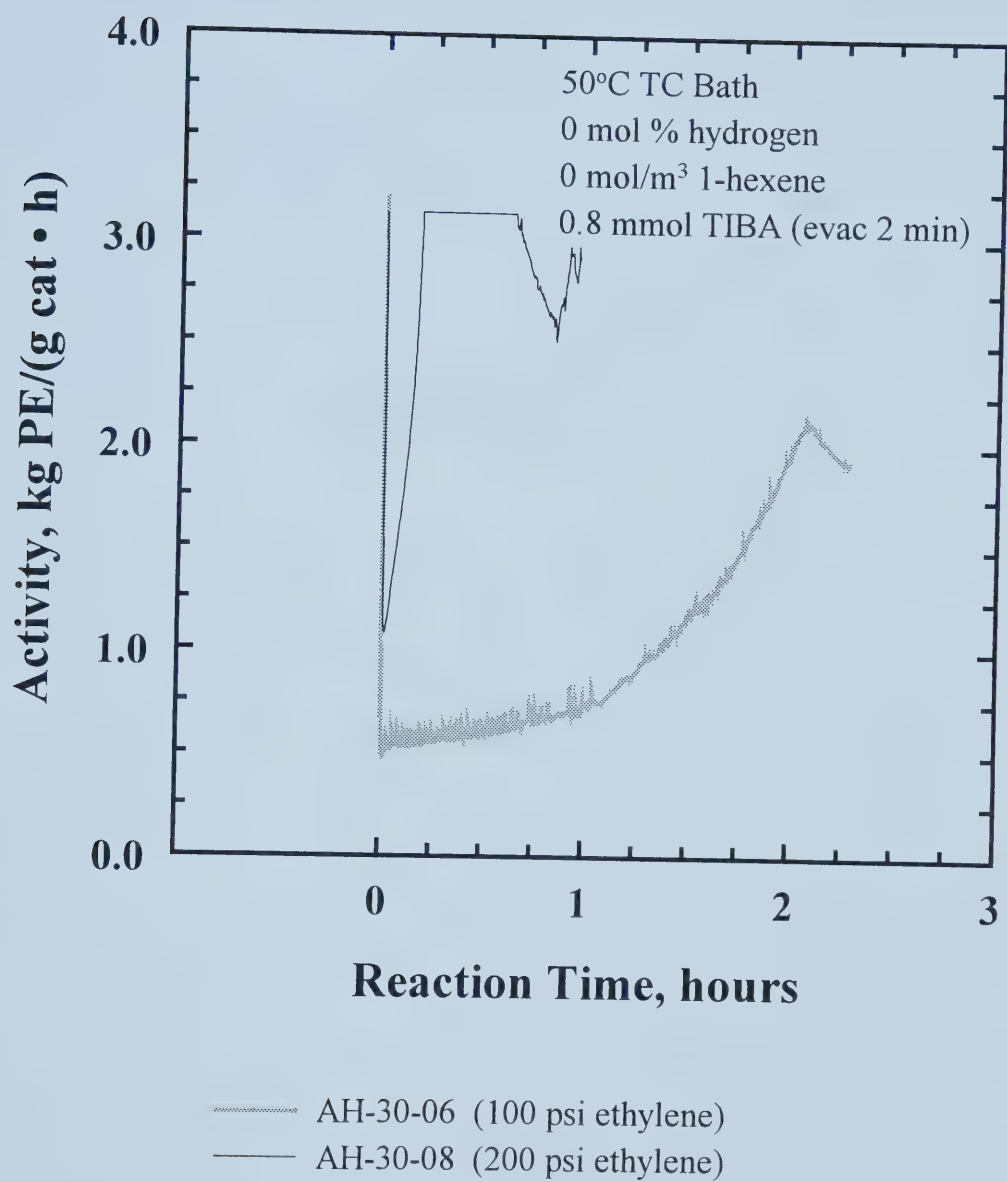


Figure 4.18. Activity profiles for CAT-30 at different ethylene pressures.

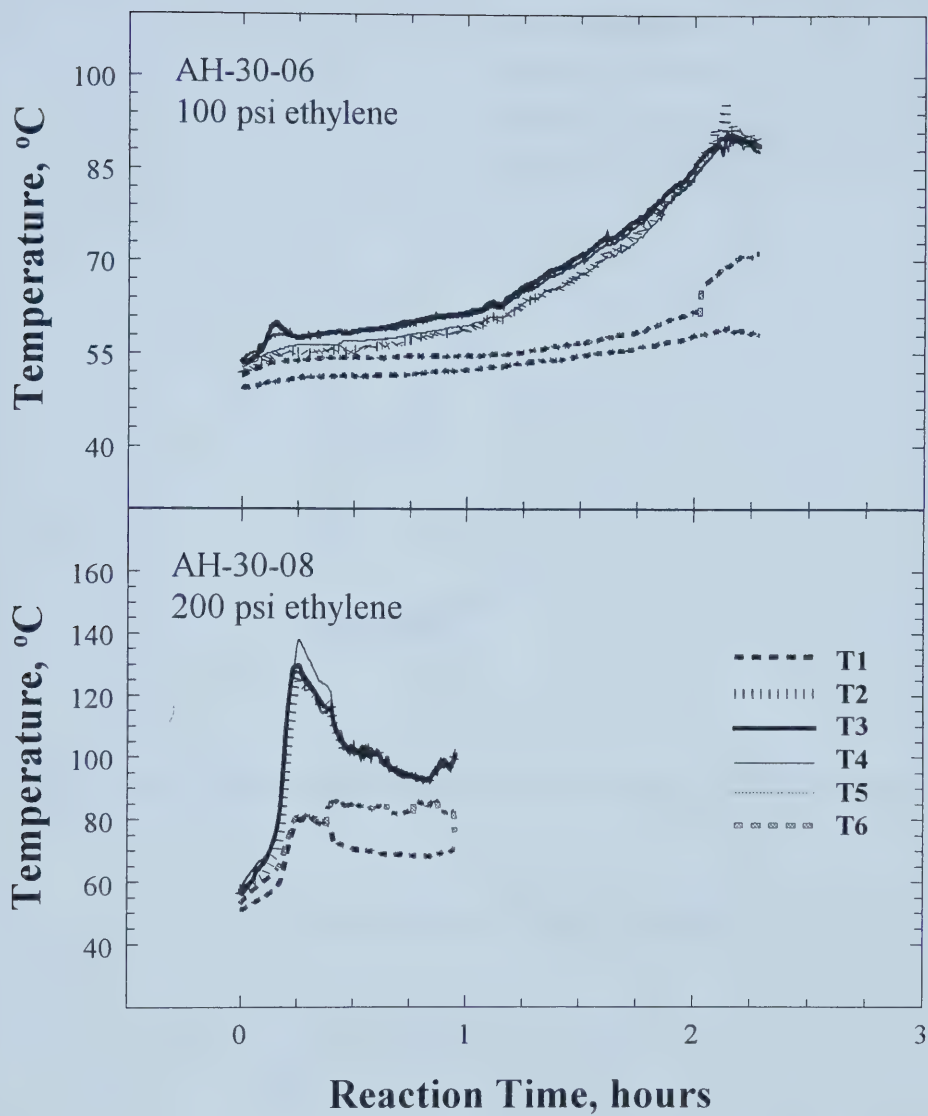


Figure 4.19. Temperature profiles for CAT-30 at different ethylene pressures.

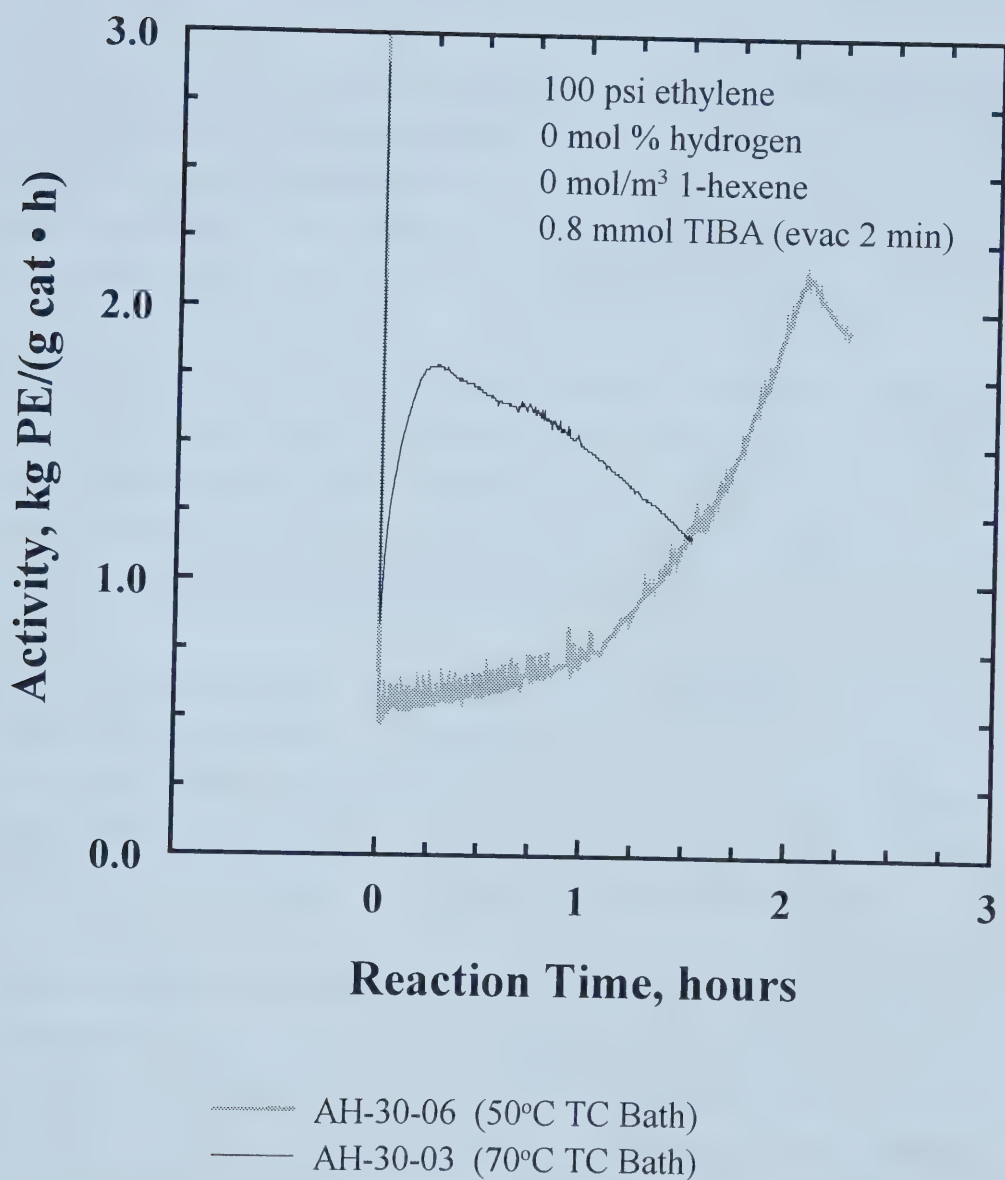


Figure 4.20. Activity profiles for CAT-30 at different TC bath temperatures.

4.7 Effect of Temperature on Activity

The results for CAT-27 (Figure 4.17) and CAT-30 (Figure 4.20) illustrated that activity increased with reactor temperature. The corresponding temperature profiles (Figures 4.21 and 4.22) showed steadily increasing gas-phase temperatures due to poor heat transfer to the circulating silicone oil bath. Some experiments were performed to examine the sensitivity of catalyst activation to temperature.

In one experiment (AH-30-10), a helical mixer blade was installed in the center position on the stirrer shaft in an attempt to improve mixing of the reactor contents. Better mixing resulted in better gas-phase temperature control (Figure 4.23). The activity for this experiment was initially the same as that for the paddle-type blades (AH-30-06), but the activity rapidly dropped (Figure 4.24).

Sodium chloride was used as a seedbed to disperse catalyst particles. An experiment (AH-31-03) was performed with twice the usual amount of salt to raise the overall heat transfer efficiency of the reactor. Consequently, the gas-phase temperature profiles (Figure 4.23) showed a more gradual increase over time, and a higher maximum activity was attained after a longer induction period (Figure 4.24).

The shape of the activity profile is very sensitive to gas-phase temperature; the rates of activation and deactivation increase at higher temperatures. When isothermal conditions were maintained (AH-30-10), the activity profile showed a period of activation followed by rapid deactivation. For the cases with poor temperature control (AH-30-06 and AH-31-03), the activity profiles had the unusual feature of rapid activation after a long induction period during which time the gas-phase temperature was slowly rising. The profiles showed there was a period of continuous activation when the gas-phase temperature was slowly rising and deactivation was delayed until the gas-phase temperature exceeded 100°C.

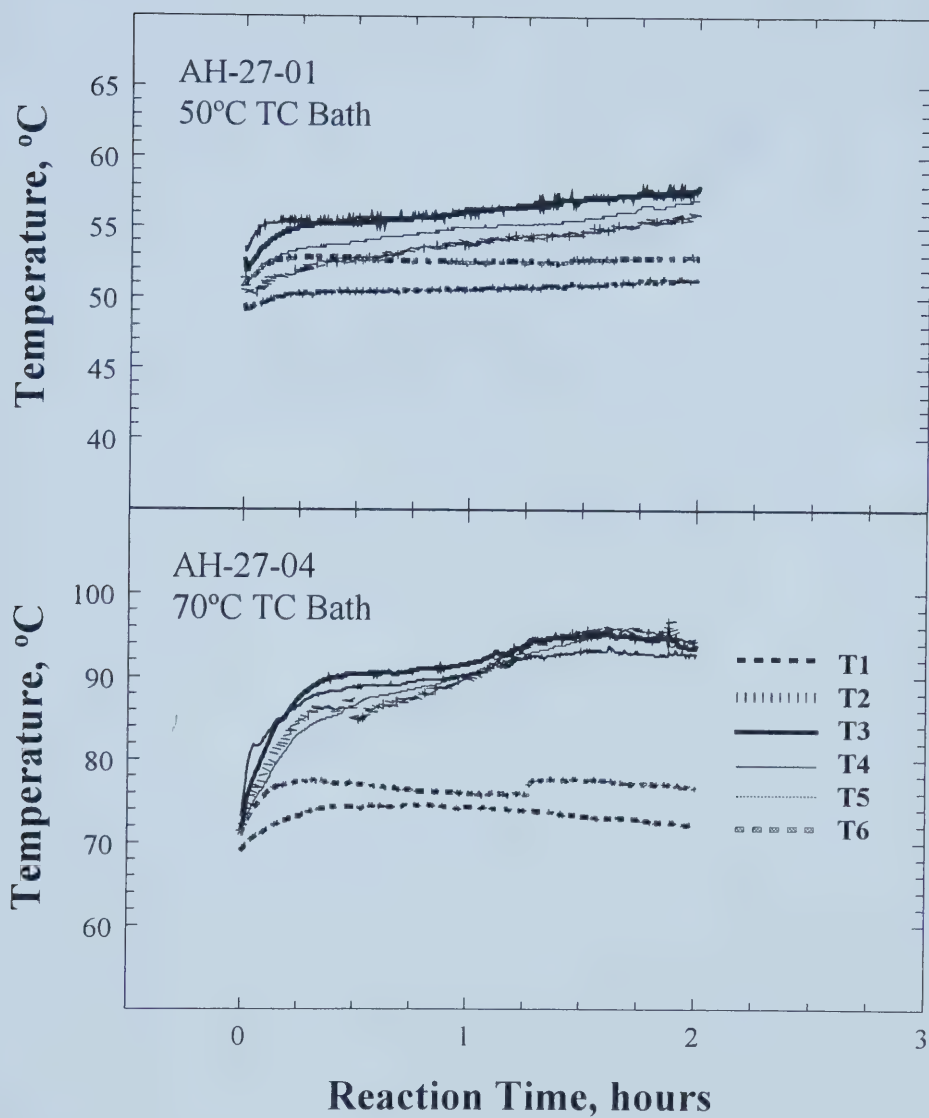


Figure 4.21. Temperature profiles for CAT-27 at different TC bath temperatures.

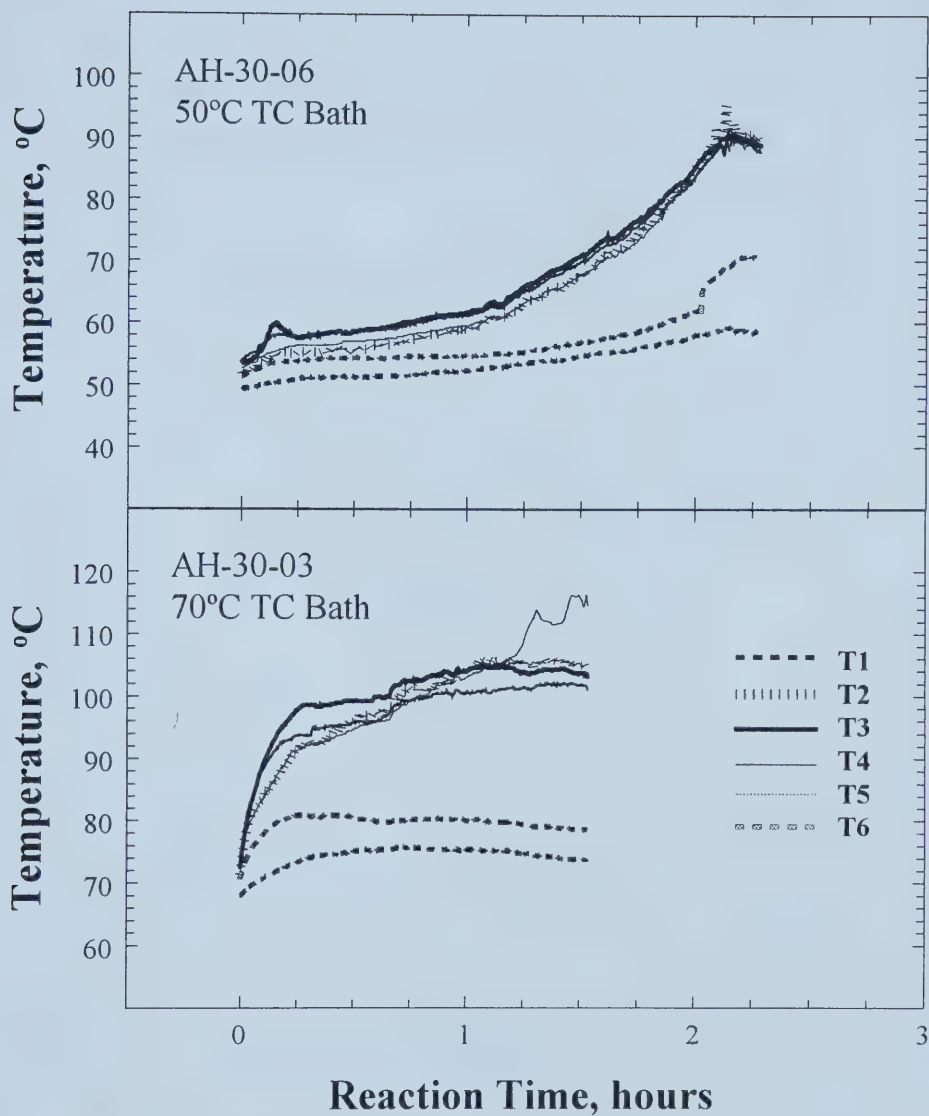


Figure 4.22. Temperature profiles for CAT-30 at different TC bath temperatures.

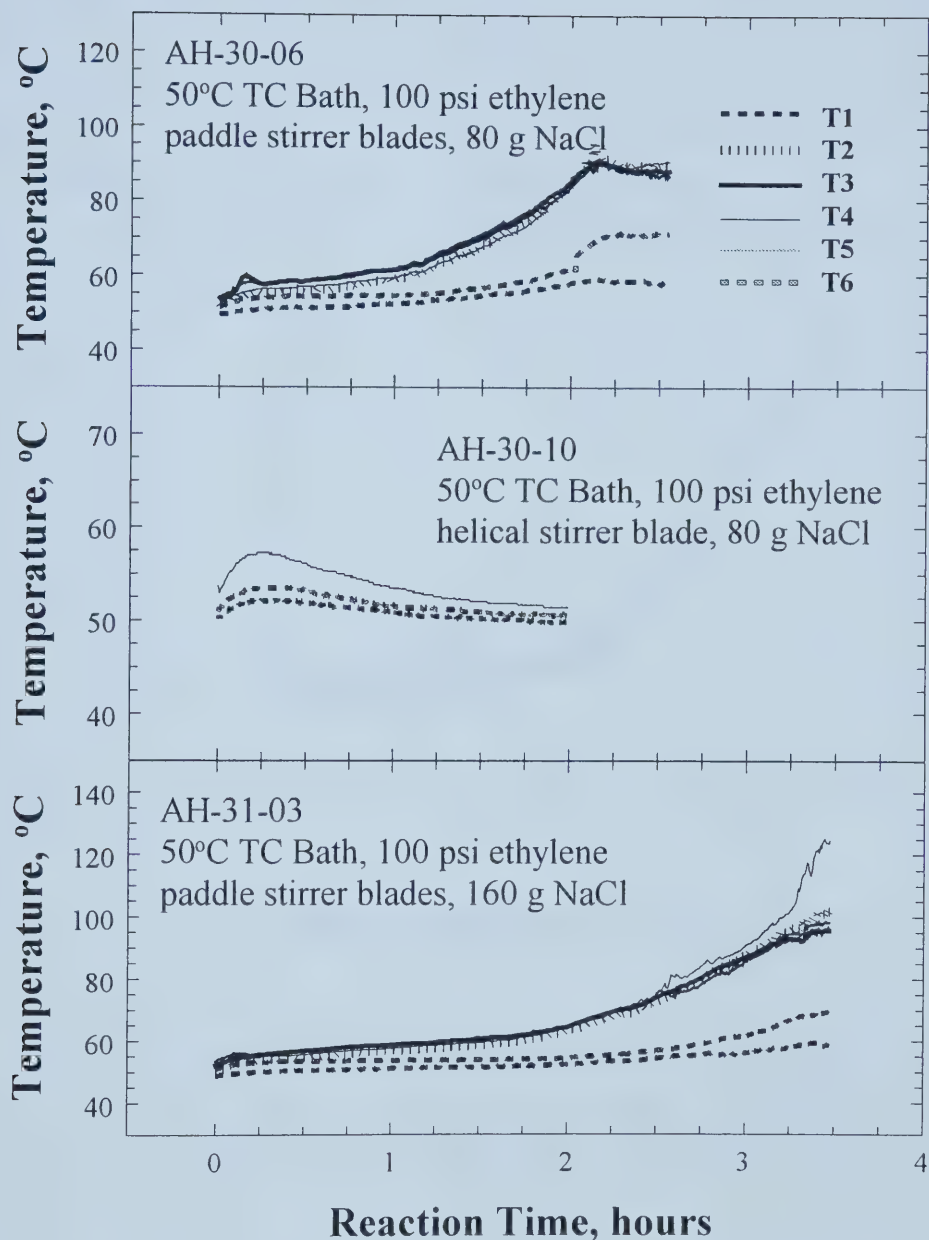


Figure 4.23. Temperature profiles showing the effect of mixing and heat transfer.

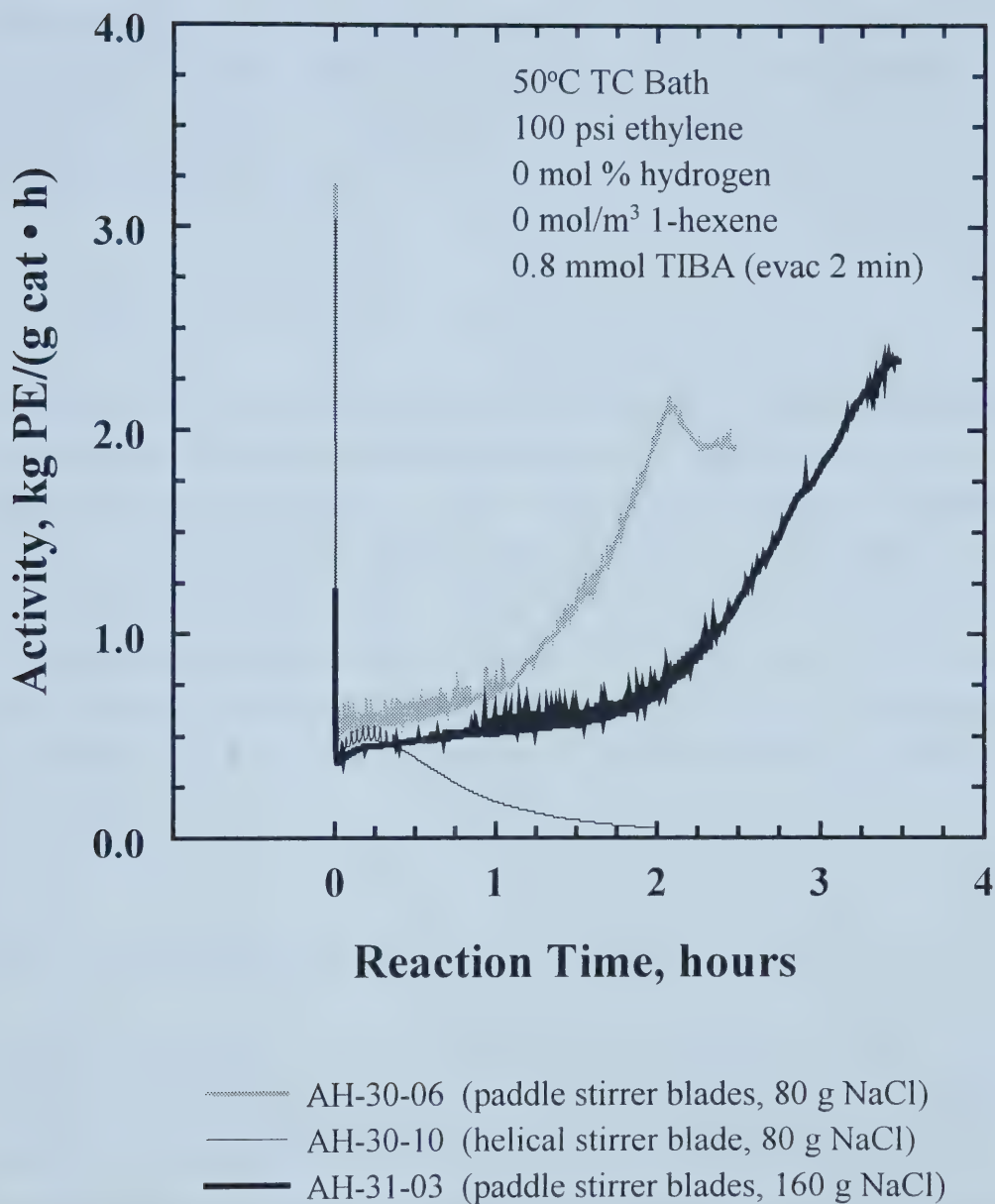


Figure 4.24. Activity profiles showing the effect of mixing and heat transfer.

Unfortunately, heat transfer from the reaction zone to the circulating oil bath was inadequate because the activities were too high. When hydrogen was present, the activity was suppressed (Figure 4.25) so there was better gas-phase temperature control (Figure 4.26); the activity profiles with hydrogen were somewhat flatter in comparison to those with poor temperature control.

4.8 Effect of Hydrogen

Hydrogen acts as a chain transfer agent that alters the rate of chain termination in polymerization. In addition to reducing molar masses, the polymerization activity is typically suppressed by hydrogen. A set of experiments was designed with different hydrogen concentrations to evaluate the effect on activity and molar masses. The experiments were performed with both the bimetallic polyphenoxide (Ti/Mg/Ligand/Silica) and bimetallic silyloxide (Ti/Mg/Silica) catalysts to evaluate the propagation rates for different catalytic sites. In some polymerization experiments, the reactor gas was sampled to assess the quantity of hydrogen consumed.

4.8.1 Effect of Hydrogen Concentration on Activity

As expected, hydrogen suppressed the activity of the Ti-Mg polyphenoxide catalyst (Figure 4.27). The activity profile for the polymerization experiment with hydrogen showed an initial period of activation followed by slow and steady deactivation. As previously discussed, there was better gas-phase temperature control with hydrogen (Figure 4.28), which affected the shape of the activity profile.

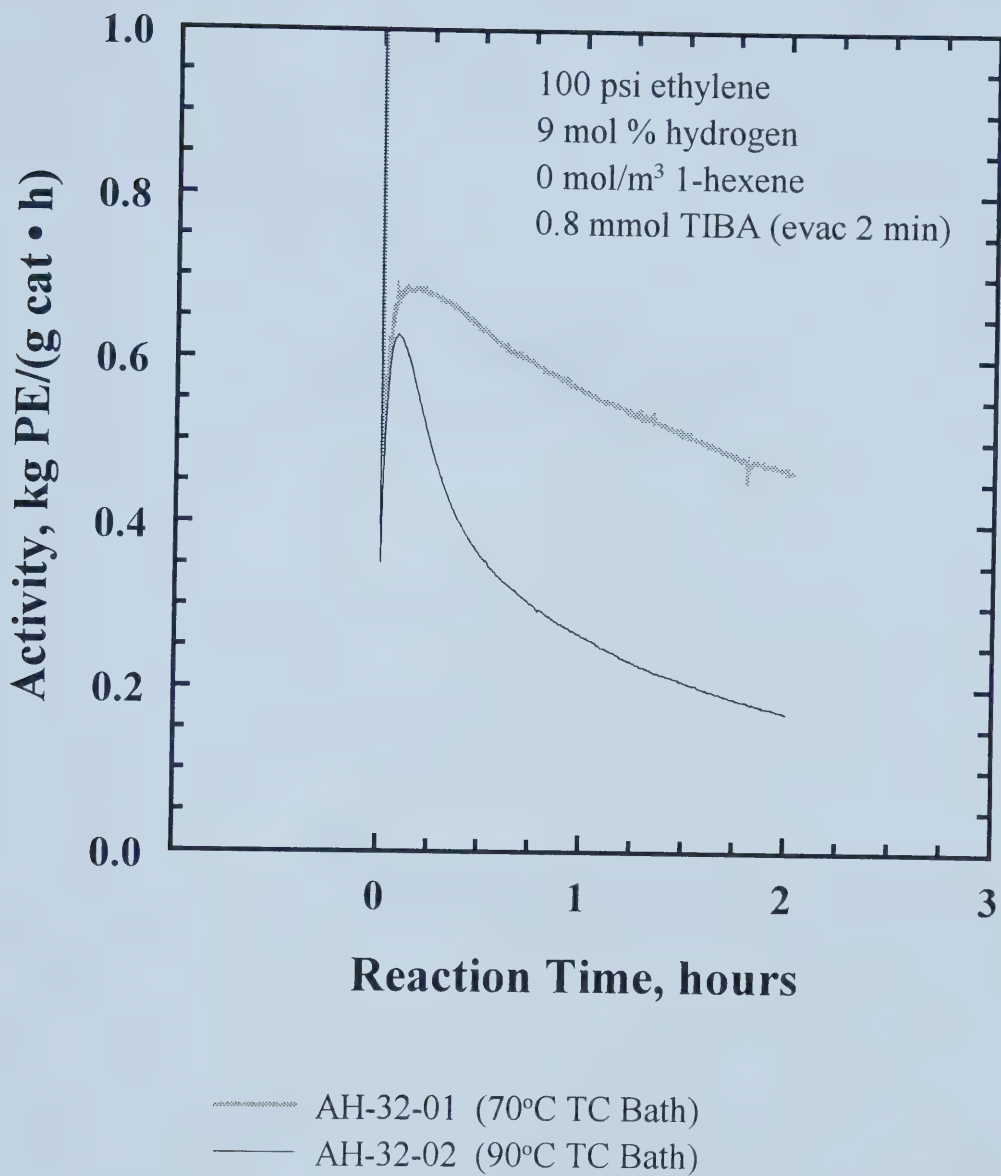


Figure 4.25. Activity profiles with hydrogen at different TC bath temperatures.

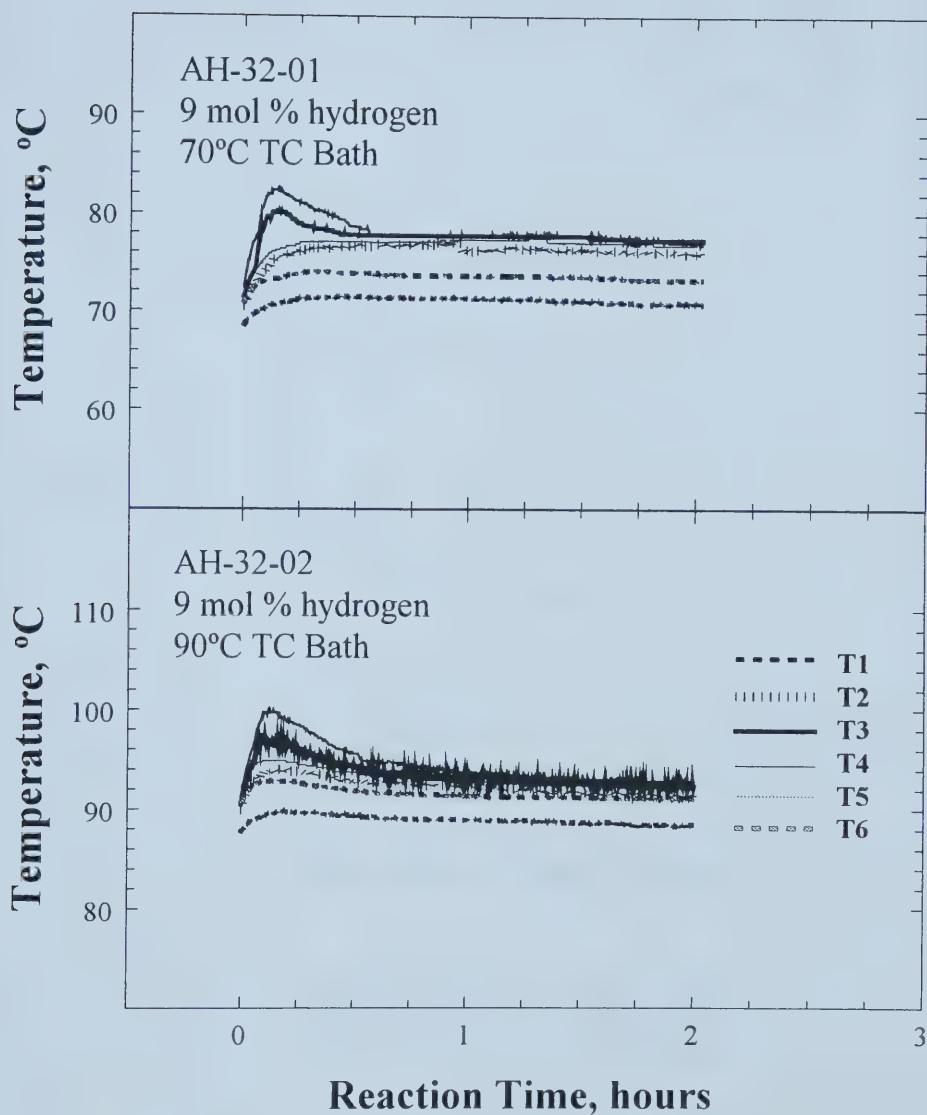


Figure 4.26. Temperature profiles with hydrogen at different TC bath temperatures.

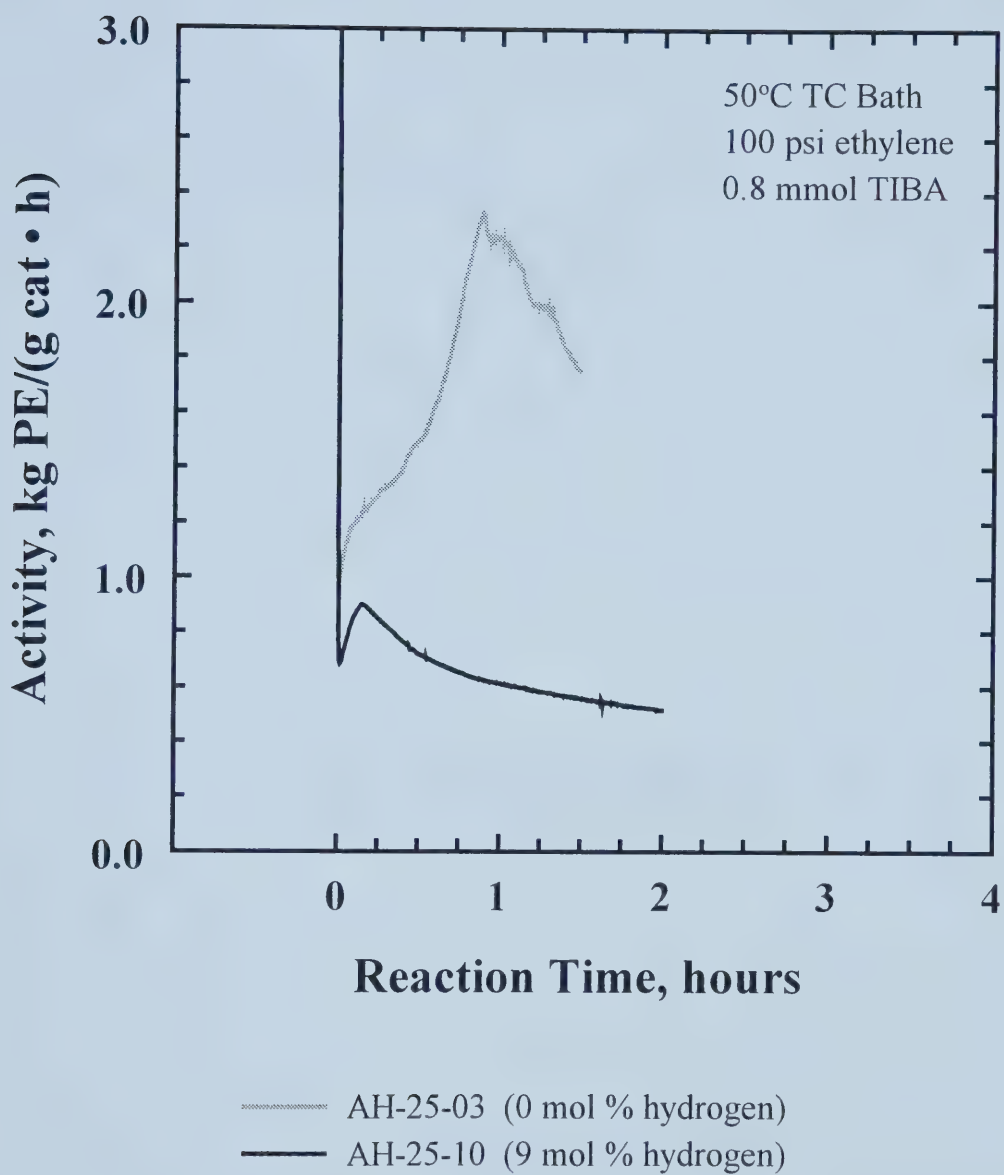


Figure 4.27. Activity profiles showing effect of hydrogen.

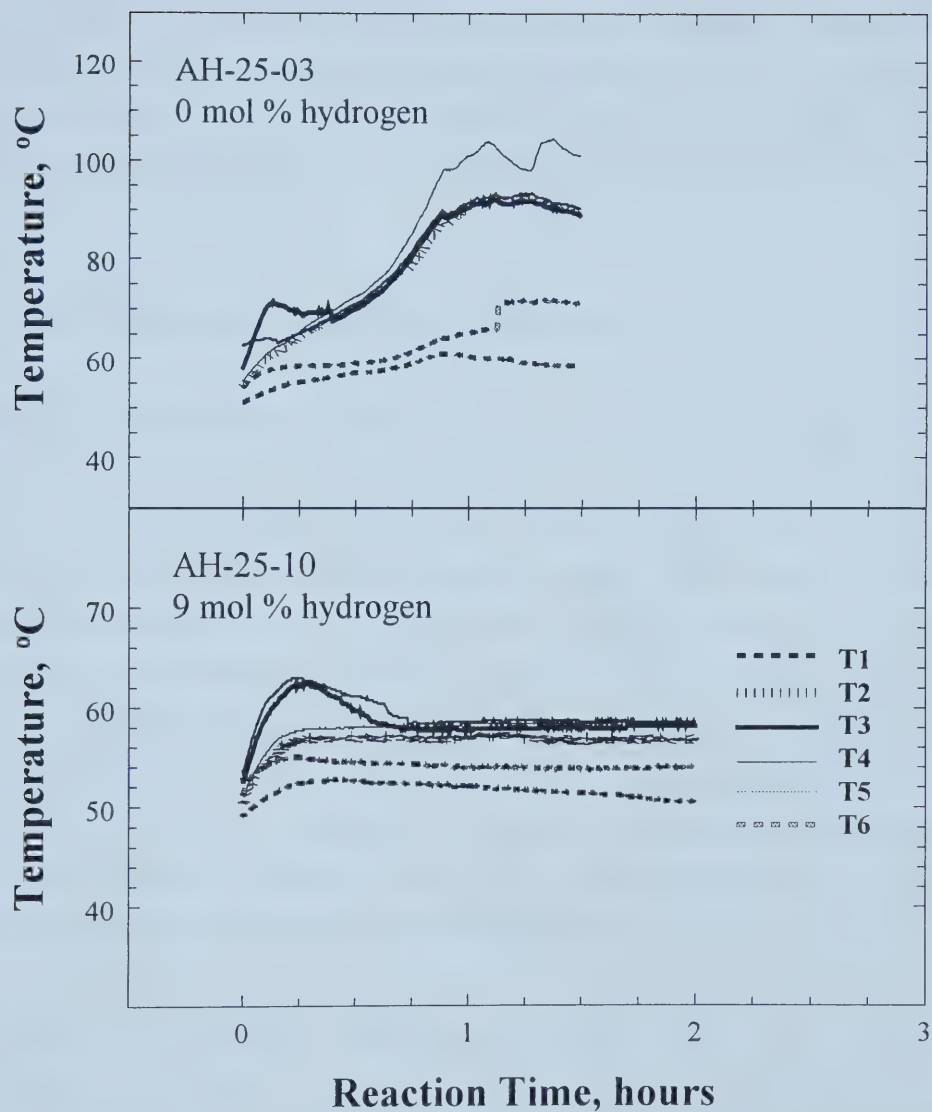


Figure 4.28. Temperature profiles for polymerization experiments performed with and without hydrogen.

The activity decreased as the hydrogen concentration increased for both the Ti-Mg polyphenoxide (Figure 4.29) and Ti-Mg silica (Figure 4.30) catalysts. Deviations from the trends were probably due to inconsistent catalyst injections. The Ti-Mg polyphenoxide catalyst was still very active even with high hydrogen concentrations of 29 mole %; its activity was about twice that for the corresponding experiment with the Ti-Mg silica catalyst (cf AH-31-05 and AH-33-05).

4.8.2 Effect of Hydrogen Concentration on Molar Mass

Initially, the polymerization experiments were performed without hydrogen. Table 4.1 lists molar masses for polymer samples produced with different methods of titanium (IV) chloride addition. The trends were the same for both ethylene homopolymer and ethylene/1-hexene copolymer samples; molar masses for the vapour deposition method were lower than those for slurry addition. The molar masses were lower for longer contact times with the vapour deposition method (CAT-20). The activity for the catalysts prepared with the vapour deposition method (CAT-19 and CAT-20) was much higher than that for the catalyst prepared with the slurry method (CAT-17). Consequently, the gas-phase temperatures were much higher in the experiments with CAT-19 and CAT-20. The observed trends in molar masses could be the result of elevated gas-phase temperature during polymerization.

The ligand loading on silica had an effect on molar masses (see Table 4.2). Very high molar masses were obtained for CAT-26, which was prepared without the polyphenoxide ligand. The molar mass distribution for AH-26-04 was also broader as indicated by the polydispersity of 6.9. Similar SEC results were reported in the literature for other sterically hindered Group IV aryloxide complexes (Matilainen et al., 1996; van der Linden et al., 1995). The other SEC results were representative for the two ligand loadings examined in this work; lower molar masses were obtained for

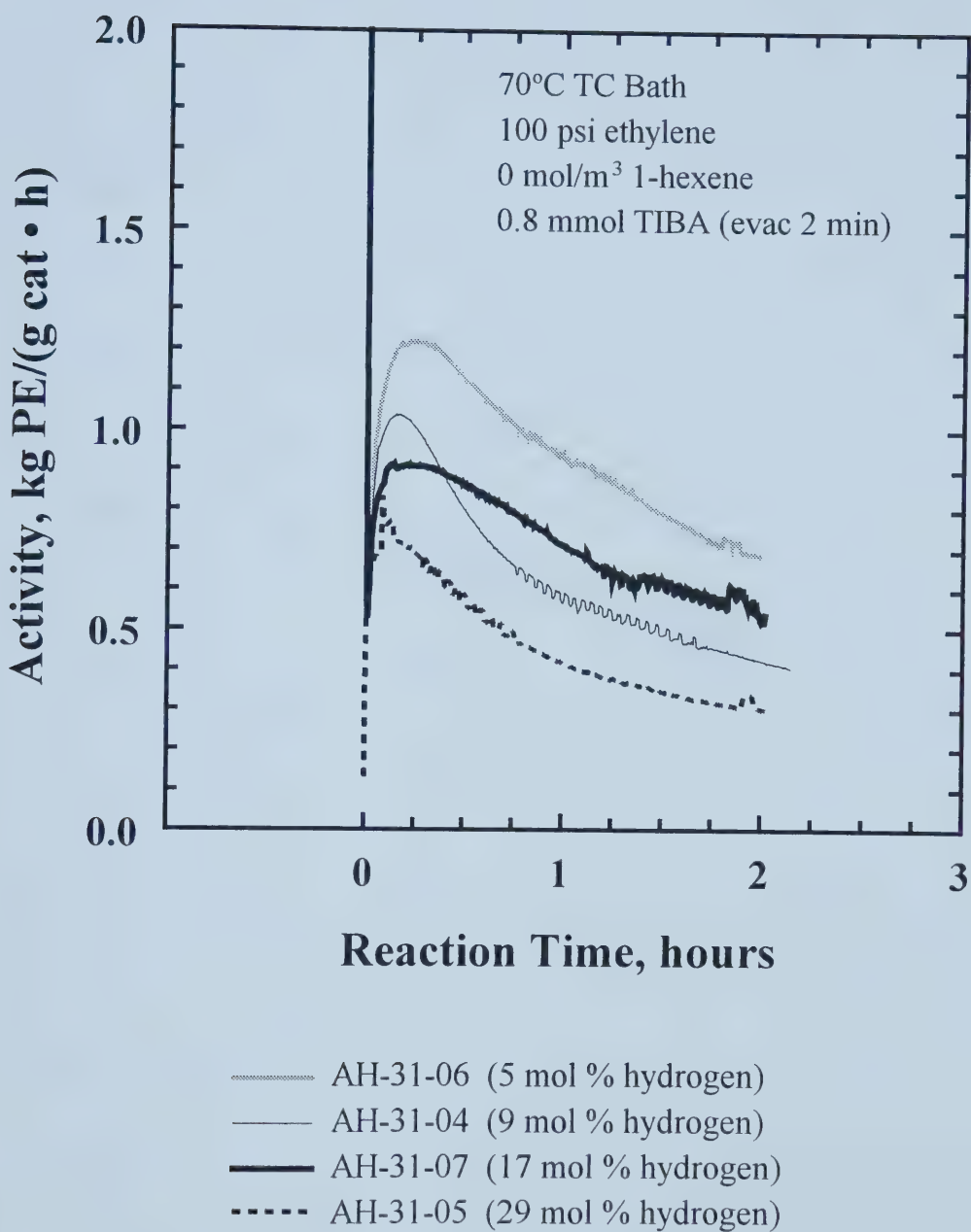


Figure 4.29. Activity profiles for the Ti-Mg polyphenoxide catalyst at different hydrogen concentrations.

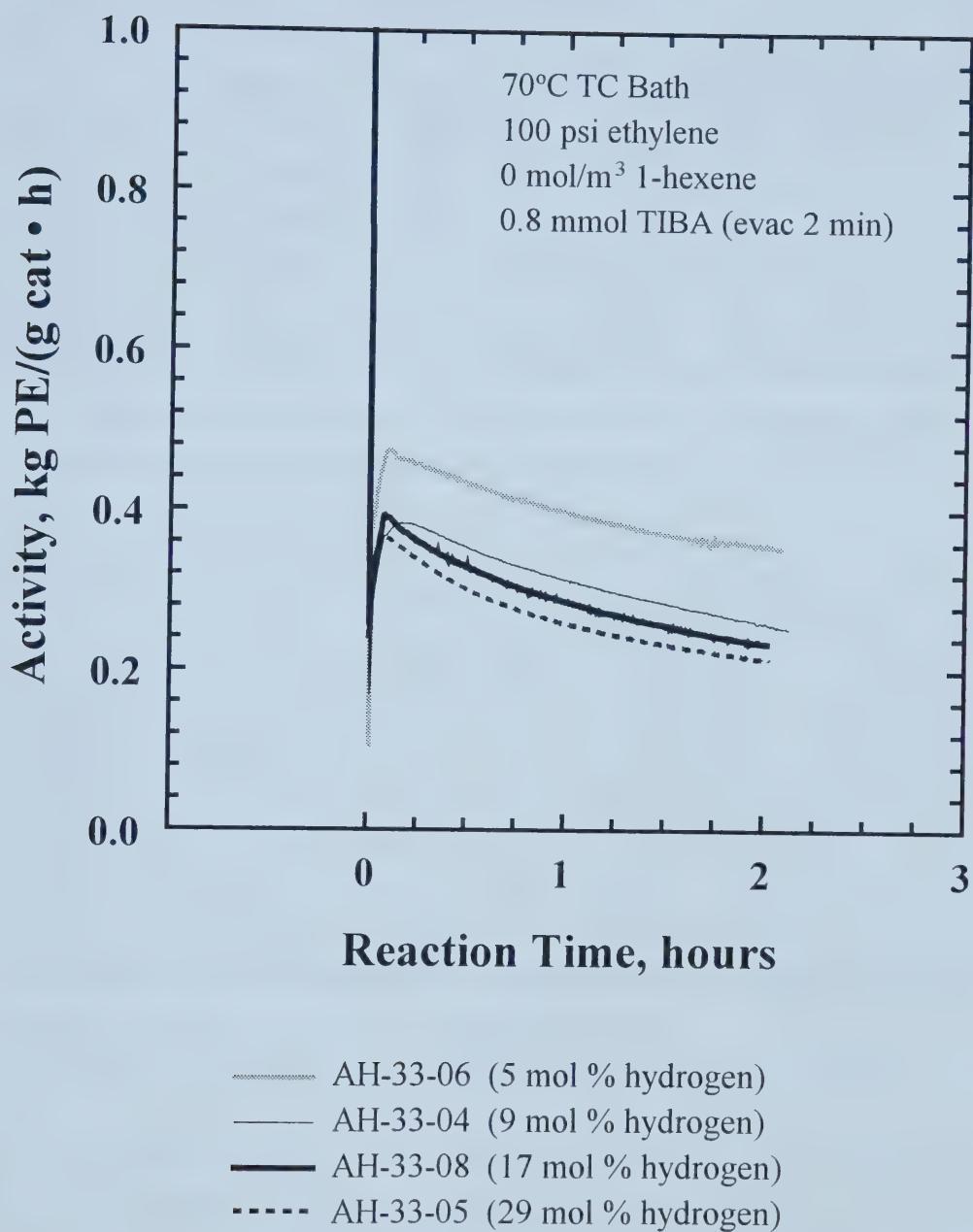


Figure 4.30. Activity profiles for the Ti-Mg silica catalyst at different hydrogen concentrations.

Table 4.1: SEC Results Comparing TiCl_4 Addition Methods.

Run ID	TiCl_4 Addition Method ^a	Polymer Type ^b	Averaged SEC Results		
			Mn ($\times 10^{-3}$)	Mw ($\times 10^{-3}$)	PD
AH-17-02	S (Toluene)	Homo	184	423	2.3
AH-17-03	S (Toluene)	Co	151	706	4.7
AH-19-01	V (10 min)	Homo	147	327	2.2
AH-19-02	V (10 min)	Co	128	438	3.4
AH-20-01	V (5.5 h)	Homo	105	276	2.6
AH-20-02	V (5.5 h)	Co	88	261	3.0

a S (solvent) for slurry method or V (contact time) for vapour deposition method

b Homo for ethylene homopolymer and Co for ethylene/1-hexene copolymer

Table 4.2: SEC Results Comparing Ligand Loadings on Silica.

Run ID	Ligand Loading ^a	Polymer Type ^b	Averaged SEC Results		
			Mn ($\times 10^{-3}$)	Mw ($\times 10^{-3}$)	PD
AH-26-04	No Ligand	Homo	174	1193	6.9
AH-20-01	47.8 mg/g	Homo	105	276	2.6
AH-20-02	47.8 mg/g	Co	88	261	3.0
AH-25-03	38.8 mg/g	Homo	187	776	4.2
AH-25-06	38.8 mg/g	Co	136	516	3.8
AH-27-04	38.9 mg/g	Homo	186	733	3.9
AH-27-06	38.9 mg/g	Co	196	643	3.3

a All catalysts prepared with vapour deposition of TiCl_4

b Homo for ethylene homopolymer and Co for ethylene/1-hexene copolymer

the higher ligand loading (CAT-20). The molar mass distribution was also narrower for the higher ligand loading with unusually low polydispersities for conventional Ti-Mg catalysts. The Ti-Mg polyphenoxide catalyst has at least two types of magnesium environments; magnesium aryloxides are formed with the ligand and magnesium silyloxides are produced from the residual silanols. The differences in

polydispersity with ligand loading suggested ligand functionality affected the molar mass distributions.

Table 4.3 lists molar masses for polymer samples produced at different hydrogen concentrations. The data revealed that the molar masses for the Ti-Mg polyphenoxide polymer samples (CAT-31) were higher than those for the corresponding polymer samples for the Ti-Mg silica catalyst (CAT-33). As expected, the polydispersities increased for higher hydrogen concentrations, and lower polydispersities were obtained with the Ti-Mg polyphenoxide catalyst.

Table 4.3: Molar Masses for Homopolymers Produced with Hydrogen.

Run ID	Catalyst Type ^a	H ₂ Concentration (mol %)	SEC Results		
			Mn (x10 ⁻³)	Mw (x10 ⁻³)	PD
AH-31-02	Ligand	0	45	1117	2.5
AH-31-06	Ligand	5	97	325	3.4
AH-31-04	Ligand	9	84	298	3.6
AH-31-07	Ligand	17	49	201	4.1
AH-31-05	Ligand	29	33	147	4.5
AH-33-06	Silyloxide	5	83	321	3.9
AH-33-04	Silyloxide	9	66	258	3.9
AH-33-08	Silyloxide	17	38	186	4.9
AH-33-05	Silyloxide	29	26	139	5.3

a Ligand for Ti/Mg/Ligand/Silica catalyst and Silyloxide for Ti/Mg/Silica catalyst

Jaber and Ray (1993) give the correlation between number average molar mass (Mn) and hydrogen concentration ([H₂]) as

$$\frac{1}{Mn} = a + b[H_2]^n \quad (4)$$

Usually, an order of 0.5 or 1.0 for hydrogen concentration is used. The inverse number average molar masses (M_n^{-1}) were plotted as a function of hydrogen pressure to examine the hydrogen termination kinetics for both the Ti-Mg polyphenoxide (Figure 4.31) and Ti-Mg silica (Figure 4.32) catalysts. Based on the fittings for hydrogen termination kinetics, the dependence of M_n with respect to hydrogen concentration could be described by either first- or half-order for both catalysts. The catalysts might possess different types of active sites with different hydrogen termination kinetics; one site might be first-order and the other site could trend towards $n < 1.0$ (Huang et al., 1997).

It has been well established that Ziegler-Natta catalysts have different types of active sites that result in broad molar mass distributions with typical polydispersities ranging between 4 and 5 (Kissin et al., 1999). The differences in the fitting parameters for hydrogen termination kinetics (Figures 4.31 and 4.32) indicated the two catalysts had different responses to hydrogen. The molar mass distributions for the Ti-Mg polyphenoxide (Figure 4.33) and Ti-Mg silica (Figure 4.34) catalysts were bimodal, which revealed the presence of multiple types of active sites in both catalysts. These sites had different sensitivities to hydrogen because one peak in the distribution shifted as the hydrogen concentration was varied; at least one site type was responsive to hydrogen and another site type was fairly insensitive to hydrogen concentration.

The molar mass data supported the hypothesis that the Ti-Mg polyphenoxide catalyst had either different ratios of the same types of active sites or different types of active sites than the Ti-Mg silica catalyst. The Ti-Mg silica catalyst was prepared for comparison purposes because the Ti-Mg polyphenoxide catalyst possessed some magnesiated silanols. The differences in propagation rates and polydispersities indicated the active site environment of the ligand had some effect on polymerization kinetics. Higher ligand loadings had the effect of producing narrower molar mass

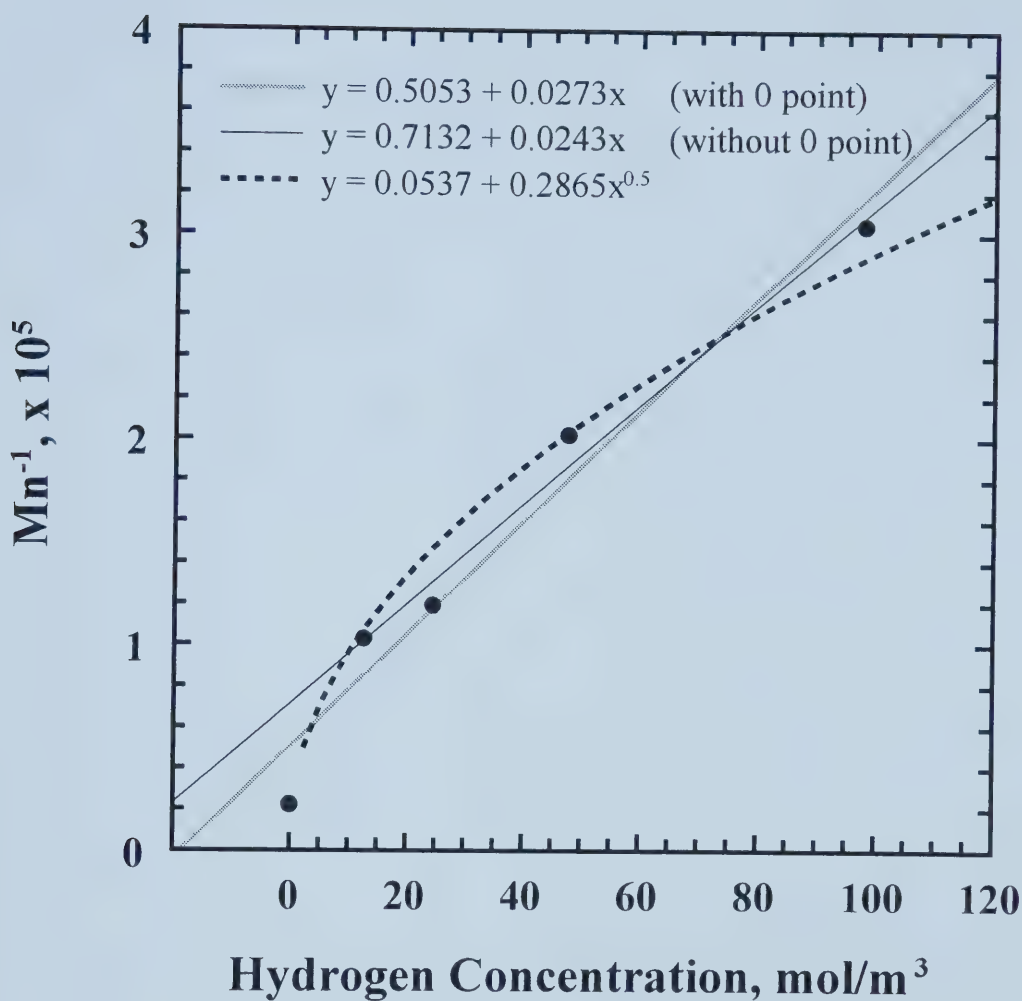


Figure 4.31. Fitting of hydrogen termination kinetics for the Ti-Mg polyphenoxide catalyst.

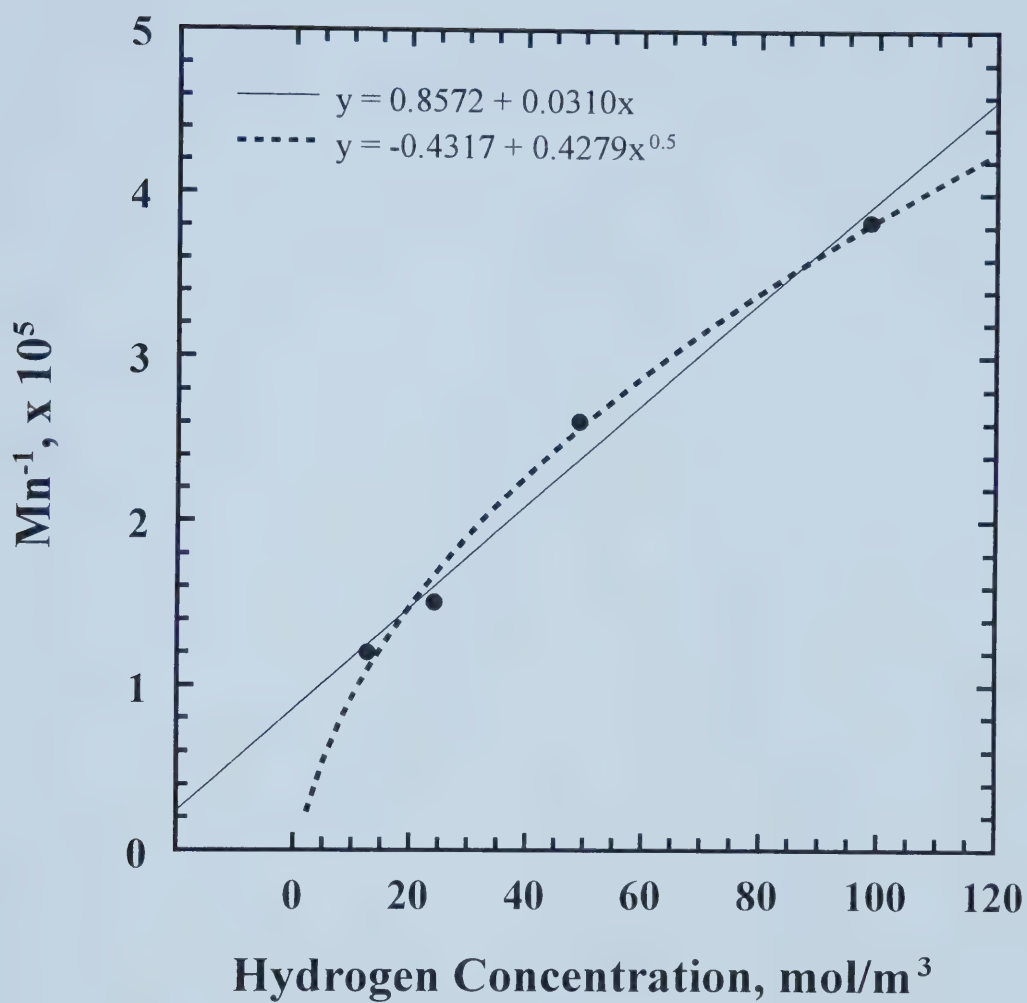


Figure 4.32. Fitting of hydrogen termination kinetics for the Ti-Mg silica catalyst.

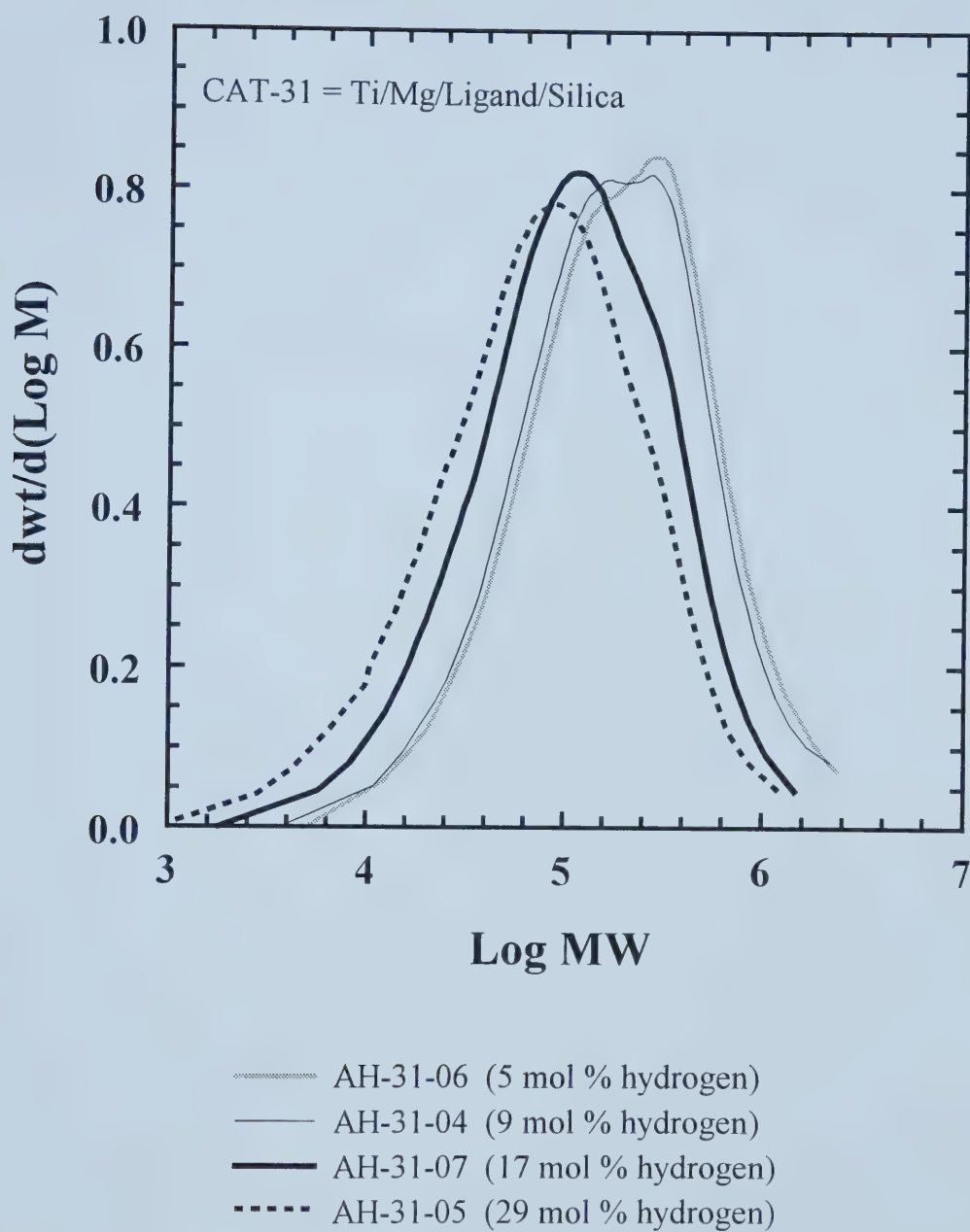
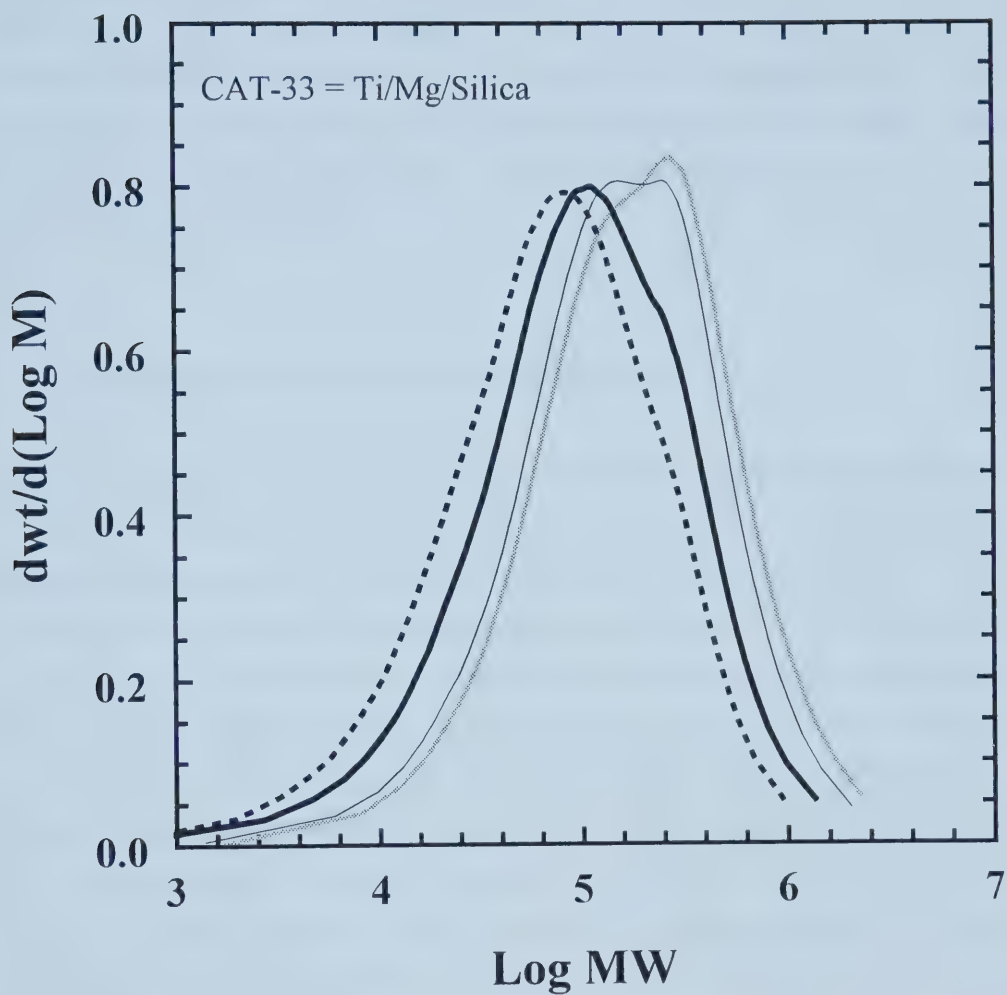


Figure 4.33. Molar mass distributions for the Ti-Mg polyphenoxide catalyst.



- AH-33-06 (5 mol % hydrogen)
- AH-33-04 (9 mol % hydrogen)
- AH-33-08 (17 mol % hydrogen)
- AH-33-05 (29 mol % hydrogen)

Figure 4.34. Molar mass distributions for the Ti-Mg silica catalyst.

distributions with unusually low polydispersities for conventional Ti-Mg catalysts. There was a higher fraction of magnesium aryloxide sites than magnesium silyloxide sites at the higher ligand loading so it is possible that the ligand created a more homogeneous surface on the support thus controlling the ratio of active sites. Alternatively, the magnesium aryloxide functionality created different types of active sites with different polymerization kinetics.

4.8.3 Hydrogen Consumption During Polymerization

Gas chromatographic results for reactor gas samples taken at the beginning and end of several experiments are given in Table 4.4. For most of the experiments, the hydrogen concentration did not change appreciably during the experiment. The results for AH-31-06 and AH-07 showed that some hydrogen was consumed during polymerization; however, there was no appreciable change in hydrogen concentration for AH-31-05, which was performed with the same catalyst at a higher hydrogen concentration. It would be reasonable to expect there would be consumption at higher concentrations when the GC results showed some hydrogen was consumed at lower concentrations. In general, hydrogen was effective in lowering the molar masses by chain termination, but the amount of hydrogen consumed by chain termination is small (see Appendix C).

Table 4.4: Hydrogen Concentration during Polymerization.

Run ID	H ₂ Concentration (mol %)	% H ₂ Peak Area at Start		% H ₂ Peak Area at End	
		Sample 1	Sample 2	Sample 1	Sample 2
AH-29-06	10	18.46	18.87	18.85	18.62
AH-30-05	9	17.29	17.01	17.02	16.60
AH-31-05	29	43.79	43.88	43.15	43.27
AH-31-06	5	10.87	10.18	8.27	7.93
AH-31-07	17	28.37	28.10	24.79	24.82

4.9 Effect of 1-Hexene

Catalyst activity for Ziegler-Natta catalysts is typically higher in ethylene/1-hexene copolymerization than ethylene homopolymerization (Kissin et al., 1999); this enhancement is commonly referred to as the comonomer effect. Varying the hydrogen concentration showed there were at least two types of active sites in the catalysts that had different responses to hydrogen. Similar experiments were performed with a series of 1-hexene concentrations to assess comonomer incorporation for the bimetallic polyphenoxide (Ti/Mg/Ligand/Silica) and bimetallic silyloxide (Ti/Mg/Silica) catalysts. The molar masses were measured and the polymer samples were analyzed with TREF to evaluate short-chain branching due to comonomer incorporation. Because very high activities were obtained in ethylene/1-hexene copolymerization experiments, there was concern that all the 1-hexene injected into the reactor at the start would be consumed during the 2-hour experiments. The reactor gas was sampled at regular intervals in a few experiments to monitor 1-hexene consumption.

4.9.1 Effect of 1-Hexene Concentration on Activity

Activities were much higher for ethylene/1-hexene copolymerization than for ethylene homopolymerization with the Ti-Mg polyphenoxide catalyst (Figures 4.35 and 4.36). Smaller amounts of catalyst were used in an attempt to keep the ethylene flow rate below the maximum reading of the flow meter. The activity profiles for copolymerization showed more rapid activation after catalyst injection than for homopolymerization. After a period of high activity, the activity decayed to a lower rate then stayed approximately constant for the rest of the experiment. The gas-phase temperature increased, and it was not uncommon for temperatures to exceed 130°C; the rapid rate of deactivation was probably caused by the temperature excursions.

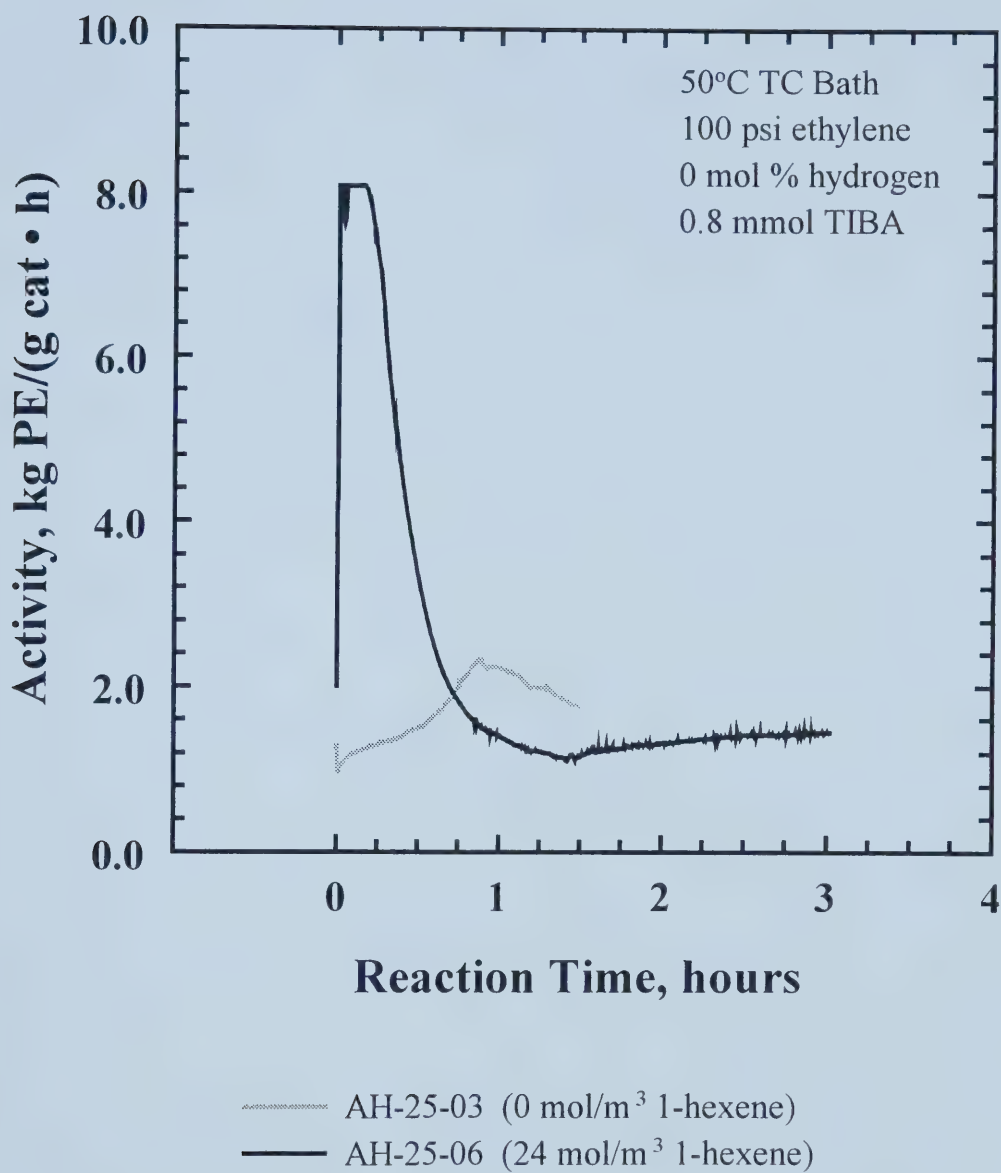


Figure 4.35. Activity profiles showing effect of 1-hexene without hydrogen.

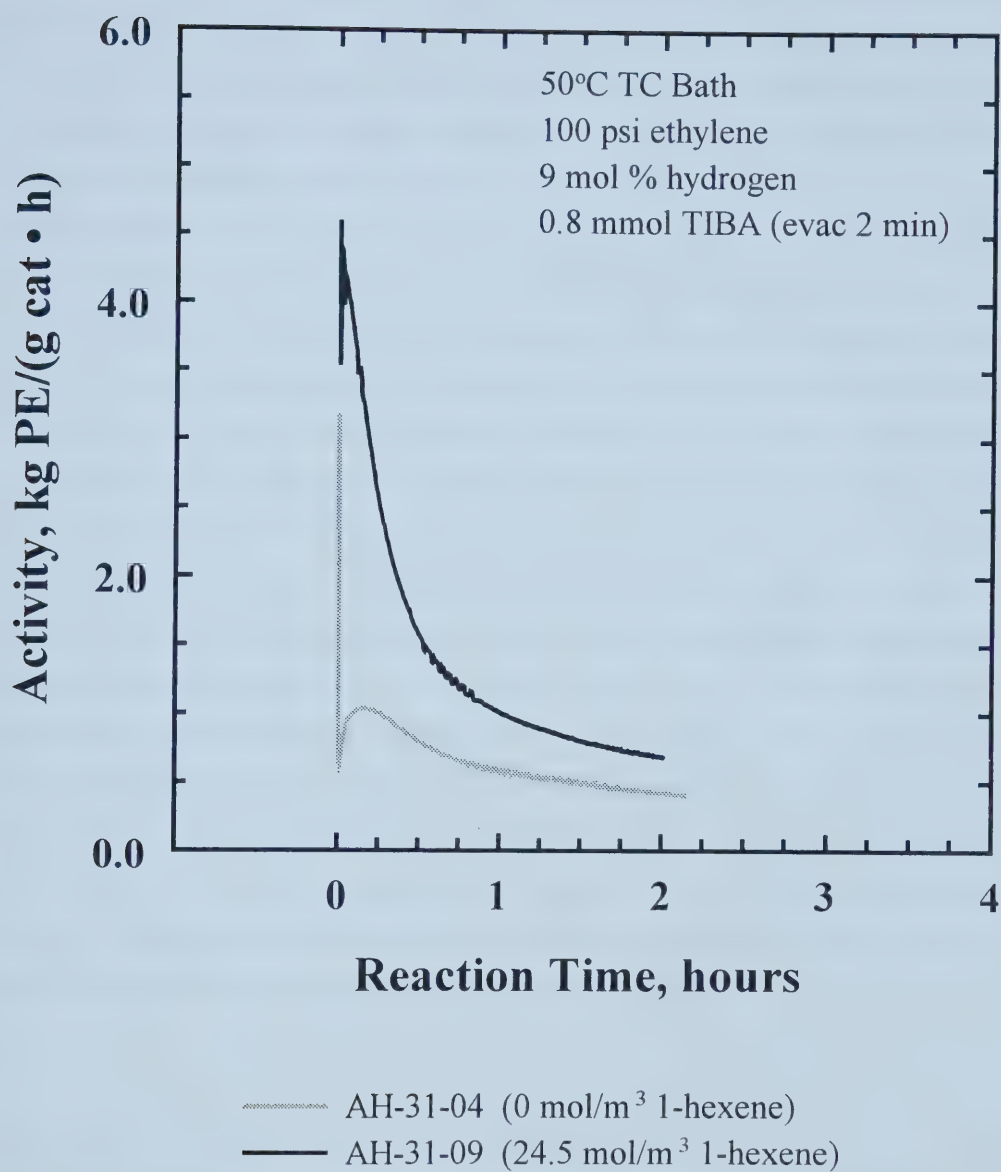
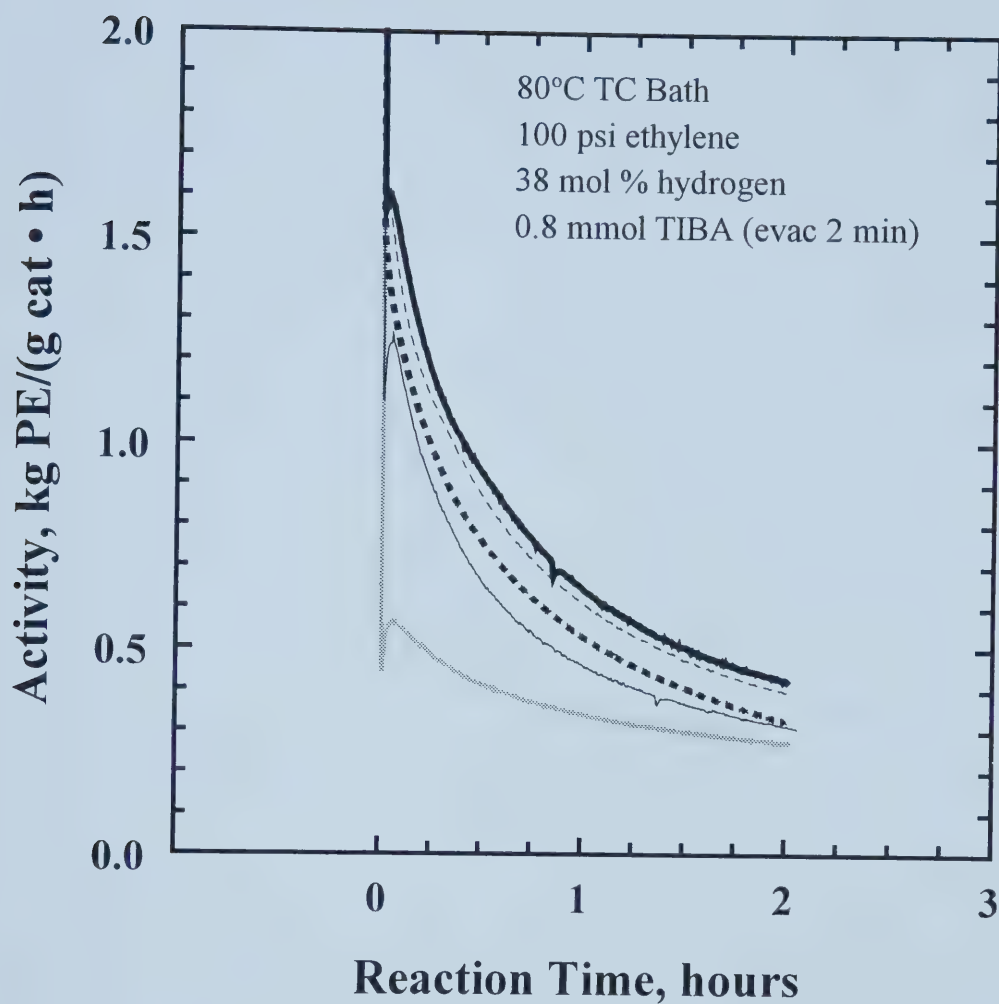


Figure 4.36. Activity profiles showing effect of 1-hexene with hydrogen.

A series of experiments was performed with different 1-hexene concentrations for both the Ti-Mg polyphenoxide and Ti-Mg silica catalysts, and hydrogen was used in the ethylene/1-hexene copolymerization experiments to control molar masses. The 1-hexene concentration is reported on the basis of the volume of 1-hexene fed to the 1 L reactor at the start of the experiment. Although there were deviations from the trends probably due to irreproducible catalyst injection, the activity generally increased as the 1-hexene concentration increased up to a certain point for both the Ti-Mg polyphenoxide (Figure 4.37) and Ti-Mg silica (Figure 4.38) catalysts. At the higher 1-hexene concentrations of 50-60 mol/m³ corresponding to the injection of about 6-7 mL 1-hexene, there were smaller differences in the rate of activation for both catalysts. The 1-hexene vapour pressure for these runs might have been similar because some 1-hexene could have condensed on the colder reactor surfaces such as the top flange and hollow mixer shaft. During the 1-hexene calibration (refer to Section 3.3.2), it was observed that the 1-hexene peak area in the gas chromatogram did not change appreciably above 4 mL likely because some 1-hexene condensed in the sampling valve and tubing, which were at room temperature. The activity profiles for the Ti-Mg silica catalyst seemed to have a second maximum just before the one-hour mark for the two experiments with higher 1-hexene concentrations (AH-33-09 and AH-33-14), but this behaviour was not observed for the Ti-Mg polyphenoxide catalyst. This observation could indicate the two catalysts have different types of active sites with different responses for 1-hexene incorporation.

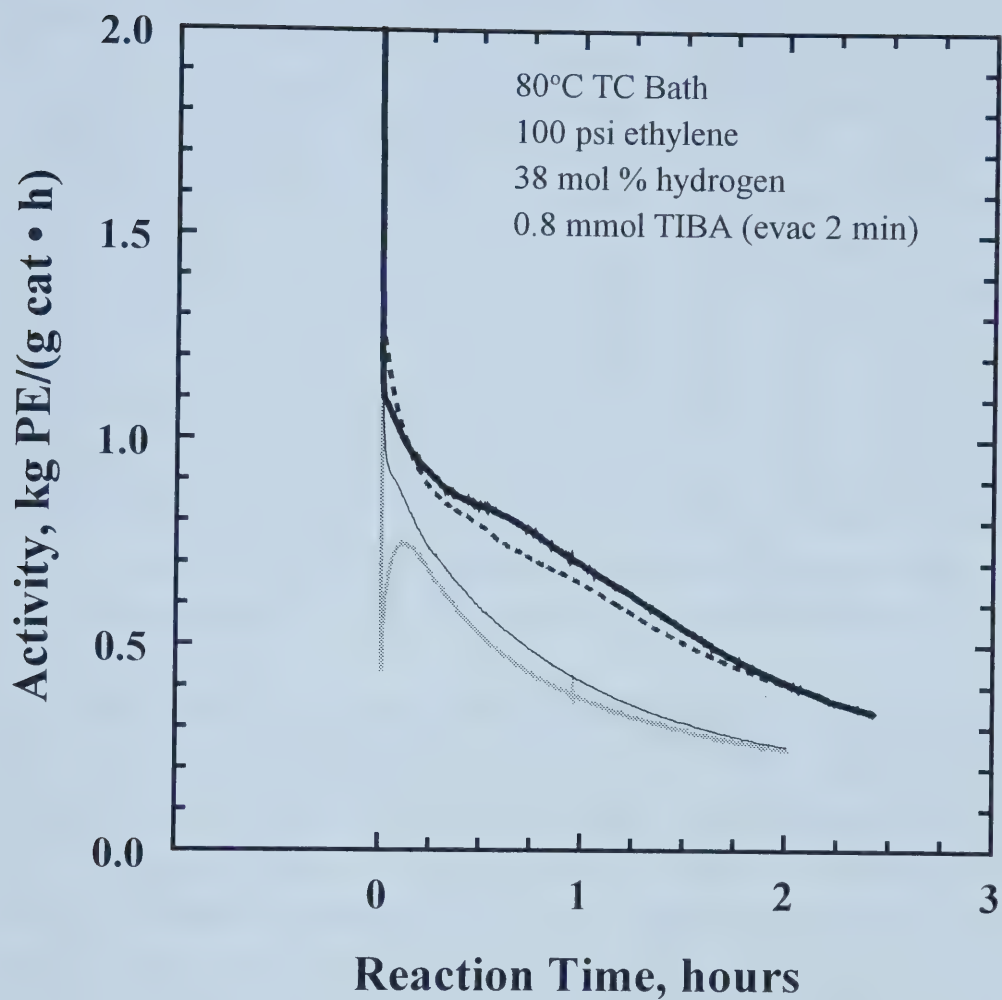
4.9.2 Effect of 1-Hexene Concentration on Molar Mass

Table 4.5 gives the molar masses for homopolymer and copolymer samples produced with about 2.85 mL (24.0 mol/m³) 1-hexene at different hydrogen concentrations.



- AH-32-08 (0 mol/m³ 1-hexene)
- AH-32-05 (16.7 mol/m³ 1-hexene)
- AH-32-07 (33.7 mol/m³ 1-hexene)
- AH-32-04 (50.3 mol/m³ 1-hexene)
- AH-32-06 (58.3 mol/m³ 1-hexene)

Figure 4.37. Activity profiles for the Ti-Mg polyphenoxide catalyst at different 1-hexene concentrations.



- AH-33-11 (17.5 mol/m³ 1-hexene)
- AH-33-13 (33.3 mol/m³ 1-hexene)
- AH-33-09 (49.8 mol/m³ 1-hexene)
- AH-33-14 (58.8 mol/m³ 1-hexene)

Figure 4.38. Activity profiles for the Ti-Mg silica catalyst at different 1-hexene concentrations.

Table 4.5: Molar Masses of Copolymers Produced with Hydrogen.

Run ID ^a	H ₂ Concentration (mol %)	SEC Results		
		Mn ($\times 10^{-3}$)	Mw ($\times 10^{-3}$)	PD
AH-31-02	0	450	1117	2.5
AH-31-06	5	97	325	3.4
AH-31-04	9	84	298	3.6
AH-31-09 ^b	9	47	191	4.1
AH-31-07	17	49	201	4.1
AH-31-11 ^b	17	33	145	4.1
AH-31-05	29	33	147	4.5
AH-31-10 ^b	29	21	96	4.5
AH-31-12 ^b	37	17	80	4.7

a All runs performed with bimetallic polyphenoxide catalyst Ti/Mg/Ligand/Silica

b Copolymerization with ~2.85 mL 1-hexene (no 1-hexene for other polymers)

The weight average molar masses (Mw) were lower for the ethylene/1-hexene copolymer samples, but hydrogen had a more dramatic effect in reducing molar masses. Table 4.6 gives the molar masses for polymer samples produced with 38 mole % hydrogen at different 1-hexene concentrations. In general, the molar masses for both the catalysts decreased as the 1-hexene concentration increased. The polydispersities for the Ti-Mg polyphenoxide samples were lower than those for the corresponding Ti-Mg silica samples, which suggested there were differences in the ratio or types of active sites with respect to their response to 1-hexene. Two experiments (AH-32-09 and AH-33-10) were performed with a shorter polymerization time of 30 minutes compared to the usual 2-hour duration. Comparing the molar mass results for the 30-minute experiments to the corresponding 2-hour experiments (AH-32-04 and AH-33-09), it can be seen that the 30-minute experiments produced polymer with lower molar masses, which is an indication that both catalysts have multiple types of active sites. Some active sites could incorporate 1-hexene into the growing polymer chain at the start of

polymerization then these sites could become deactivated as polymerization proceeds thus resulting in less comonomer incorporation at longer times into the experiments.

Table 4.6: Molar Masses for Ethylene/1-Hexene Copolymers.

Run ID	Catalyst Type ^a	Initial 1-Hexene Conc. (mol/m ³) ^b	SEC Results ^c		
			Mn (x10 ⁻³)	Mw (x10 ⁻³)	PD
AH-32-08	Ligand	0.0	17	93	5.6
AH-32-05	Ligand	16.8	15	70	4.8
AH-32-07	Ligand	33.7	14	66	4.7
AH-32-09 ^d	Ligand	51.3	10	52	5.2
AH-32-04	Ligand	50.3	11	56	5.1
AH-32-06	Ligand	58.4	11	55	4.8
AH-33-11	Silyloxide	17.5	13	77	5.8
AH-33-13	Silyloxide	23.6	13	67	5.4
AH-33-10 ^d	Silyloxide	51.7	10	53	5.6
AH-33-09 ^e	Silyloxide	49.8	15	94	6.1
AH-33-14	Silyloxide	58.8	12	61	5.1

a Ligand for Ti/Mg/Ligand/Silica catalyst and Silyloxide for Ti/Mg/Silica catalyst

b 1-Hexene concentration based on 0.95 L internal reactor volume

c Polymerization performed with 38 mole % hydrogen

d Polymerization time of 0.5 hours

e Polymerization time of 2.4 hours

4.9.3 1-Hexene Consumption During Polymerization

On-line GC sampling of the reactor gas stream was performed at regular intervals for two experiments (AH-29-07 and AH-30-07). The reactor gas was sampled at a flow rate between 20-30 mL/min through the GC sampling port on the reactor. The 1-hexene concentrations were calculated using a response factor of 4.3 for the ratio of 1-hexene peak area to ethylene peak area (refer to Figure 3.13 in Section 3.3.2).

Figures 4.39 and 4.40 show the concentration results relative to the activity profiles. The activity profiles show small increases in activity at the sampling times because the ethylene flow rate increased when the sample valve was open to the GC. The first measured 1-hexene concentration in AH-29-07 was outside the calibration range (maximum 10 mole % 1-hexene) so this concentration value is not reliable. For both experiments, most of the 1-hexene seemed to be consumed at the start of the experiments; however, 1-hexene is soluble in polyethylene (Moore, 2001) so there could just be more 1-hexene adsorbed into the polymer as polymerization progressed. Most importantly, 1-hexene was detected at the end of the experiments despite the high productivities. There was concern that all the 1-hexene would be consumed during the 2-hour experiments resulting in the production of a homopolymer fraction.

4.9.4 1-Hexene Incorporation

The TREF profiles, which are plots of polymer concentration versus elution temperature, were examined to evaluate the degree of comonomer incorporation. TREF profiles for common types of polyethylene have been characterized in the literature (Kelusky et al., 1987). There can be narrow peaks for homogeneous polymers or broad distributions for polymer chains with varying degrees of short-chain branching. High-density polyethylene samples typically have narrow peaks centered around 100°C while the short-chain branching distributions for ethylene/1-hexene copolymers can be broad and extend below elution temperatures of 40°C; polymer with lower crystallizability elutes at lower temperatures indicating there is more comonomer incorporated into the polymer chains.

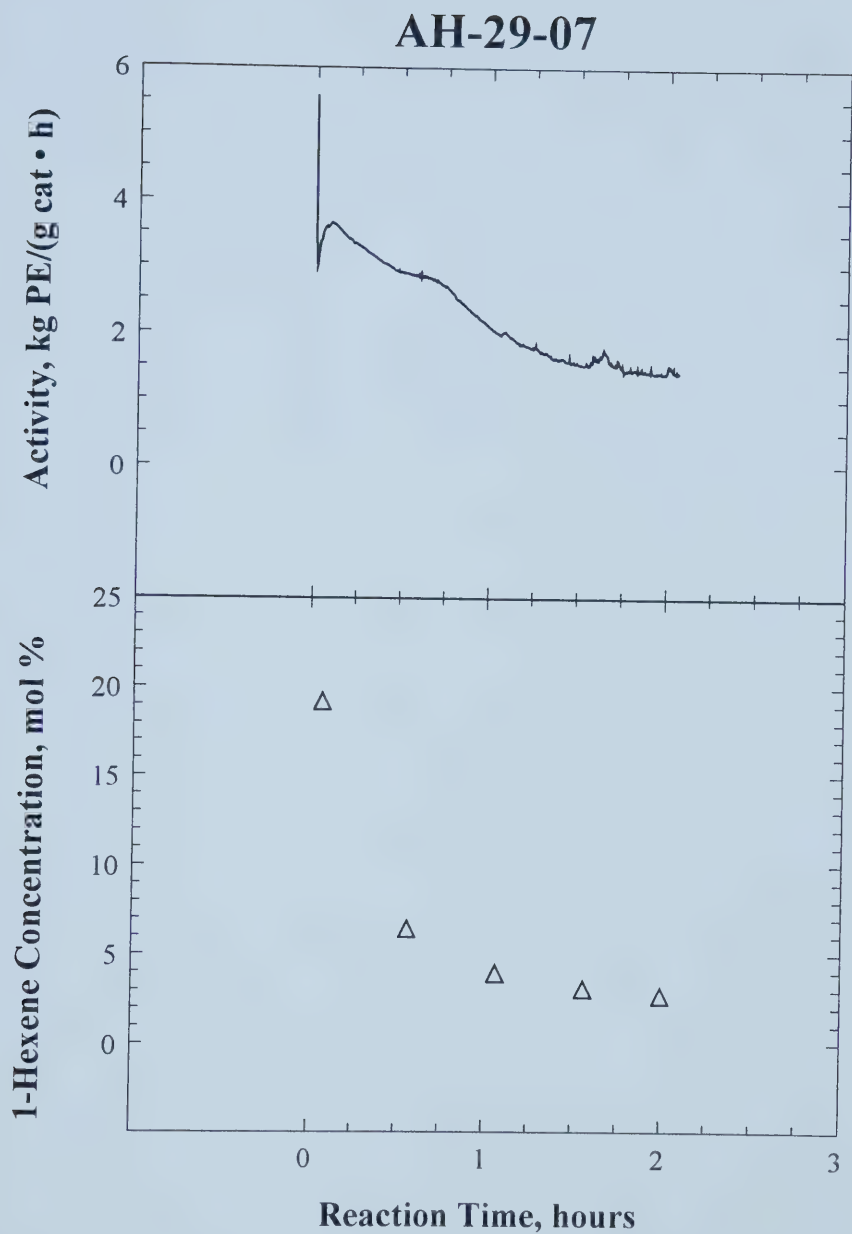


Figure 4.39. 1-Hexene concentration during polymerization for AH-29-07.

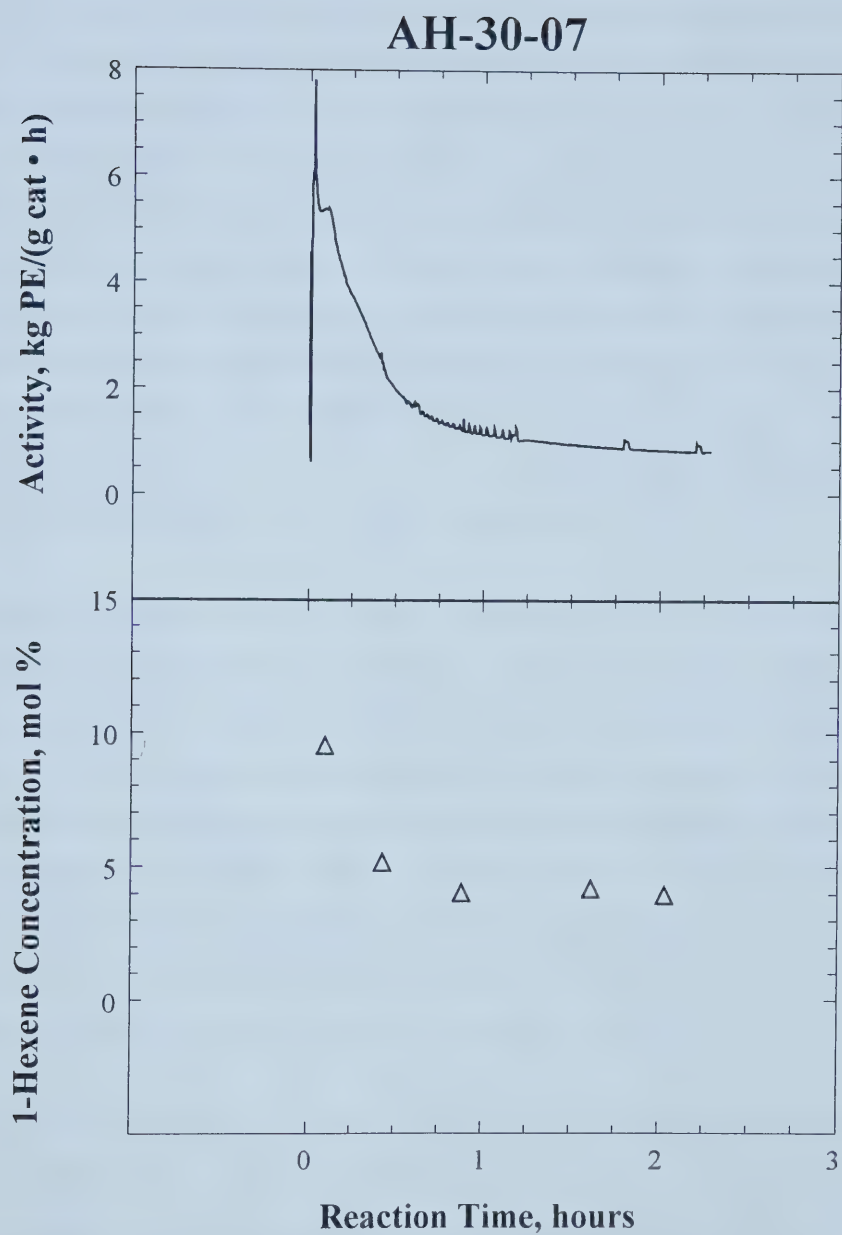


Figure 4.40. 1-Hexene concentration during polymerization for AH-30-07.

Figure 4.41 compares the TREF profiles for the Ti-Mg polyphenoxide catalyst at different hydrogen concentrations with an initial 1-hexene concentration of 24 ± 2 mol/m³ in the reactor; the IR signal was normalized to make relative comparisons between the different samples. All the polyethylene should elute below about 105°C, but the TREF profiles for the lower hydrogen concentrations (9 and 17 mole %) showed peaks at higher temperatures. The samples for AH-31-09 and AH-31-11 had higher molar masses (see Table 4.5) because lower hydrogen concentrations (9 mole % and 17 mole %, respectively) were used so the solvent likely swelled the polymer and the solution did not elute until higher temperatures were reached. High quality TREF profiles were collected for samples produced at higher hydrogen concentrations (AH-31-10 and AH-31-12) so all subsequent ethylene/1-hexene copolymers were produced with the 38 mole % hydrogen.

To permit a wide range of 1-hexene concentrations, the ethylene/1-hexene copolymerization experiments were performed at 80°C. The TREF profiles for the Ti-Mg polyphenoxide catalyst at different 1-hexene concentrations are given in Figure 4.42. The homopolymer sample AH-32-08 was analyzed for comparison purposes; however, the appearance of the TREF profile indicated there was swelling of the polymer by the eluting solvent. Similarly, Figure 4.43 shows the TREF profiles for the Ti-Mg silica catalyst for the same range of 1-hexene concentrations. In general, all the ethylene/1-hexene copolymers for both catalysts had a large homopolymer fraction as evident by the peak centered around 100°C.

The short-chain branching distributions for the copolymer samples were determined from the TREF results. The methylene sequence distribution was obtained using a correlation between elution temperature (T) and methyl group concentration ($[\text{CH}_3]_T$) (Kumkaew et al., 2003). Equation (5) was used to calculate the average concentration of CH_3 per 1000 carbon atoms (Cn) as a function of elution time (t) or elution temperature (T) with the time-varying output of the IR cell $(\text{IR})_{\text{signal}}$ during elution.

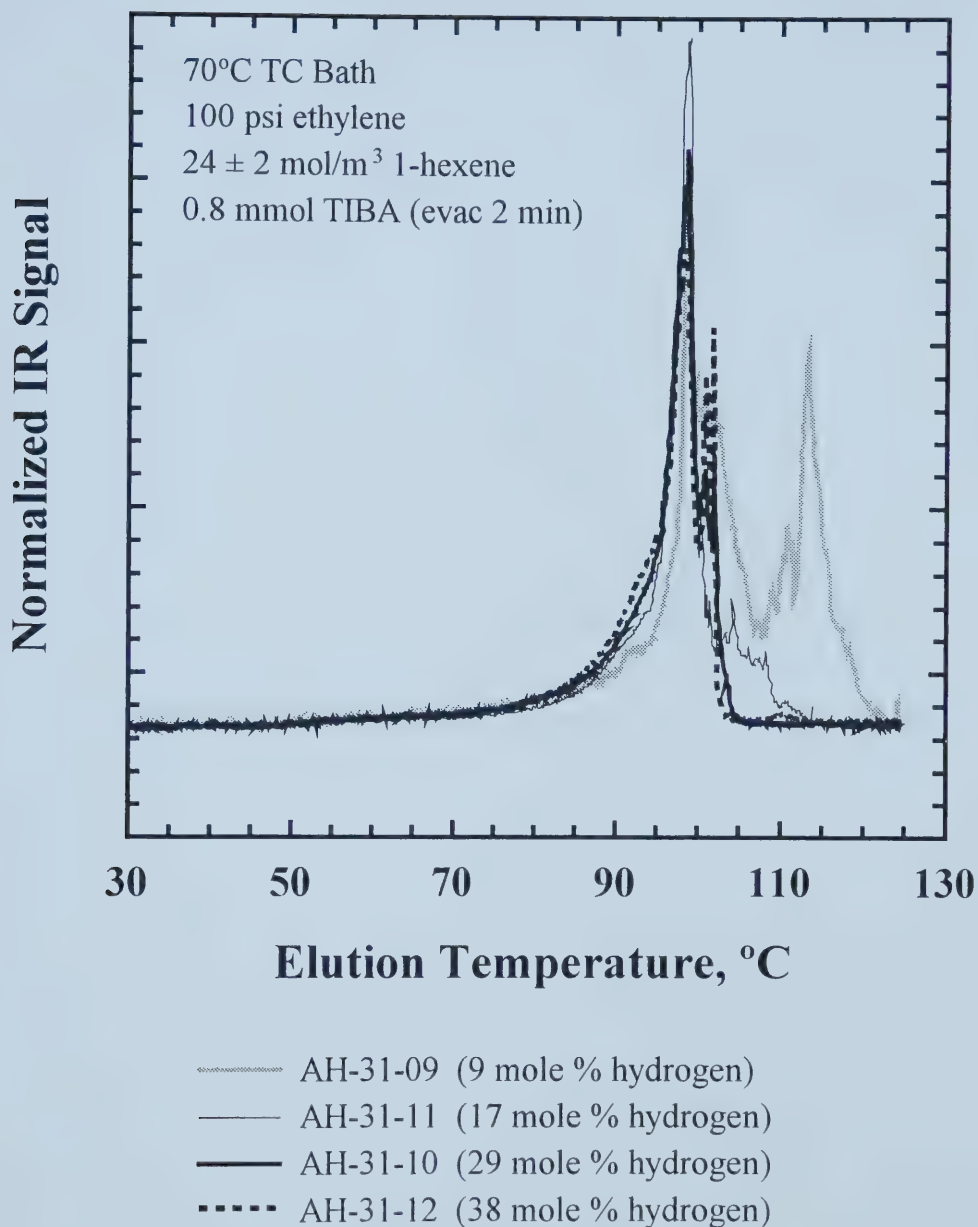


Figure 4.41. TREF profiles for the Ti-Mg polyphenoxide catalyst at different hydrogen concentrations.

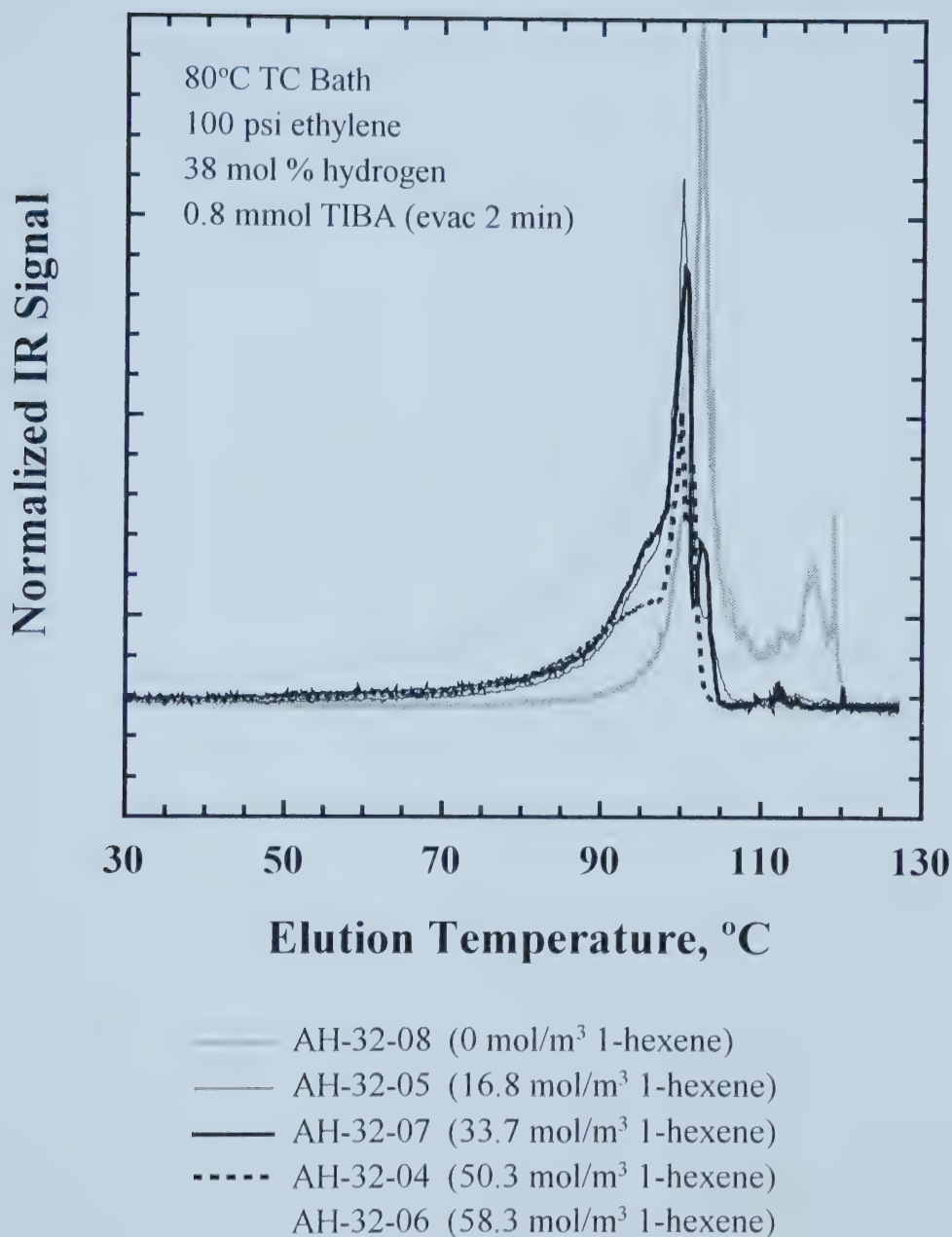


Figure 4.42. TREF profiles for the Ti-Mg polyphenoxide catalyst at different 1-hexene concentrations.

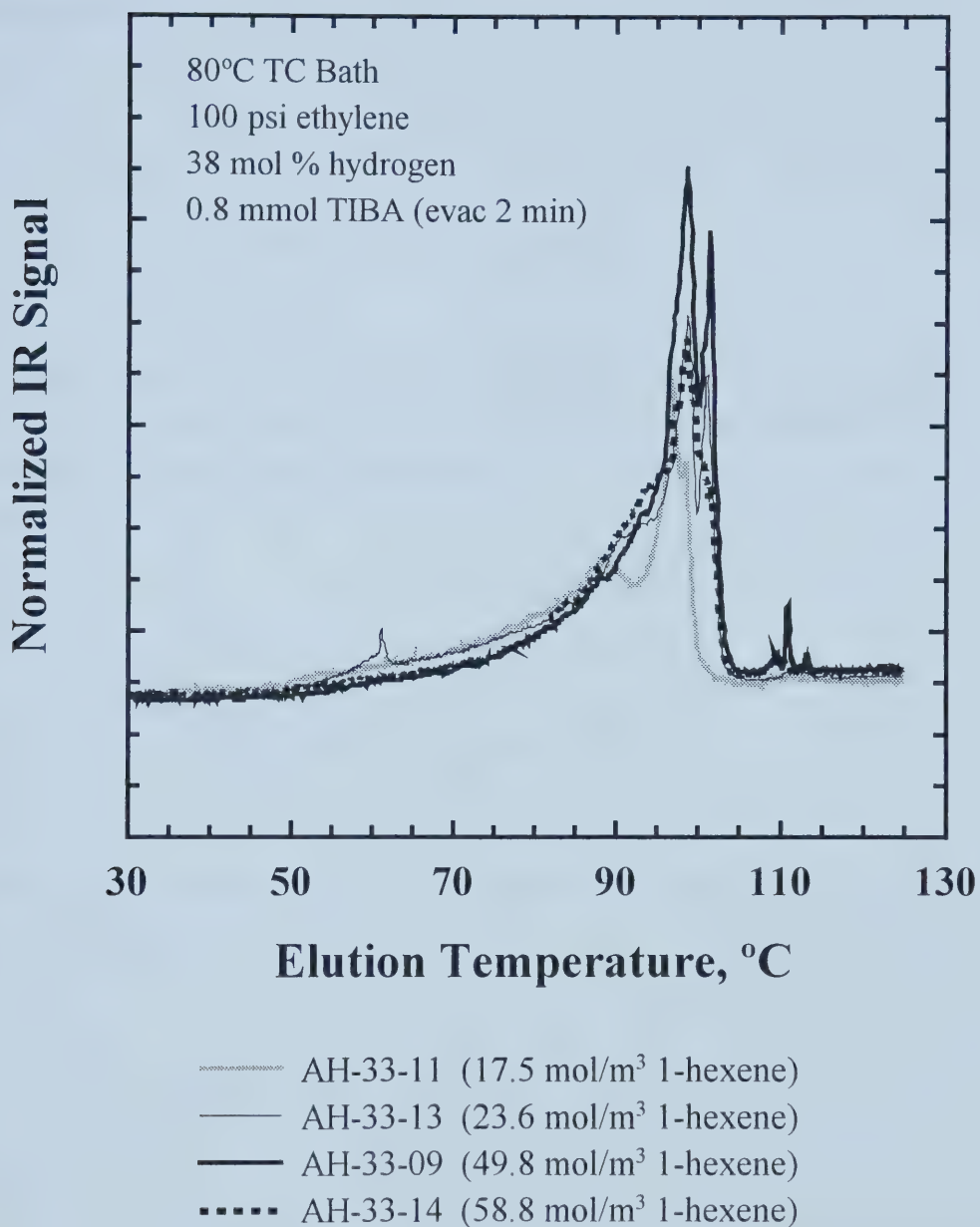


Figure 4.43. TREF profiles for the Ti-Mg silica catalyst at different 1-hexene concentrations.

Appendix D contains more details about the correlation for methylene sequence distribution as well as the individual TREF profiles for the polymer samples.

$$Cn = \frac{\int_{t_0}^{t_f} (IR)_{\text{signal}} [CH_3]_t dt}{\int_{t_0}^{t_f} (IR)_{\text{signal}} dt} = \frac{\int_{T_0}^{T_f} (IR)_{\text{signal}} [CH_3]_T dT}{\int_{T_0}^{T_f} (IR)_{\text{signal}} dT} \quad (5)$$

The elution temperature can be substituted for the elution time because temperature was a linear function of time. The ratio of Cw/Cn gives an indication of the distribution of methyl group concentrations in the sample with Cw defined in Equation (6).

$$Cw = \frac{\int_{t_0}^{t_f} (IR)_{\text{signal}} [CH_3]_t^2 dt}{\int_{t_0}^{t_f} (IR)_{\text{signal}} [CH_3]_t dt} = \frac{\int_{T_0}^{T_f} (IR)_{\text{signal}} [CH_3]_T^2 dT}{\int_{T_0}^{T_f} (IR)_{\text{signal}} [CH_3]_T dT} \quad (6)$$

Homopolyethylene is eluted above 90.5°C so the fraction of homopolymer (F_{HOMO}) is given by Equation (7).

$$F_{\text{HOMO}} = \frac{\int_{90.5}^{T_f} (IR)_{\text{signal}} [CH_3]_T dT}{\int_{T_0}^{T_f} (IR)_{\text{signal}} dT} \quad (7)$$

Table 4.7 lists the short-chain branching distributions for the Ti-Mg polyphenoxide catalyst as a function of hydrogen concentration; there was low 1-hexene incorporation with about 3 CH₃ per 1000 carbon atoms for all the samples. Except

for AH-31-09, the homopolymer fraction decreased slightly as more hydrogen was used in the polymerization experiments likely because some active sites were more sensitive to hydrogen. The pressure profile for AH-31-09 showed that the solvent swelled the polymer during elution from the column (see Appendix D), which could explain the deviation from the trend.

Table 4.7: Methylene Branching in Copolymers Produced with Hydrogen.

Run ID ^{a,b}	H ₂ Concentration (mol %)	CH ₃ Branching Results			
		Cn ^c	Cw ^d	Cw/Cn	F _{HOMO} ^e
AH-31-09	9	3.3	8.8	2.6	0.74
AH-31-11	17	2.9	8.1	2.8	0.84
AH-31-10	29	3.1	7.8	2.6	0.79
AH-31-12	37	3.3	8.8	2.6	0.74

a All runs performed with bimetallic polyphenoxide catalyst Ti/Mg/Ligand/Silica

b Runs performed with ~2.85 mL 1-hexene

c Average concentration of CH₃ groups per 1000 carbon atoms

d This quantity is similar to an average weight concentration of CH₃ groups

e Fraction of polymer eluted above 90.5°C (homopolymer fraction)

The methylene branching distributions were also calculated for the Ti-Mg polyphenoxide and Ti-Mg silica catalysts for different initial 1-hexene concentrations (Table 4.8). Both catalysts had a similar extent of methylene branching (about 3-7 CH₃ per 1000 carbon atoms), but the trends with 1-hexene concentration were opposite. For higher initial 1-hexene concentrations, the CH₃ branching increased for the Ti-Mg polyphenoxide catalyst but decreased for the Ti-Mg silica catalyst. Also, polymer produced with the Ti-Mg polyphenoxide catalyst had lower homopolymer fractions for higher initial 1-hexene concentrations. Conversely, the homopolymer fraction increased for higher initial 1-hexene concentrations with the Ti-Mg silica catalyst. These results suggested that the two catalysts likely have different ratios or types of active sites that controlled 1-hexene incorporation.

The 30-minute polymerization experiments (AH-32-09 and AH-33-10) had lower homopolymer fractions than the corresponding >2-hour experiments (AH-32-04 and AH-33-09), which is an indication that both catalysts have multiple types of active sites. It is likely some sites incorporated 1-hexene into the growing polymer chain at the start of polymerization then these sites became deactivated as polymerization progressed resulting in less comonomer incorporation at longer polymerization times.

Table 4.8: Methylene Branching in Ethylene/1-Hexene Copolymers.

Run ID ^a	Catalyst Type ^b	Initial 1-Hexene Conc. (mol/m ³) ^c	CH ₃ Branching Results			
			Cn ^d	Cw ^e	Cw/Cn	F _{HOMO} ^f
AH-32-05	Ligand	16.8	3.2	7.3	2.3	0.73
AH-32-07	Ligand	33.7	4.3	10.7	2.5	0.68
AH-32-09 ^g	Ligand	51.3	6.4	12.4	1.9	0.48
AH-32-04	Ligand	50.3	4.7	10.5	2.2	0.62
AH-32-06	Ligand	58.4	5.4	11.6	2.2	0.58
AH-33-11	Silyloxide	17.5	6.4	13.2	2.1	0.51
AH-33-13	Silyloxide	33.3	5.5	11.7	2.1	0.63
AH-33-10 ^g	Silyloxide	51.7	5.9	11.8	2.0	0.49
AH-33-09 ^h	Silyloxide	49.8	3.4	8.6	2.5	0.78
AH-33-14	Silyloxide	58.8	4.1	9.8	2.4	0.56

a Polymerization performed with 38 mole % hydrogen

b Ligand for Ti/Mg/Ligand/Silica catalyst and Silyloxide for Ti/Mg/Silica catalyst

c 1-Hexene concentration based on 0.95 L internal reactor volume

d Average concentration of CH₃ groups per 1000 carbon atoms

e This quantity is similar to an average weight concentration of CH₃ groups

f Fraction of polymer eluted above 90.5°C (homopolymer fraction)

g Polymerization time of 0.5 hours

h Polymerization time of 2.4 hours

4.10 SEM of Polymer Samples

SEM images were collected for two polymer samples (AH-20-01 and AH-20-02). There was no observable difference between the particle morphology for ethylene homopolymer and ethylene/1-hexene copolymer samples.

Figures 4.44 and 4.47 show there was a wide distribution of polymer particle sizes, and the particles were irregularly shaped with no well-structured morphology. The image in Figure 4.45, which gives a closer view of outer surface features, was representative of all particles examined. Overall, the particles appeared to be porous and it seemed the particles fractured to form a network of cracks between the denser sections of polymer as polymerization progressed. Figure 4.46, which shows a higher magnification view inside a crack, revealed that the denser sections consisted of tendrils of polymer interconnected by thin fibers.

The silica fractured during polymerization to give irregularly shaped particles, and the salt crystals provided a secondary surface to influence polymer particle morphology. It was previously mentioned that some salt crystals remained in the polymer samples even though they were rinsed repeatedly with copious amounts of water. Figures 4.48 and 4.49 show that thin layers of polymer grew around the salt crystals or out of imperfections in the lattice.

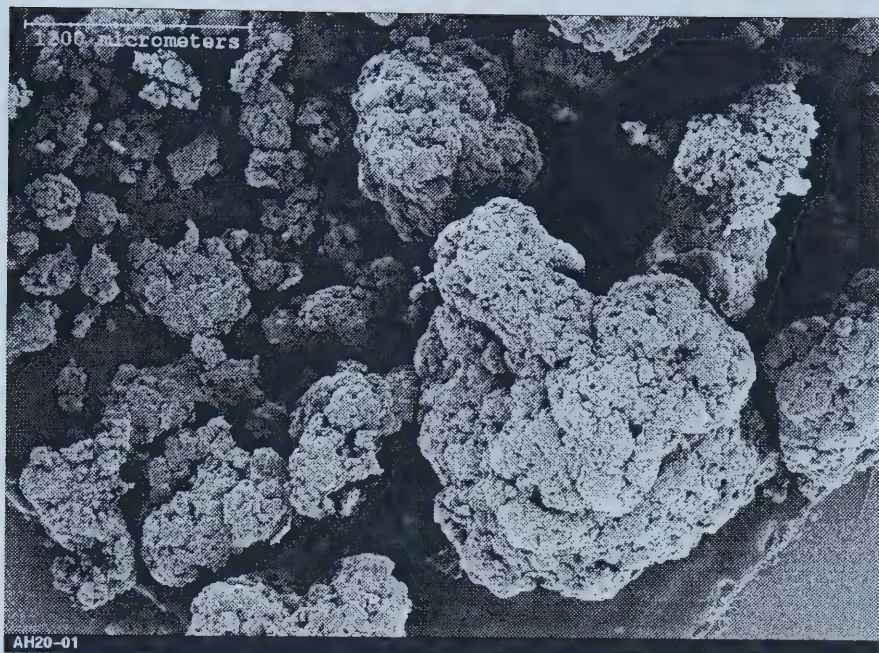


Figure 4.44. SEM picture showing view of many particles.

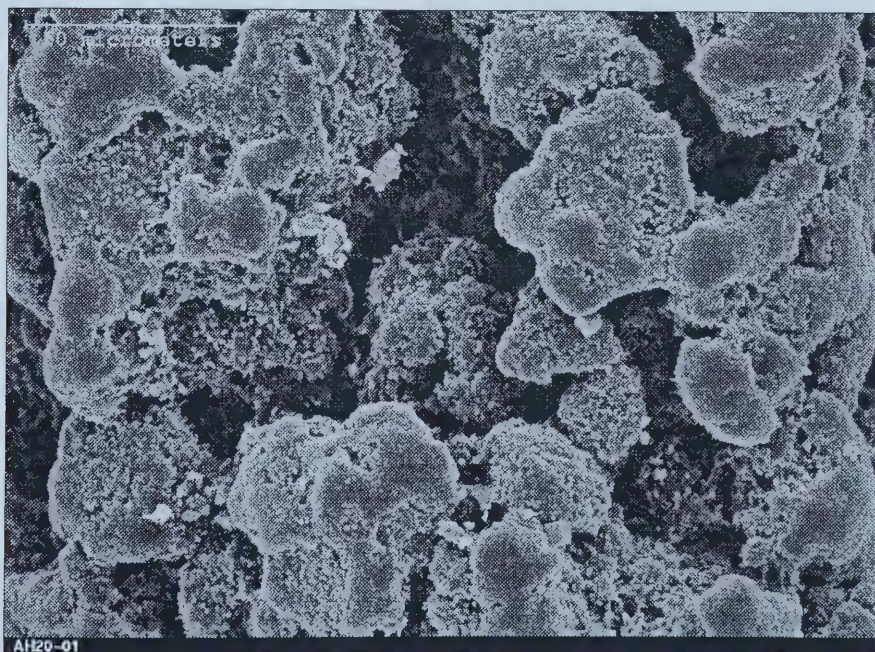


Figure 4.45. SEM picture showing outer surface of one particle.

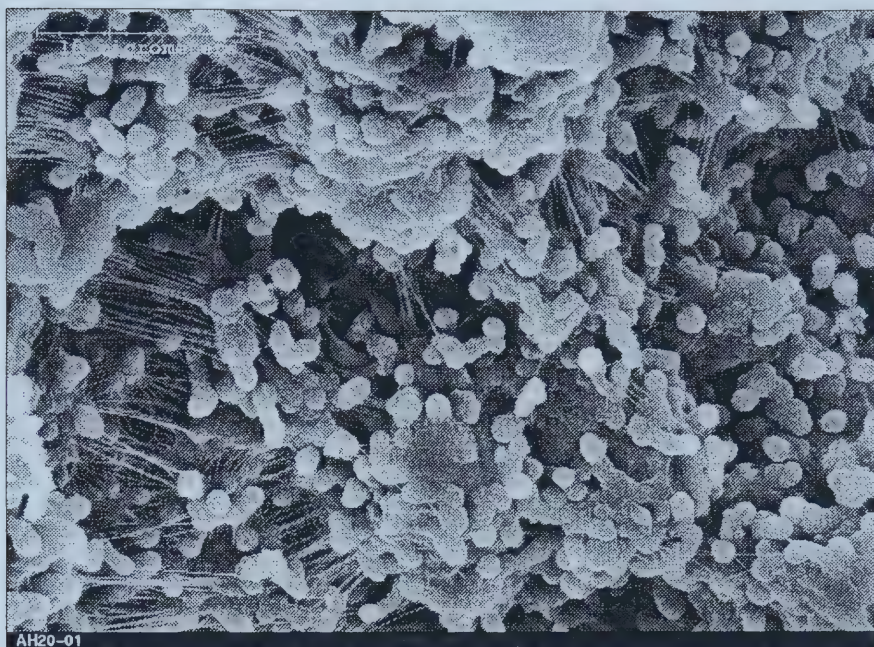


Figure 4.46. SEM picture showing inner structure of one particle.

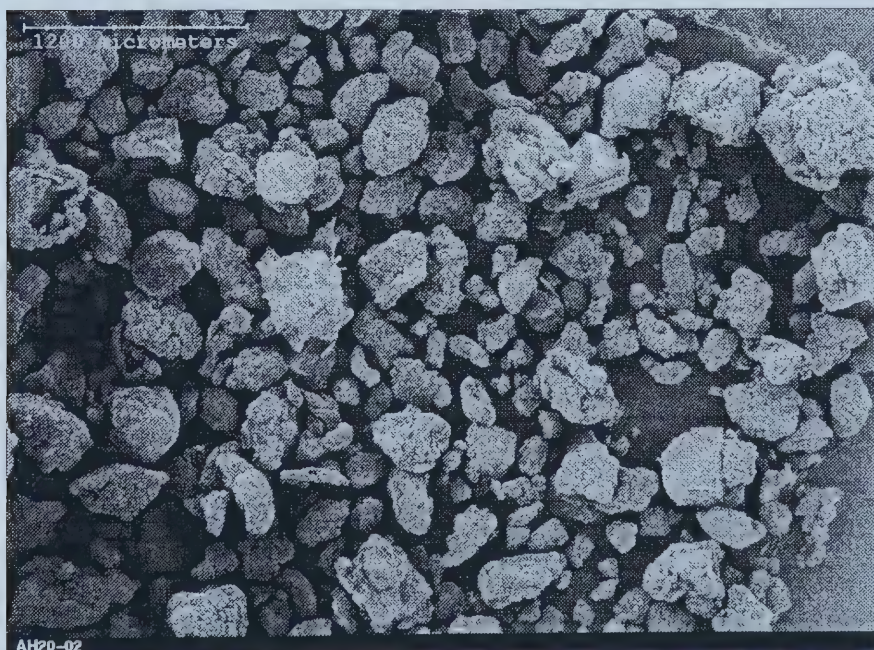


Figure 4.47. SEM picture showing view of many particles.

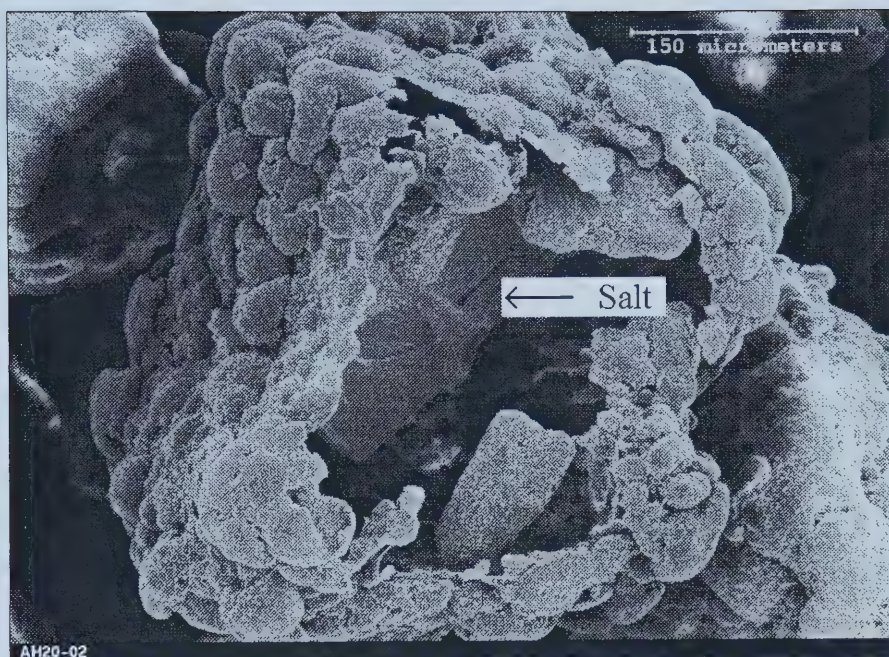


Figure 4.48. SEM picture showing partially dissolved salt crystal.

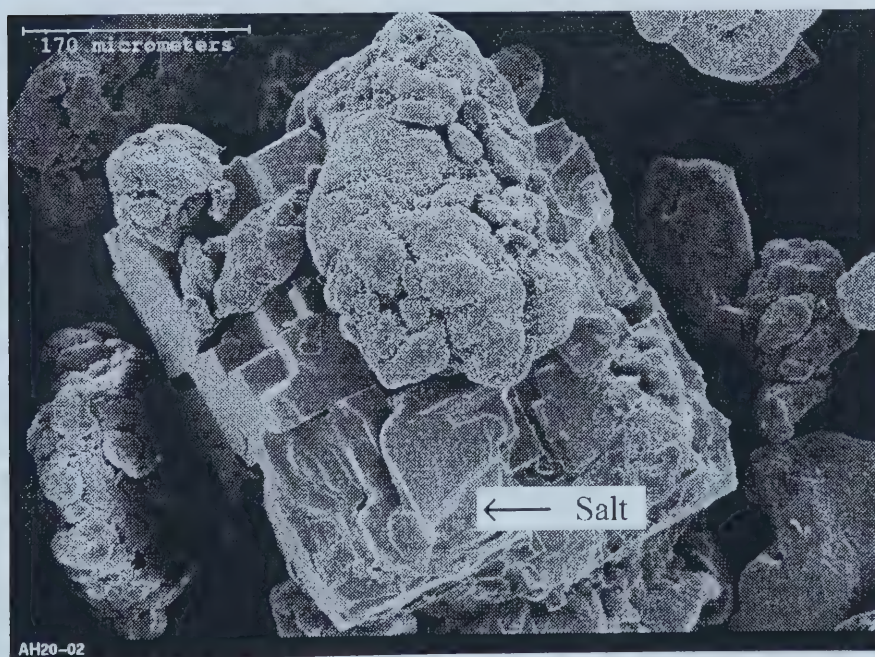


Figure 4.49. SEM picture showing polymer growth on a salt crystal.

5.0 CATALYST CHARACTERIZATION

Surface areas and pore size distributions for the support and catalysts were determined by nitrogen adsorption. The BET measurements were informative because monomer diffusion is affected by pore size (Muñoz-Escalona et al., 1990); deposition of the catalyst components on the support could create many small pores that would likely not be accessible to monomers during polymerization. Particle sizes were also measured because it was desirable to assess whether the thermal treatment affected the silica particle size because sintering was possible at temperatures exceeding 500°C (Ullmann's Encyclopedia of Industrial Chemistry, 1993). The titanium, magnesium, and chlorine contents were also determined for many of the catalysts. The Ti/Mg ratio was useful in explaining polymerization activities for the different batches of catalyst as well as evaluating the catalyst preparation conditions.

5.1 Surface Areas and Pore Size Distributions

Surface areas for several thermally treated silica samples (Batches 3, 5, and 6) and two silica-supported catalysts (CAT-32 and CAT-33) were measured by nitrogen adsorption with the BET method; the results are tabulated in Table 5.1. The average surface area for the three thermally treated silica samples was about 300 m²/g; the variation between the different batches was within experimental error and likely not the result of the differences in heating time because there was no trend in the surface areas with heating time. Deposition of the catalyst components did not seem to significantly affect the pore volumes of the support because the surface areas of the two catalysts were similar to that for the thermally treated silica.

The pore size distributions, as determined by the BJH method, were also determined. Figure 5.1 shows the pore size distributions for the three thermally treated silica samples. The pore radii ranged between 30 to 200 Å with a majority of the pore sizes

between 50 to 100 Å; these pore sizes are typical for silica gel (Ullmann's Encyclopedia of Industrial Chemistry, 1993).

Table 5.1. Surface Areas for Silica and Catalysts.

Sample ID	Batch ID	Silica Drying Conditions	Surface Area (m ² /g)
Silica	Batch 3	500°C, 9 h	300
Silica	Batch 5	520°C, 11 h	310
Silica	Batch 6	500°C, 16 h	275
Ti/Mg/Ligand/Silica	CAT-32	520°C, 11 h	320
Ti/Mg/Silica	CAT-33	520°C, 11 h	290

The surface areas of the catalysts were similar to that for the thermally treated silica, but the pore size distributions were different (see Figure 5.2). The catalysts had a wider range of pore sizes than the thermally treated silica; deposition of the catalyst components seemed to create pores with radii <30 Å and >200 Å, but most of the pore radii were still in the range of 50 to 100 Å.

5.2 Particle Size Distributions

Figure 5.3 gives the particle size distributions for several silica samples, both unheated and thermally treated, as determined with the Mastersizer 2000 using the refractive index 1.544 for silica. All the silica samples have particle sizes in the range of 2 to 200 µm, which is the typical distribution for silica gel with a surface area of 300 m²/g (Ullmann's Encyclopedia of Industrial Chemistry, 1993). Overall, the silica samples that were heated to about 500°C for different times had particle size distributions with similar shapes, and there were only slight differences in the mean particle sizes, as listed in Table 5.2. Compared to the unheated silica, the thermally treated silica samples had narrower particle size distributions (see Figure 5.3).

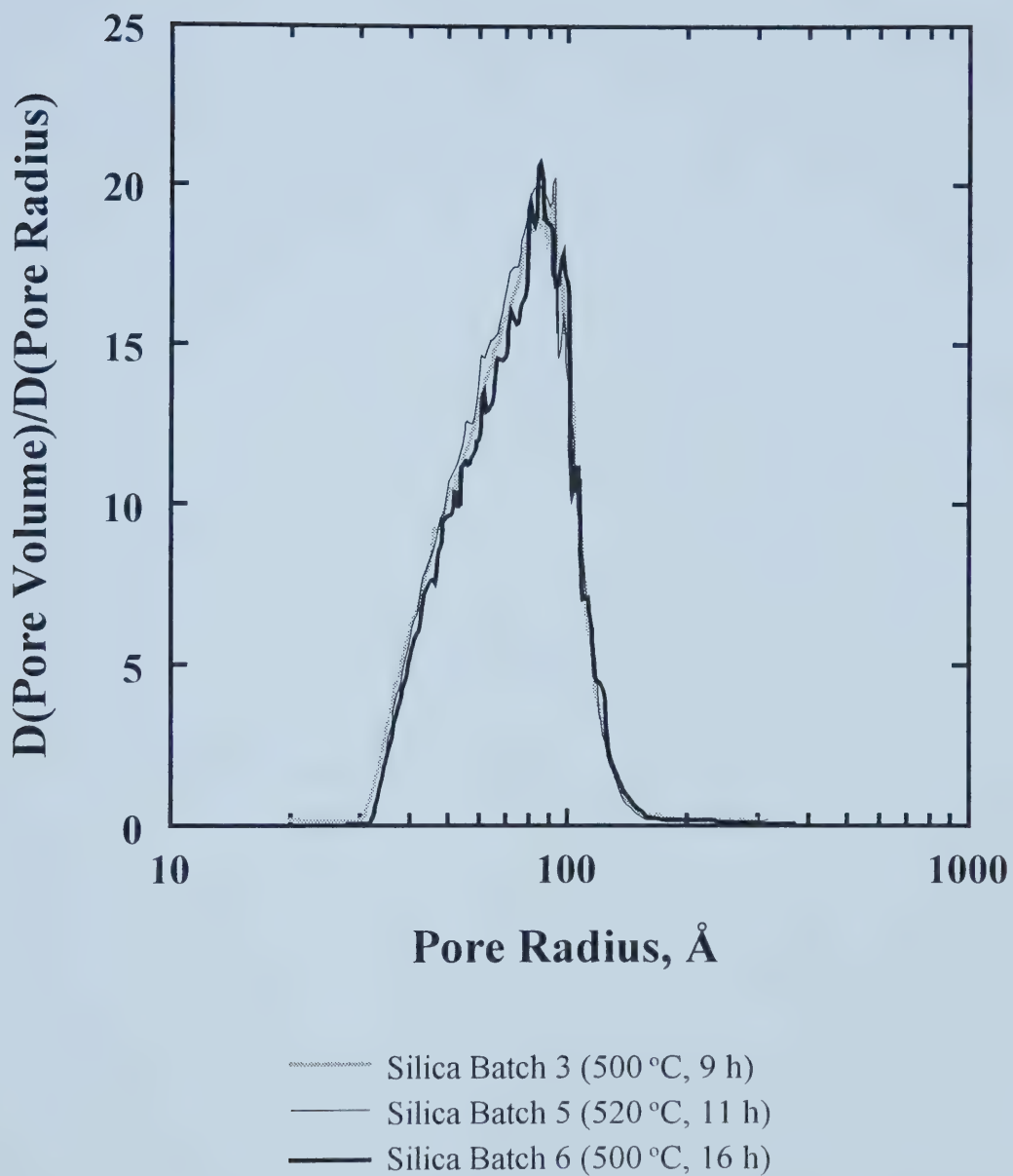


Figure 5.1. Pore size distributions for thermally treated silica.

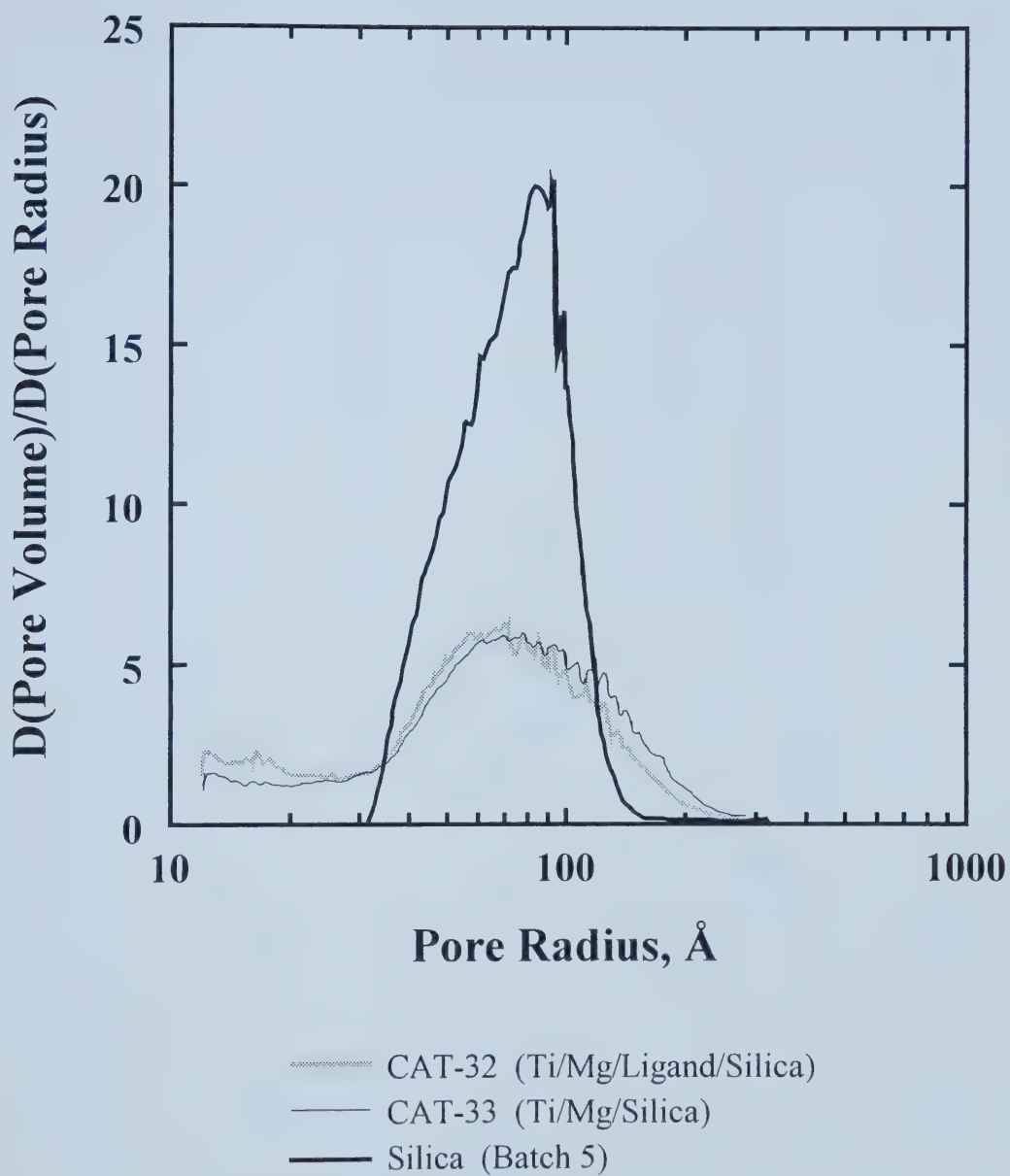
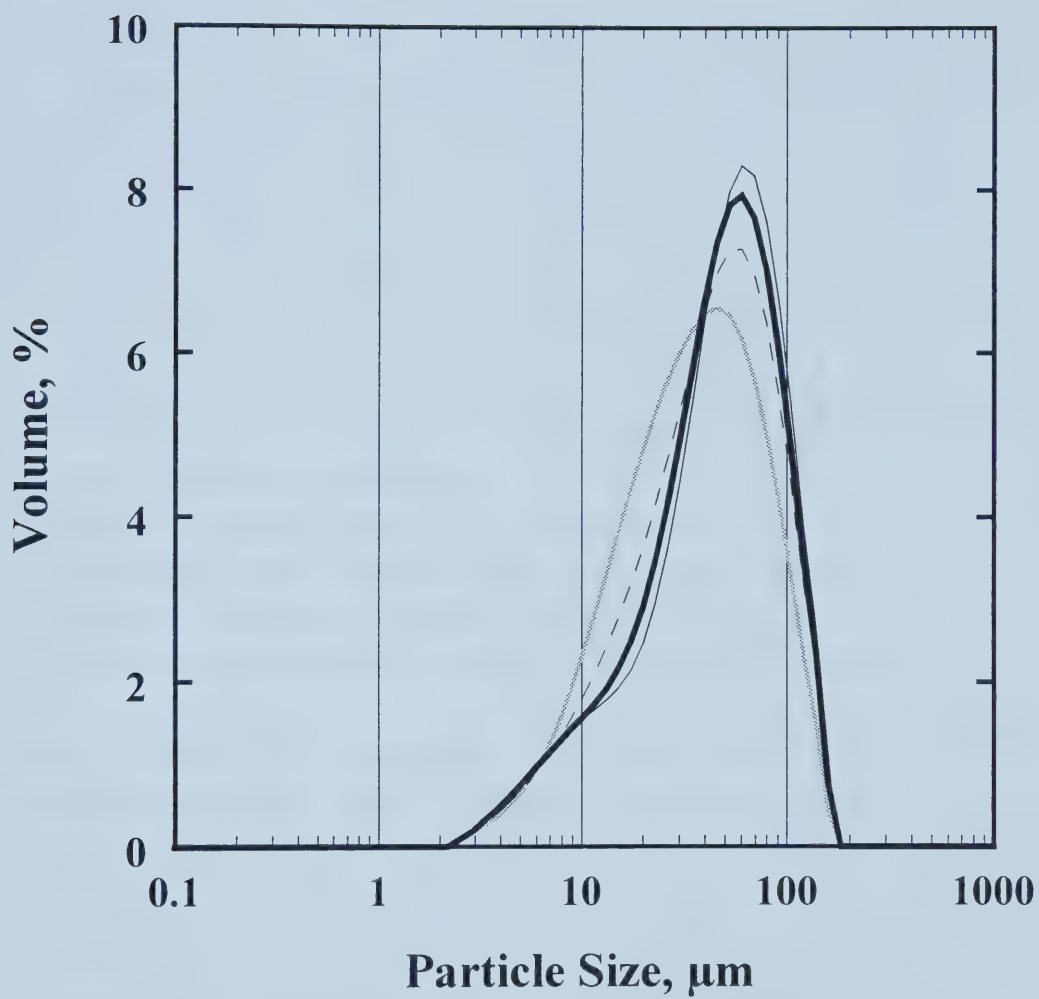


Figure 5.2. Pore size distributions for silica and catalysts.



- Silica (Unheated)
- Silica-Batch 3 (500°C, 9 h)
- Silica-Batch 5 (520°C, 11 h)
- Silica-Batch 6 (500°C, 16 h)

Figure 5.3. Particle size distributions for silica.

Table 5.2: Particle Size Statistics for Silica.

Particle Size Results	Silica (Unheated)	Silica Batch 3 (500°C, 9 h)	Silica Batch 5 (520°C, 11 h)	Silica Batch 6 (500°C, 16 h)
Surface Area ^a , m ² /g	0.277	0.232	0.241	0.250
Vol. Mean ^b , μm	40.851	51.361	49.056	46.651
Surface Mean ^c , μm	21.638	25.874	24.924	23.990
Uniformity ^d	0.683	0.555	0.557	0.619
d(0.1) ^e , μm	10.214	11.318	11.200	10.980
d(0.5) ^e , μm	33.197	46.827	43.832	40.356
d(0.9) ^e , μm	83.56	97.324	94.334	92.184

- a External surface area of the particles
- b Weighted mean particle size based on volume of particles
- c Weighted mean particle size based on external surface area of particles
- d Uniformity of particle size distribution (1 for symmetric distribution)
- e d(#) for particle size including # fraction of total particles in the distribution

Different particle size distributions were also observed for CAT-32 (Ti/Mg/Ligand/Silica) and CAT-33 (Ti/Mg/Silica) as compared to Batch 5 of the thermally treated silica that was used in their preparation (see Figure 5.4). The corresponding statistics for the particle size distributions are given in Table 5.3. The thermally treated silica had a broader particle size distribution than both the catalysts, and larger particle sizes were measured for the bare silica support. Also, CAT-33 (Ti/Mg/Silica) had larger particle sizes than CAT-32 (Ti/Mg/Ligand/Silica), and the distribution for CAT-33 was bimodal; the peak between 2-10 μm is usually attributed to air bubbles in the water but the analysis was repeated to give the same pore size distribution. It was unusual that the thermally treated silica had larger particle sizes than the catalysts. A possible explanation for the observed particle sizes is that the refractive index for silica changed with the incorporation of the catalyst components. In summary, the results only provided a measure of the range of particle sizes.

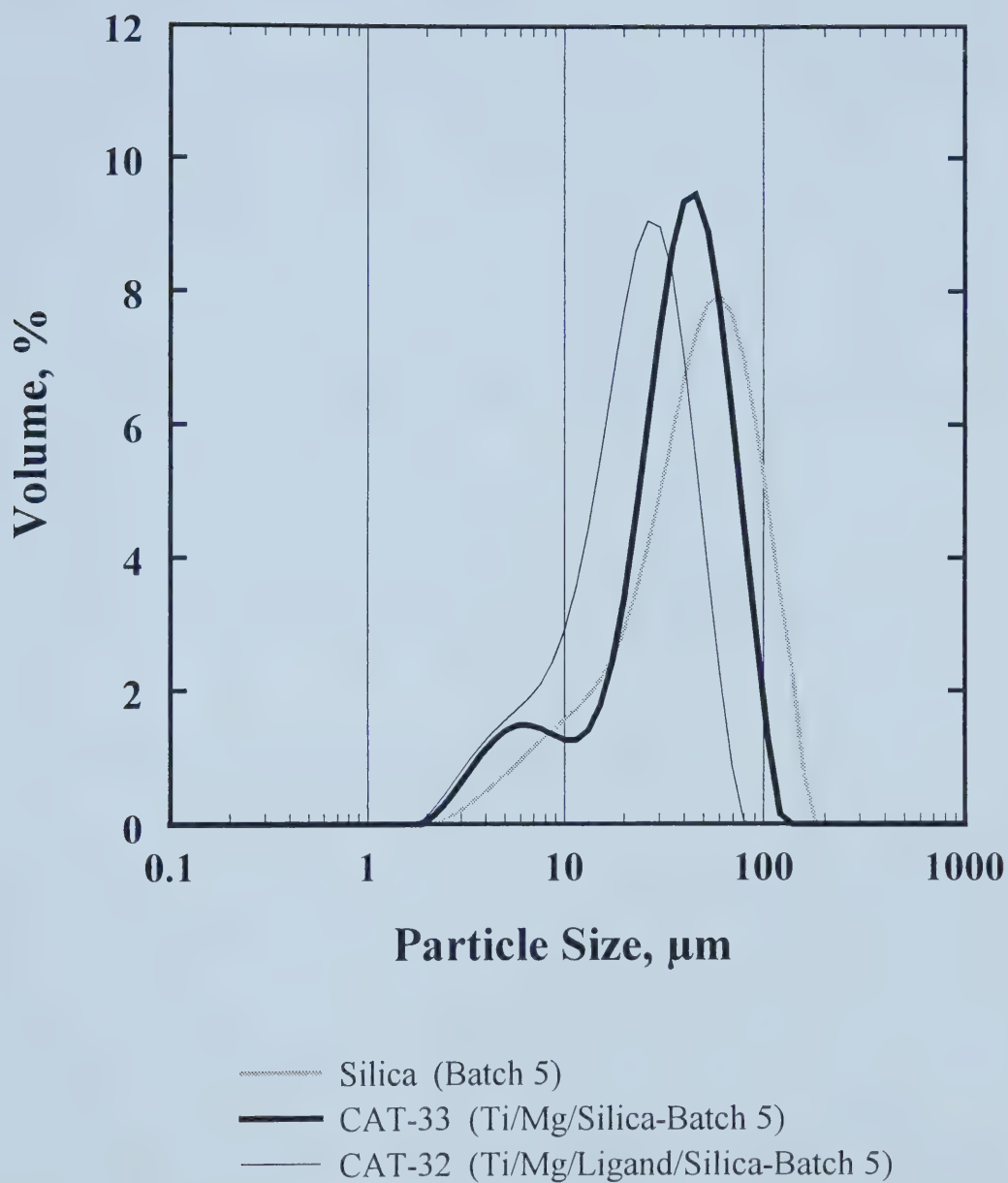


Figure 5.4. Particle size distributions for silica and catalysts.

Table 5.3: Particle Size Statistics for Catalysts.

Particle Size Results	Silica (Batch 5)	Ti/Mg/Silica (CAT-33)	Ti/Mg/Ligand/Silica (CAT-32)
Surface Area ^a , m ² /g	0.241	0.311	0.434
Vol. Mean ^b , μm	49.056	37.255	23.025
Surface Mean ^c , μm	24.924	19.327	13.845
Uniformity ^d	0.557	0.487	0.512
d(0.1) ^e , μm	11.200	7.912	6.501
d(0.5) ^e , μm	43.832	35.238	21.631
d(0.9) ^e , μm	94.334	66.700	41.946

- a External surface area of the particles
- b Weighted mean particle size based on volume of particles
- c Weighted mean particle size based on external surface area of particles
- d Uniformity of particle size distribution (1 for symmetric distribution)
- e d(#) for particle size including # fraction of total particles in the distribution

5.3 Titanium and Magnesium Elemental Analysis

Neutron activation was used in the elemental analysis of the polymerization catalysts; titanium and magnesium contents were measured (see Table 5.4) because the activity is strongly influenced by the Ti/Mg ratio (Muñoz-Escalona et al., 1990). The chlorine content was also determined by INAA (see Table 5.5) as well as calculated from the Ti, Mg data by accounting for the molar ratios of Cl in the catalyst ingredients (i.e. 1 Cl per mole methyl magnesium chloride, 4 Cl per mole titanium (IV) chloride). In addition, catalyst preparation conditions are summarized in Table 5.6 to compare Ti/Mg ratios.

The Mg contents for the different batches of magnesiated catalyst precursor (Mg/Ligand/Silica) were all similar with an average value of about 3.0 wt %. Excess

methyl magnesium chloride was used in catalyst preparation and the silica thermal treatment was performed for different lengths of time. The similarity of the Mg contents between batches of catalyst was encouraging because it showed the catalyst preparation procedures were adequate to ensure reproducibility; unbound magnesium compounds were removed when the catalyst precursor was washed with THF and the different heating times during the silica thermal treatment likely did not significantly alter the silanol content of the support.

Table 5.4: Ti and Mg Contents for the Polymerization Catalysts.

Catalyst Name	Catalyst Components on Silica ^a	Ti wt %	Error ^b	Mg wt %	Error ^b
CAT-12	Ti + Ligand	0.22	0.02	< 0.05	N/A
CAT-13	Ti	0.33	0.02	< 0.05	N/A
CAT-17	Ti + Mg + Ligand	1.78	0.10	3.49	0.14
CAT-19 ^c	Ti + Mg + Ligand	2.8	0.1	Unknown	N/A
CAT-20	Ti + Mg + Ligand	4.95	0.09	3.13	0.08
CAT-22	Ti + Mg + Ligand	4.77	0.14	2.95	0.13
CAT-24	Ti + Mg + Ligand	4.71	0.07	3.10	0.06
CAT-25	Ti + Mg + Ligand	4.92	0.08	2.98	0.07
CAT-26	Ti + Ligand	3.05	0.06	< 0.05	N/A
CAT-28	Ti + Mg + Ligand	4.60	0.07	3.06	0.06
CAT-29	Ti + Mg + Ligand	4.52	0.07	3.00	0.06
CAT-30	Ti + Mg + Ligand	4.42	0.07	3.05	0.06
CAT-31	Ti + Mg + Ligand	3.83	0.07	3.04	0.06
CAT-32	Ti + Mg + Ligand	2.93	0.06	3.14	0.07
CAT-33	Ti + Mg + Silica	2.37	0.05	3.05	0.06
CAT-34	Ti + Mg + Ligand	1.47	0.06	3.55	0.10
CAT-34B	Ti + Mg + Ligand	4.78	0.07	3.11	0.06

a Ti for TiCl₄, Mg for CH₃MgCl, Ligand for tris(2,6-dihydroxyphenyl)ethene

b All uncertainties +/- 1 standard deviation (68% confidence level)

c Ti content determined with colorimetric method (see Appendix A)

Table 5.5: Cl Contents for the Polymerization Catalysts.

Catalyst Name	Catalyst Components on Silica ^a	Cl wt % (Measured)	Cl wt % (Calculated)	% Difference
CAT-12	Ti + Ligand	0.24	N/A	N/A
CAT-13	Ti	0.34	N/A	N/A
CAT-17	Ti + Mg + Ligand	6.97	10.4	48.7
CAT-19 ^b	Ti + Mg + Ligand	Unknown	N/A	N/A
CAT-20	Ti + Mg + Ligand	10.81	19.2	77.8
CAT-22	Ti + Mg + Ligand	10.18	18.4	81.1
CAT-24	Ti + Mg + Ligand	11.94	18.5	54.7
CAT-25	Ti + Mg + Ligand	11.93	18.9	58.5
CAT-26	Ti + Ligand	1.92	N/A	N/A
CAT-28	Ti + Mg + Ligand	11.74	18.1	54.1
CAT-29	Ti + Mg + Ligand	12.01	17.8	47.9
CAT-30	Ti + Mg + Ligand	11.36	17.6	54.6
CAT-31	Ti + Mg + Ligand	10.83	15.8	45.6
CAT-32	Ti + Mg + Ligand	10.15	13.3	30.8
CAT-33	Ti + Mg + Silica	8.82	11.5	30.3
CAT-34	Ti + Mg + Ligand	12.39	9.5	23.2
CAT-34B	Ti + Mg + Ligand	7.15	18.7	161.7

a Ti for TiCl₄, Mg for CH₃MgCl, Ligand for tris(2,6-dihydroxyphenyl)ethene

b Ti content determined with colorimetric method (see Appendix A)

The calculated Cl content was significantly higher than the measured value by INAA; there are no neutron interference reactions that could have caused the discrepancy. It is possible that incorporation of titanium (IV) chloride into the catalyst precursor produced hydrogen chloride (HCl) due to reaction with residual silanols. Excess titanium (IV) chloride vapour was condensed into its Schlenk flask after contact with the catalyst precursor, and the last step in the catalyst preparation procedure was to evacuate the catalyst holder until the pressure was below atmospheric. Consequently, HCl could have been condensed into the Schlenk flask or removed from the catalyst during evacuation, thus giving lower Cl contents. In addition, a soluble magnesium

byproduct, $\text{MgCl}_2(\text{THF})_2$, could have been produced during the incorporation of magnesium onto the supported ligand (Fujita, 2001). It was subsequently removed during filtration of the magnesiated catalyst precursor thus contributing to the lower chloride content.

Table 5.6: Summary of Catalyst Preparation Conditions versus Ti/Mg

Catalyst Name	Catalyst Components on Silica ^a	Mg/Ligand/Silica Batch ^{b, c}	TiCl ₄ Addition	Ti/Mg Molar Ratio
CAT-12	Ti + Ligand	N/A (7.1 mg/g)	V (45 min)	N/A
CAT-13	Ti	N/A (0 mg/g)	V (1.5 h)	N/A
CAT-17	Ti + Mg + Ligand	2 (51.4 mg/g)	S (toluene)	0.26
CAT-19	Ti + Mg + Ligand	2 (47.8 mg/g)	V (15 min)	Unknown
CAT-20	Ti + Mg + Ligand	3 (47.8mg/g)	V (5.5 h)	0.80
CAT-22	Ti + Mg + Ligand	3 (47.8mg/g)	S (hexane)	0.82
CAT-24	Ti + Mg + Ligand	4 (38.8 mg/g)	V (7.5 h)	0.77
CAT-25	Ti + Mg + Ligand	4 (38.8 mg/g)	V (6 h)	0.84
CAT-26	Ti + Ligand	N/A (38.8 mg/g)	V (10 h)	N/A
CAT-28	Ti + Mg + Ligand	5 (38.9 mg/g)	V (6 h)	0.76
CAT-29	Ti + Mg + Ligand	5 (38.9 mg/g)	V (6 h)	0.76
CAT-30	Ti + Mg + Ligand	5 (38.9 mg/g)	V (6 h)	0.74
CAT-31	Ti + Mg + Ligand	6 (39.0 mg/g)	V (8.5 h)	0.64
CAT-32	Ti + Mg + Ligand	6 (39.0 mg/g)	V (7 h)	0.47
CAT-33	Ti + Mg + Silica	N/A (0 mg/g)	V (6 h)	0.39
CAT-34	Ti + Mg + Ligand	7 (39.6 mg/g)	V (8 h)	0.21
CAT-34B	Ti + Mg + Ligand	7 (39.6 mg/g)	V (23 h)	0.78

a Ti for TiCl₄, Mg for CH₃MgCl, Ligand for tris(2,6-dihydroxyphenyl)ethene

b N/A if catalyst does not contain the polyphenoxide ligand or magnesium

c Ligand loading in mg ligand/g silica is given in parentheses

The activity of the Ti-Mg polyphenoxide catalysts was affected most significantly by the method for titanium (IV) chloride addition; the slurry and vapour deposition methods were evaluated. The Ti-Mg polyphenoxide catalysts that were prepared with

the vapour deposition method had higher activities in ethylene homopolymerization (Figure 4.9) and ethylene/1-hexene copolymerization (Figure 4.10) than catalysts prepared with the slurry method. In general, the Ti-Mg polyphenoxide catalysts had titanium contents of about 3-5 wt % for the vapour deposition method, but it is possible some titanium was not active for polymerization. When the Ti-Mg polyphenoxide catalyst was suspended in toluene, the solvent turned orange in colour. Presuming all the unbound compounds were removed when the magnesiated catalyst precursor was washed with THF, this observation indicated some titanium (IV) chloride was leached from the supported catalyst.

The contact time in the vapour deposition method for titanium (IV) chloride was also examined. CAT-19 was prepared with a shorter contact time than CAT-20 to determine whether diffusion or reaction times for titanium (IV) chloride affected the activity; both catalysts were prepared from the same batch of magnesiated catalyst precursor. Lower activities were obtained in gas-phase polymerization experiments for CAT-19 (cf AH-19-01 and AH-20-01 in Figure 4.9; cf AH-19-02 and AH-20-02 in Figure 4.10), which had the lower titanium content of 2.8 wt % versus 4.95 wt % for CAT-20.

Larger batches of Ti-Mg polyphenoxide catalysts were prepared after CAT-30; previously batches of <0.4 g catalyst were made to test the different catalyst preparation conditions. The titanium addition for CAT-34 was completed in two stages; about 1.7 g of magnesiated catalyst precursor was contacted with titanium (IV) chloride vapour for 8 hours (CAT-34) then the same batch was exposed for an additional 15 hours (CAT-34B). The larger batch of catalyst was intended for use in slurry polymerization experiments. The slurry polymerization activity for CAT-34 was lower than previously obtained for other catalysts (CAT-22 and CAT-31); hence the need for the second addition of titanium (IV) chloride. The different titanium contents (1.5 wt% Ti for CAT-34 and 4.8 wt% Ti for CAT-34B) indicated that

contact time is important to prepare active catalysts and care should be taken to consider the appropriate time for diffusion of titanium (IV) chloride, based on the amount of magnesiated catalyst precursor.

The more active Ti-Mg polyphenoxide catalysts had higher Ti contents of about 4-5 wt %, and the Ti/Mg ratio for these catalysts was about 0.75. Various Ti/Mg ratios are reported in the literature for Ti-Mg silica catalysts. One of the early Chemplex/Quantum Ti-Mg silica catalysts was composed of 2.44 mmol Mg and 1.2 mmol Ti per gram of silica that was thermally pretreated at 280°C for 16 hours (Pullukat and Hoff, 1999), which corresponds to a Ti/Mg ratio of 0.49. The magnesiated product was filtered and washed before adding titanium (IV) chloride. Nowlin et al. (1988) prepared Ti-Mg silica catalysts with higher Ti/Mg ratios of 1.8 to 3.8 for similar silica thermal treatment conditions; however, excess quantities of magnesium compounds were added and the magnesiated product was not washed before titanium (IV) chloride addition so some magnesium compounds were likely precipitated onto the silica surface. Overall, the Ti-Mg polyphenoxide catalyst had higher activities than the Ti-Mg silica catalyst that was prepared to compare ligand environments (CAT-33). The more active Ti-Mg polyphenoxide catalysts had Ti/Mg ratios of about 0.75, whereas the Ti-Mg silica catalyst (CAT-33) had Ti/Mg of 0.4, which was similar to the Chemplex/Quantum catalyst. The higher Ti/Mg ratio in the polyphenoxide catalysts may be the result of silica surface modification by the polyphenoxide catalyst.

6.0 CONCLUSIONS AND RECOMMENDATIONS

Very active titanium (IV) chloride-based olefin polymerization catalysts were prepared with the polyphenoxide ligand tris(2,6-dihydroxyphenyl)ethene. No supported aryloxide ligand complexes were found in the literature to compare to the silica-supported polyphenoxide catalyst used in the current gas-phase polymerization studies; other researchers explored the activity of homogeneous transition metal catalysts with sterically hindered aryloxide ligands. Direct comparisons of gas-phase and slurry polymerization activities are not possible for high activity catalysts due to differences in activation and deactivation processes, but the silica-supported bimetallic (Ti-Mg) polyphenoxide catalyst had a much higher activity than the conventional Ti-Mg silica catalyst that was prepared to examine the role of ligand functionality. The gas-phase polymerization experiments were useful in evaluating catalyst activity under different reactor conditions, and some conclusions and suggestions for future work can be made regarding catalyst preparation.

The main distinction between the aryloxide-based transition metal catalysts described in the literature and the polyphenoxide catalyst used in this research is the incorporation of magnesium (II) to create bimetallic (Ti-Mg) coordination complexes. Higher polymerization activities were obtained for third generation heterogeneous Ziegler-Natta catalysts with the use of magnesium compounds such as MgCl_2 as the support for titanium halides. Similarly, incorporation of magnesium onto the supported tris(2,6-dihydroxyphenyl)ethene ligand resulted in higher activities. Perhaps, incorporation of magnesium (II) into the aryloxide catalysts reported in the literature will increase their polymerization activities. Interestingly, the aryloxide-based transition metal catalysts described in the literature are soluble in toluene, unlike the tris(2,6-dihydroxyphenyl)ethene ligand. An industrially practical endeavor would be to develop soluble magnesium polyaryloxide complexes to resolve issues associated with solution process operations and resin processing with the current

Ziegler-Natta catalyst systems; agglomerations of insoluble catalyst particles can form in the reactor that could result in catalyst injector port blockages and gel formation during polyethylene film processing. The literature contains examples of toluene-soluble, multinuclear magnesium aryloxide complexes that were obtained in the absence of donor solvents such as THF; use of dialkyl magnesium compounds (e.g. butyl ethyl magnesium (BEM)) in hydrocarbons (e.g. heptane) could enable preparation of soluble magnesium aryloxides. Extending the work of Fujita (2001), it would be worthwhile to explore the polymerization activity of titanium (IV) chloride-based catalysts prepared with magnesium aryloxide complexes containing sterically hindered ligands that are similar in structure to the polyphenoxide ligand and soluble in hydrocarbons such as toluene (e.g. calixarenes). The literature reported that dimers consisting of terminal and bridged sterically hindered phenoxide ligands were formed in the preparation of magnesium compounds for olefin polymerization; the oligomeric nature of the calixarene ligands may be suitable for the formation of intramolecular magnesium dimers. Calix[4]arene and calix[6]arene are commercially available, and a series of substituted calixarenes could be prepared to examine the effect of electron donating ability of the para-substituents (e.g. H, ^tBu, CH₂Cl, etc.) on polymerization activity and polymer properties, specifically MWD and comonomer incorporation. It would also be necessary to perform control experiments with the TiCl₄-BEM catalyst system. Care should be taken to use the appropriate Ti/Mg ratio and Lewis acid (e.g. TEAL) concentration in the reactor to realize the full potential of the catalyst systems. Consideration of these ideas could yield the first homogeneous Ti-Mg catalyst system for olefin polymerization.

As previously mentioned, much higher polymerization activities were obtained when magnesium was incorporated onto the silica-supported polyphenoxide ligand; methyl magnesium chloride was used to prepare the magnesiated polyphenoxide complex. Use of dialkyl magnesium reagents might enable examination of the effect of chloride on polymerization activity and polymer properties. Further, the activity may vary

with the extent of magnesium coordination to the polyphenoxide ligand. To date, all catalysts were prepared with excess Grignard reagent to convert free hydroxyl groups on the ligand into magnesium aryloxides. If it could be ensured that the silanol portion of the support would not consume Grignard reagent, it would be desirable to prepare catalysts with different magnesium contents.

In conventional heterogeneous Ziegler-Natta catalyst systems, internal electron donors form complexes with active catalyst components to enhance the polymerization activity and/or increase stereospecificity. Given that incorporation of magnesium (II) onto the silica-supported polyphenoxide ligand resulted in higher polymerization activities for the Ti-Mg catalyst system, it is possible the ligand participated as an internal electron donor to create active sites for titanium (IV) chloride attachment. Perhaps, incorporation of the polyphenoxide ligand into MgCl_2 -supported titanium (IV) chloride catalysts will reveal information about its electron donor ability. These MgCl_2 -supported catalysts would also enable comparisons to the silica-supported catalysts; the interaction of the polyphenoxide ligand with the silica surface may have contributed to its polymerization behaviour.

The gas-phase experiments with the different Ti-Mg catalysts revealed that ligand functionality affected polymerization activity and polymer properties. The activity was much higher for the Ti-Mg polyphenoxide catalyst compared to the Ti-Mg silica catalyst. Other supported catalysts could be prepared to examine the effect of ligand functionality. The polyphenoxide ligand tris(2,6-dihydroxyphenyl)ethene was designed to resemble the structure of calix[4]arene, but the fourth phenol was cleaved from ethene during the last synthetic step. Perhaps the structural rigidity of the phenol-substituted ethene molecules contributed to the polymerization behaviour; the ortho-substituted phenols in tris(2,6-dihydroxyphenyl)ethene are tied to its central ethene. Besides electronic and steric effects, it is possible the close proximity of hydroxyls to each other in the polyphenoxide ligand created the appropriate

intramolecular distances to form bridged Ti-Mg sites. Structurally, the polyphenoxide ligand can be seen as being composed of 2-methyl-1,3-benzenediol (also known as 2-methylresorcinol) monomers. Comparison of activity profiles and polymer properties for silica-supported catalysts containing calix[4]arene or 2-methylresorcinol would expand our understanding of the effect that ligand functionality has on polymerization activity.

The laboratory-scale gas-phase reactor proved invaluable in evaluating the catalyst preparation conditions. Specifically, the addition of titanium (IV) chloride was judged to be more effective via vapour deposition rather than slurry addition; the solvent appeared to have detrimental effects on the polymerization activity of the supported polyphenoxide catalyst. Consequently, slurry polymerization experiments would have been more complicated, as experienced by other researchers with similar Ti-Mg polyaryloxide catalysts (Fujita, 2001) because an optimal time may exist before the Ti-Mg ligand complex deactivated or dissociated in solution.

The titanium content of the catalyst varied with contact time for vapour deposition of titanium (IV) chloride; longer contact times yielded higher titanium contents likely due to slow diffusion into the porous support. The process of vapour deposition could have been accelerated by heating the Schlenk flask containing titanium (IV) chloride, but too much may have condensed onto the supported catalyst. Titanium contents about 4-5 wt % were measured for the higher activity Ti-Mg polyphenoxide catalysts, but it is possible some of the titanium was not active for polymerization because it was observed that titanium (IV) chloride leached from the supported catalyst into toluene. The Ti/Mg ratio for the more active Ti-Mg polyphenoxide catalysts was about 0.75, which was higher than the Ti-Mg silica catalyst prepared for comparison purposes. The higher Ti/Mg ratio may be the result of surface modification of silica by the polyphenoxide catalyst.

Great care was taken to thoroughly dry the silica-supported, magnesiated polyphenoxide ligand before the addition of titanium (IV) chloride because higher activities were obtained when the magnesiated catalyst precursors were dried for longer times at room temperature. This preparation step was deemed important because titanium (IV) chloride is deactivated by THF, which solvated the Grignard reagent used to incorporate magnesium onto the supported ligand. The magnesiated catalyst precursors were dried on the high vacuum line at temperatures between 50-90°C, and the ionization gauge readings were used to judge drying time. THF was likely coordinated to magnesium, but the drying conditions seemed adequate at removing uncoordinated THF because high activities were obtained regardless of drying temperature. A toluene or heptane solution of the magnesium reagent would facilitate easier and faster catalyst preparation, and possibly give higher catalyst activities. Unfortunately, the effect of drying temperature on activity could not be thoroughly examined because there was poor control over the gas-phase temperature during the polymerization experiments. However, some differences in the initial polymerization activities were observed with respect to drying temperature when gas-phase temperatures were similar between experiments; the extent of THF coordination to magnesium may have been the cause of the activity differences because THF acts as an internal electron donor in conventional Ziegler-Natta catalysts.

The polymer properties for polyethylene produced with the Ti-Mg polyphenoxide catalyst yielded both expected and unusual results. Very little comonomer incorporation was measured by TREF for the ethylene/1-hexene copolymers (3-7 CH₃ per 1000 carbon atoms), which is typical for Ti-Mg catalysts. However, polymer from the Ti-Mg polyphenoxide catalyst contained lower homopolymer fractions as the initial 1-hexene concentration in the reactor was increased, whereas the trend was opposite for the Ti-Mg silica catalyst. These results suggested the two catalysts likely had different ratios or types of active sites that controlled 1-hexene incorporation. Bimodal molar mass distributions were observed for both types of catalyst indicating

multiple types of active sites were present with different sensitivities to hydrogen, but it was interesting that polymer samples for the Ti-Mg polyphenoxide catalyst had unusually narrow molar mass distributions compared to conventional Ziegler-Natta catalysts. Molar mass data also supported the hypothesis that the Ti-Mg polyphenoxide catalyst had either different ratios or different types of active sites than the Ti-Mg silica catalyst. Differences in propagation rates for the two catalysts indicated the active site environment created by the polyphenoxide ligand affected the polymerization kinetics. The polyphenoxide ligand might have created a more homogeneous surface on the support thus controlling the ratio of active sites. Alternatively, the magnesium aryloxide functionality created active sites with different polymerization kinetics due to electronic or steric effects. Examination of molar mass distributions for several silica-supported catalysts prepared with different polyphenoxide ligand loadings may reveal whether the magnesiated silanol portion of the supported catalysts contributed to the multiple-site behaviour. The silanol content can be controlled with the dehydroxylation temperature; a series of catalysts could be prepared and the polydispersity examined as a function of silanol content. Extrapolation of the data to zero silanol concentration may reveal whether single-site behaviour is possible with the bimetallic polyphenoxide catalyst. As well, the multiple-site behaviour could be examined by using a suitably functionalized polymer support instead of silica to eliminate the Ti-Mg silica sites; the polymer support would have to possess functional groups capable of binding the polyphenoxide ligand (compare Si-O-C and C-O-C bond strengths). Polymer particle morphology would be improved with use of a spherical polymer support, and there might be better control of the gas-phase temperature during polymerization.

It was observed that aluminum alkyl (e.g. TIBA) was needed to activate the Ti-Mg polyphenoxide catalyst in olefin polymerization. An optimal aluminum alkyl concentration may exist to give higher activities in gas-phase polymerization. The reactor pretreatment and operating procedures were effective in ensuring good

reproducibility in activity profiles, but different amounts of aluminum alkyl were consumed in scavenging impurities because it was not possible to control the day-to-day impurity levels in the laboratory-scale reactor. One option to further explore the role of aluminum alkyls in the polymerization mechanism would be to incorporate aluminum compounds (e.g. MAO) into the supported catalyst. Internal aluminum alkyl may protect the catalyst from deactivation.

The activity profiles for most of the polymerization experiments with the Ti-Mg polyphenoxide catalyst had unusual shapes; many profiles showed a steep rise in activity after a long induction period. The rapid increase in activity can likely be attributed to elevated gas-phase temperatures. In most experiments, the gas-phase temperature increased slowly during the induction period because the circulating oil bath was not capable of adequate heat removal for the high activity catalysts. In the few experiments with good temperature control, the activity profiles for the Ti-Mg polyphenoxide catalyst were fairly flat. Ideally, polymerization experiments should be performed under isothermal conditions because the shape of the activity profile is affected by the deactivation of active sites. During periods of high activity, some sites become deactivated and the rate eventually decays to a lower steady-state level; temperature oscillations are prone to occur with changes in activity and the possibility of polymer particle agglomeration exists. Flat activity profiles would reduce the likelihood of temperature oscillations thus providing greater process stability to gas-phase reactors. In addition, kinetic parameters can be determined when isothermal conditions are maintained; the propagation kinetics can be evaluated as a function of reactor temperature and ethylene pressure.

In summary, the laboratory-scale gas-phase olefin polymerization experiments showed the high activity of the silica-supported, bimetallic (Ti-Mg) catalyst with tris(2,6-dihydroxyphenyl)ethene could be attributed to the active site environment created by the polyphenoxide ligand. The role of the ligand in olefin polymerization

was explored by comparing activity profiles and polymer properties for various catalysts and preparation conditions. Future work might reveal its potential to enhance gas-phase reactor operation; flat activity profiles may be obtained under isothermal conditions. As well, extension of this research may lead to improvements in solution polymerization processes through the development of titanium (IV) chloride-based catalysts with soluble magnesium aryloxide compounds composed of sterically hindered ligands that are similar in structure to the polyphenoxide ligand. The results for the control experiments with the TiCl_4 -BEM catalyst system may prove surprising because the accepted understanding in conventional Ziegler-Natta catalyst systems is that MgCl_2 is the necessary component. It was likely never considered that alkyl nucleophiles (e.g. CH_3CH_2^- , $\text{CH}_3\text{CH}_2\text{CH}_2\text{CH}_2^-$) are stronger Lewis bases than Cl^- . Consequently, the electron donating ability of the alkyl nucleophiles to magnesium (II) may be the factor affecting the polymerization behaviour of Ziegler-Natta catalyst systems.

REFERENCES

Bu, N., D.T. Lynch, and S.E. Wanke, "Kinetics of Catalytic Gas-Phase Homopolymerization of Ethylene over $\text{SiO}_2/\text{MgCl}_2$ -Supported TiCl_4 Catalysts", *Polymer Reaction Engineering*, **3**(1), 1-22 (1995).

Chakravarty, J., *Characterization of Polyolefins by Temperature Rising Elution Fractionation (TREF)*, M.Sc. Thesis, University of Alberta, Edmonton, Alberta, Canada, 1993.

Calabrese, J., M.A. Cushing, and S.D. Ittel, "Sterically Hindered Magnesium Aryloxides", *Inorganic Chemistry*, **27**, 867-870 (1988).

Chemical Economics Handbook, SRI Consulting, 2002.

Chemical Industries Newsletter, "Linear Low-Density Polyethylene (LLDPE) Resins", SRI Consulting, **3**, 2000.

Chen, Y., Y. Zhang, Z. Shen, R. Kou, and L. Chen, "Ethylene Polymerization Catalyzed by Rare Earth Calixarene Catalytic System", *European Polymer Journal*, **37**, 1181-1184 (2001).

Choi, K.Y. and W.H. Ray, "Recent Developments in Transition Metal Catalyzed Olefin Polymerization—A Survey. I. Ethylene Polymerization", *Journal of Macromolecular Science Reviews of Macromolecular Chemistry Physic*, **C25**(1), 1-55 (1985).

Choi, K.Y. and W.H. Ray, "The Dynamic Behaviour of Fluidized Bed Reactors for Solid Catalyzed Gas Phase Olefin Polymerization", *Chemical Engineering Science*, **40**, 2261-2279 (1985b).

Czaja, K., L.A. Novokshonova, N. Kovaleva, "Deactivation of Oxide-Supported Titanium Catalysts in the Ethylene Polymerization Process", *Macromolecular Chemistry and Physics*, **200**, 983-988 (1999).

Dzwiniel, T., Department of Chemistry, University of Alberta, Edmonton, Alberta, Canada, personal communication.

Firth, A.V., J.C. Stewart, A.J. Hoskin, and D.S. Stephan, "Ancillary Aryloxide Ligands in Ethylene Polymerization Catalyst Precursors", *Journal of Organometallic Chemistry*, **591**, 185-193 (1999).

Fuhrmann, H. and M.M. Pohl, "Ziegler-Natta Polymerization of Ethylene with Ti-Mg Catalysts Anchored on Polymeric Supports", *Acta Polymerica*, **44**, 156-162 (1993).

Fujita, M., *Coordination Chemistry of the New Preorganized Polyphenoxide Ligand Tetrakis(2-hydroxyphenyl)ethene Derivatives. Attempts to Create Surface-Models for Classic Ziegler-Natta Olefin Polymerization Catalysts*, Ph.D. Thesis, University of Alberta, Edmonton, Alberta, Canada, 2001.

Furuyama, R., J. Saito, S. Ishii, M. Mitani, S. Matsui, Y. Tohi, H. Makio, N. Matsukawa, H. Tanaka, T. Fujita, "Ethylene and Propylene Polymerization Behavior of a Series of Bis(phenoxy-imine)titanium Complexes", *Journal of Molecular Catalysis A-Chemical*, **200**, 31-42, 2003.

Galli, P., L. Luciani, and G. Cecchin, "Advances in the Polymerization of Polyolefins with Coordination Catalysts", *Die Angewandte Makromolekulare Chemie*, **94**, 63-89 (1981).

Grabbe, A., T.A. Michalske, W.L. Smith, "Strained Siloxane Rings on the Surface of Silica: Their Reaction with Organosiloxanes, Organosilanes, and Water", *Journal of Physics and Chemistry*, **99**, 4648-4654 (1995).

Gorbach, A.B., S.D. Naik, and W.H. Ray, "Dynamics and Stability Analysis of Solid Catalyzed Gas-Phase Polymerization of Olefins in Continuous Stirred Bed Reactors", *Chemical Engineering Science*, **55**, 4461-4479 (2000).

Gregg, S.J. and K.S.W. Sing, In *Adsorption, Surface Area and Porosity*, 2nd ed., Academic Press, London, 1982.

Han-Adebekun, G.C., J.A. Debling, W.H. Ray, "Polymerization of Olefins Through Heterogeneous Catalysis. XVI. Design and Control of a Laboratory Stirred Bed Copolymerization Reactor", *Journal of Applied Polymer Science*, **64**, 373-382 (1997).

Henderson, K.W., G.W. Honeyman, A.R. Kennedy, R.E. Mulvey, J.A. Parkinson, and D.C. Sherrington, "Magnesium Aryloxides: Synthesis, Structure, and Magnesiato Ion Formation", *Dalton Transactions*, 1365-1372 (2003).

Hlatky, G.G., "Heterogeneous Single-Site Catalysts for Olefin Polymerization", *Chemical Reviews*, **100**, 1347-1376 (2000).

Huang, J. and G.L. Rempel, "Ziegler-Natta Catalysts for Olefin Polymerization: Mechanistic Insights from Metallocene Systems", *Progress in Polymer Science*, **20**, 459-526 (1995).

Huang, J.C.-K., Y. Lacombe, D.T. Lynch, and S.E. Wanke, "Effects of Hydrogen and 1-Butene Concentration on the Molecular Properties of Polyethylene Produced by Catalytic Gas-Phase Polymerization", *Industrial & Engineering Chemistry Research*, **36** (4), 1136-1143 (1997).

Hutchinson, R.A. and W.H. Ray, "Polymerization of Olefins Through Heterogeneous Catalysis. VII. Particle Ignition and Extinction Phenomena", *Journal of Applied Polymer Science*, **34**, 657-676 (1987).

Jaber, I.A. and W.H. Ray, "Polymerization of Olefins through Heterogeneous Catalysis. XII. The Influence of Hydrogen in the Solution Copolymerization of Ethylene", *Journal of Applied Polymer Science*, **49**, 1695-1707 (1993).

Jejelowo, M.O., D.T. Lynch, and S.E. Wanke, "Comparison of Ethylene Polymerization in Gas-Phase and Slurry Reactors", *Macromolecules*, **24**, 1755-1761 (1991).

Karol, F.J. and S.C. Kao, "Ligand Effects at Transition Metal Centers for Ethylene Polymerization", *New Journal of Chemistry*, **18**, 97-103 (1994).

Kelusky, E.C., C.T. Elston, and R.E. Murry, "Characterizing Polyethylene-Based Blends with Temperature Rising Elution Fractionation (TREF) Techniques", *Polymer Engineering and Science*, **27**(20), 1562-1571 (1987).

Kissin, Y.V., In *Isospecific Polymerization of Olefins with Heterogeneous Ziegler-Natta Catalysts*, 3rd ed., Springer-Verlag, New York, 1985.

Kissin, Y.V., R.I. Mink, T.E. Nowlin, and A.J. Brandolini, "Kinetics and Mechanism of Ethylene Homopolymerization and Copolymerization Reactions with Heterogeneous Ti-Based Ziegler-Natta Catalysts", *Topics in Catalysis*, **7**, 69-88 (1999).

Kumkaew, P., L.Wu, P. Praserttham, and S.E. Wanke, "Rates and Product Properties of Polyethylene Produced by Copolymerization of 1-Hexene and Ethylene in the Gas-Phase with (n-BuCp)₂ZrCl₂ on Supports with Different Pore Sizes", submitted to *Polymer* (2003).

Kruger, P., In *Principles of Activation Analysis*, 1st ed., Wiley-Interscience, New York, 1971.

Lacombe, Y., *TREF and SEC Characterization of Ethylene/1-Butene Copolymers Produced at Various 1-Butene and Hydrogen Pressures*, M.Sc. Thesis, University of Alberta, Edmonton, Alberta, Canada, 1995.

Liu, W., *Gas-Phase Ethylene/1-Hexene Copolymerization over MgCl₂-Supported Ziegler-Natta Catalysts*, Ph.D. Thesis, University of Alberta, Edmonton, Alberta, Canada, 2002.

Lynch, D.T. and S.E. Wanke, "Reactor Design and Operation for Gas-Phase Ethylene Polymerization Using Ziegler-Natta Catalysts", *The Canadian Journal of Chemical Engineering*, **69**, 332-339 (1991).

Lyon, W.S. In *Guide to Activation Analysis*, 1st ed., D. Van Nostrand Company, Inc., New Jersey, 1964.

Mannan, T., H. Hammawa, D.T. Lynch, and S.E. Wanke, "A Reactor for Gas-Phase Olefin Polymerization", submitted to *The Canadian Journal of Chemical Engineering* (2003).

Matilainen, L., M. Klinga, and M. Leskelä, "Group 4 Metal Alkoxide Complexes as Catalysts for Olefin Polymerization", *Journal of the Chemical Society Dalton Transactions*, 219-225 (1996).

McAuley, K.B., D.A. Macdonald, and P.J. McLellan, "Effects of Operating Conditions on Stability of Gas-Phase Polyethylene Reactors", *American Journal of Chemical Engineering*, **41**, 868-879 (1995).

Muñoz-Escalona, A., A. Fuentes, J. Liscano, and A. Albornoz, "High Active Ziegler-Natta Catalysts for Homo- and Copolymerization of Ethylene by Supporting a Grignard Compound and TiCl_4 on SiO_2 ", *Study of Surface Science and Catalysis*, **56**, 377-404 (1990).

Nait Ajjou, J.A. and S.L. Scott, "Reactions of Tetraalkylchromium(IV) with Silica: Mechanism of Grafting and Characterization of Surface Organometallic Complexes", *Organometallics*, **16**, 86-92 (1997).

Nowlin, T.E., Y.V. Kissin, and K.P. Wagner, "High Activity Ziegler-Natta Catalysts for the Polymerization of Ethylene Copolymers", *Journal of Polymer Science: Part A: Polymer Chemistry*, **26**, 755-764 (1988).

Odian, G., In *Principles of Polymerization*, 1st ed., McGraw-Hill Book Company, New York, 1970.

Ozerov, O.V., N.P. Rath, and F.T. Ladipo, "Synthesis, Characterization, and Reactivity of Titanium (IV) complexes Supported by Proximally Bridged p-tert-butylcalix[4]arene Ligands", *Journal of Organometallic Chemistry*, **586**, 223-233 (1999).

Pullukat, T.J. and R.E. Hoff, "Silica-Based Ziegler-Natta Catalysts: A Patent Review", *Catalysis Reviews: Science and Engineering*, **41**, 389-428 (1999).

Repo, T., G. Jany, M. Salo, M. Polamo, and M. Leskelä, "Phenoxy Substituted Zirconocenes in Ethylene Polymerization", *Journal of Organometallic Chemistry*, **541**, 363-366 (1997).

Rice, G.L. and S.L. Scott, "Characterization of Silica-Supported Vanadium(V) Complexes Derived from Molecular Precursors and Their Ligand Exchange Reactions", *Langmuir*, **13**, 1545-1551 (1997).

Shreve, A.P., R. Mulhaupt, W. Fultz, J. Calabrese, W. Robbins, and S.D. Ittel, "Sterically Hindered Aryloxide-Substituted Alkylaluminum Compounds", *Organometallics*, **7**, 409-416 (1988).

Smith, G.M., C.F. Tirendi, R.J. Amata, E.I. Band, "Alkoxymagnesium Halide Supports for Heterogeneous Ziegler-Natta Polymerization Catalysts", *Inorganic Chemistry*, **32**, 1161-1166 (1993).

Soares, J.B.P. and A.E. Hamielec, "Metallocene/Aluminoxane Catalysts for Olefin Polymerization. A Review", *Polymer Reaction Engineering*, **3**, 131-200 (1995).

Sobota, P., J. Utko, J. Ejfler, and L.B. Jerzykiewicz, "Syntheses and Molecular Structures of $[\text{Mg}_4(\text{THFFO})_6(\text{OSiPh}_3)_2]$ and $[\text{Al}_3\text{Mg}(\mu_3\text{-O})(\text{THFFO})_3(\text{Me})_6]$ Relevant to Ziegler-Natta Catalyst Intermediates (THFFO = 2-Tetrahydrofurfuroxide)", *Organometallics*, **19**, 4929-4931, (2000).

Sobota, P., J. Utko, K. Sztajnowska, J. Ejfler, and L.B. Jerzykiewicz, "Polynuclear Magnesium and Magnesium-Titanium Species. Syntheses and Crystal Structures of $[\text{Mg}_4(\mu_3, \eta^2\text{-ddbfo})_2(\mu, \eta^2\text{-ddbfo})_2(\mu, \eta^1\text{-ddbfo})_2(\eta^1\text{-ddbfo})_2]$, $[\text{Mg}_4(\mu_3\text{-OME})_2(\mu, \eta^2\text{-ddbfo})_2(\mu, \eta^1\text{-ddbfo})_2(\eta^1\text{-ddbfo})_2(\text{CH}_3\text{OH})_5]$, and $[\text{Mg}_4(\mu_3, \eta^2\text{-thffo})_2(\mu, \eta^2\text{-thffo})_2(\mu, \eta^1\text{-thffo})_2\{\mu\text{-OTi}(\text{DIPP})_3\}_2]$ Aggregates", *Inorganic Chemistry*, **39**, 235-239 (2000b).

Soga, K and T. Shiono, "Ziegler-Natta Catalysts for Olefin Polymerizations", *Progress in Polymer Science*, **22**, 1503-1546 (1997).

Thorn, M.G., Z.C. Etheridge, P.E. Fanwick, and I.P. Rothwell, "Cationic Group 4 Metal Alkyl Compounds Containing Aryloxide Ligation: Synthesis, Reactivity and Polymerization Studies", *Journal of Organometallic Chemistry*, **591**, 148-162 (1999).

Ullmann's Encyclopedia of Industrial Chemistry, 5th ed., Vol. A23, VCH Publishers Inc., Weinheim, 1993.

van der Linden, A., C.J. Schaverien, N. Meijboom, C. Ganter, and A.G. Orpen, "Polymerization of α -Olefins and Butadiene and Catalytic Cyclotrimerization of 1-Alkynes by a New Class of Group IV Catalysts. Control of Molecular Weight and Polymer Microstructure via Ligand Tuning in Sterically Hindered Chelating Phenoxide Titanium and Zirconium Species", *Journal of the American Chemical Society*, **117**, 3008-3021 (1995).

Vogel, A.I., In *A Text-Book of Quantitative Inorganic Analysis Including Elementary Instrumental Analysis*, 3rd ed., Longmans, London, 1961.

Vollmert, B., In *Polymer Chemistry*, 1st ed., Springer-Verlag, New York, 1973.

Wells, G.J. and W.H. Ray, "Effects of Catalyst Activity Profiles on Polyethylene Reactor Dynamics", *American Institute of Chemical Engineering Journal*, **47**, 2768-2780 (2001).

Wu, L., D.T. Lynch, and S.E. Wanke, "Kinetics of Gas-Phase Ethylene Polymerization with Morphology-Controlled MgCl_2 -Supported TiCl_4 Catalyst", *Macromolecules*, **32**, 7990-7998 (1999).

Xie, T., K.B. McAuley, J.C.C. Hsu, and D.W. Bacon, "Gas Phase Ethylene Polymerization: Production Processes, Polymer Properties, and Reactor Modeling", *Industrial & Engineering Chemistry Research*, **33**, 449-479 (1994).

Yasuda, M., Department of Chemistry, University of Alberta, Edmonton, Alberta, Canada, personal communication.

Zechmann, C.A., T.J. Boyle, M.A. Rodriguez, and R.A. Kemp, "Solvent Influences on the Molecular Aggregation of Magnesium Aryloxides: Synthesis, Crystal Structure, and Solution Characterization of $\text{Mg}(\text{OAr})_2(\text{L})_3$ ($\text{OAr} = \text{DMP}, \text{DIP}, \text{TCP}$) and $[\text{Mg}(\text{DIP})_2]_3$ ", *Polyhedron*, **19**, 2557-2564 (2000).

Zechmann, C.A., T.J. Boyle, M.A. Rodriguez, R.A. Kemp, "Synthesis, Characterization, and Structural Study of Sterically Hindered Magnesium Alkoxide and Siloxide Compounds", *Inorganica Chimica Acta*, **319**, 137-146 (2001).

APPENDIX A: Catalyst Preparation Conditions

Catalyst preparation was described in Section 3.1. Some additional information is presented here; specifically, Table A.2 lists the batches of magnesiated catalyst precursor (Mg/Ligand/Silica) that were divided into portions before the addition of titanium (IV) chloride. As well, Figure A.1 shows the glassware used to dry the catalyst precursor on the high vacuum line in the laboratory. The glassware with the Teflon stopcock and without the vacuum hose side arm was better at preventing contamination by air and/or moisture than the greased stopcocks because striations in the grease were observed over time that could admit air and/or moisture into the flask and deactivate the magnesiated catalyst precursor. The Teflon stopcock glassware was used in the preparation of CAT-17 and all subsequent catalysts.

Table A.1: Thermal Treatment Conditions for Silica.

Silica Batch Number	Heating Temperature (°C)	Heating Time (hours)
1	500	8.5
2	500	6.0
3	500	9.0
4	500	16.5
5	520	11.0
6	500	16.0

Table A.2: Batches of Catalyst Precursor Mg/Ligand/Silica.

Catalyst Name	Silica Batch ^a	Mg/Ligand/Silica Batch ^b	Ligand Loading (mg/g)	Drying Temp ^c (°C)	Drying Time ^d (days)
CAT-12	1	N/A	7.1	RT	< 1
CAT-13	2	N/A	N/A	RT	< 1
CAT-14	2	1	55.7	RT + heat	3
CAT-15	3	N/A	N/A	RT + heat	8
CAT-16 ^e	N/A	N/A	42.1	RT + heat	8
CAT-17	3	2	51.4	60	3
CAT-18 ^f	3	2	51.4	60	3
CAT-19	3	3	47.8	RT	6
CAT-20	3	3	47.8	RT	6
CAT-21	3	3	47.8	RT	8
CAT-22	3	3	47.8	RT	6
CAT-23	3	3	47.8	RT	8
CAT-24 ^f	4	4	38.8	RT + 50	6 + 1
CAT-25	4	4	38.8	RT + 50	6 + 1
CAT-26	4	N/A	38.8	RT	7
CAT-27	4	5	38.9	90	5
CAT-28	4	5	38.9	70	5
CAT-29	4	5	38.9	80	5
CAT-30	4	5	38.9	60	5
CAT-31	5	6	39.0	60	5.5
CAT-32	5	6	39.0	70	5
CAT-33	5	N/A	N/A	70	7
CAT-34	6	7	39.6	70	7

a Refer to Table A.1 for details

b N/A if catalyst does not contain the polyphenoxide ligand or magnesium

c Temperature for resistance heater, RT for room temperature, or heat for heat gun

d Drying time on high vacuum line at specified drying temperature

e Used HEMA PS-DVB as support

f Catalyst discoloured after drying (some exposure to air)

Table A.3: Summary of Catalyst Preparation Conditions.

Catalyst Name	Silica Batch ^a	Ligand ^b (mg [mmol])	Ligand Loading (mg/g)	Grignard ^c (mmol)	Drying Temp ^d (°C)	TiCl ₄ Addition ^e
CAT-12	1	18.1 [0.051]	7.1	None	RT	V (45 min)
CAT-13	2	None	N/A	None	RT	V (1.5 h)
CAT-14	2	56.4 [0.160]	55.7	3.8	RT + heat	V (5.5 h)
CAT-15	3	None	N/A	4.0	RT + heat	V (5.5 h)
CAT-16 ^f	N/A	21.4 [0.061]	42.1	7.3	RT + heat	V (75 min)
CAT-17	3	51.2 [0.145]	51.4	2.4	60	S (toluene)
CAT-18 ^g	3	51.2 [0.145]	51.4	2.4	60	V (15 min)
CAT-19	3	58.3 [0.165]	47.8	3.8	RT	V (10 min)
CAT-20	3	58.3 [0.165]	47.8	3.8	RT	V (5.5 h)
CAT-21	3	58.3 [0.165]	47.8	3.8	RT	V (5.5 h)
CAT-22	3	58.3 [0.165]	47.8	3.8	RT	S (hexane)
CAT-23	3	58.3 [0.165]	47.8	3.8	RT	V (5.5 h)
CAT-24 ^g	4	77.7 [0.220]	38.8	4.1	RT + 50	V (7.5 h)
CAT-25	4	77.7 [0.220]	38.8	4.1	RT + 50	V (6 h)
CAT-26	4	77.7 [0.220]	38.8	None	RT	V (10 h)
CAT-27	4	84.6 [0.240]	38.9	5.9	90	V (6 h)
CAT-28 ^g	4	84.6 [0.240]	38.9	5.9	70	V (6 h)
CAT-29	4	84.6 [0.240]	38.9	5.9	80	V (6 h)
CAT-30	4	84.6 [0.240]	38.9	5.9	60	V (6 h)
CAT-31	5	99.0 [0.281]	39.0	5.3	60	V (8.5 h) ^h
CAT-32	5	99.0 [0.281]	39.0	5.3	70	V (7 h)
CAT-33	5	None	N/A	3.1	70	V (6 h)
CAT-34	5	63.2 [0.179]	39.6	3.1	70	V (8, 15 h) ⁱ

a Refer to Table A.1 for details

b MW of 1,1,2-tris(2,6-dihydroxyphenyl)ethene = 352.34 g/mol

c Used 3M solution of CH₃MgCl in THF (density = 1.013 g/mL)

d Temperature for resistance heater, RT for room temperature, or heat for heat gun

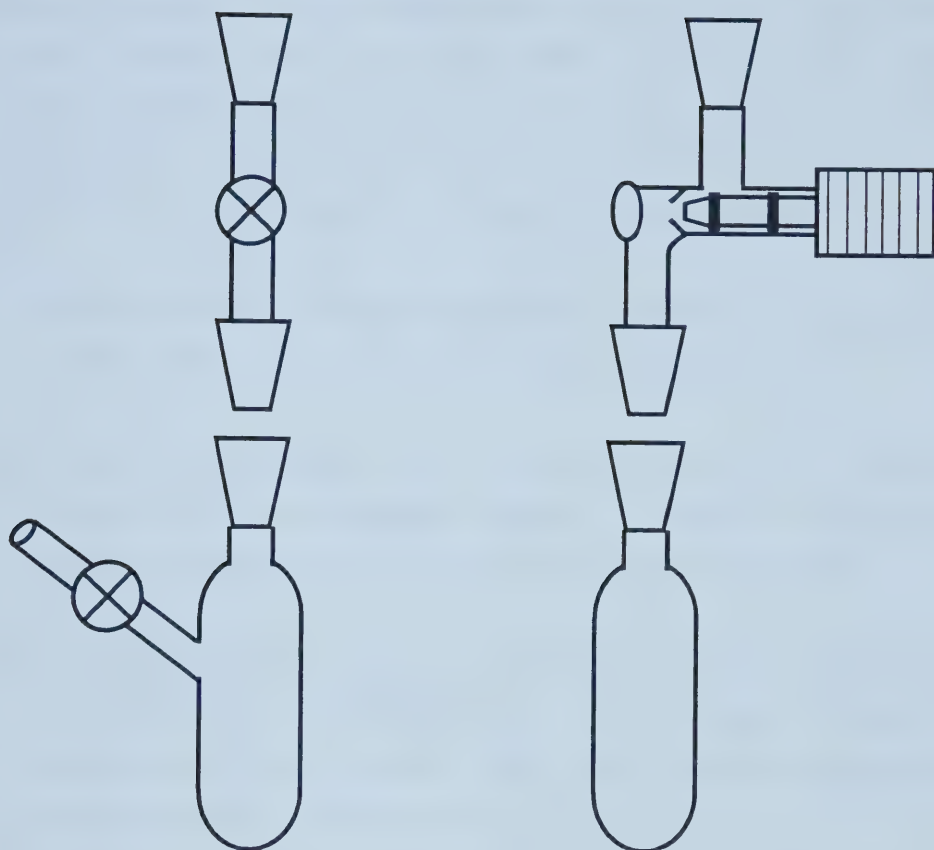
e S (solvent) for slurry method or V (contact time) for vapour deposition method

f Used HEMA PS-DVB as support

g Catalyst discoloured after drying (some exposure to air)

h Catalyst heated at 60°C during vapour deposition of TiCl₄

i Vapour deposition performed in two stages



~20 mL Schlenk flask
 Side arm for vacuum hose
 14/20 sized joints
 Greased stopcocks

~20 mL Schlenk flask
 14/20 sized joints
 Teflon stopcock with o-rings

Figure A.1. Glassware used to dry catalyst precursor before TiCl_4 addition.

For the most part, the titanium contents of the polymerization catalysts were determined with neutron activation analysis because it is a highly sensitive, multi-element technique, but the colorimetric method was initially used for some catalysts (CAT-17 through CAT-20). In aqueous solution, Ti^{4+} forms a yellow-coloured complex in the presence of hydrogen peroxide (H_2O_2). The reaction permits determination of the titanium content for the polymerization catalysts. The colorimetric procedure (Vogel, 1961) consisted of the following steps:

1. Sufficient catalyst (0.10-0.15 g) was accurately weighed (± 0.001 g) to give about 2 mg Ti^{4+} when digested, and it was placed in a Kjeldahl flask.
2. About 3-4 mL concentrated sulfuric acid (H_2SO_4) and 0.5 mL concentrated perchloric acid (HClO_4) were added to the flask. The solution was gently swirled in the flask while digesting the catalyst, and it was heated until colourless.
3. The solution was allowed to cool to room temperature then it was cautiously diluted with 10-15 mL de-ionized water. After cooling, the solution was transferred to a 100-mL volumetric flask. The Kjeldahl flask was thoroughly rinsed with water for a quantitative transfer.
4. More concentrated H_2SO_4 (5 mL) was slowly added to the volumetric flask and the solution was again cooled to room temperature.
5. The yellow-coloured complex immediately formed upon the addition of 10 mL dilute hydrogen peroxide solution (1:7 vol/vol). Finally, the volumetric flask was filled to the 100-mL mark with water.
6. Calibration solutions were prepared by pipetting 0.5, 1, 2, 3, 4, 5, 6, and 7 mL of 1 mg/mL Ti^{4+} atomic absorption standard (Aldrich) to separate 100-mL

volumetric flasks. About 50 mL de-ionized water was added to each flask followed by 8 mL concentrated H_2SO_4 . The solutions were cooled to room temperature then Step 5 was performed.

The absorbance of the solutions was measured at a wavelength of 410 nm with a 1-cm pathlength uv/visible spectrophotometer (Phillips, Model PU 8740). The titanium content of the catalysts was determined from the calibration curve in Figure A.2. It was necessary to avoid agitating the catalyst solutions before the colorimetric analysis because silica particles, which do not dissolve in acidic media, would make the solutions turbid and give falsely high absorbance measurements.

Table A.4: Colorimetric Results for Ti Content.

Catalyst Name	Catalyst Components on Silica ^a	Ti wt% (Colorimetric)	Ti wt% (Neutron Activation)
CAT-17	Ti + Mg + Ligand	2.1	1.78
CAT-19	Ti + Mg + Ligand	2.8	N/A
CAT-20	Ti + Mg + Ligand	5.9	4.95

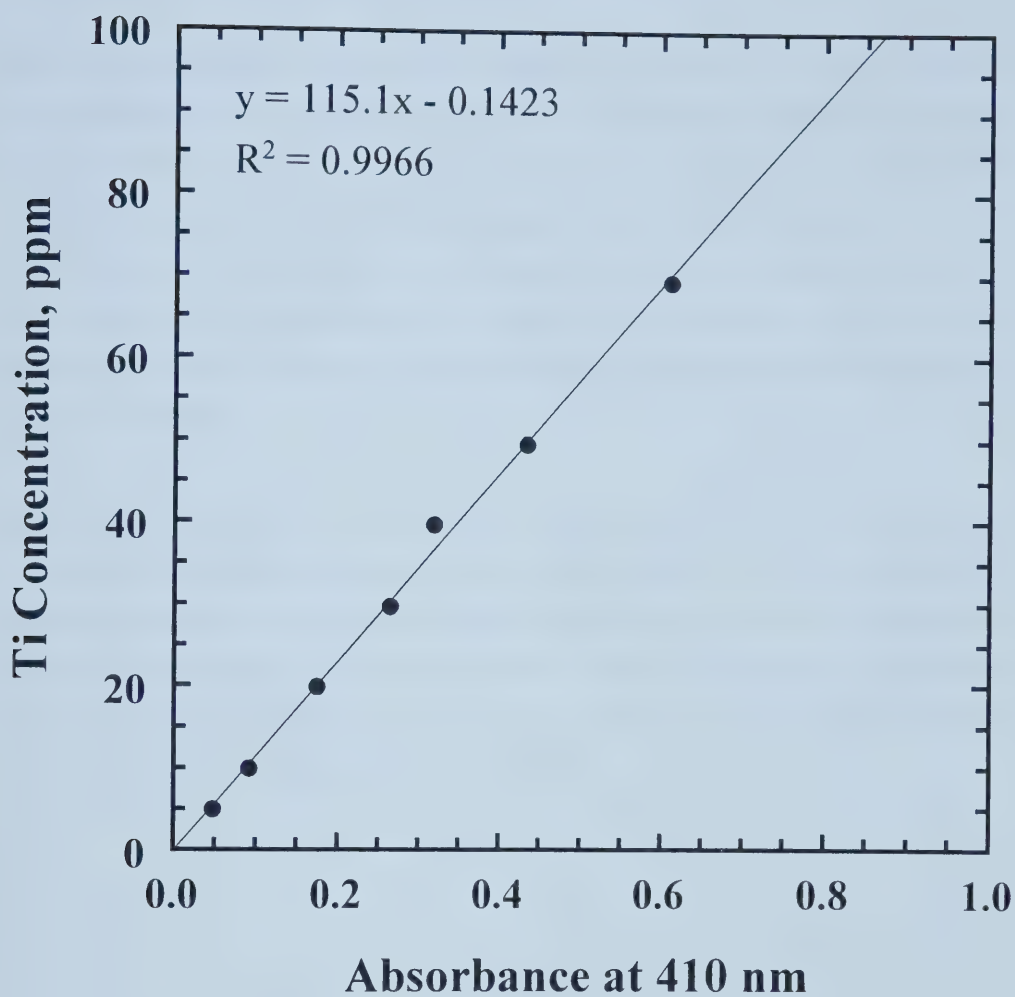


Figure 3.14. Calibration for Ti content with the colorimetric method.

APPENDIX B: Summary of Polymerization Results

Table B.1 summarizes polymerization conditions and yields for all the experiments performed with CAT-12 through CAT-33. Not all of the polymerization experiments were discussed in Chapter 4.0 because some problems were encountered during the experiments (e.g. catalyst injector port plugged, ethylene flow rate restriction, etc.). The ethylene flow rate profiles were integrated to give the calculated PE yield; in some instances the measured yield is higher than the calculated yield due to the presence of residual salt (i.e. some salt remained despite repeatedly rinsing the polymer with water).

The pressure, ethylene flow rate, and temperature profiles for all the polymerization experiments discussed in Chapter 4.0 are given after Table B.1. The polymerization experiments were named with the notation AH-XX-YY, where XX refers to the catalyst number and YY gives the run number. Blank-1 and Blank-2 were collected with the same experimental procedure as the polymerization experiments, except no catalyst or co-catalyst was injected into the reactor.

Table B.1: Summary of Polymerization Conditions and Yields

Run ID	Amount of Catalyst (mg)	TC Bath Temperature ^a (°C)	TIBA Concentration ^b (evac time)	Partial Pressures		Amount of 1-Hexene (mL)	Run Time (h)	Measured PE Yield ^c (g)	Calculated PE Yield ^d (g)
				Ethylene (psi)	Hydrogen (psi)				
Blank-1	0.0	50	N/A	100	0	0.00	N/A	0.0	N/A
Blank-2	0.0	50	N/A	200	0	0.00	N/A	0.0	N/A
AH-12-01 ^e	110.0	50	2.2 mmol TEA	100, 200	0	0.00	2.0	0.2	0.5
AH-12-02 ^e	145.2	70	0.7 mmol TEA	100	0	0.00	1.0	0.0	0.1
AH-13-01 ^e	96.2	50	2.2 mmol TEA	100	0	0.00	2.0	0.2	0.4
AH-14-01	68.8	50	4.4 mmol TEA	100	0	0.00	2.0	54.6	55.4
AH-14-02	45.8	50	1.5 mmol TEA	100	0	0.00	2.0	51.8	49.1
AH-14-03 ^f	46.6	50	0.8 mmol TEA	100	0	0.00	2.1	0.0	N/A
AH-14-04	43.3	50	1.9 mmol TEA	100	0	0.00	2.0	37.0	37.2
AH-14-05	55.9	50	1.3 mmol TEA	100	0	0.00	2.1	59.5	52.6
AH-14-06 ^g	43.7	70	1.3 mmol TEA	100	0	0.00	N/A	0.0	N/A
AH-14-07 ^h	44.4	70	1.5 mmol TEA	100	0	0.00	0.5	14.2	12.5
AH-14-08	44.1	40	1.3 mmol TEA	100	0	0.00	2.0	30.7	30.6
AH-14-09 ^g	45.0	70	1.5 mmol TEA	100	0	0.00	N/A	0.0	N/A
AH-14-10 ^h	43.9	60	1.5 mmol TEA	100	0	0.00	2.0	50.0	50.4
AH-14-11	47.0	60	1.6 mmol TEA	100	0	0.00	2.0	39.8	39.6
AH-14-12 ^h	47.5	50	1.5 mmol TEA	100	0	0.00	1.5	27.7	27.5

Run ID	Amount of Catalyst (mg)	TC Bath Temperature ^a (°C)	TIBA Concentration ^b (evac time)	Partial Pressures		Amount of 1-Hexene (mL)	Run Time (h)	Measured PE Yield ^c (g)	Calculated PE Yield ^d (g)
				Ethylene (psi)	Hydrogen (psi)				
AH-14-13	42.7	50	1.5 mmol TEA	100	0	0.00	2.0	36.2	37.6
AH-14-14 ⁱ	46.7	50	1.5 mmol TEA	100	0	0.00	2.0	42.7	44.1
AH-14-15	41.0	50	0 min	100	0	0.00	2.0	61.3	58.9
AH-14-16	42.0	50	1.4 mmol TIBA	100	0	0.00	2.0	58.5	56.8
AH-14-17 ^g	45.9	50	1.4 mmol TIBA	100	0	0.00	N/A	0.0	N/A
AH-14-18	43.6	50	1.4 mmol TIBA	100	0	0.00	2.1	54.6	51.6
AH-15-01 ^j	46.5	50	1.5 mmol TEA	100	0	0.00	N/A	0.0	N/A
AH-15-02	44.6	50	1.3 mmol TEA	100	0	0.00	2.0	17.5	17.2
AH-15-03	45.1	50	1.5 mmol TEA	100	0	0.00	2.0	16.0	17.2
AH-15-04	46.0	50	1.5 mmol TEA	100	0	0.00	2.0	13.5	13.9
AH-15-05 ⁱ	42.5	50	1.3 mmol TEA	100	0	0.00	2.0	9.6	10.1
AH-15-06	45.4	50	1.5 mmol TEA	100	0	0.00	2.0	20.5	20.9
AH-15-07	43.0	50	1.6 mmol TIBA	100	0	0.00	2.0	32.2	32.1
AH-16-01	42.0	50	1.4 mmol TIBA	100	0	0.00	2.0	21.4	17.3
AH-16-02	43.4	50	1.6 mmol TIBA	100	0	0.00	2.2	18.9	17.9
AH-16-03	46.0	50	>1.6 mmol TIBA	100	0	0.00	2.0	21.4	20.7
AH-17-01	46.1	60	3 min	100	0	0.00	2.0	3.0	3.1
AH-17-02 ^k	50.5	60	2 min	100	0	0.00	2.0	13.5	13.5

Run ID	Amount of Catalyst (mg)	TC Bath Temperature ^a (°C)	TIBA Concentration ^b (evac time)	Partial Pressures		Amount of l-Hexene (mL)	Run Time (h)	Measured PE Yield ^c (g)	Calculated PE Yield ^d (g)
				Ethylene (psi)	Hydrogen (psi)				
AH-17-03 ^k	50.3	55	2 min	100	0	2.89	2.0	9.5	9.9
AH-18-01	49.3	60	2 min	100	0	0.00	2.0	12.1	12.6
AH-18-02	49.7	60	2 min	100	0	2.80	2.0	54.3	48.9
AH-18-03 ^l	26.1	60	2 min	100	0	0.00	1.3	1.7	3.3
AH-19-01 ^k	46.8	55	2 min	100	0	0.00	1.8	62.2	53.4
AH-19-02	47.5	50	2 min	100	0	2.74	1.1	129.4	99.0
AH-20-01 ^m	49.4	50	5 min	100	0	0.00	1.0	125.6	104.9
AH-20-02	20.8	50	2.5 min	100	0	2.87	1.0	187.0	N/A
AH-20-03 ^k	12.2	60	2 min	100	0	2.68	2.0	40.6	38.7
AH-20-04 ⁱ	20.4	60	3 min	100, 200	0	2.86	1.0	137.9	102.2
AH-20-05	21.4	60	2 min	100	0	2.92	0.5	51.5	44.6
AH-20-06 ⁿ	21.0	60	2 min	100	0	4.55	1.0	99.6	N/A
AH-22-01 ^k	48.2	55	2 min	100	0	0.00	1.0	6.3	8.8
AH-22-02	49.6	50	2 min	100	0	3.01	1.0	68.9	57.7
AH-23-01	19.0	50	2.5 min	100	0	4.25	1.0	93.0	83.8
AH-23-02	40.5	50	2 min	100	10	0.00	2.0	13.3	14.0
AH-23-03 ⁱ	39.4	50	2 min	100	15	0.00	2.0	12.3	12.0
AH-24-01	50.9	50	2 min	100	0	0.00	2.5	133.0	116.0

Run ID	Amount of Catalyst (mg)	TC Bath Temperature ^a (°C)	TIBA Concentration ^b (evac time)	Partial Pressures		Amount of 1-Hexene (mL)	Run Time (h)	Measured PE Yield ^c (g)	Calculated PE Yield ^d (g)
				Ethylene (psi)	Hydrogen (psi)				
AH-24-02	49.3	50	2 min	100	0	2.83	0.75	126.6	N/A
AH-24-03	21.1	50	2 min	100	0	2.68	2.0	95.2	87.8
AH-24-04	51.2	70	2 min	100	0	0.00	2.0	35.9	32.9
AH-24-05	59.8	50	2 min	100	0	0.00	2.5	92.5	86.7
AH-24-06	51.4	50	2 min	100	5	0.00	1.5	19.5	19.9
AH-24-07	41.5	50	2 min	100	0	0.00	2.0	13.8	14.4
AH-24-08	51.1	40	2 min	100	0	0.00	2.0	27.7	27.0
AH-25-01 ^o	50.0	50	2 min	100	0	0.00	2.0	unknown	31.3
AH-25-02	50.0	50	0 min	100	0	0.00	2.0	36.0	35.3
AH-25-03	50.5	50	0 min	100	0	0.00	1.5	140.3	140.7
AH-25-04	50.5	50	2 min	100	0	0.00	2.5	164.6	147.3
AH-25-05	49.4	50	12 min	100	0	0.00	3.0	49.8	46.5
AH-25-06	19.8	50	0 min	100	0	2.85	3.0	142.7	N/A
AH-25-07	20.2	50	2 min	100	0	2.84	2.0	111.0	99.0
AH-25-08	50.5	70	2 min	100	0	0.00	2.0	157.7	144.6
AH-25-09	51.0	50	0 min	90	10	0.00	2.0	58.6	56.2
AH-25-10	51.0	50	0 min	100	10	0.00	2.0	70.4	63.9
AH-26-01	51.0	50	0 min	100	0	0.00	2.0	4.5	3.7

Run ID	Amount of Catalyst (mg)	TC Bath Temperature ^a (°C)	TIBA Concentration ^b (evac time)	Partial Pressures		Amount of I-Hexene (mL)	Run Time (h)	Measured PE Yield ^c (g)	Calculated PE Yield ^d (g)
				Ethylene (psi)	Hydrogen (psi)				
AH-26-02	50.4	50	0 min	100	0	2.70	2.0	4.9	3.6
AH-26-03	50.3	50	2 min	100	0	0.00	2.0	6.5	6.3
AH-26-04	50.5	70	2 min	100	0	0.00	2.0	10.8	10.0
AH-27-01	50.4	50	2 min	100	0	0.00	2.0	42.5	40.3
AH-27-02	50.5	50	0 min	100	0	0.00	2.0	67.4	60.4
AH-27-03	50.2	50	0 min	200	0	0.00	1.0	185.3	N/A
AH-27-04	51.4	70	2 min	100	0	0.00	2.0	121.9	111.6
AH-27-05	20.4	50	2 min	100	0	2.77	2.1	30.5	29.2
AH-27-06	24.4	50	0 min	200	0	2.80	2.0	57.1	54.2
AH-28-01 ⁱ	50.5	50	0 min	100	0	0.00	2.0	166.6	141.8
AH-28-02	51.5	5	2 min	100	0	0.00	1.5	172.6	162.4
AH-28-03	49.7	50	0 min	100	0	0.00	2.0	145.8	141.8
AH-28-04	20.6	50	0 min	100	0	2.75	1.0	92.3	N/A
AH-28-05	22.2	50	0 min	100	0	2.74	1.2	61.0	57.0
AH-28-06	50.6	70	2 min	100	0	0.00	1.5	150.7	120.5
AH-28-07	51.2	50	2 min	100	10	0.00	2.0	49.8	43.8
AH-29-01 ⁱ	51.9	50	2 min	100	0	0.00	2.0	136.2	123.4
AH-29-02 ^j	50.5	50	0 min	100	0	0.00	2.0	142.8	116.3

Run ID	Amount of Catalyst (mg)	TC Bath Temperature ^a (°C)	TIBA Concentration ^b (evac time)	Partial Pressures		Amount of 1-Hexene (mL)	Run Time (h)	Measured PE Yield ^c (g)	Calculated PE Yield ^d (g)
				Ethylene (psi)	Hydrogen (psi)				
AH-29-03 ⁱ	51.3	70	2 min	100	0	0.00	2.0	160.8	115.4
AH-29-04 ⁱ	49.7	70	2 min	100	0	0.00	2.0	26.8	12.7
AH-29-05	51.0	70	2 min	100	0	0.00	2.0	175.3	160.2
AH-29-06	49.6	50	2 min	100	11	0.00	2.1	69.0	66.0
AH-29-07 ⁱ	20.2	50	0 min	100	0	2.80	2.0	101.4	100.7
AH-29-08 ⁱ	50.3	50	0 min	100	0	0.00	3.0	178.0	150.0
AH-29-09 ⁱ	50.4	50	0 min	100	0	0.00	2.0	90.8	85.6
AH-29-10	51.3	50	0 min	100	0	0.00	2.0	158.2	141.9
AH-29-11	51.2	50	2 min	100	0	0.00	2.0	201.3	162.2
AH-30-01	51.6	50	0 min	100	0	0.00	2.0	117.8	103.3
AH-30-02	50.4	50	2.5 min	100	0	0.00	2.5	149.6	126.3
AH-30-03	50.2	70	2 min	100	0	0.00	1.5	154.4	113.5
AH-30-04	50.2	50	0 min	100	0	0.00	2.0	120.4	110.4
AH-30-05	50.7	50	2 min	100	10	0.00	1.1	50.1	46.0
AH-30-06	50.0	50	2 min	100	0	0.00	2.5	164.0	150.3
AH-30-07	20.5	50	0 min	100	0	2.71	2.3	90.6	76.0
AH-30-08	51.1	50	2 min	200	0	0.00	1.0	216.5	N/A
AH-30-09 ^p	50.5	50	2 min	100	0	0.00	2.0	39.5	38.0

Run ID	Amount of Catalyst (mg)	TC Bath Temperature ^a (°C)	TIBA Concentration ^b (evac time)	Partial Pressures		Amount of 1-Hexene (mL)	Run Time (h)	Measured PE Yield ^c (g)	Calculated PE Yield ^d (g)
				Ethylene (psi)	Hydrogen (psi)				
AH-30-10 ^p	52.6	50	2 min	100	0	0.00	2.0	23.3	23.6
AH-31-01	50.6	50	2 min	100	0	0.00	2.3	149.9	129.1
AH-31-02 ^q	50.9	50	2 min	100	0	0.00	2.0	12.5	11.9
AH-31-03 ^r	51.6	50	2 min	100	0	0.00	3.5	183.2	165.3
AH-31-04	50.5	70	2 min	100	10	0.00	2.1	78.6	66.6
AH-31-05 ^s	51.8	70	2 min	100	40	0.00	2.0	53.2	47.1
AH-31-06	50.3	70	2 min	100	5	0.00	2.0	121.8	91.5
AH-31-07	51.9	70	2 min	100	20	0.00	2.0	84.6	73.6
AH-31-08 ^s	22.2	70	2 min	100	10	2.87	1.5	3.9	5.3
AH-31-09	22.3	70	2 min	100	10	2.91	2.0	70.5	66.4
AH-31-10 ^s	22.5	70	2 min	100	40	2.68	2.0	52.6	50.9
AH-31-11	23.0	70	2 min	100	20	2.84	2.2	65.1	54.5
AH-31-12 ^s	22.8	70	2 min	100	60	2.80	2.0	44.0	44.2
AH-32-01	51.9	70	2 min	100	10	0.00	2.0	61.1	58.0
AH-32-02	52.3	90	2 min	100	10	0.00	2.0	31.7	30.8
AH-32-03 ^s	25.0	80	2 min	100, 200	100	5.96	2.1	0.0	N/A
AH-32-04 ^s	25.9	80	2 min	100	60	5.98	2.0	33.1	31.1
AH-32-05 ^o	25.4	80	2 min	100	60	1.99	2.0	unknown	27.7

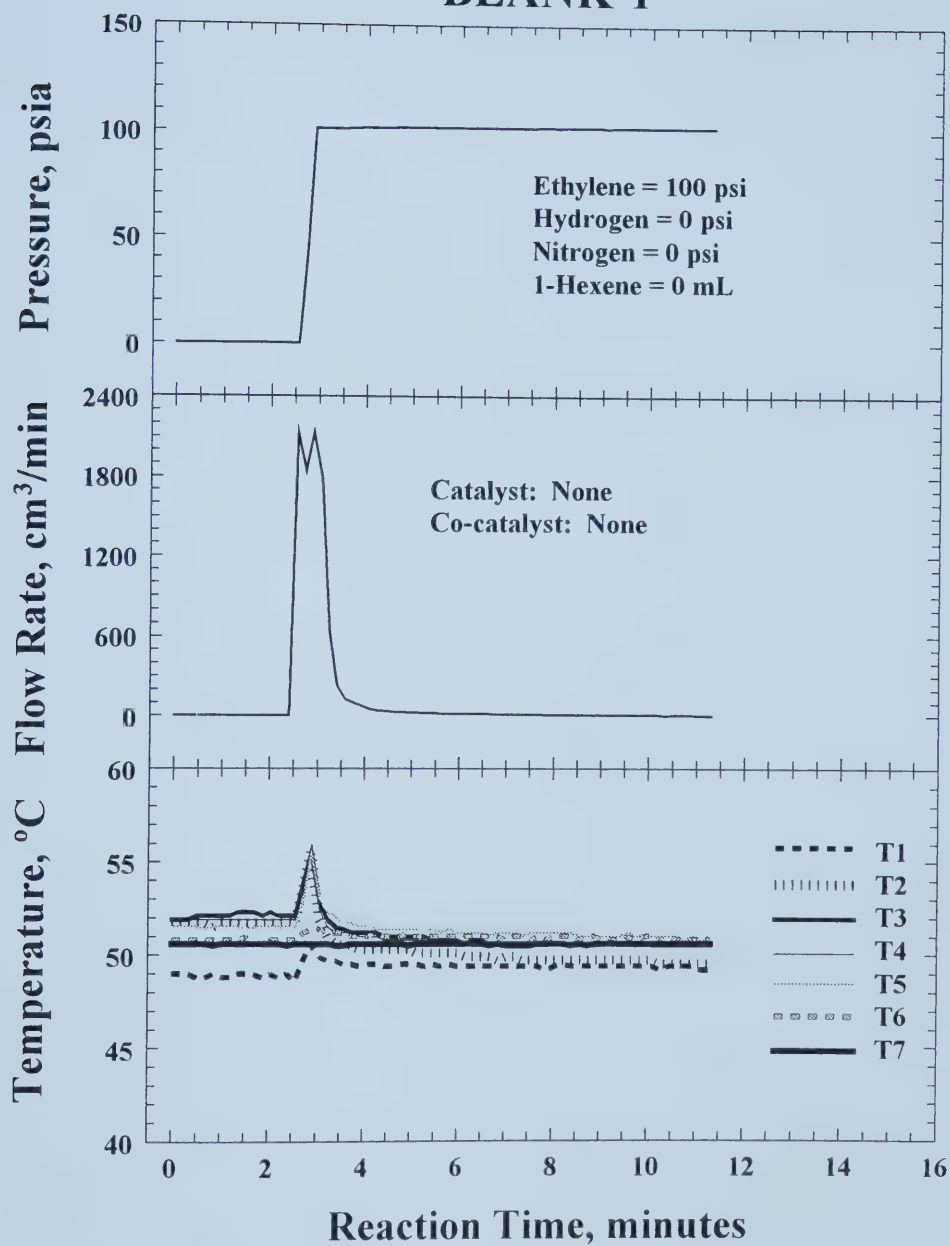
Run ID	Amount of Catalyst (mg)	TC Bath Temperature ^a (°C)	TIBA Concentration ^b (evac time)	Partial Pressures		Amount of 1-Hexene (mL)	Run Time (h)	Measured PE Yield ^c (g)	Calculated PE Yield ^d (g)
				Ethylene (psi)	Hydrogen (psi)				
AH-32-06	25.9	80	2 min	100	60	6.94	2.0	37.5	35.8
AH-32-07	26.0	80	2 min	100	60	4.00	2.0	47.4	42.9
AH-32-08	26.5	80	2 min	100	60	0.00	2.0	18.2	18.9
AH-32-09	25.2	80	2 min	100	60	6.09	0.5	7.8	8.6
AH-32-10	49.0	70	2 min	100	40	0.00	2.0	37.8	34.2
AH-32-11	50.0	70	2 min	100	40	0.00	2.0	35.3	32.3
AH-32-12	49.9	70	2 min	100	40	0.00	2.0	42.7	36.3
AH-33-01	49.9	70	2 min	100	0	0.00	2.0	53.3	50.8
AH-33-02	50.2	50	2 min	100	0	0.00	2.2	28.1	27.2
AH-33-03 ⁿ	51.0	50	2 min	100	0	3.54	2.0	59.0	57.8
AH-33-04	51.1	70	2 min	100	10	0.00	2.1	33.3	32.9
AH-33-05	50.0	70	2 min	100	40	0.00	2.0	25.4	26.5
AH-33-06	50.9	70	2 min	100	5	0.00	2.1	41.9	41.0
AH-33-07 ^t	50.8	70	2 min	100	21	0.00	1.0	0.0	N/A
AH-33-08	52.2	70	2 min	100	20	0.00	2.0	35.5	30.0
AH-33-09	27.3	80	2 min	100	60	5.91	2.4	42.5	40.3
AH-33-10	25.2	80	2 min	100	60	6.14	0.5	11.3	11.0
AH-33-11	25.4	80	2 min	100	60	2.08	2.0	23.0	21.1

Run ID	Amount of Catalyst (mg)	TC Bath Temperature ^a (°C)	TIBA Concentration ^b (evac time)	Partial Pressures		Amount of 1-Hexene (mL)	Run Time (h)	Measured PE Yield ^c (g)	Calculated PE Yield ^d (g)
				Ethylene (psi)	Hydrogen (psi)				
AH-33-12	25.1	80	2 min	100	60	4.08	2.0	8.3	8.4
AH-33-13	26.5	80	2 min	100	60	3.96	2.0	29.1	24.4
AH-33-14	26.7	80	2 min	100	60	6.98	2.0	38.3	34.8

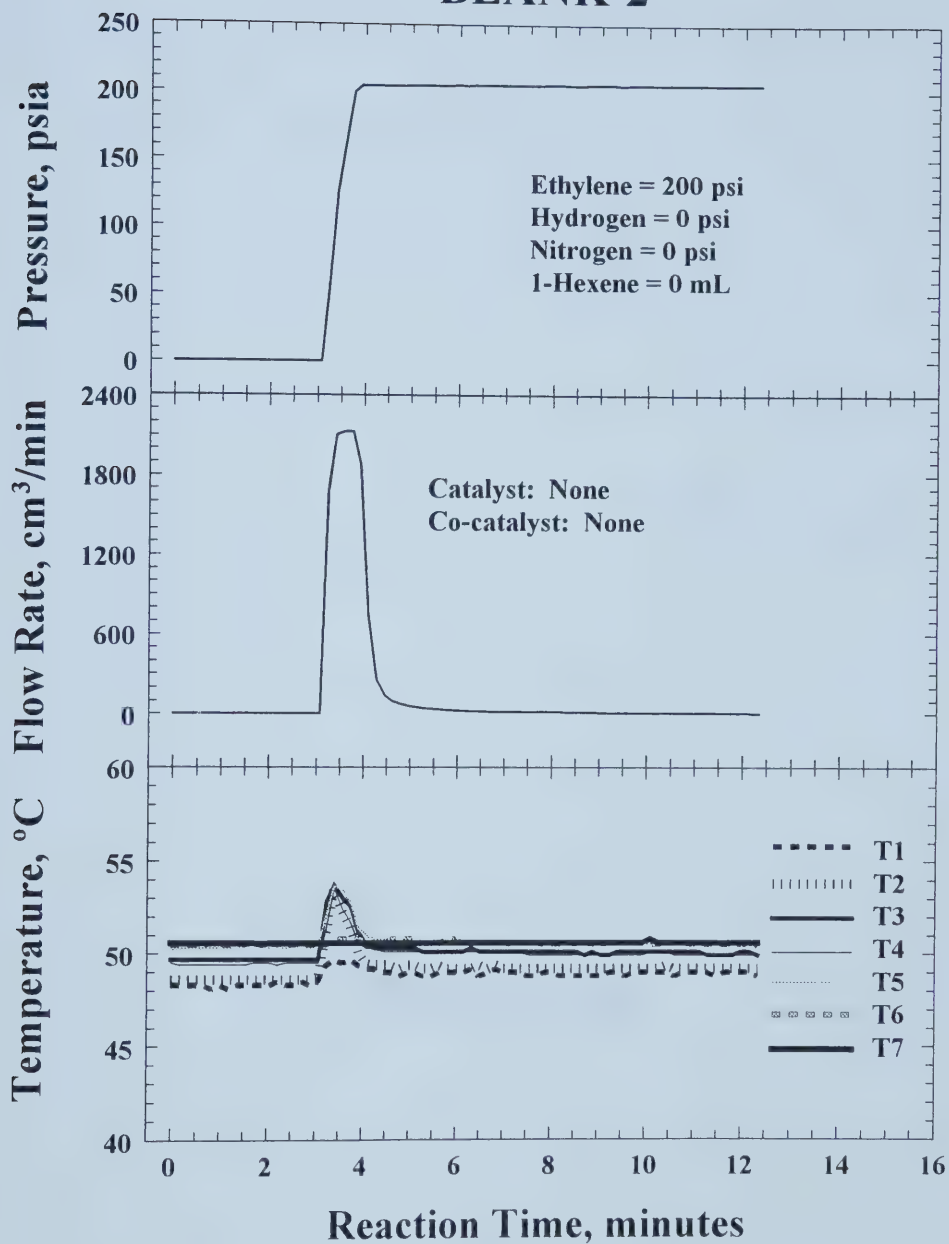
- Temperature of circulating oil bath increased above set point for high activity polymerization runs
- Unless otherwise stated, added 0.2 mL (0.8 mmol) TIBA then evacuated the reactor for the specified time after scavenging impurities
- Measured yield may be to high due to the presence of residual salt
- Calculated yield determined from integration of ethylene flow rate (N/A if maximum flow rate exceeded)
- Very low activity experiment
- Very low activity experiment (not enough TEA to scavenge impurities)
- Most of the catalyst remained in the holder after injection because the catalyst port was plugged
- Mixer noisy during the experiment (mixer shaft plugged)
- Ethylene flow rate restriction because mixer shaft plugged or very high flow rates
- Ethylene cylinder closed during experiment
- Attempted to maintain constant gas-phase temperatures by adjusting temperature of oil bath
- Did not purge end of catalyst holder properly before connecting it to the port on the top flange
- Evacuated TIBA longer than usual because vacuum line plugged with polymer

- n Accidentally added too much 1-hexene (exceeded volume to achieve saturation)
- o Lost some polymer down the sink while rinsing salt out of the product
- p Used helical stirrer blade in center position of mixer shaft
- q Stirred catalyst in the reactor with 100 psi nitrogen for 30 min before adding ethylene
- r Used 160 g NaCl seed bed
- s Some of the catalyst remained in the holder after injection
- t Reactor not sealed properly because mixer blades installed incorrectly

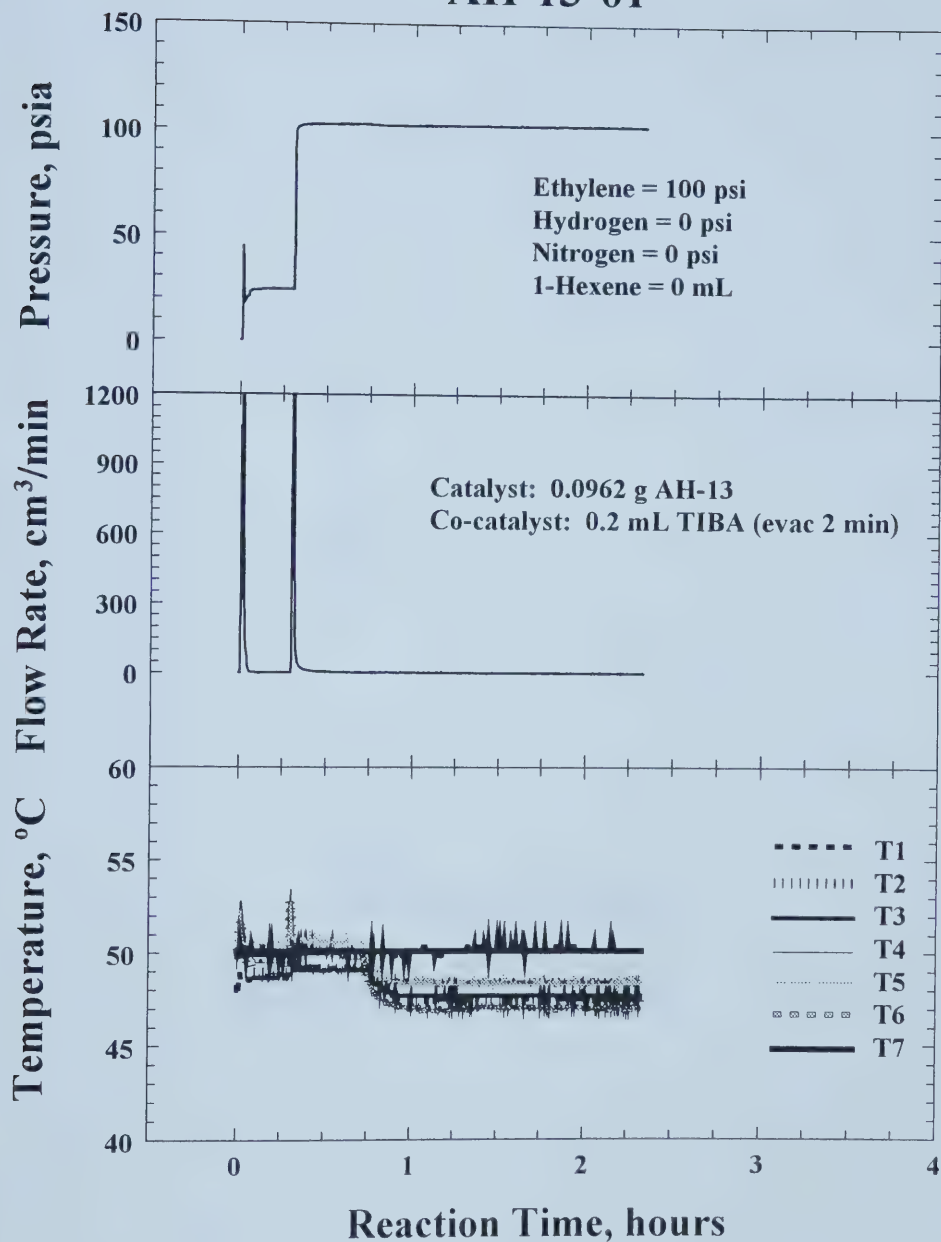
BLANK-1



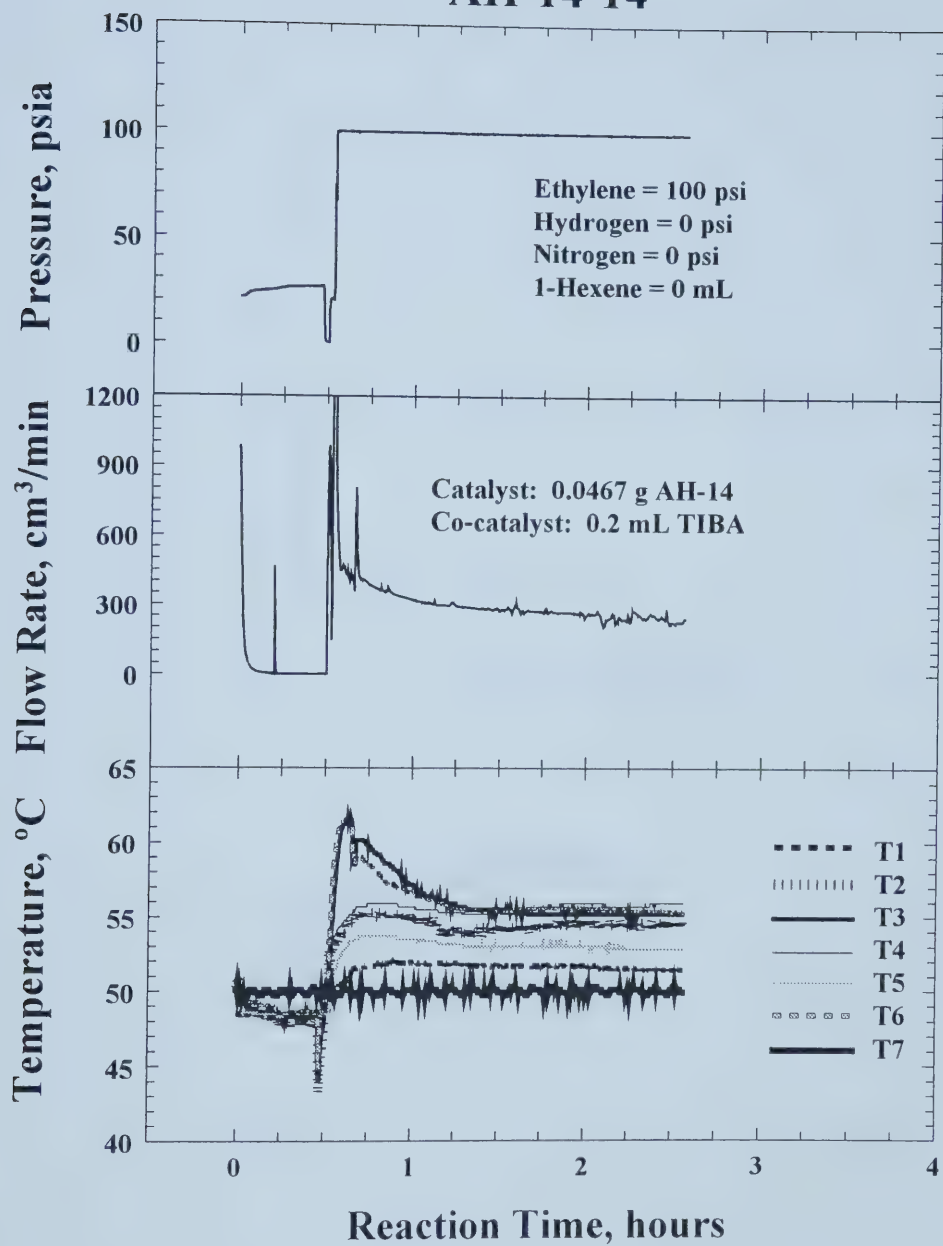
BLANK-2



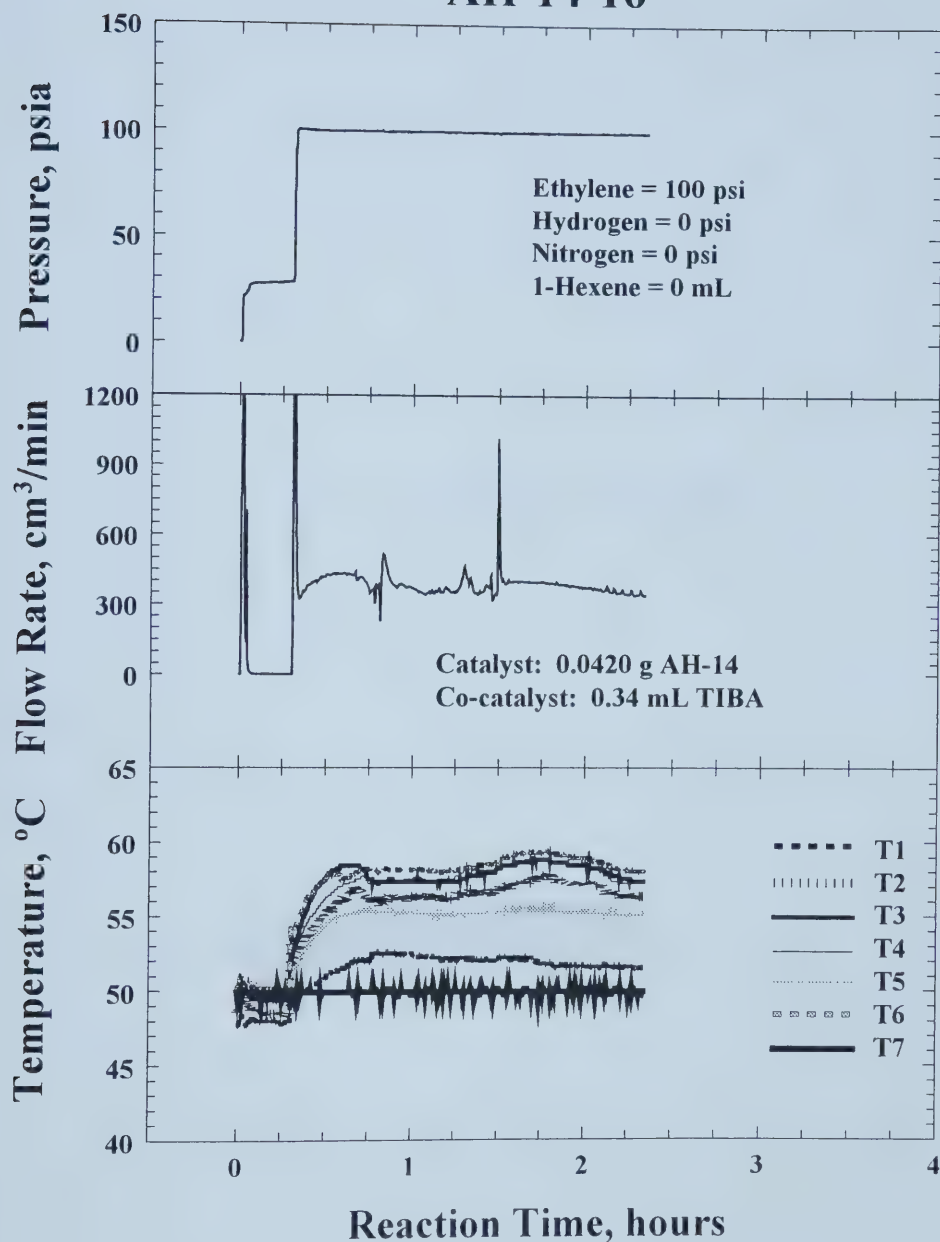
AH-13-01



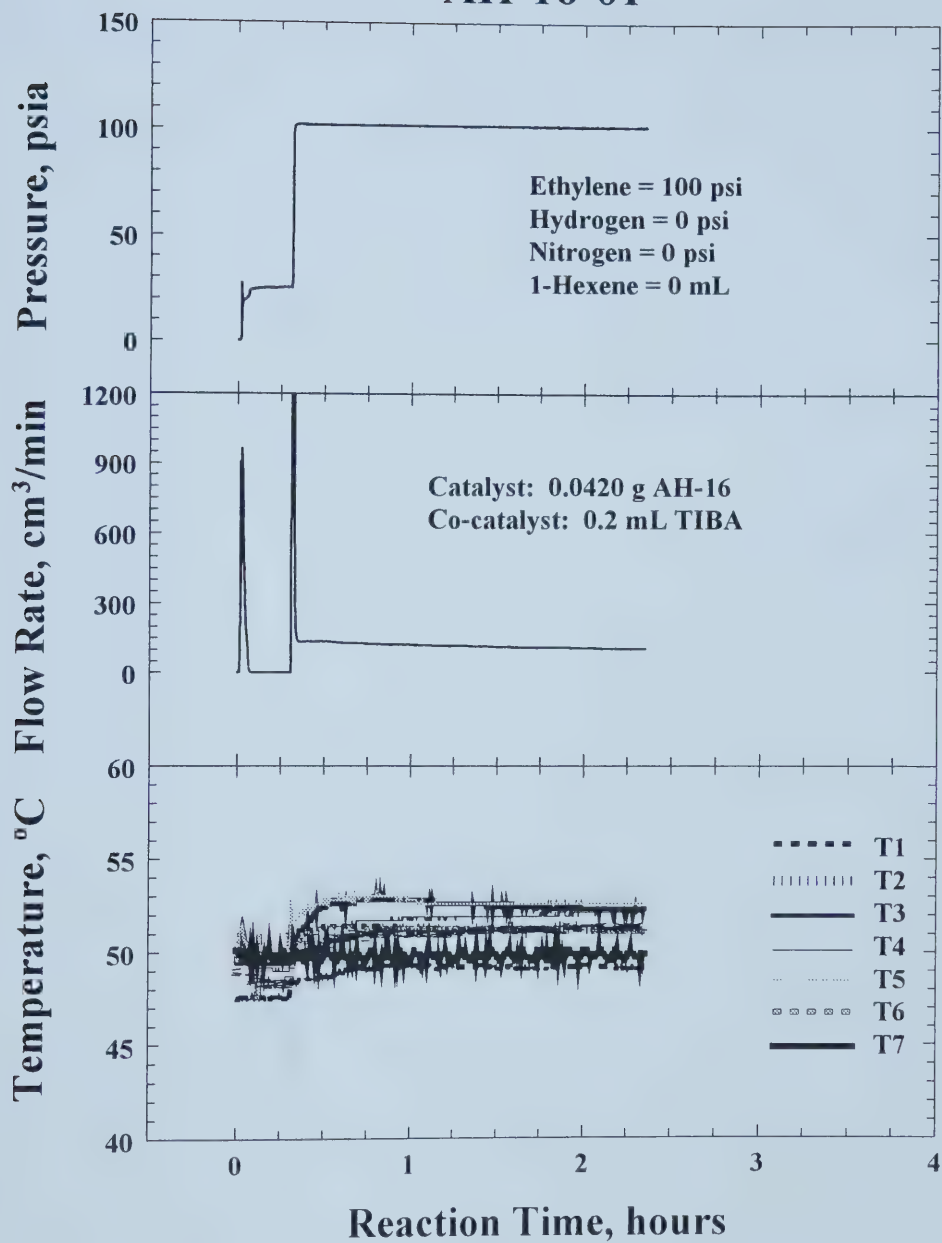
AH-14-14



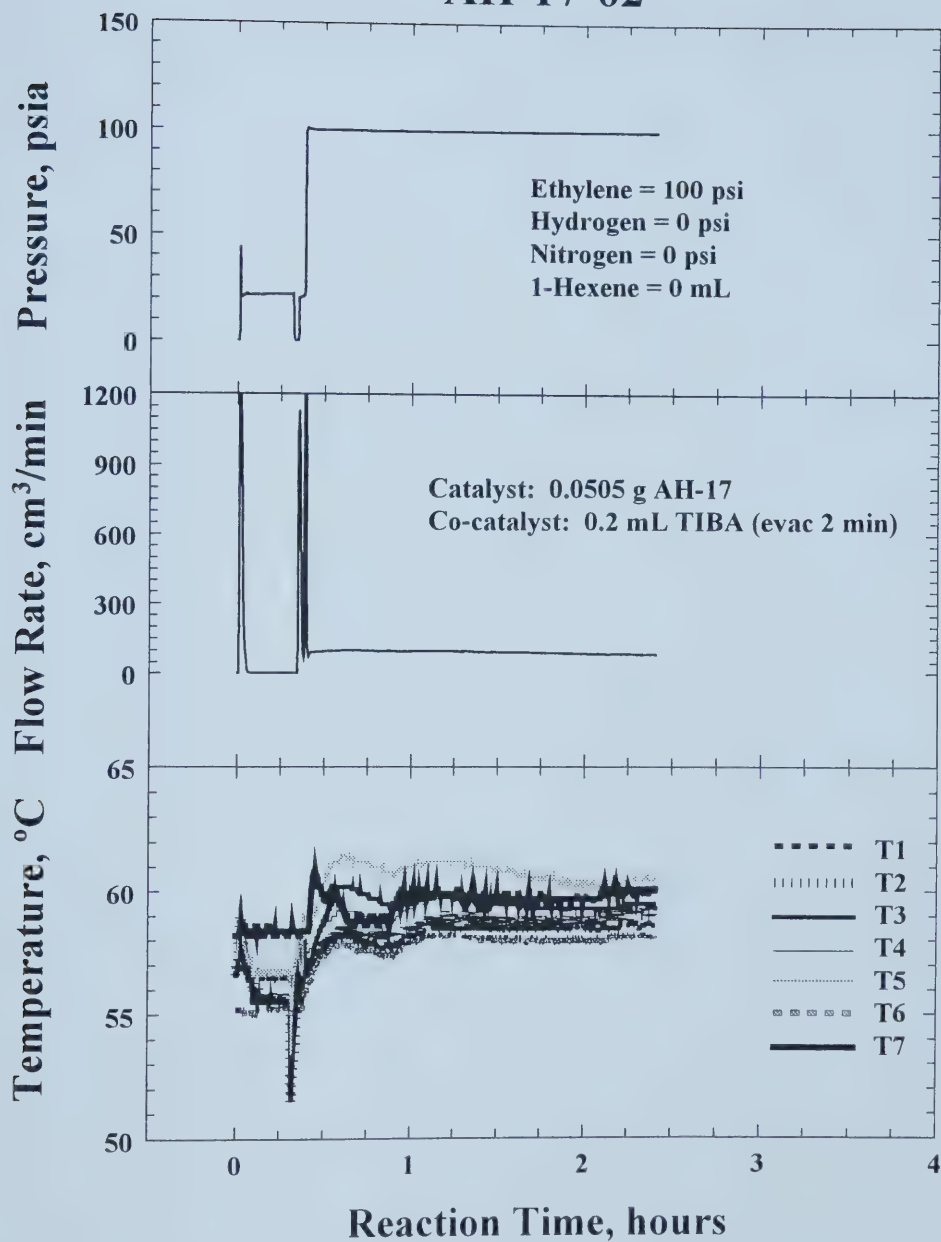
AH-14-16



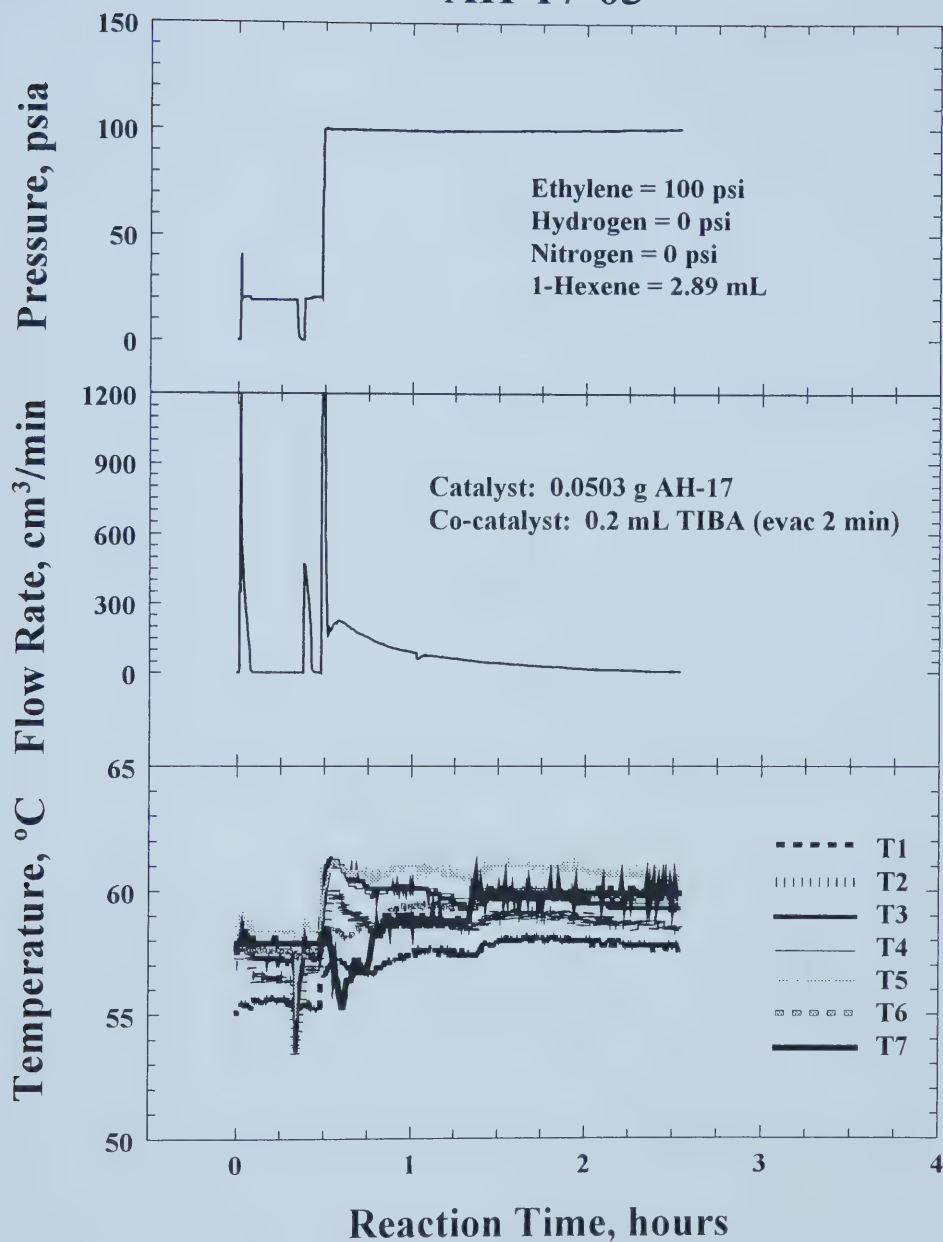
AH-16-01



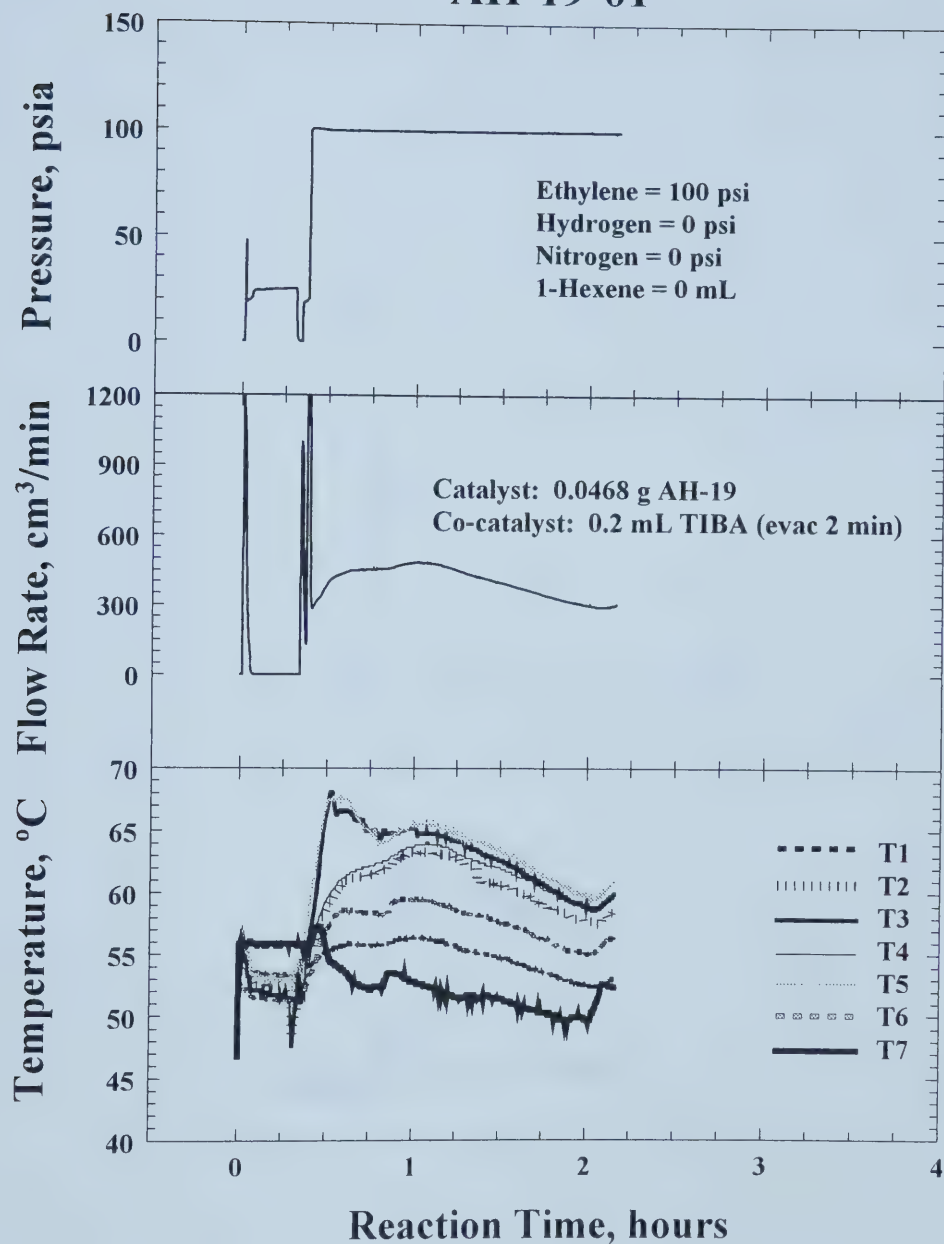
AH-17-02



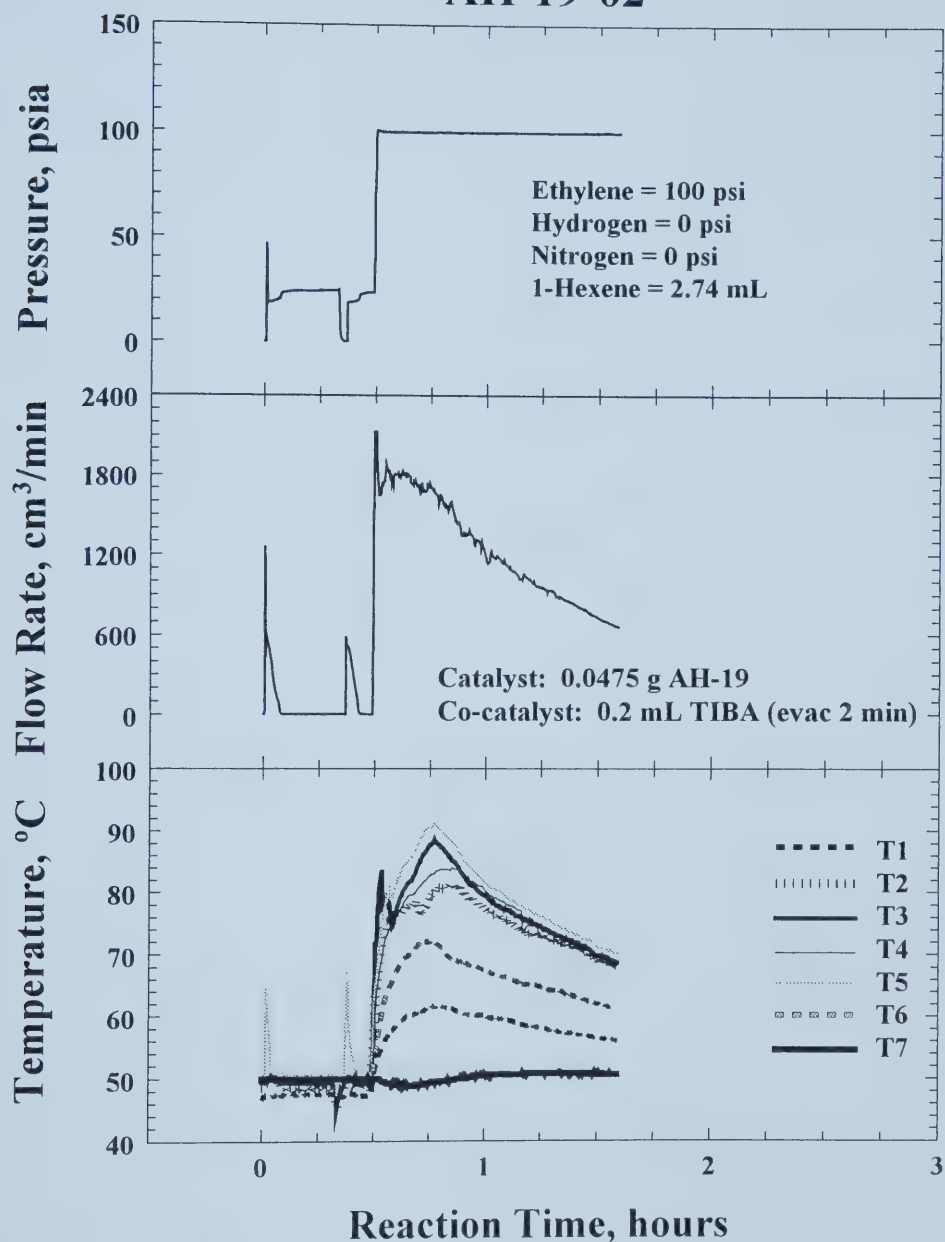
AH-17-03



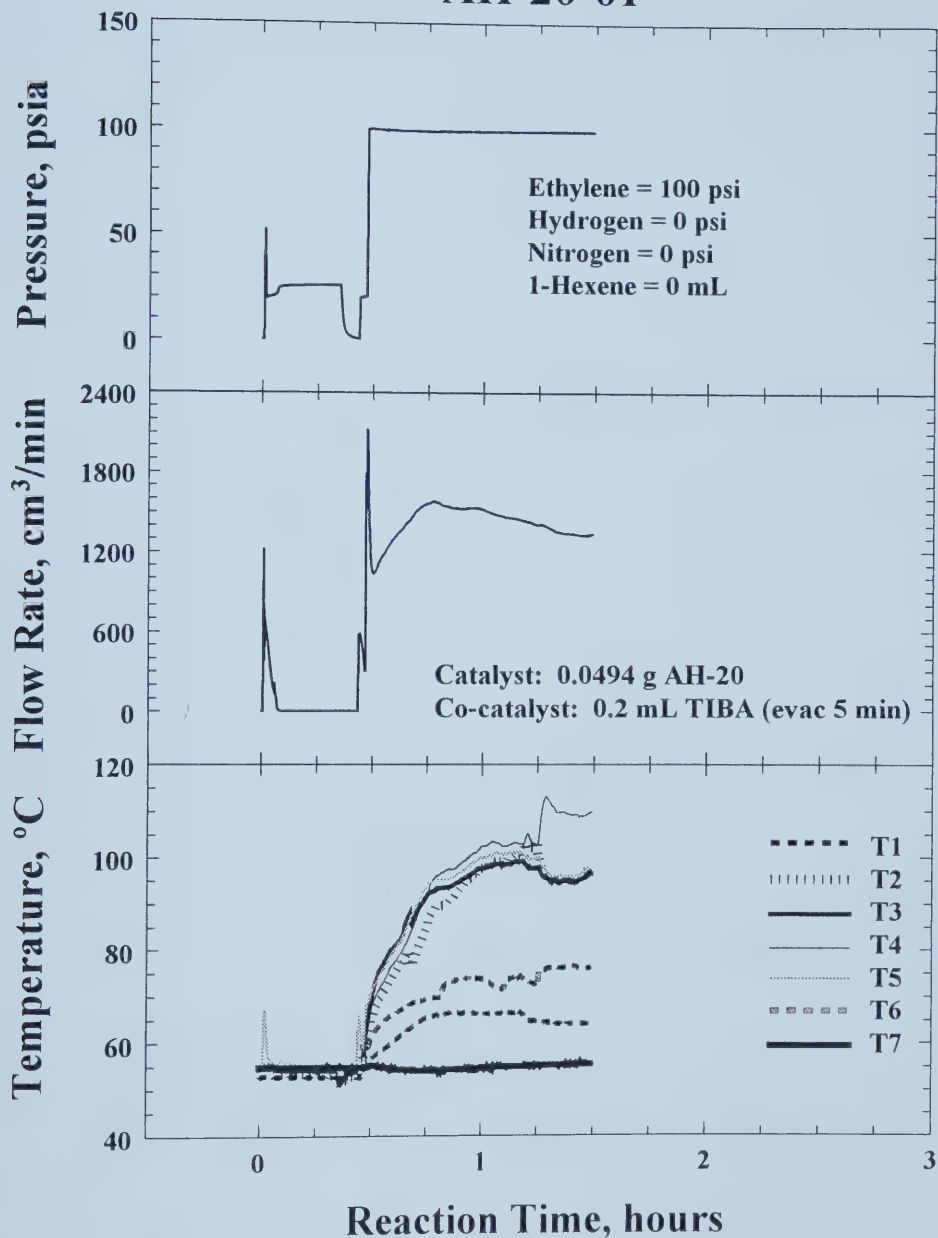
AH-19-01



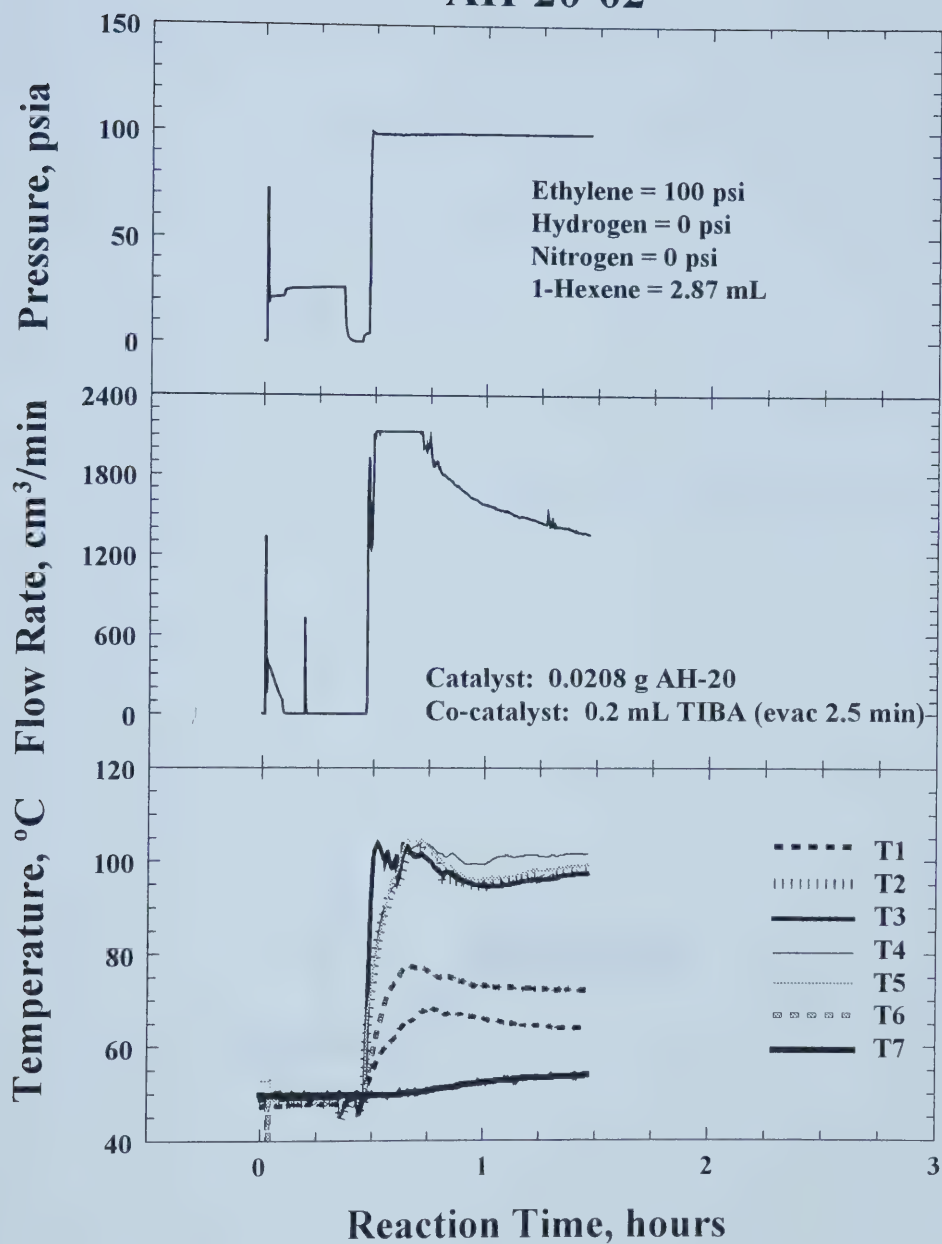
AH-19-02



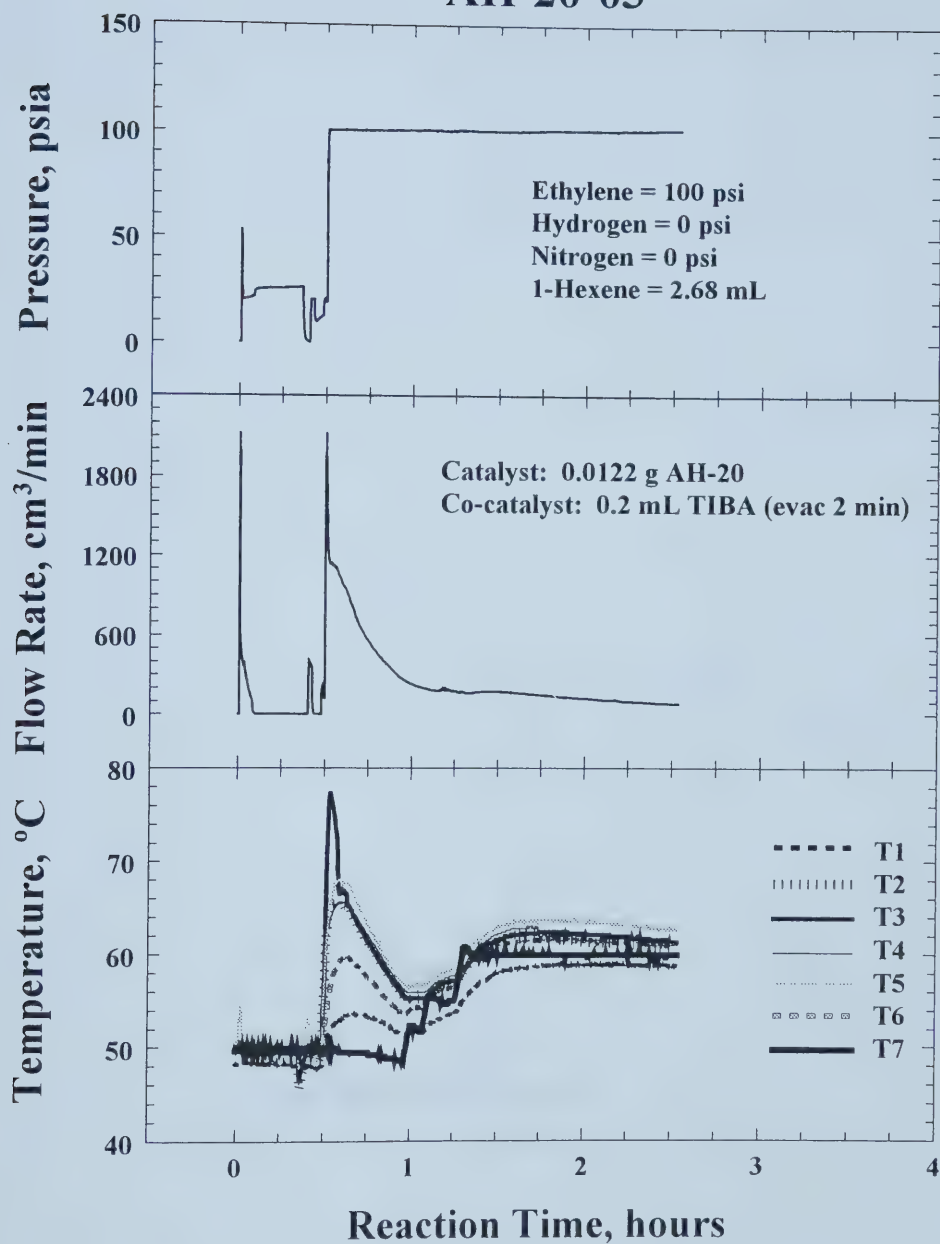
AH-20-01



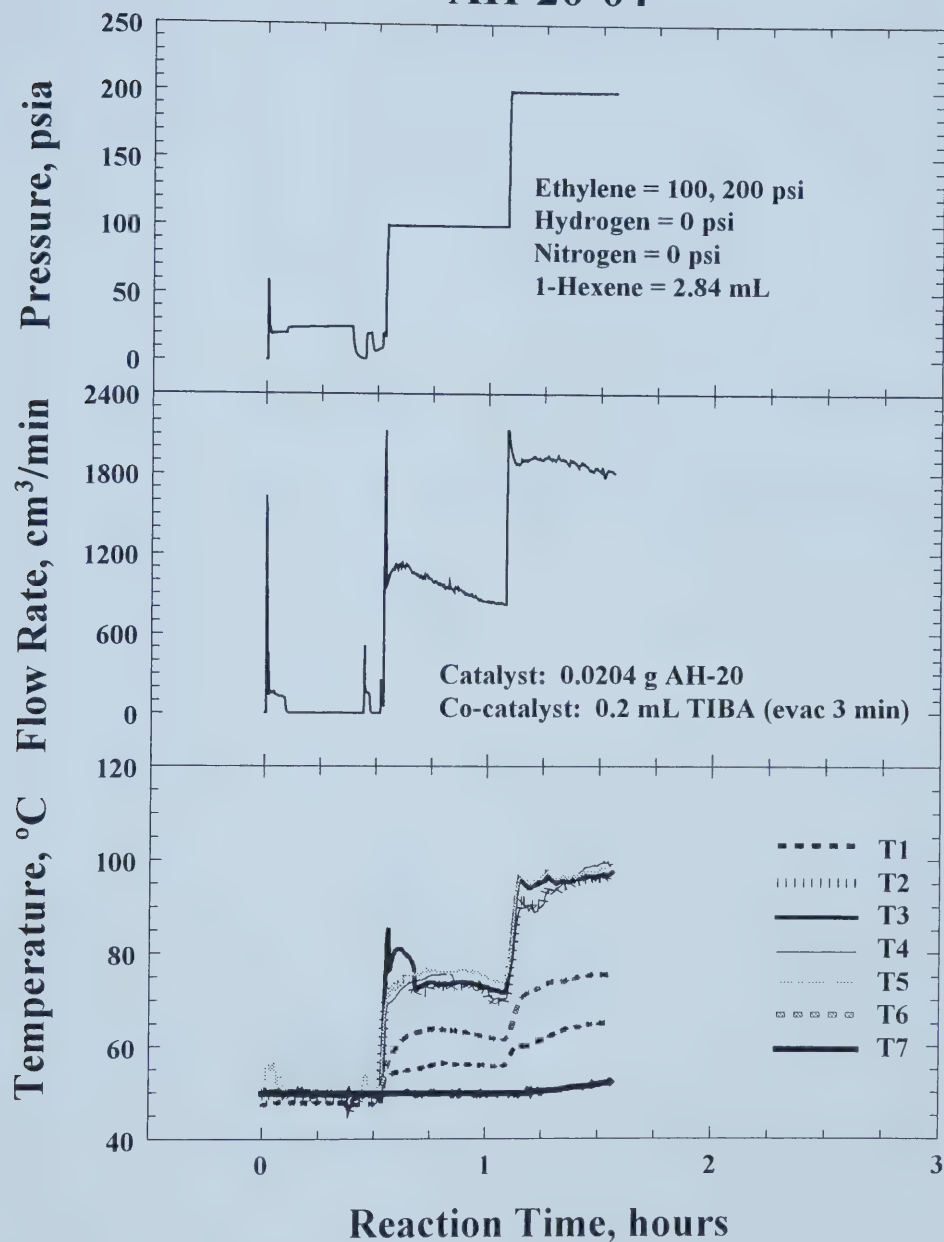
AH-20-02



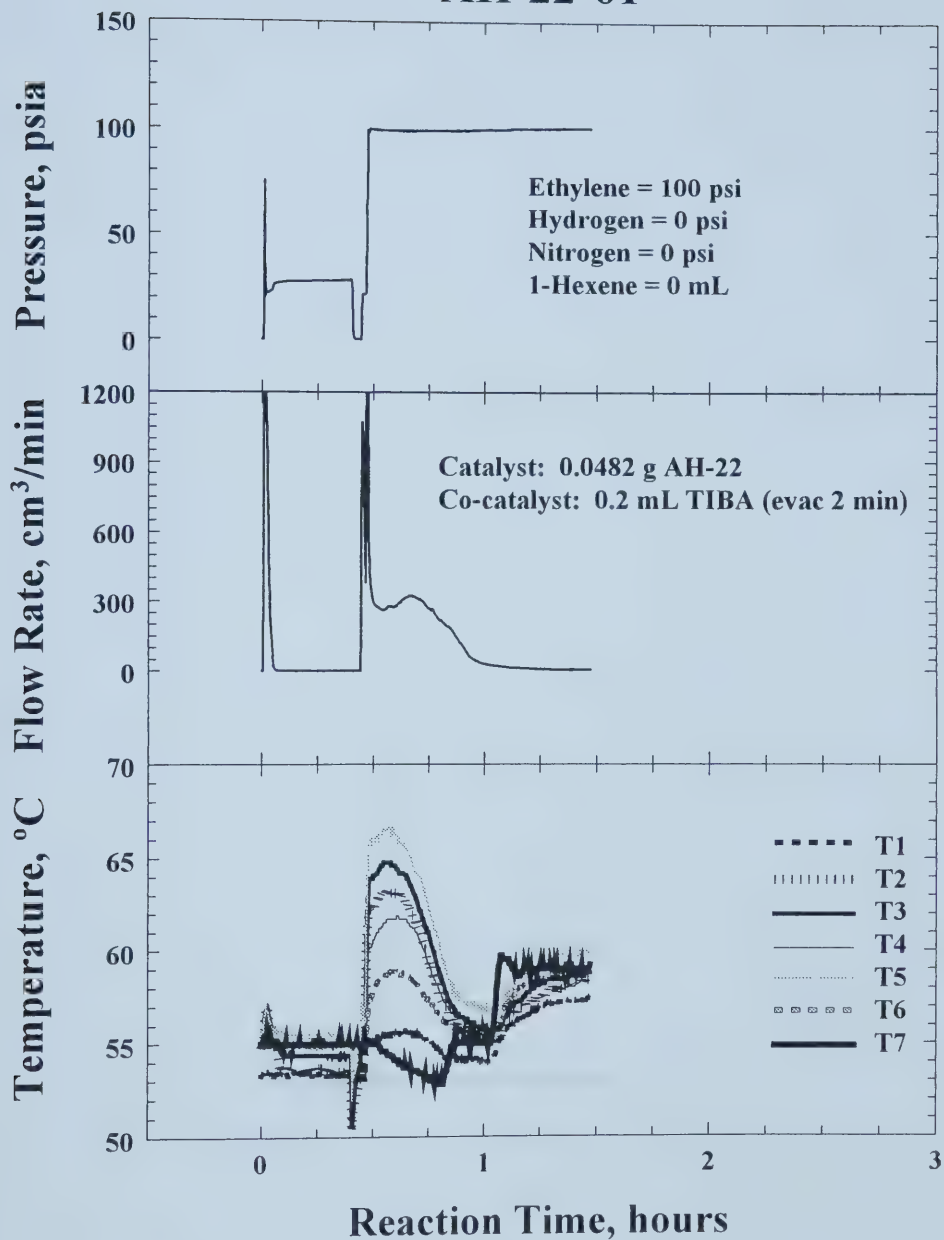
AH-20-03



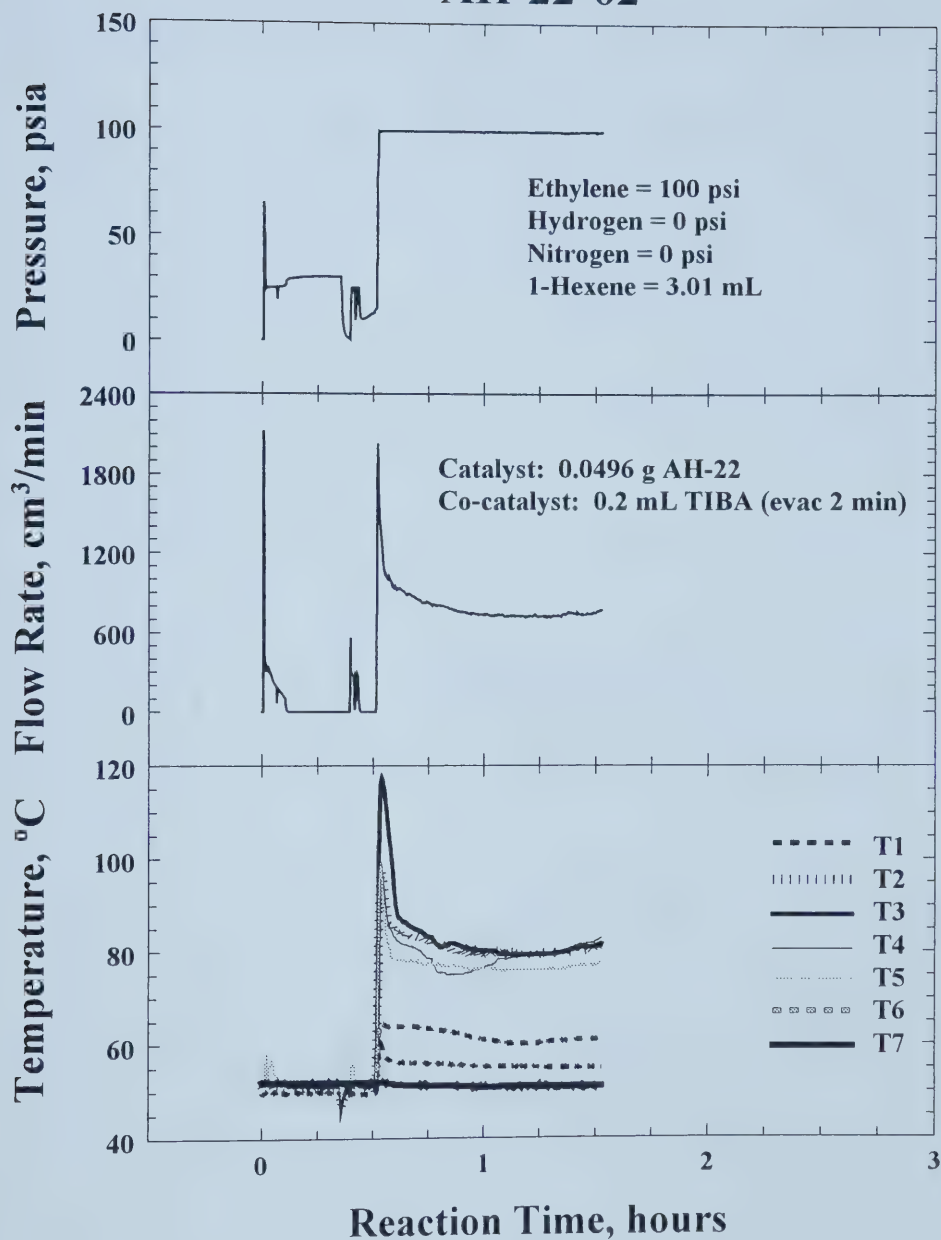
AH-20-04



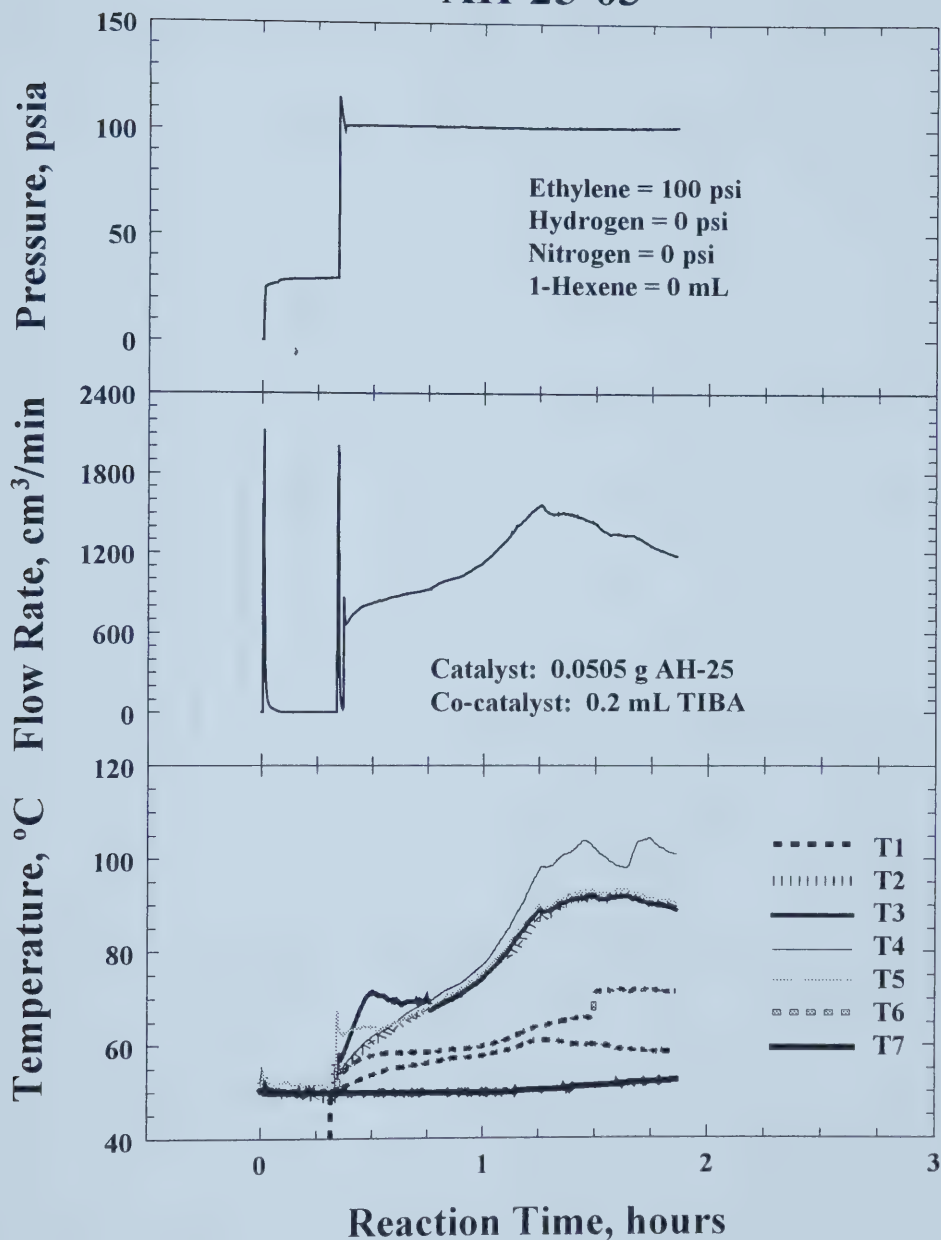
AH-22-01



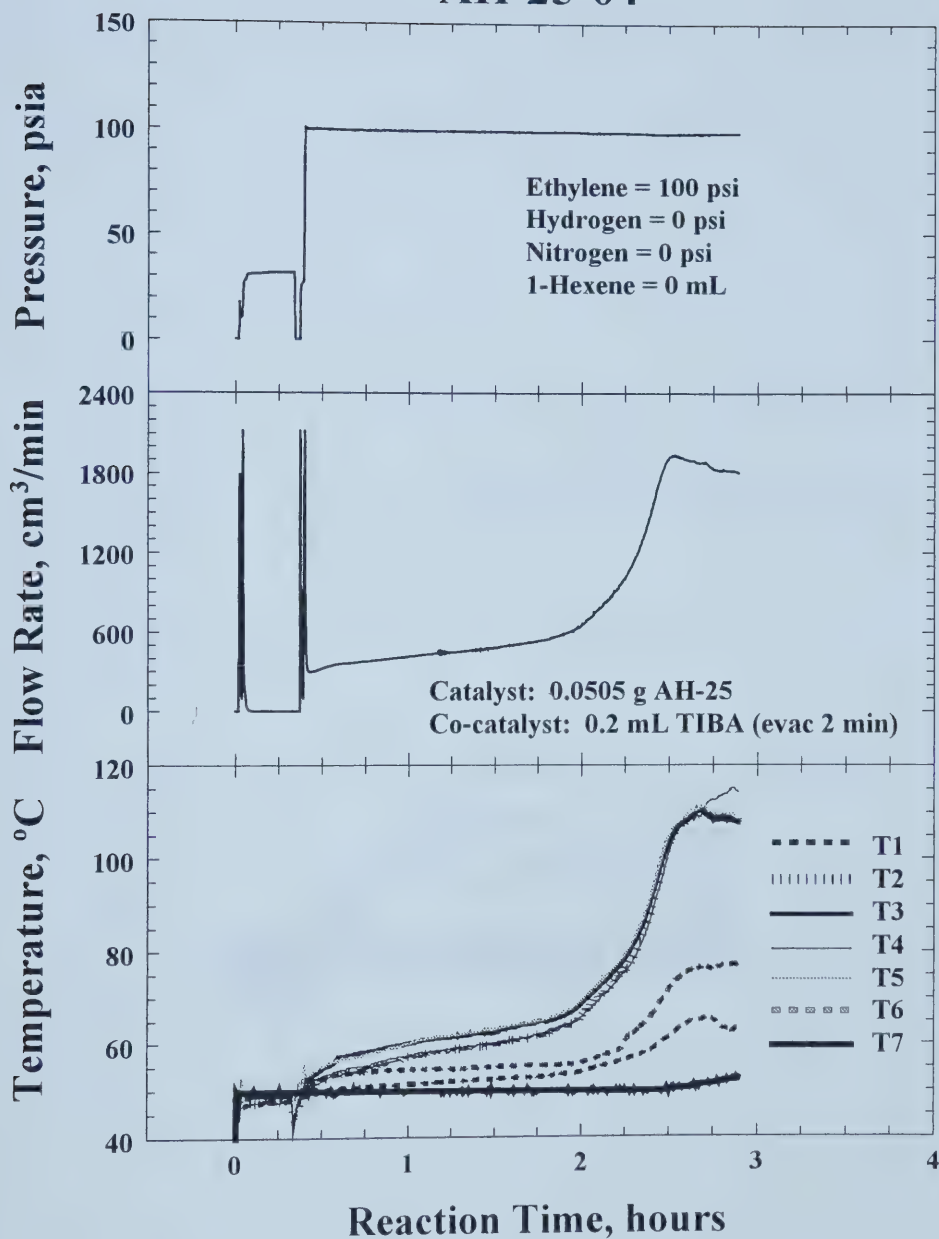
AH-22-02



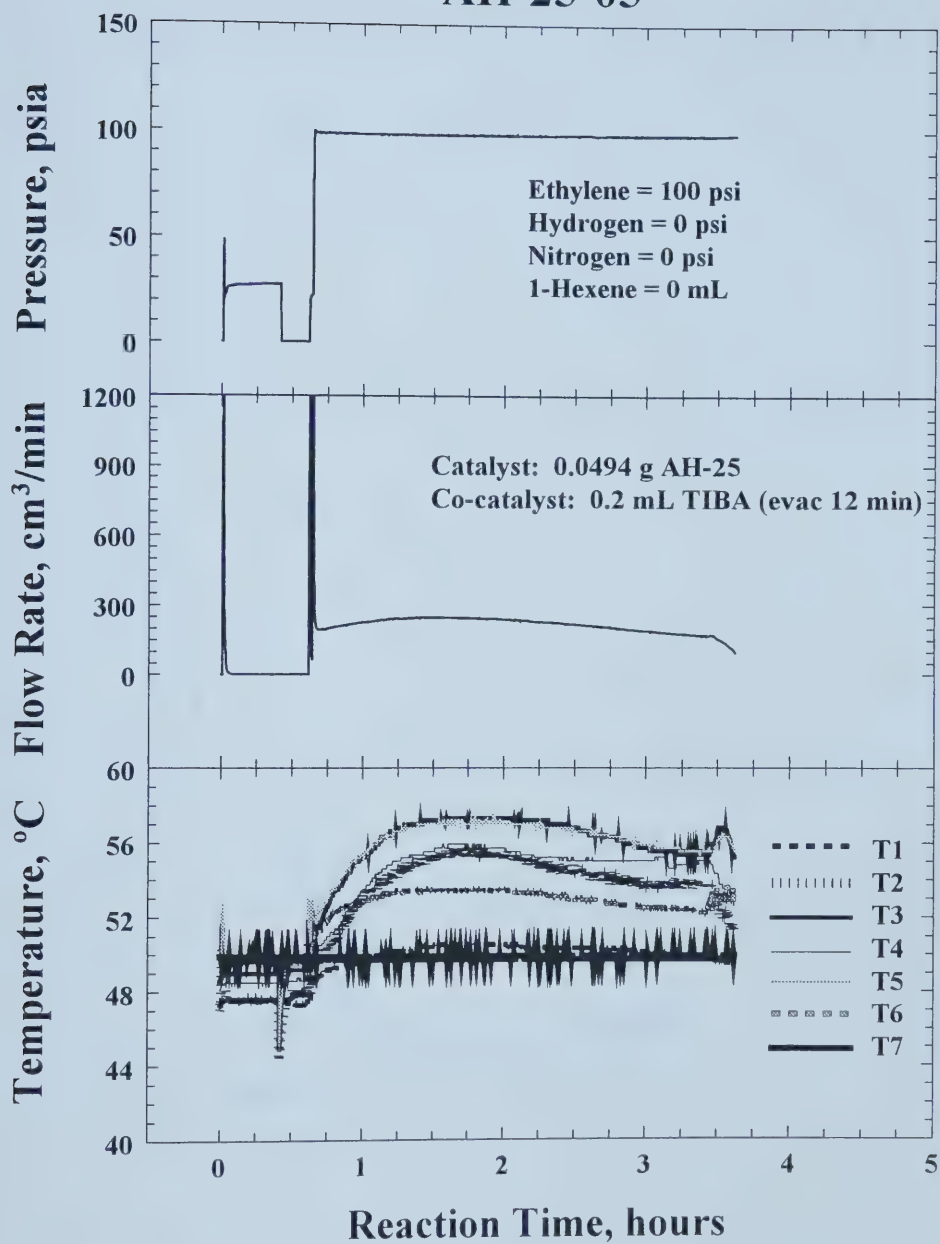
AH-25-03



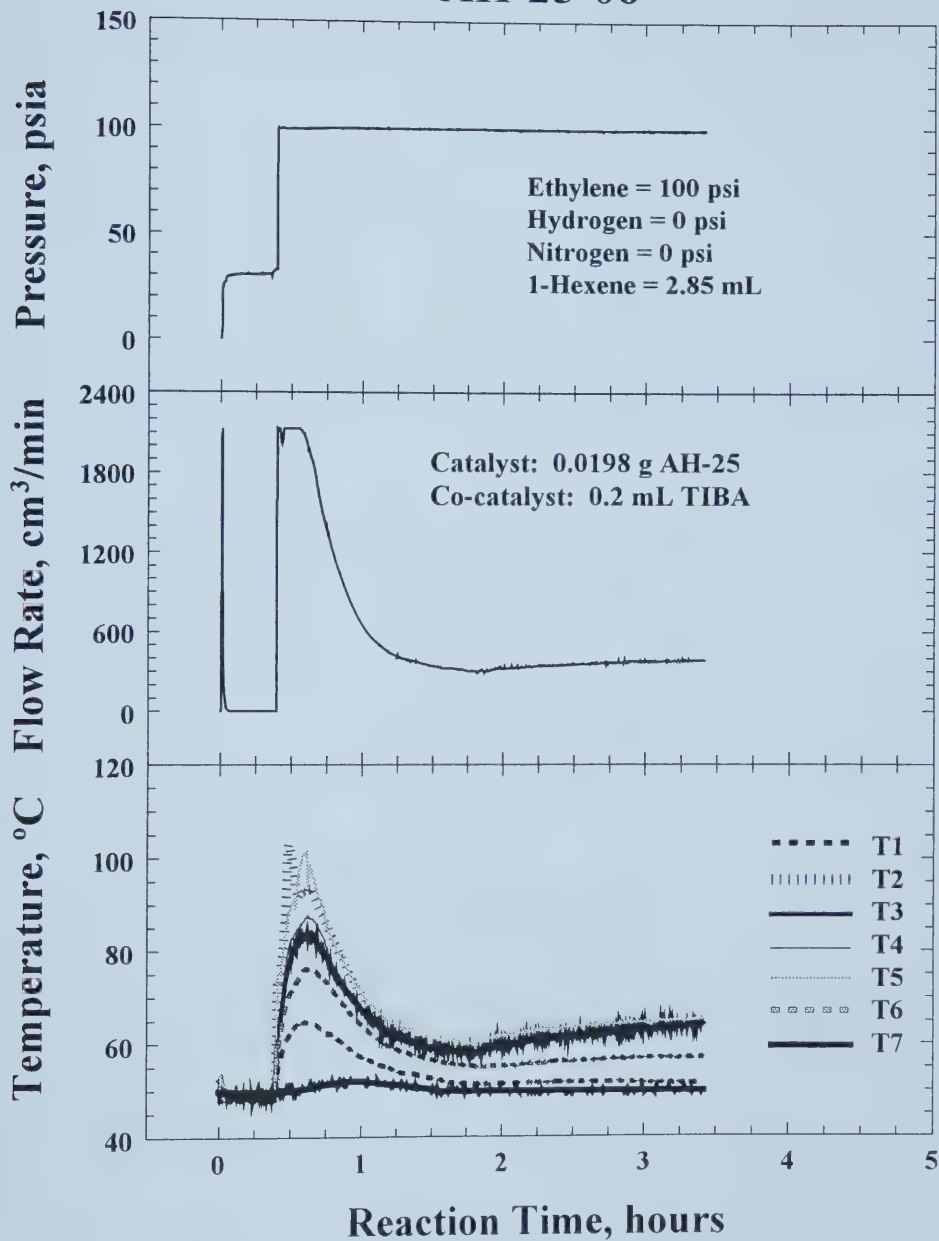
AH-25-04



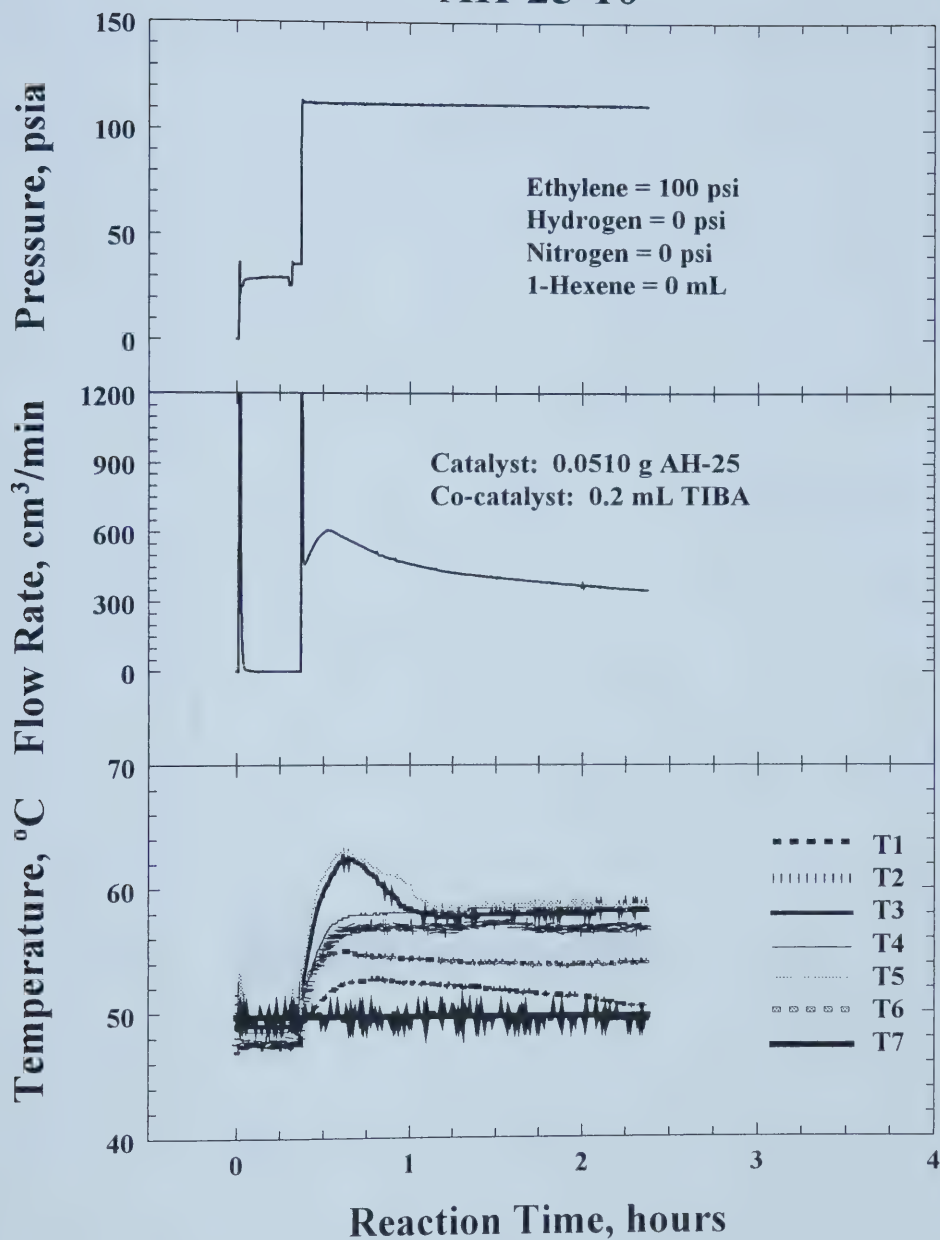
AH-25-05



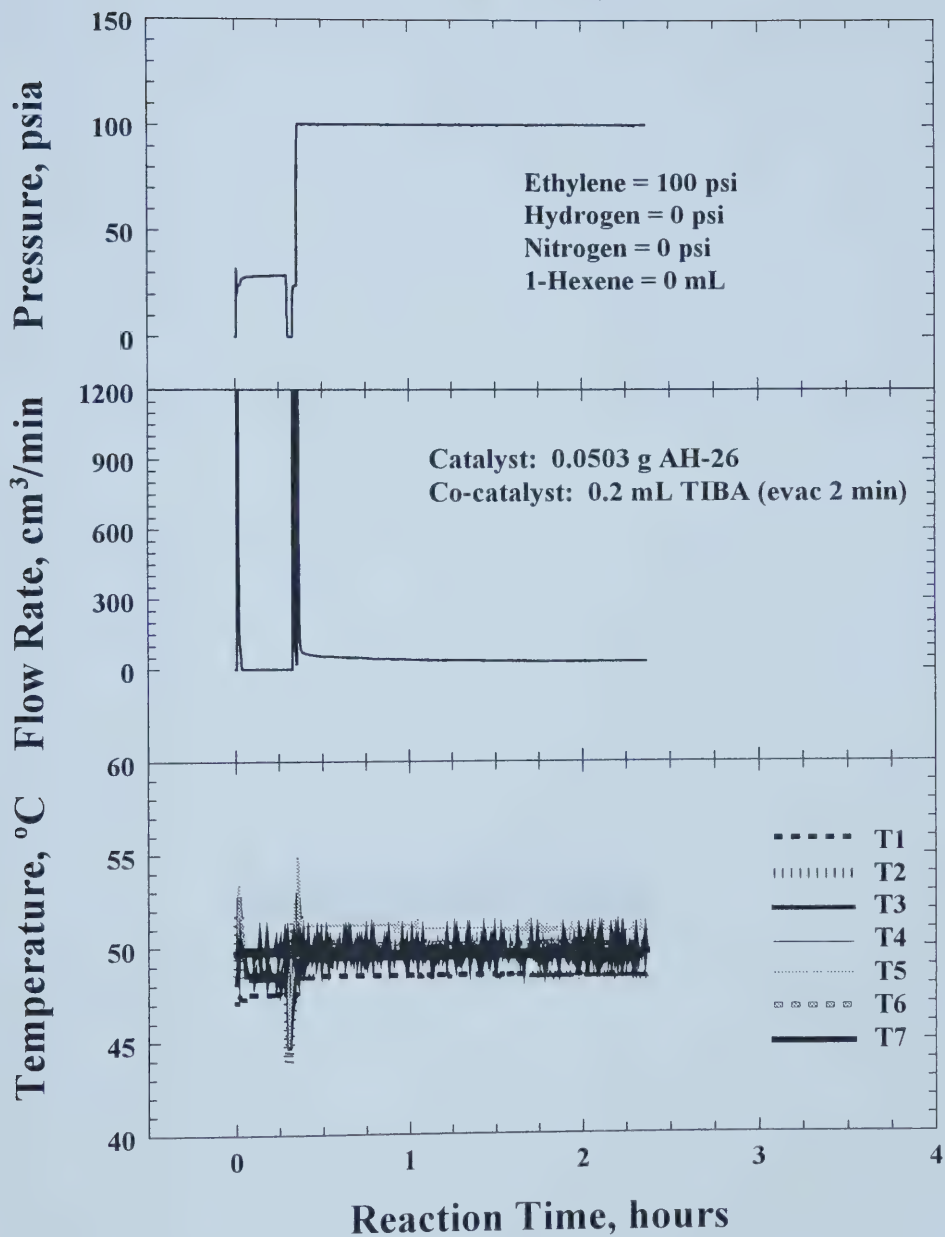
AH-25-06



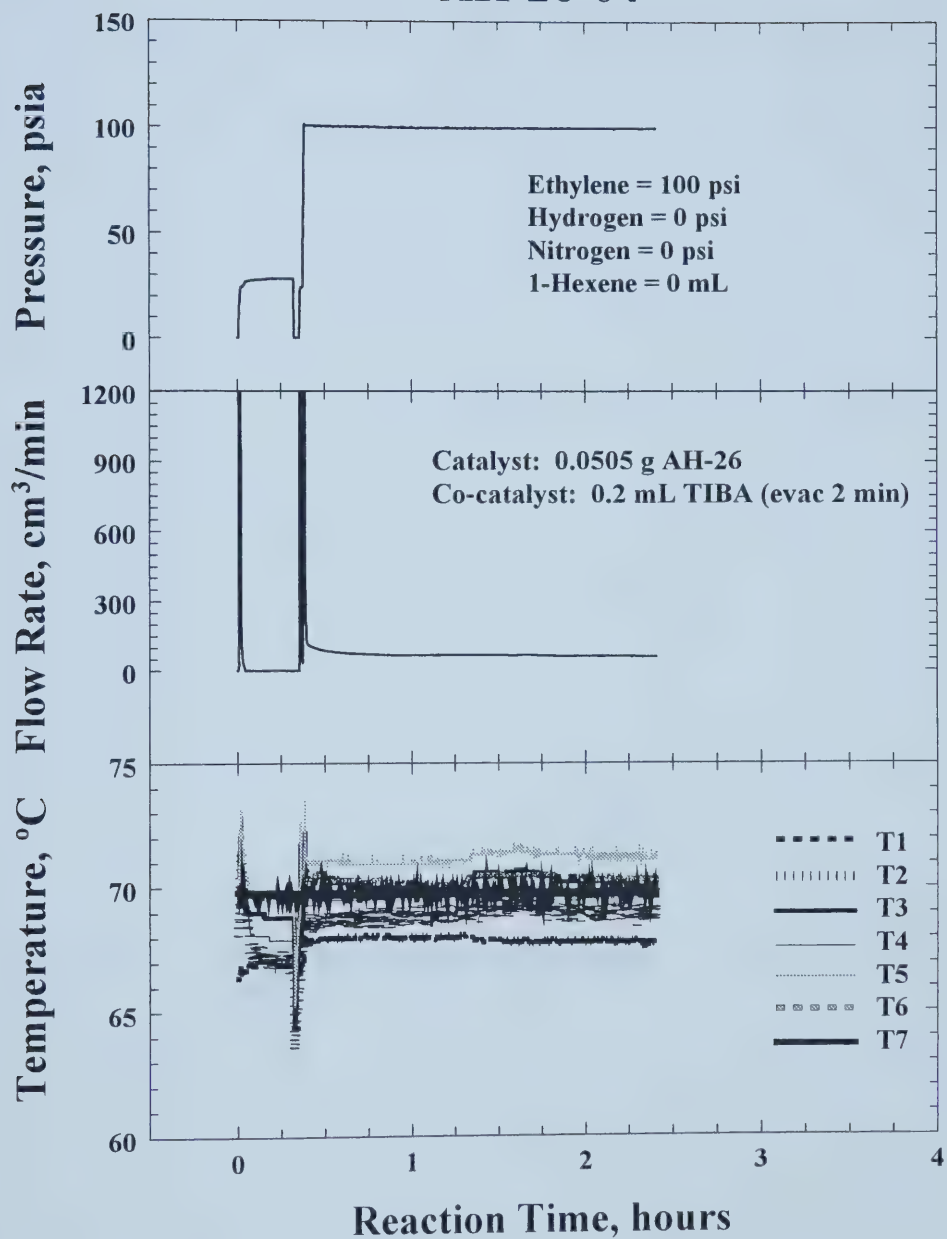
AH-25-10



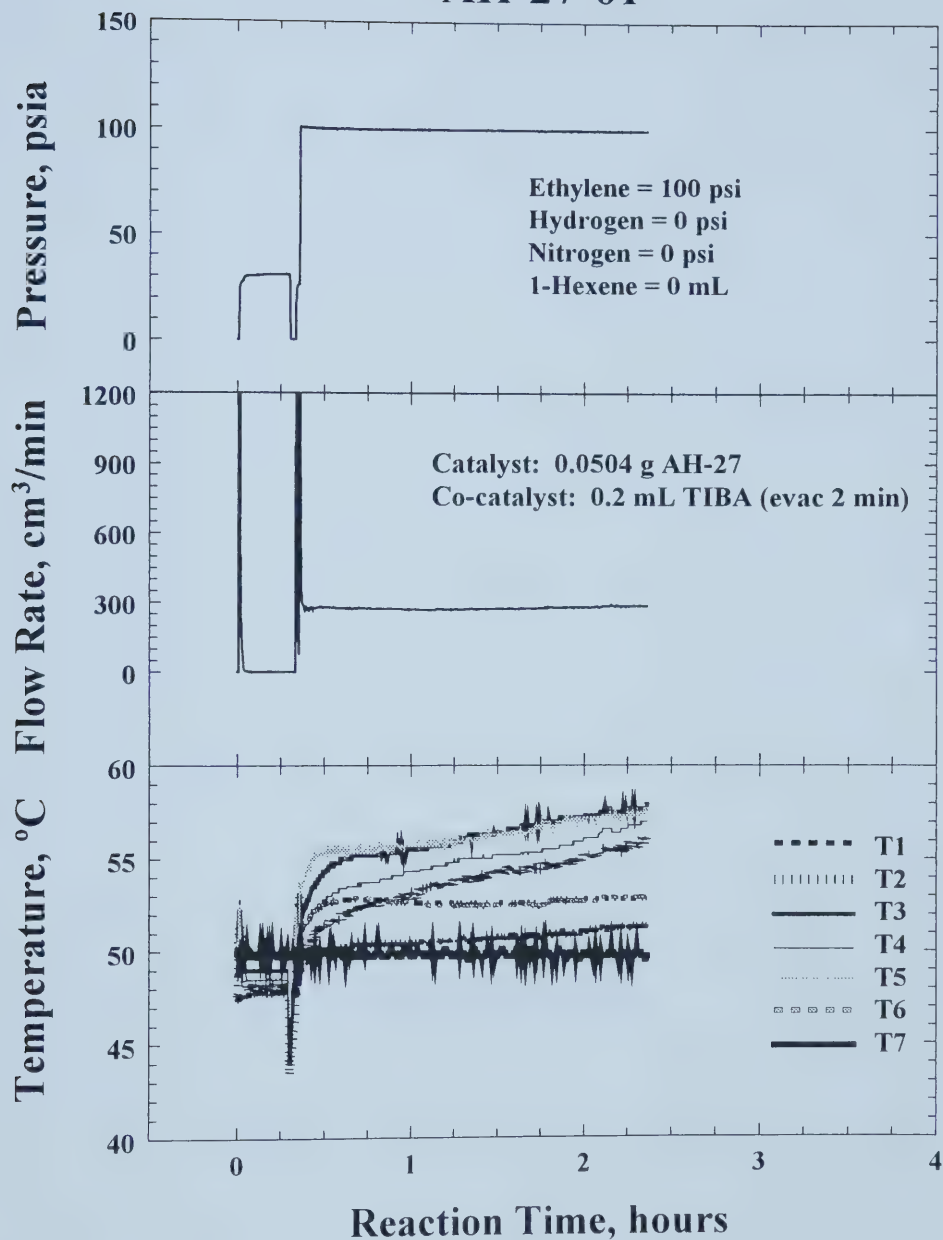
AH-26-03



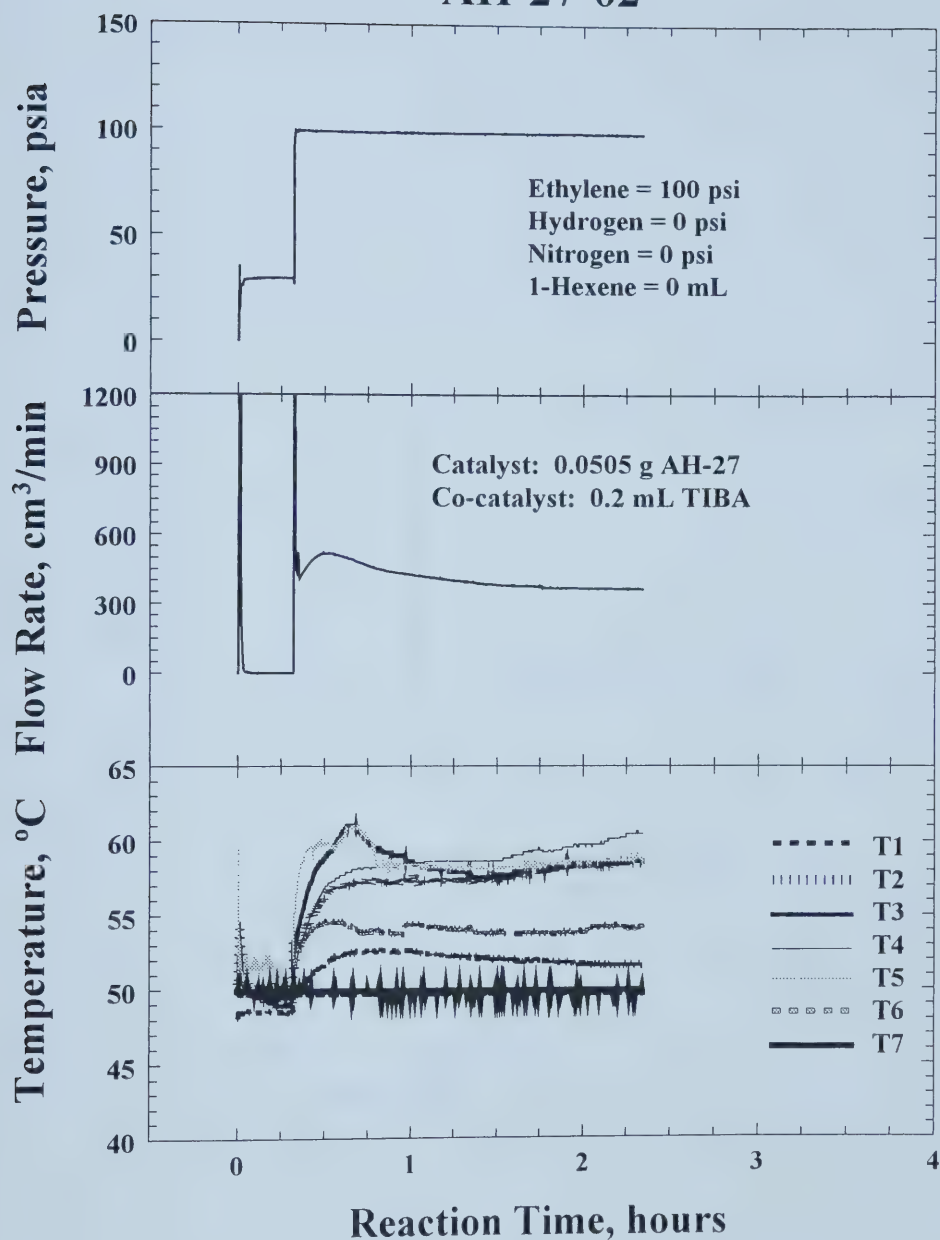
AH-26-04



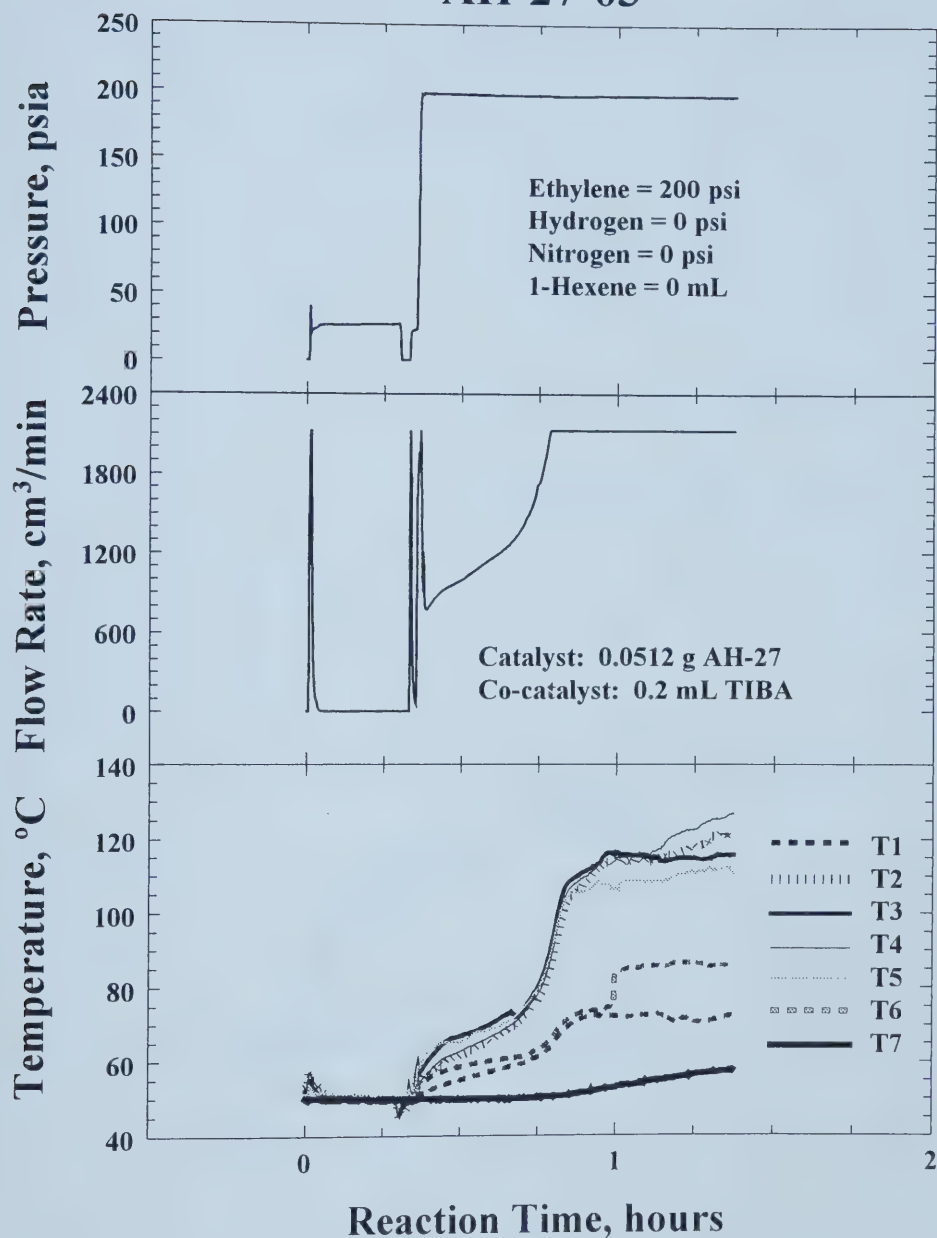
AH-27-01



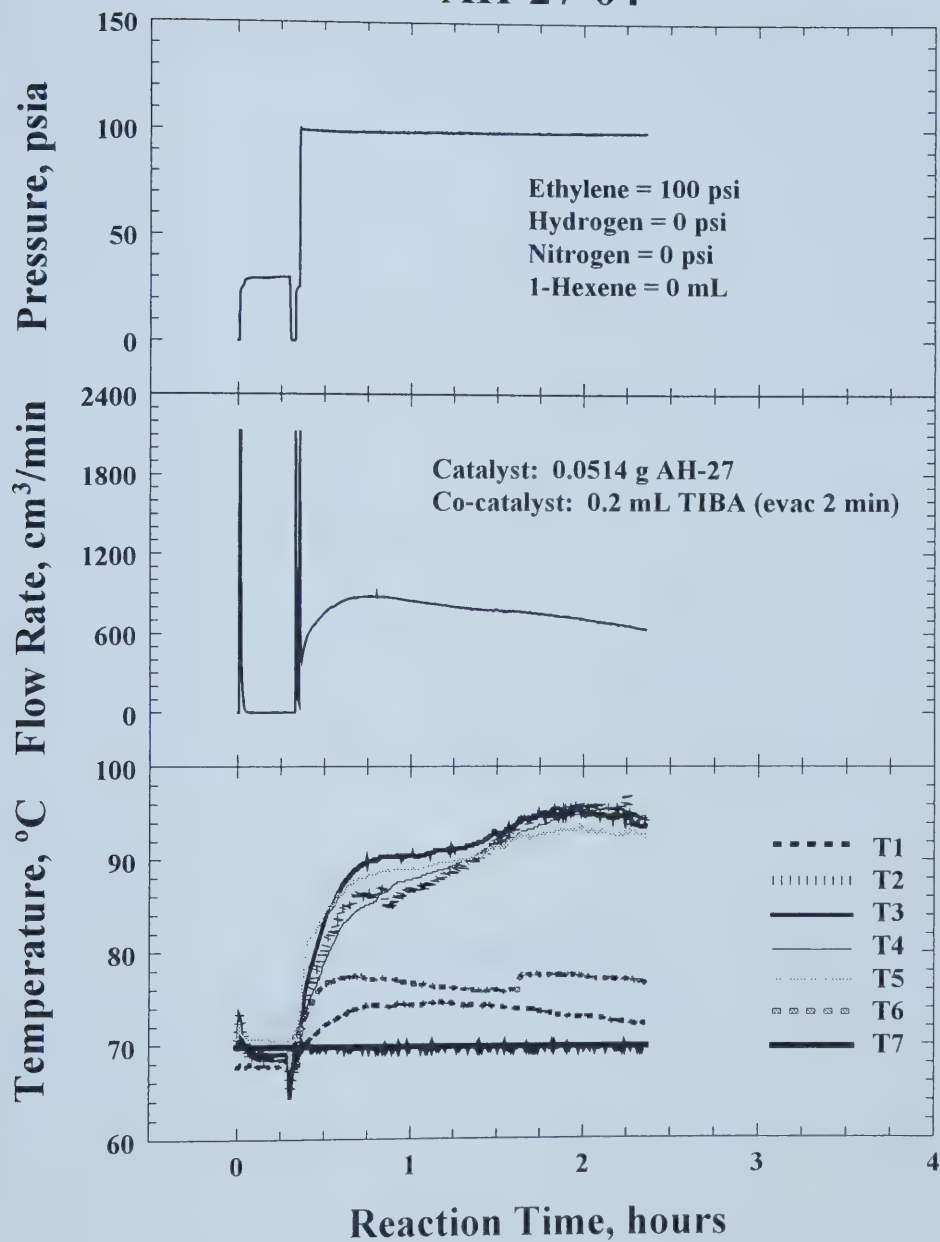
AH-27-02



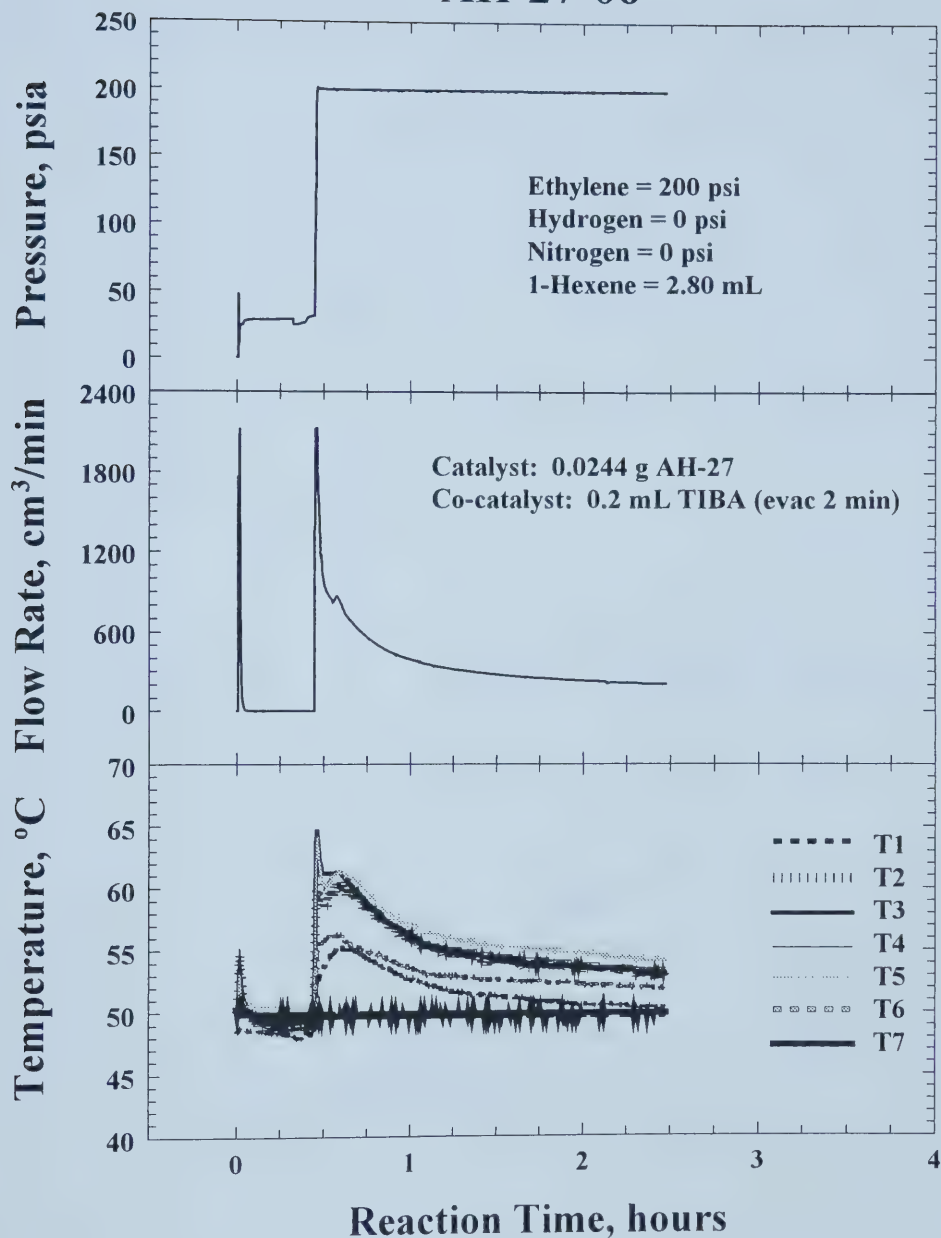
AH-27-03



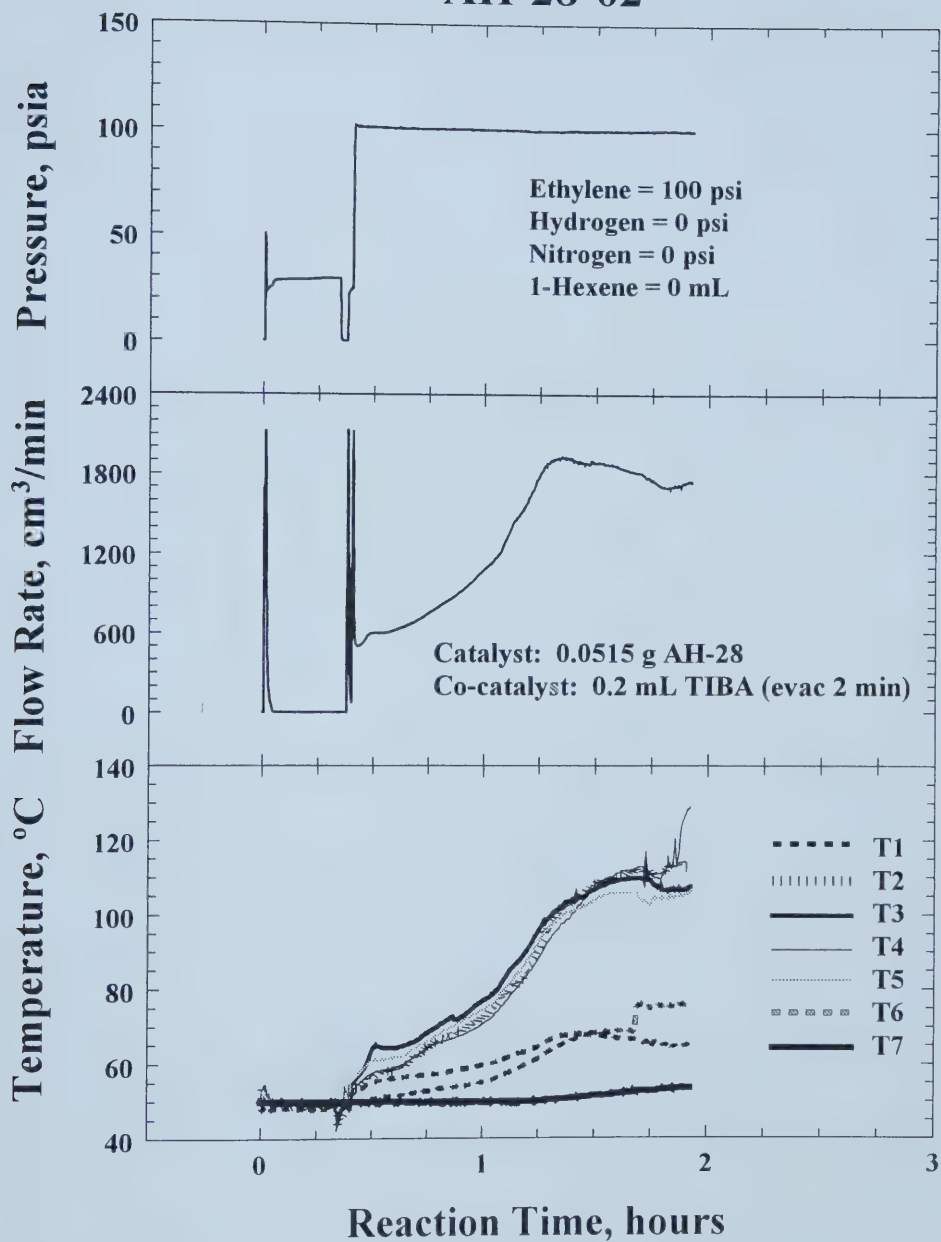
AH-27-04



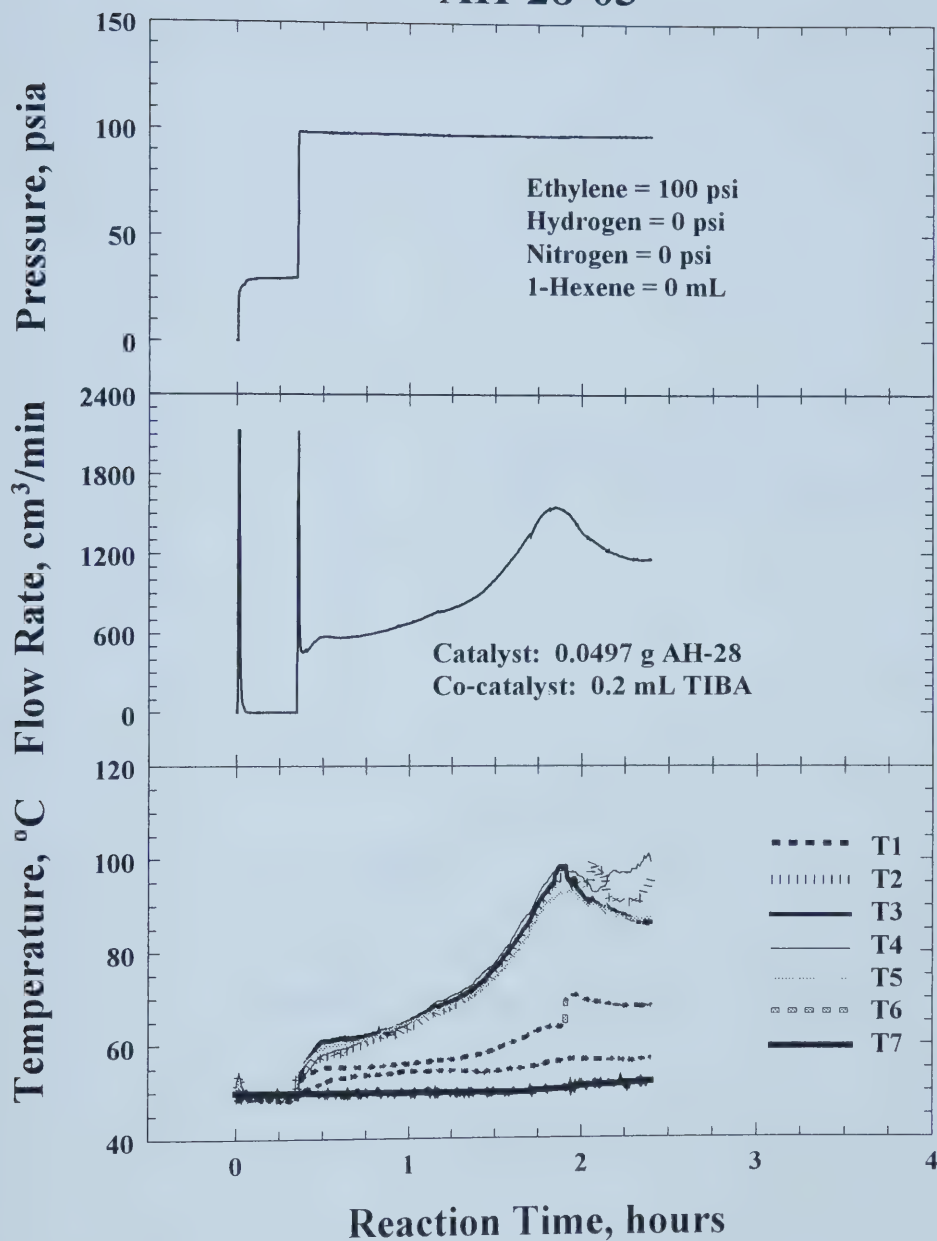
AH-27-06



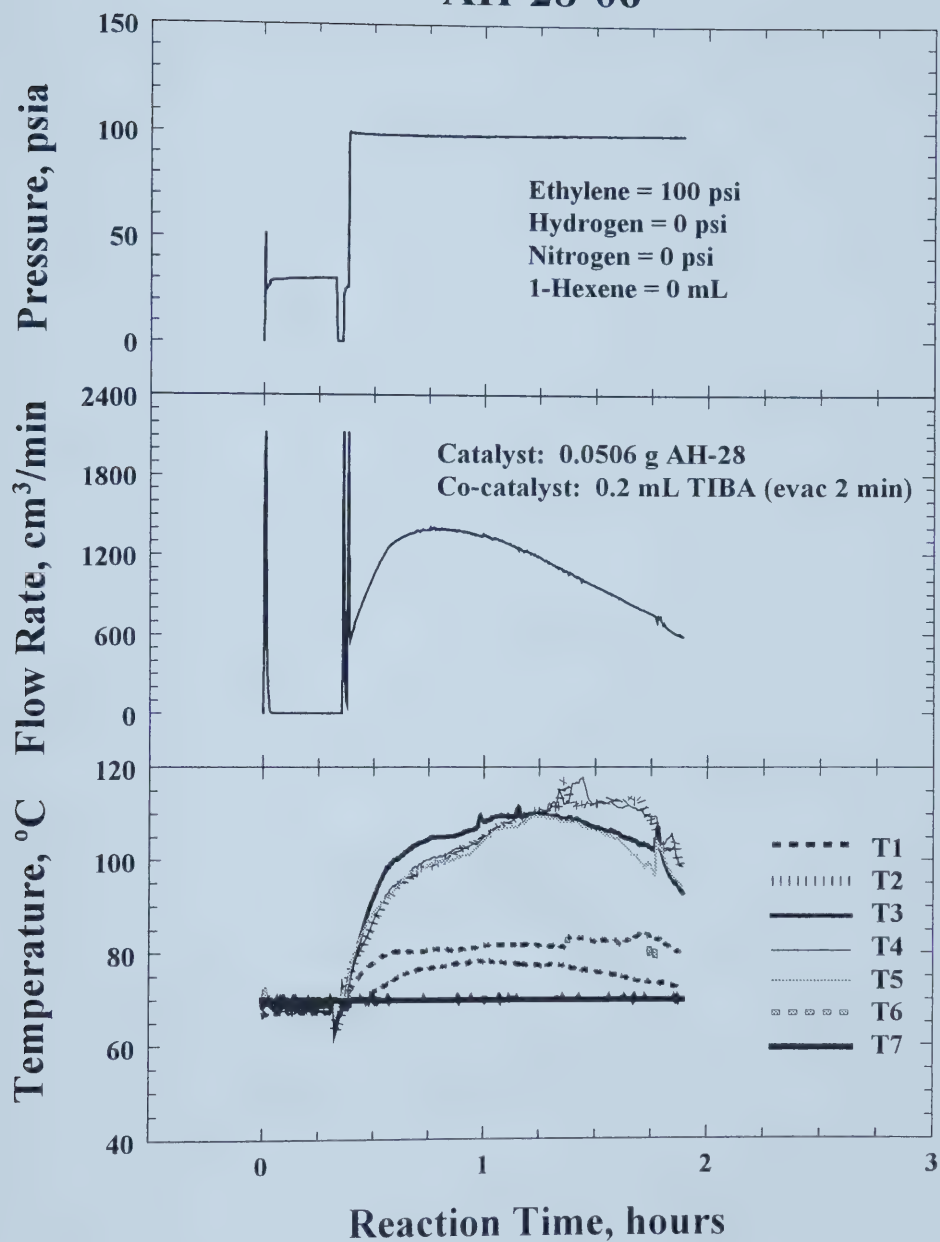
AH-28-02



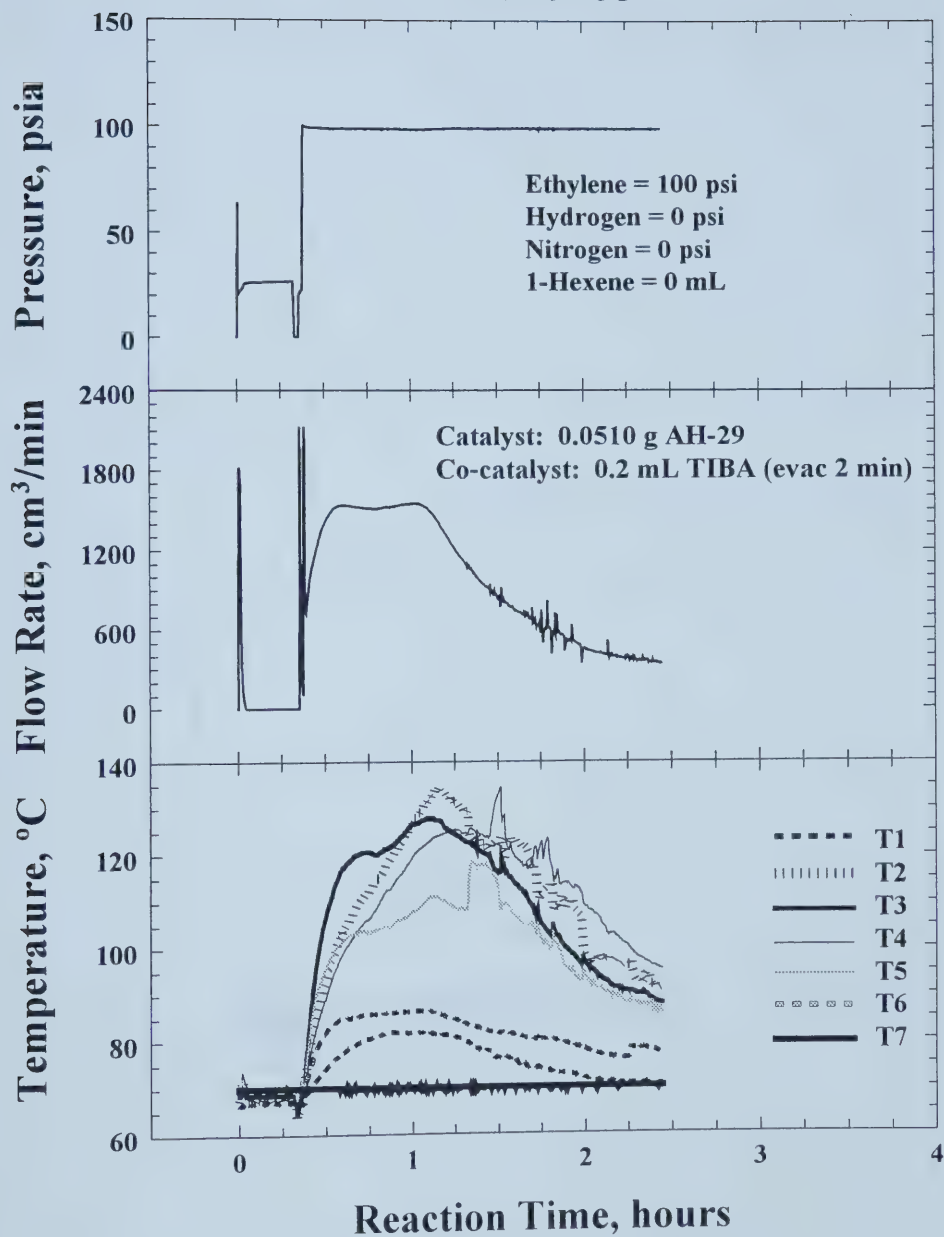
AH-28-03



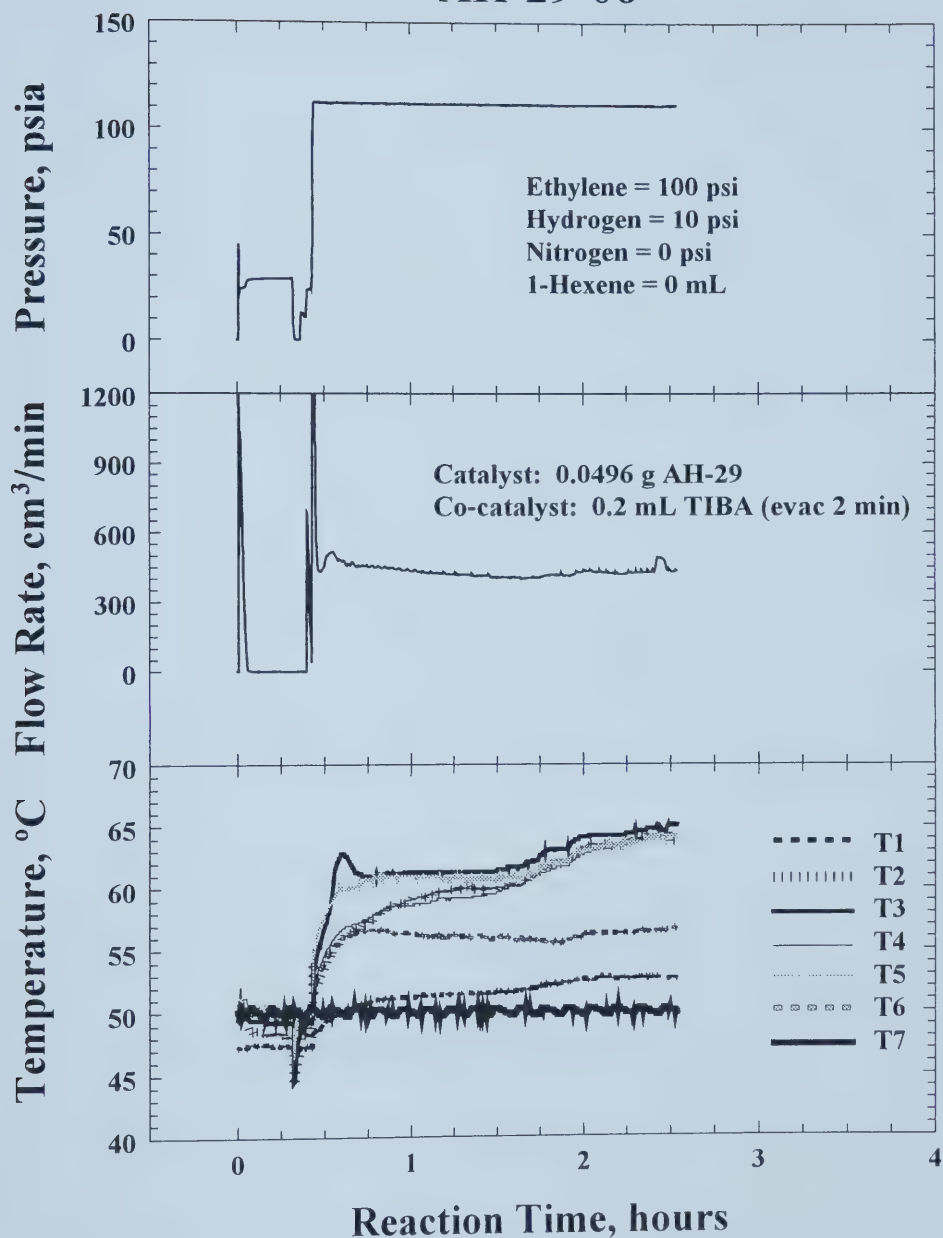
AH-28-06



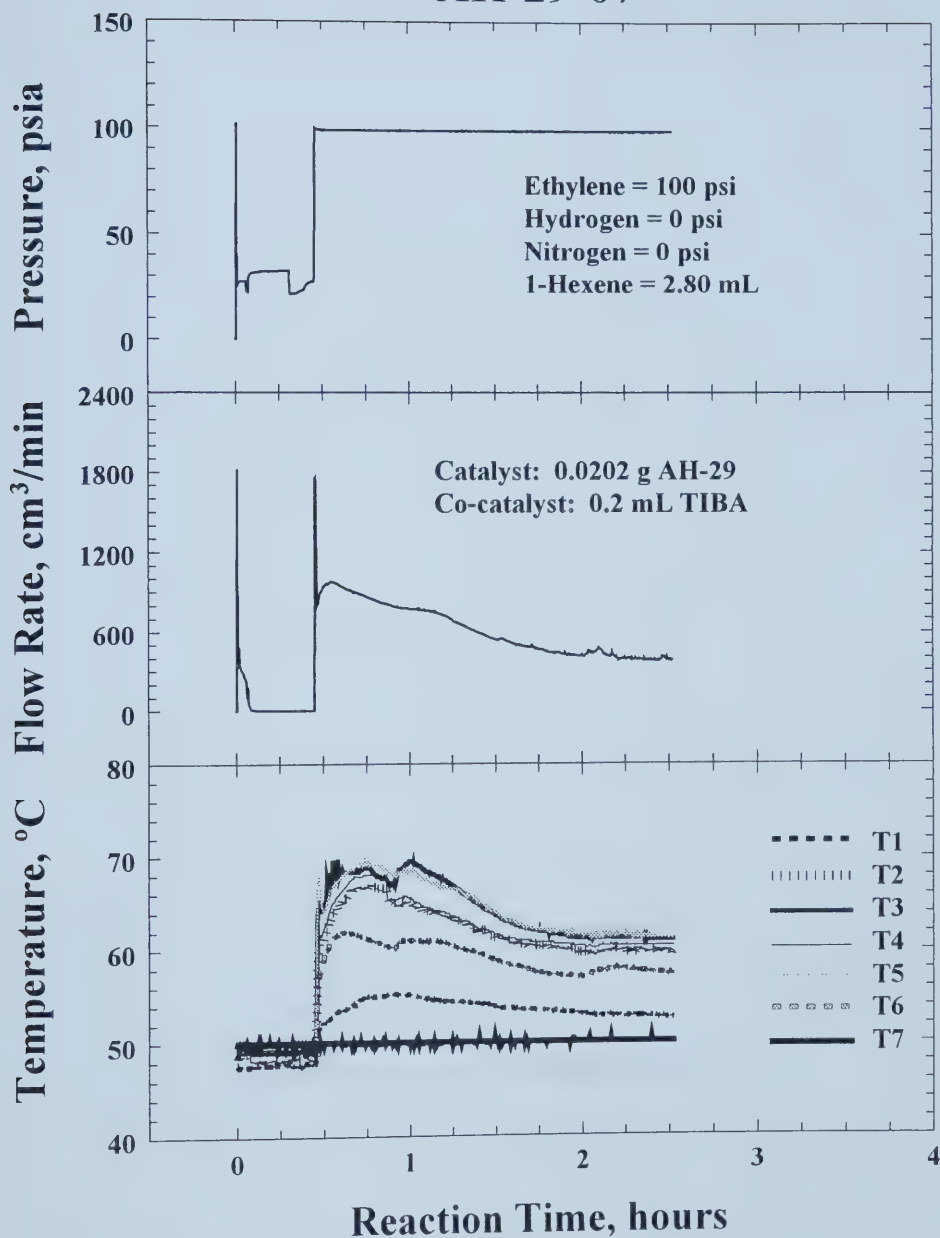
AH-29-05



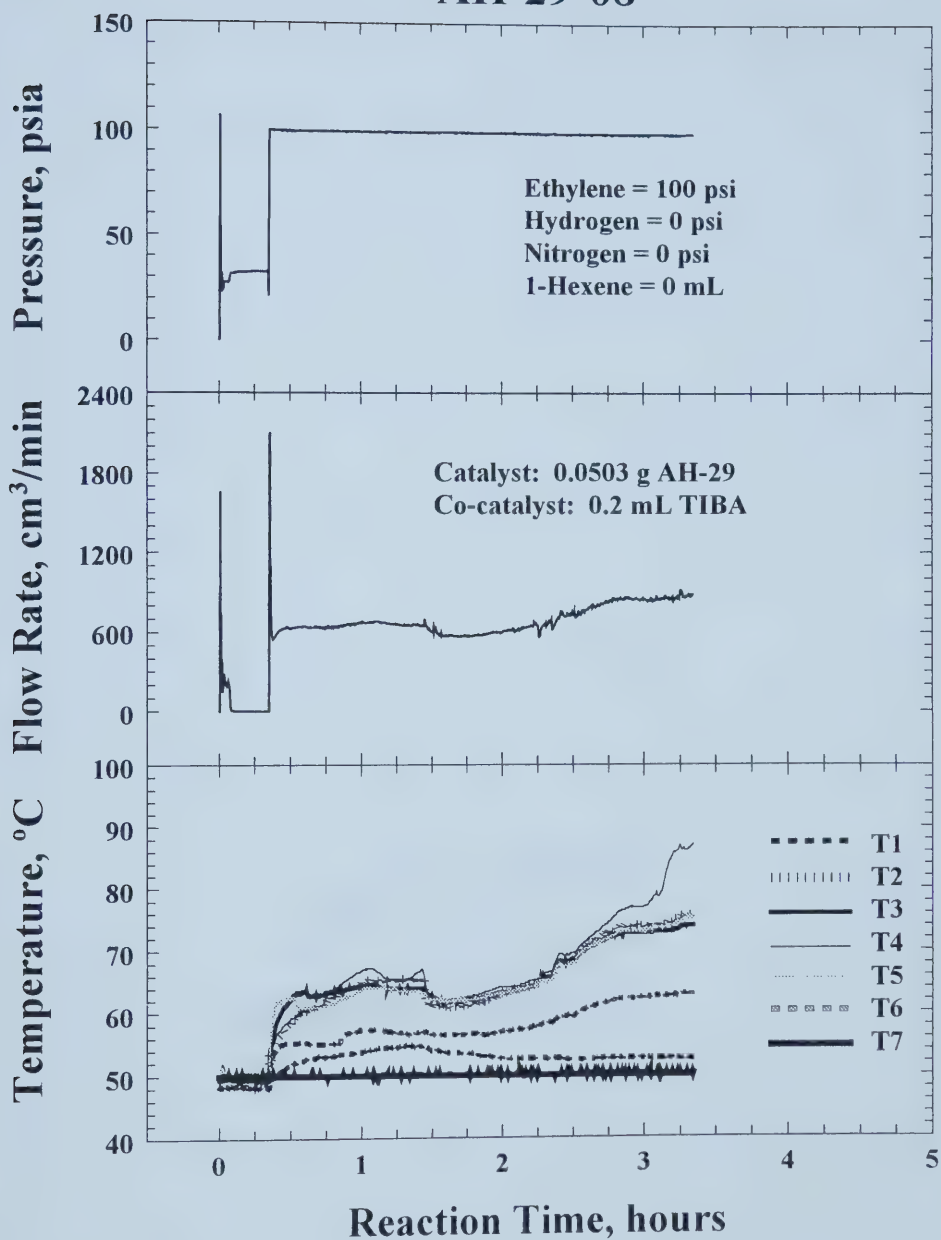
AH-29-06



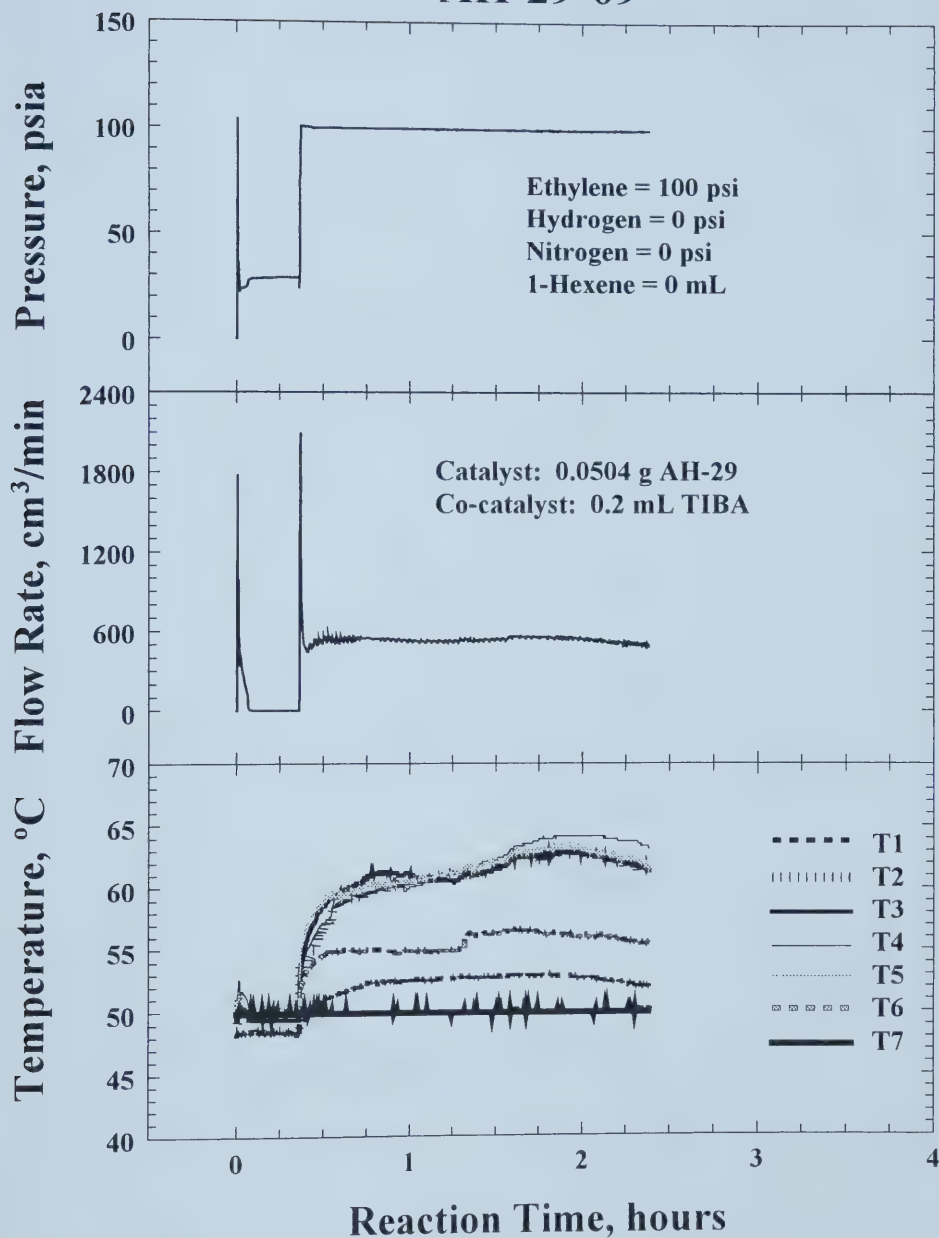
AH-29-07



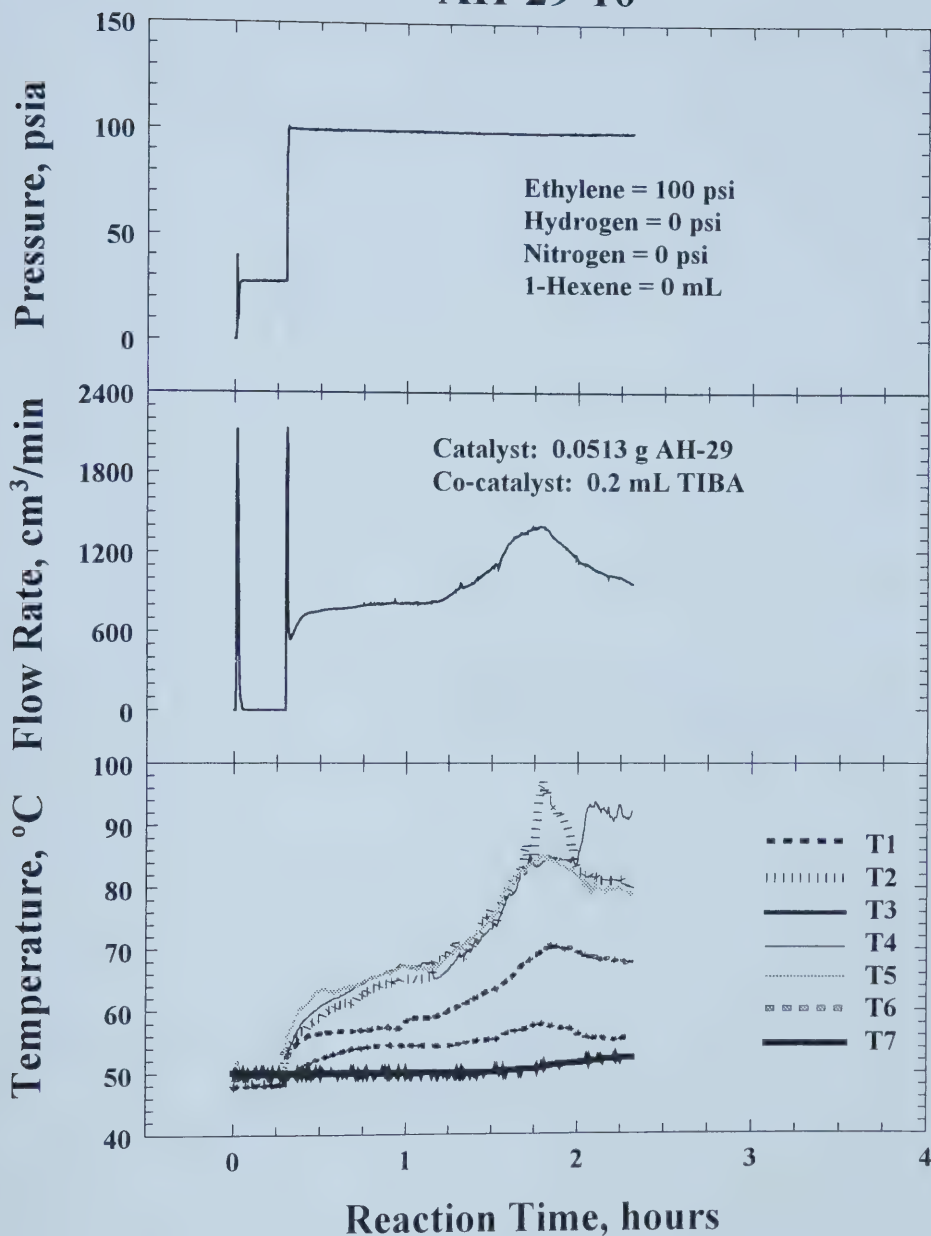
AH-29-08



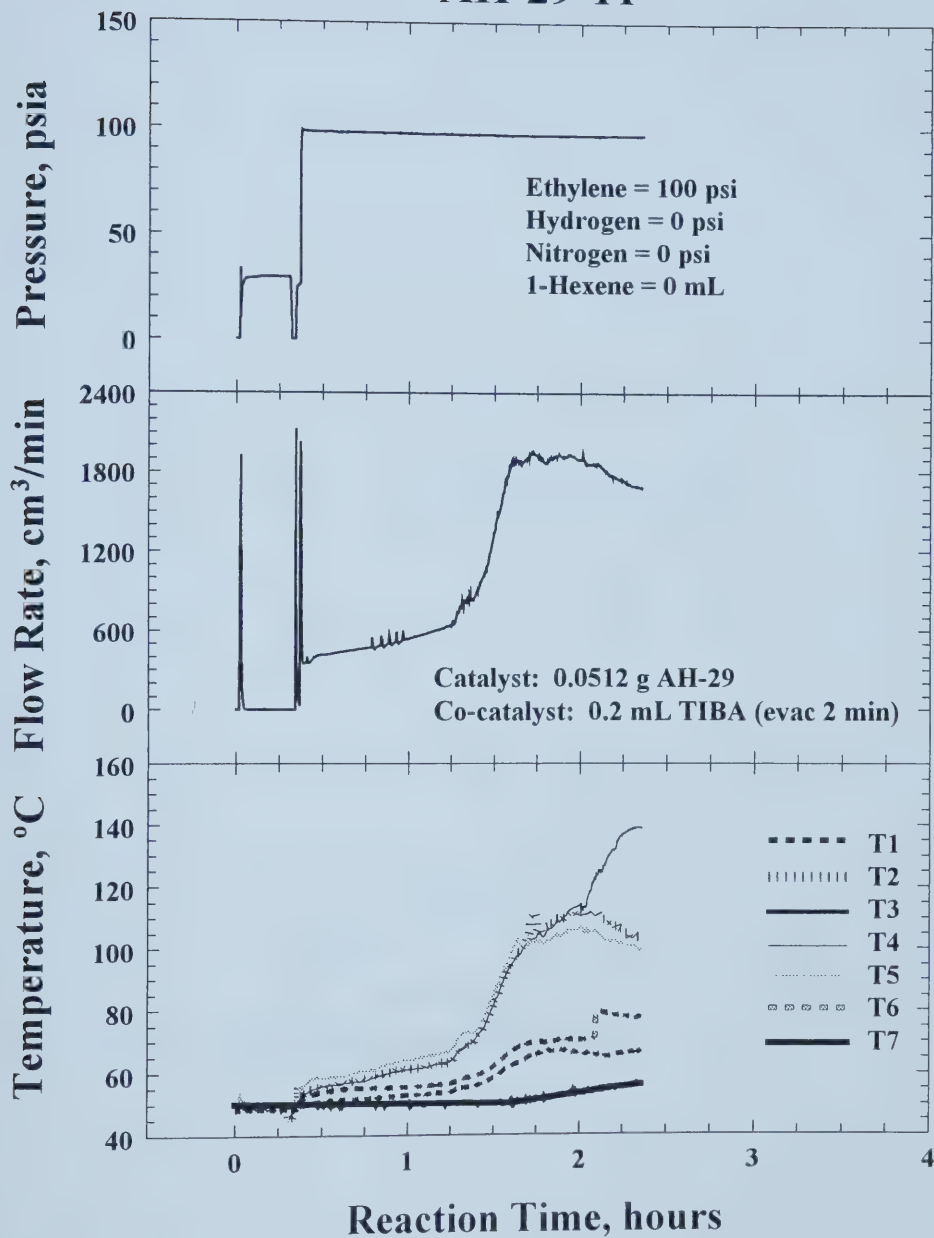
AH-29-09



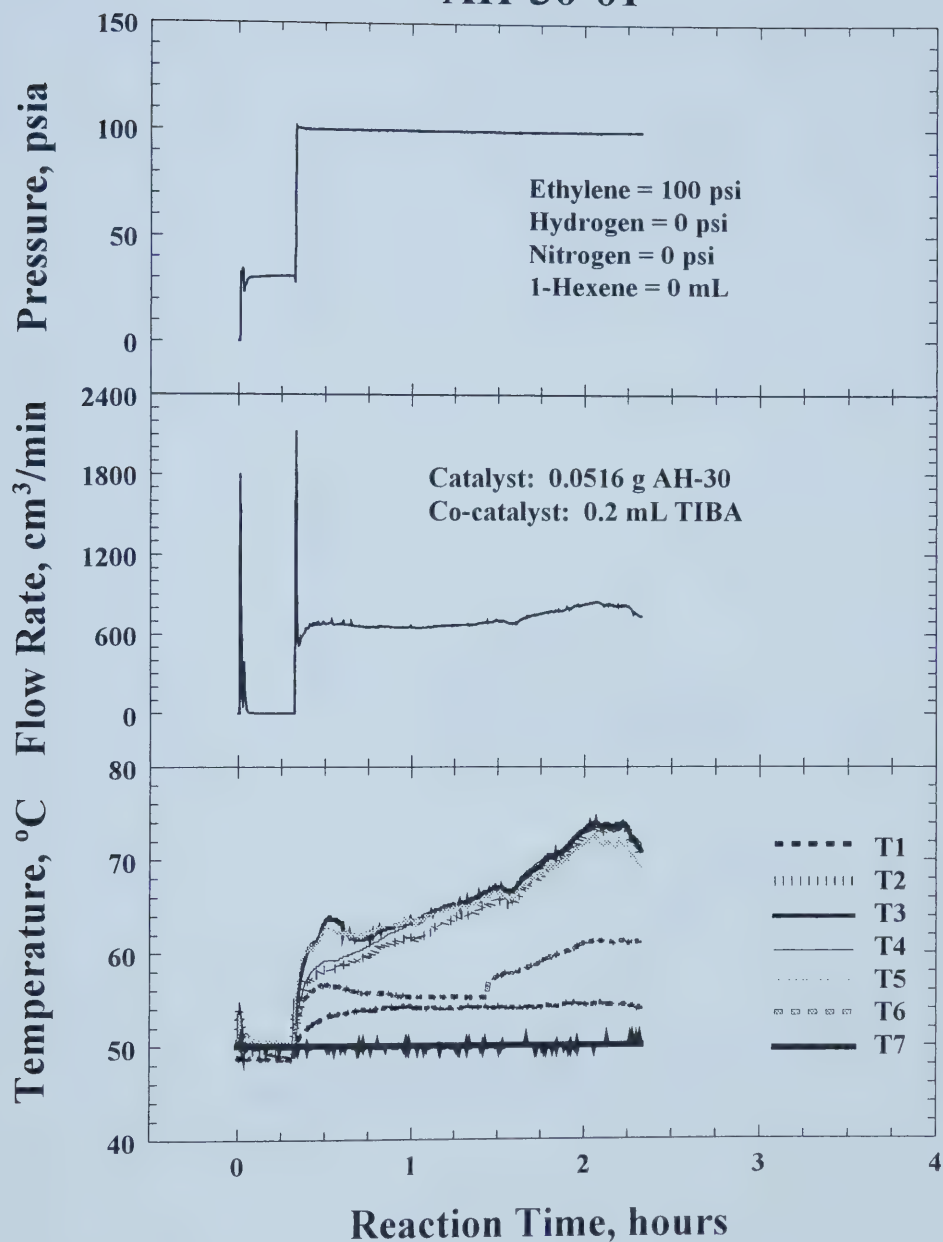
AH-29-10



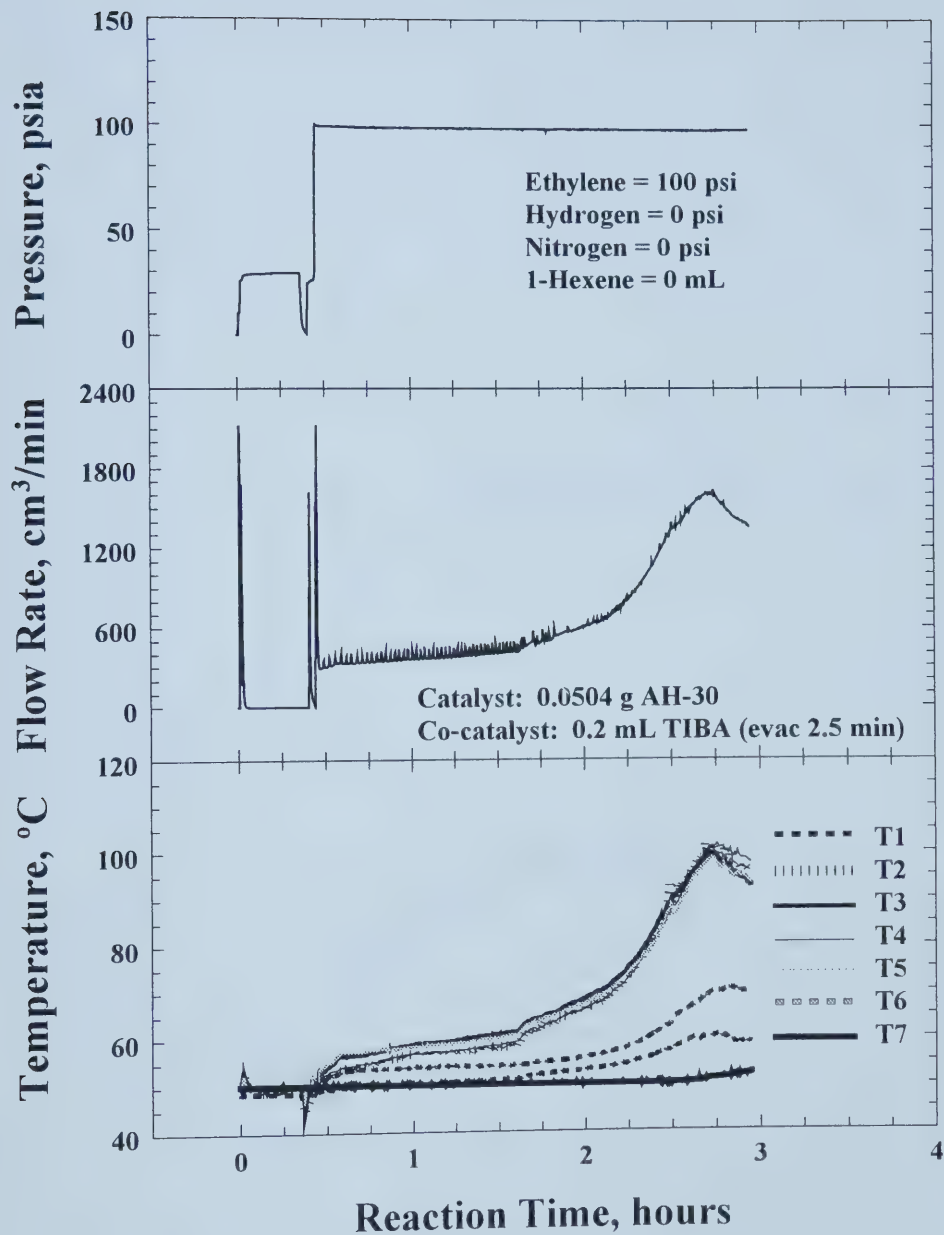
AH-29-11



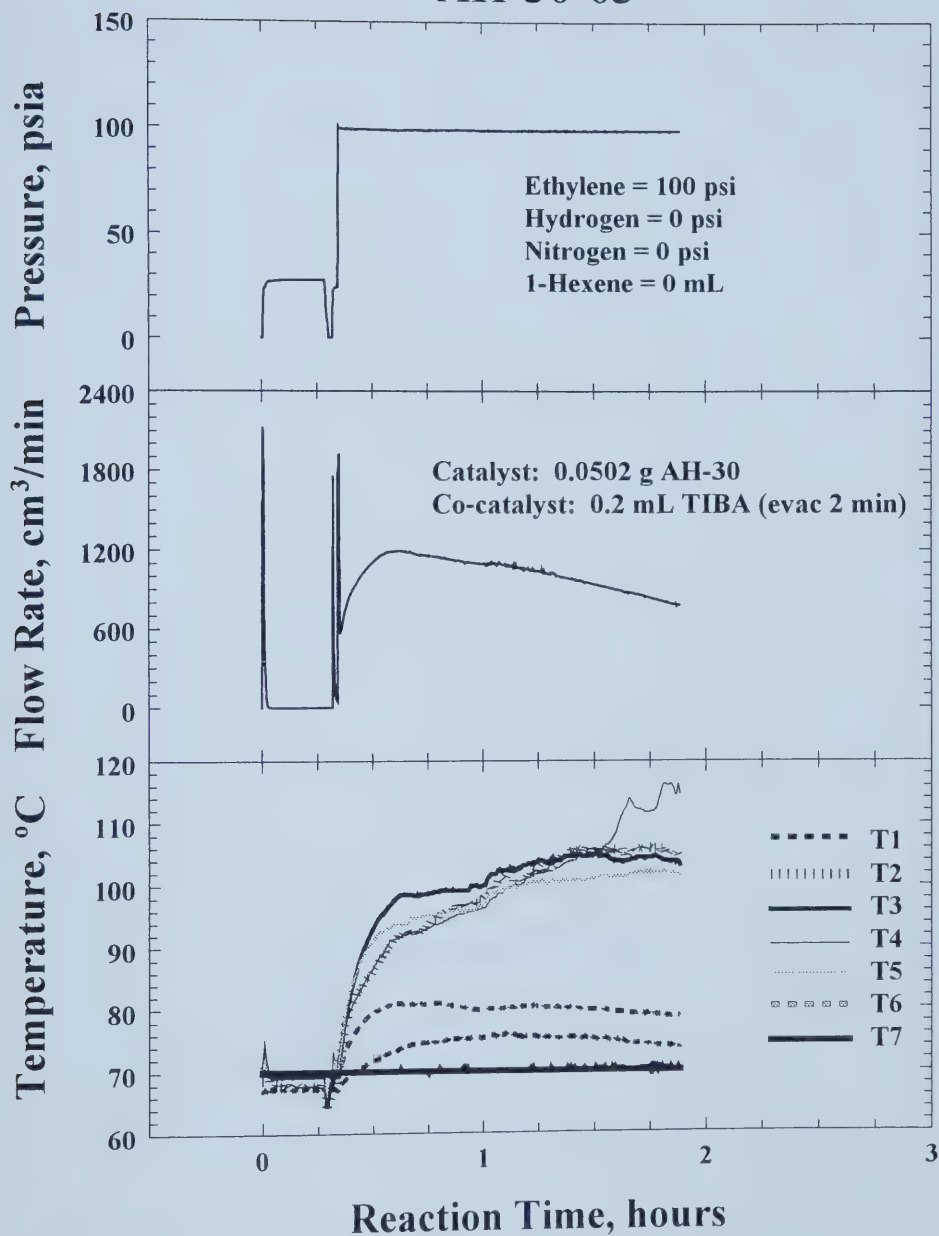
AH-30-01



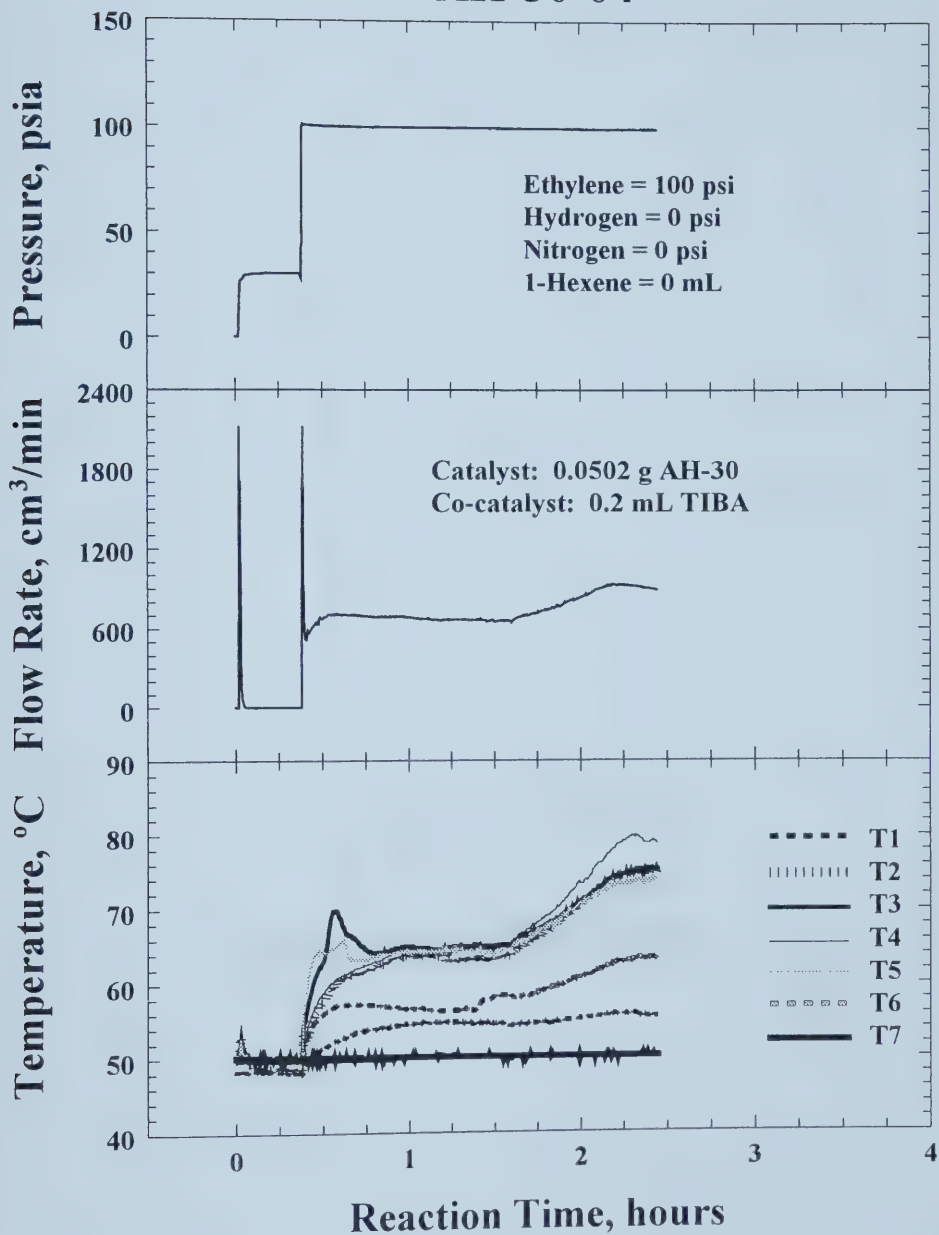
AH-30-02



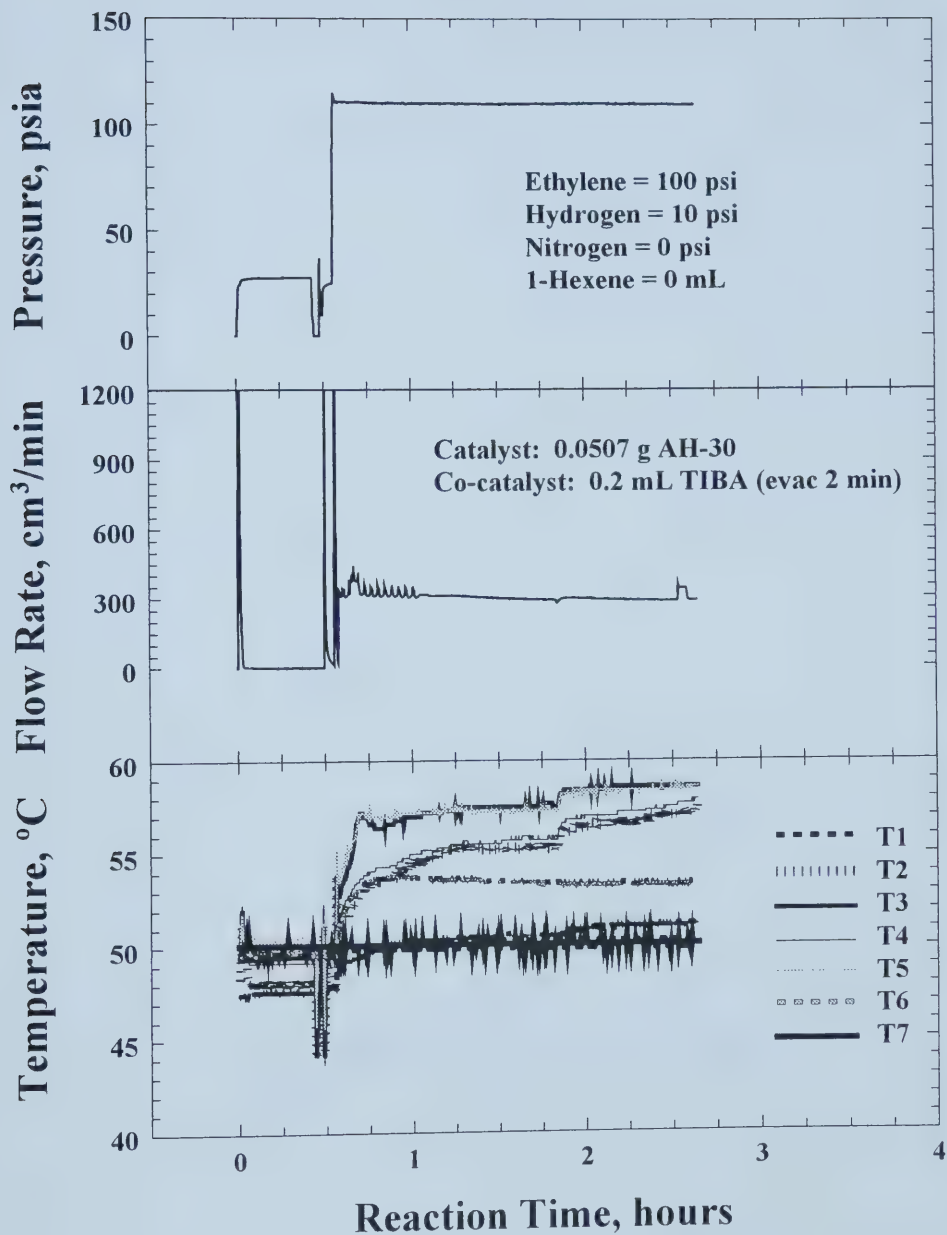
AH-30-03



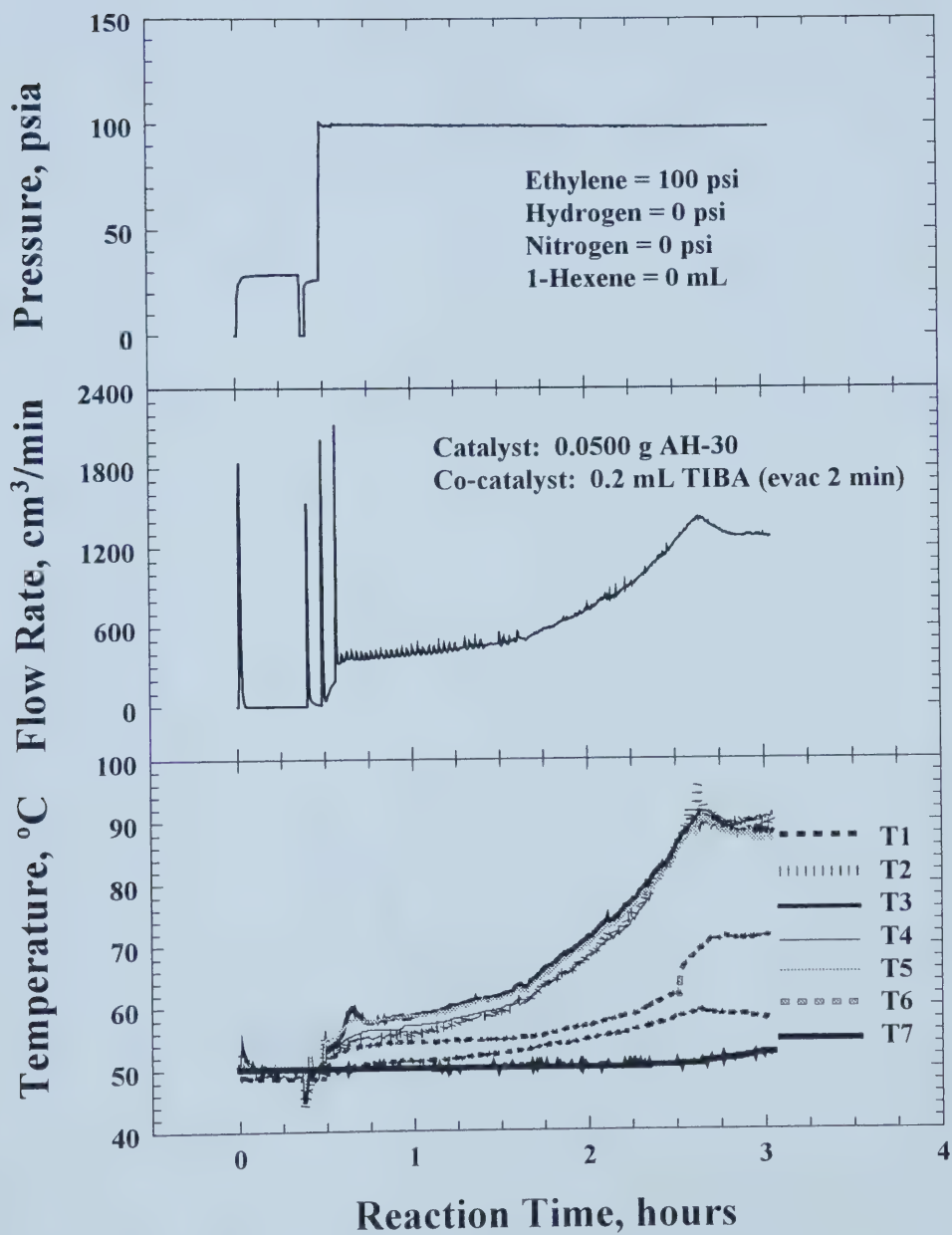
AH-30-04



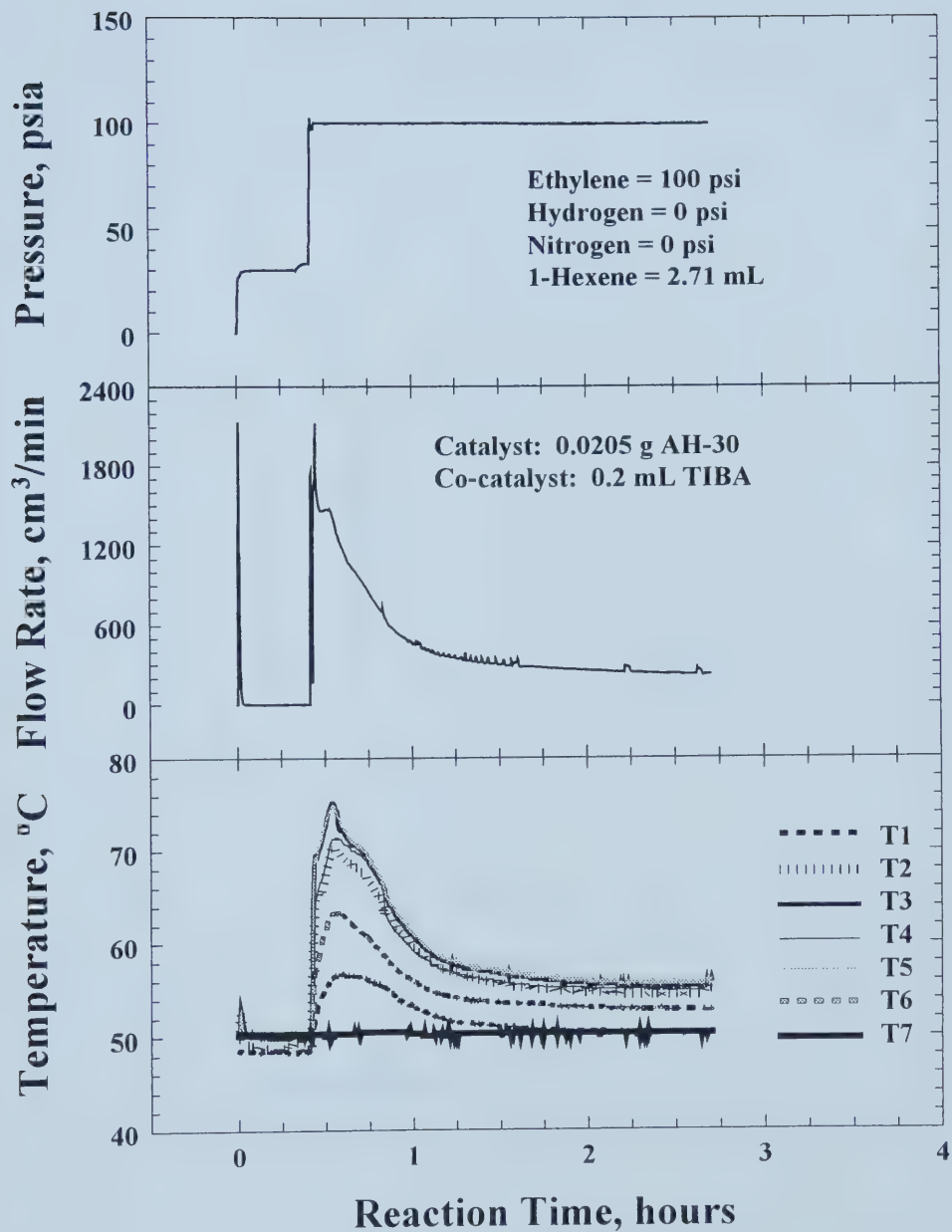
AH-30-05



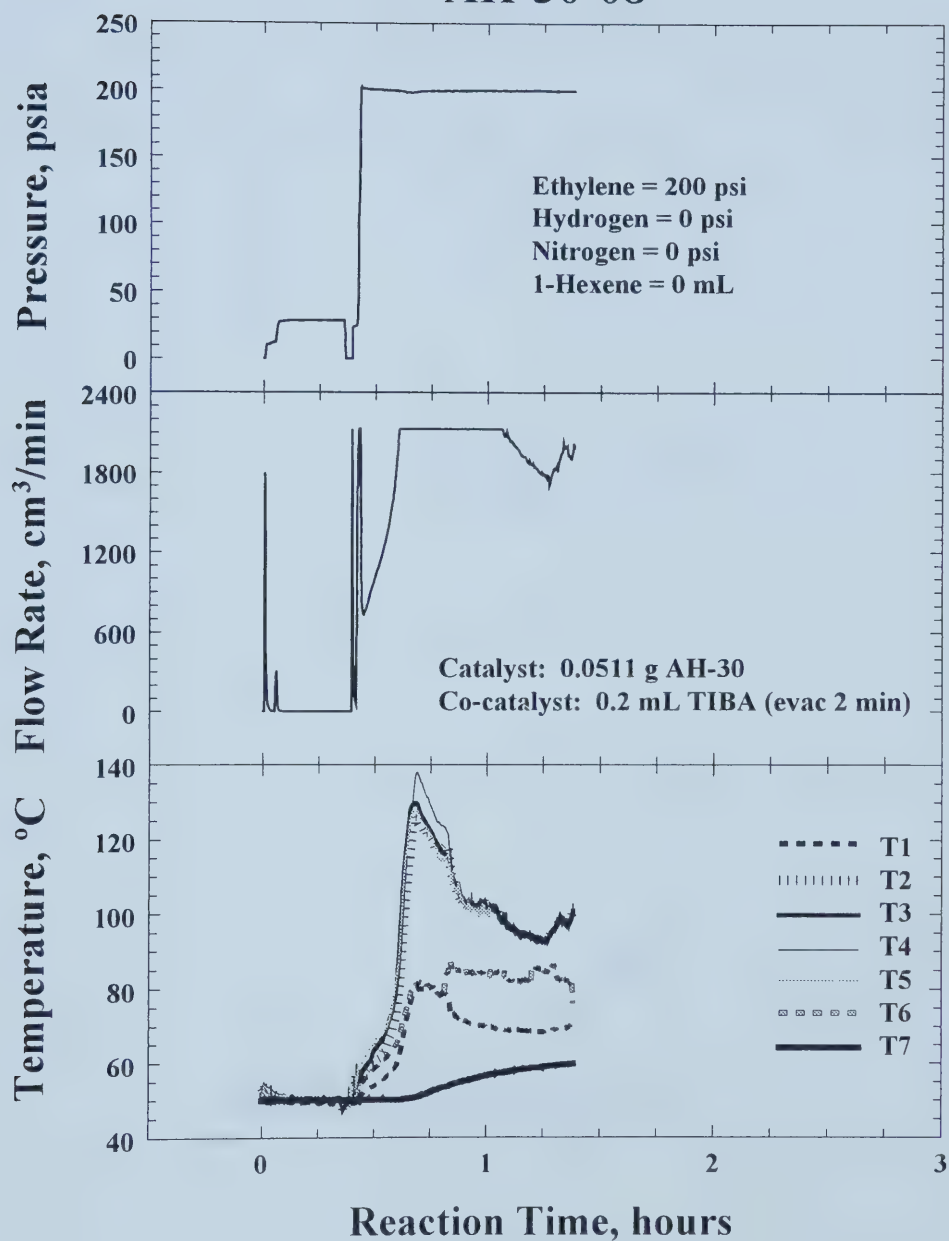
AH-30-06



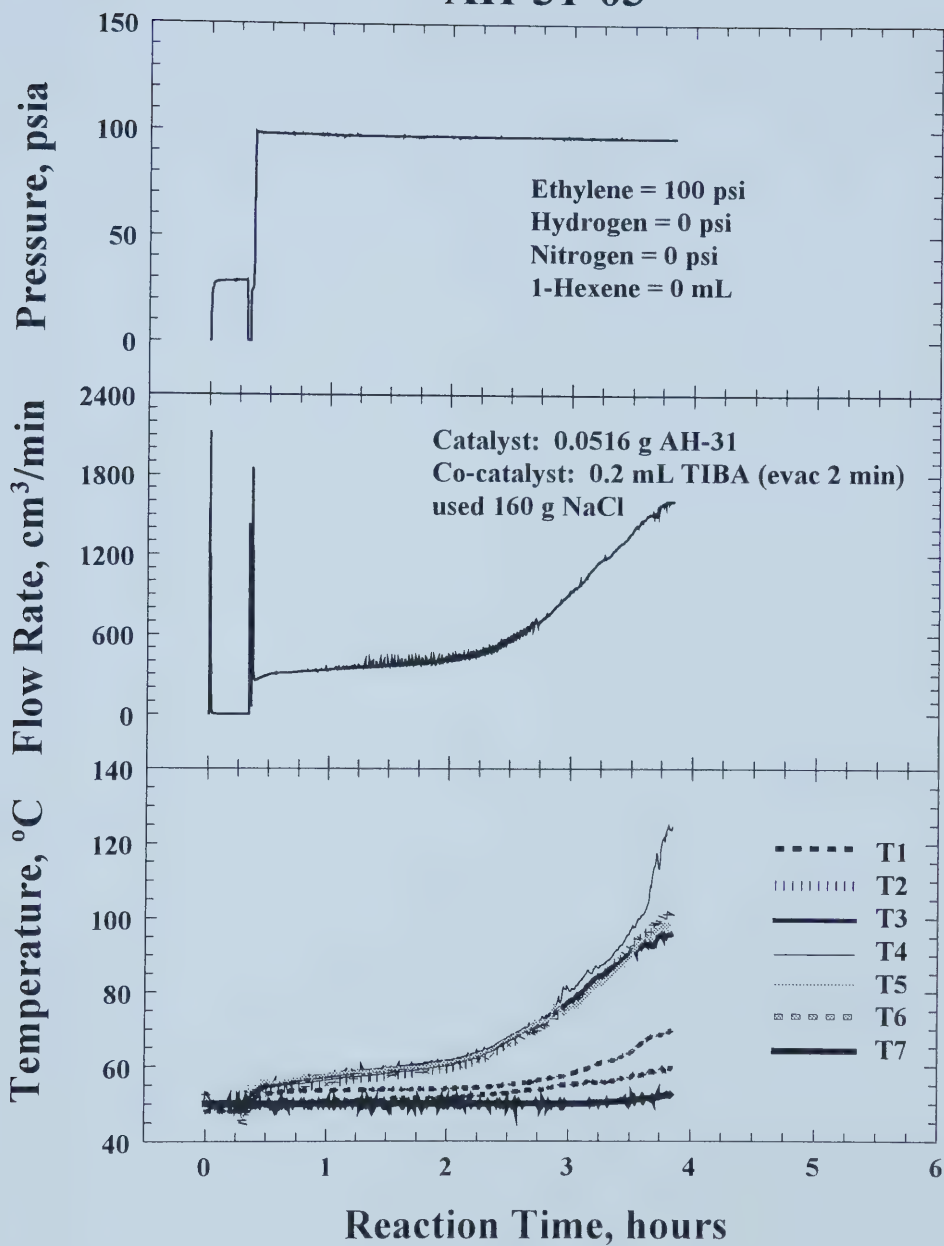
AH-30-07



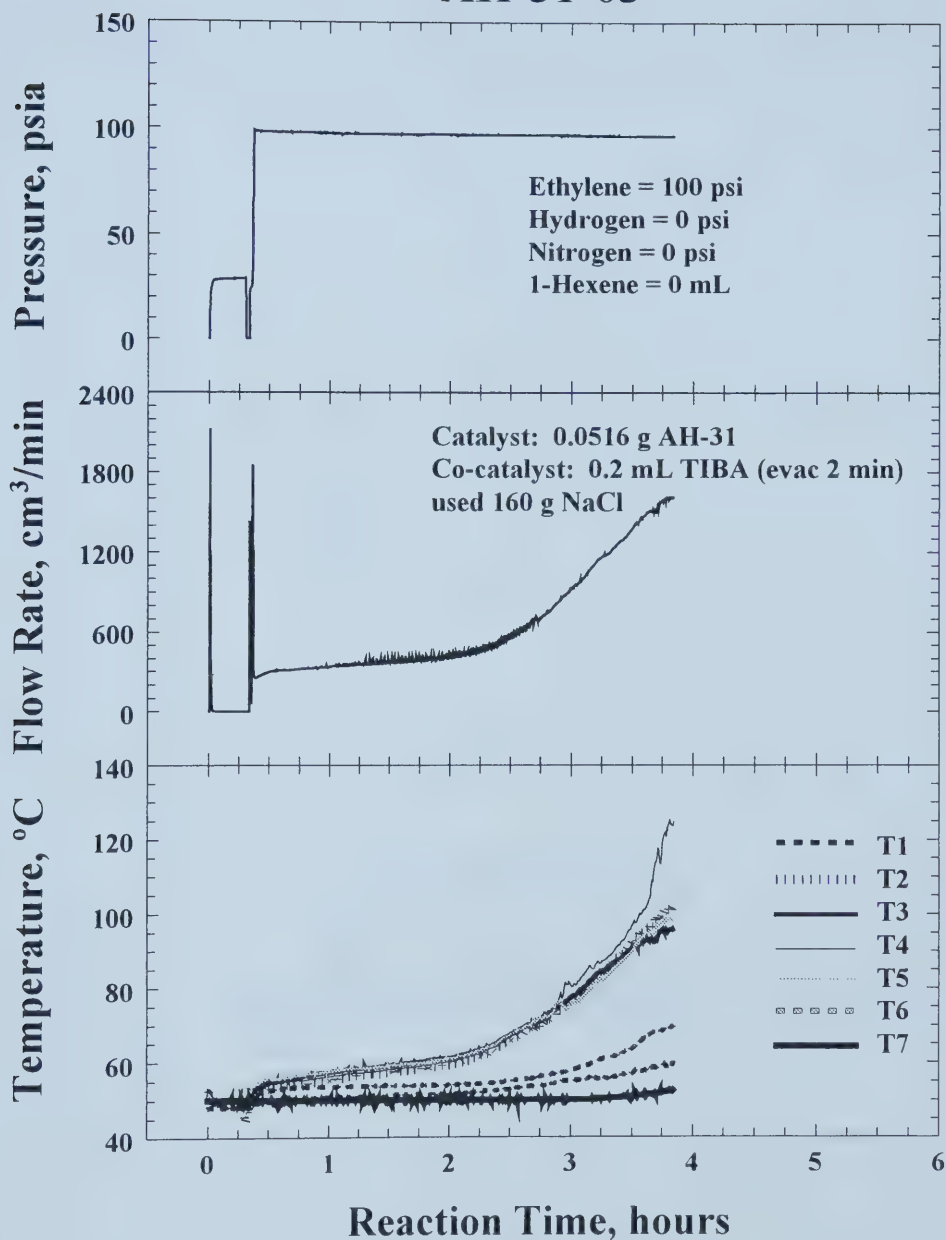
AH-30-08



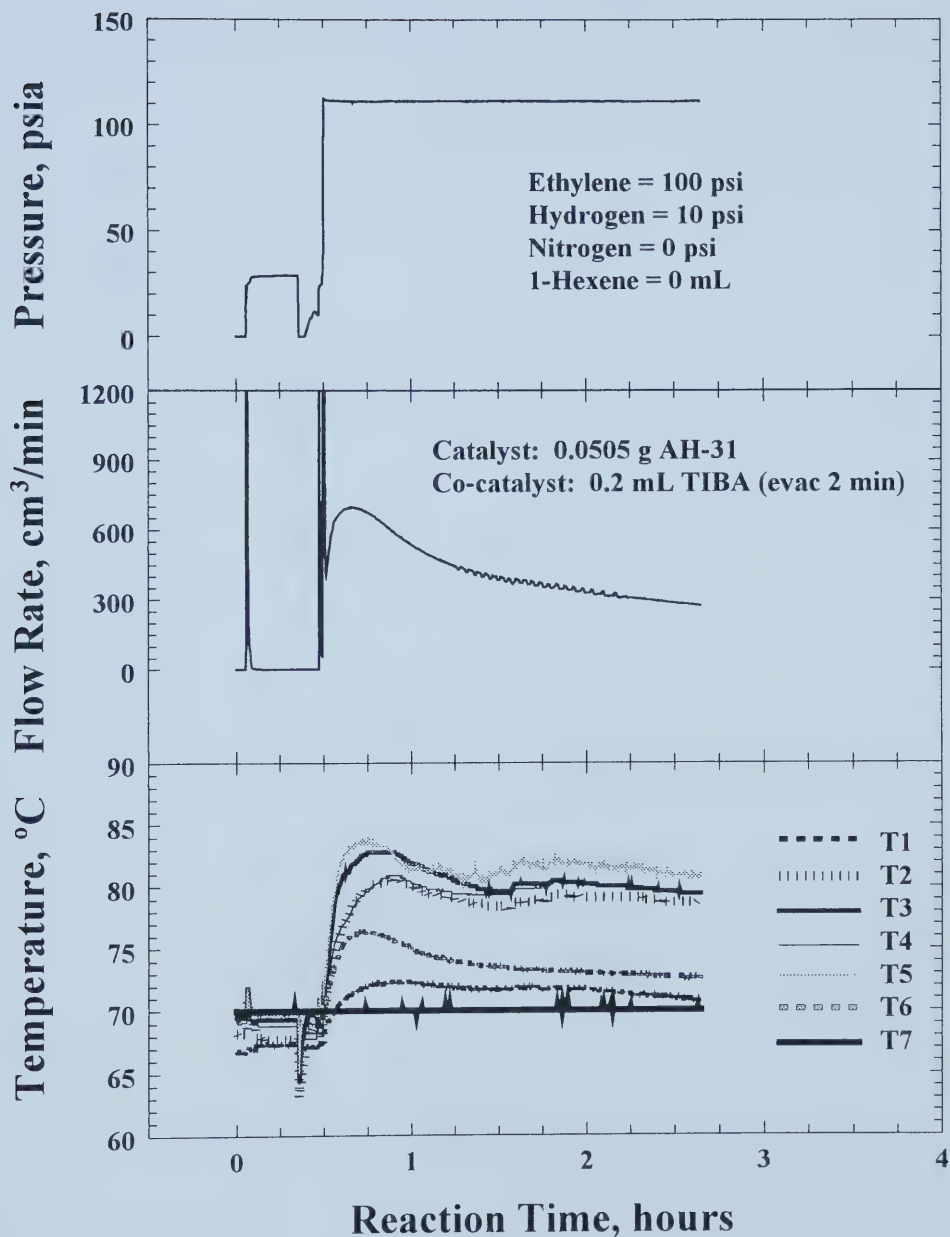
AH-31-03



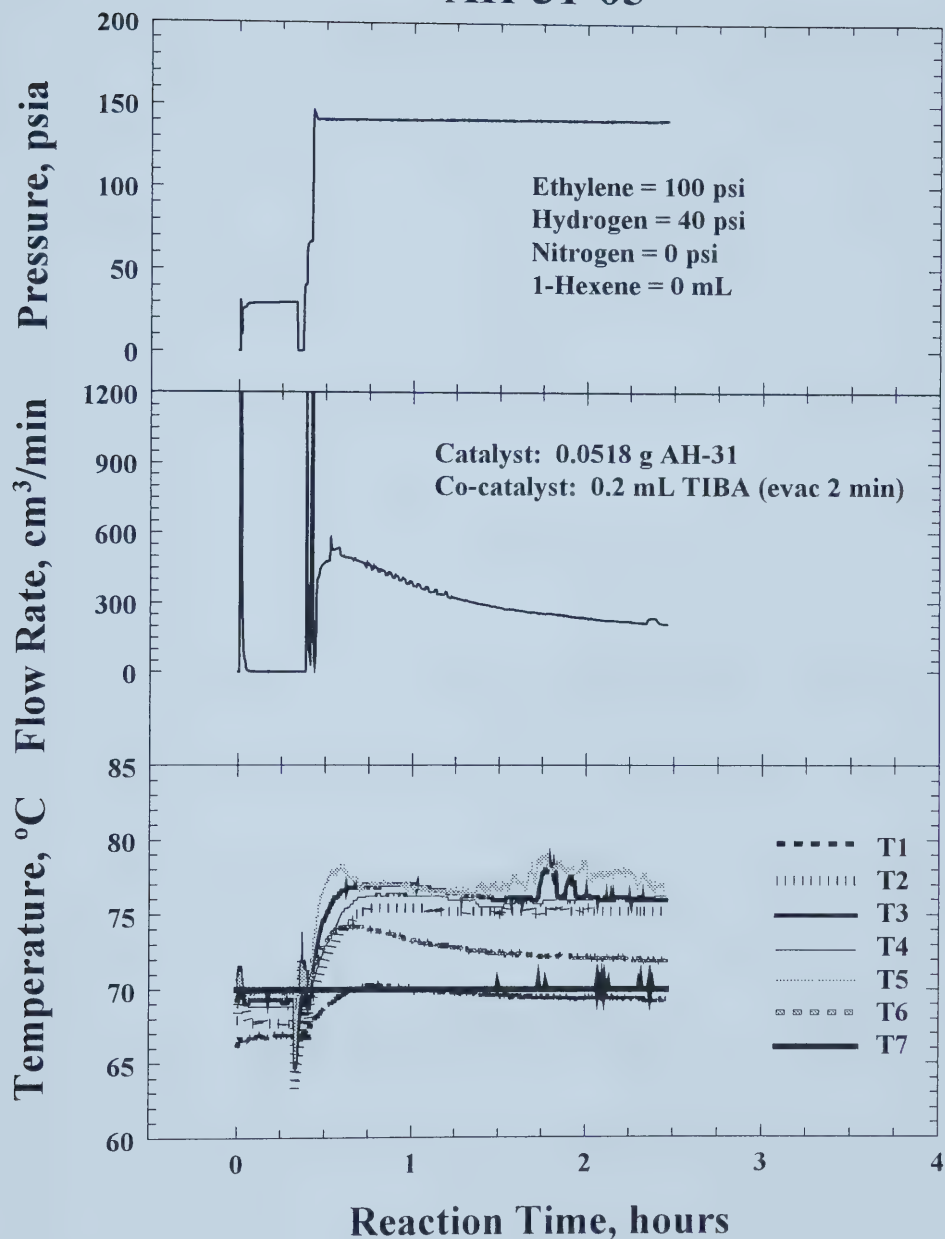
AH-31-03



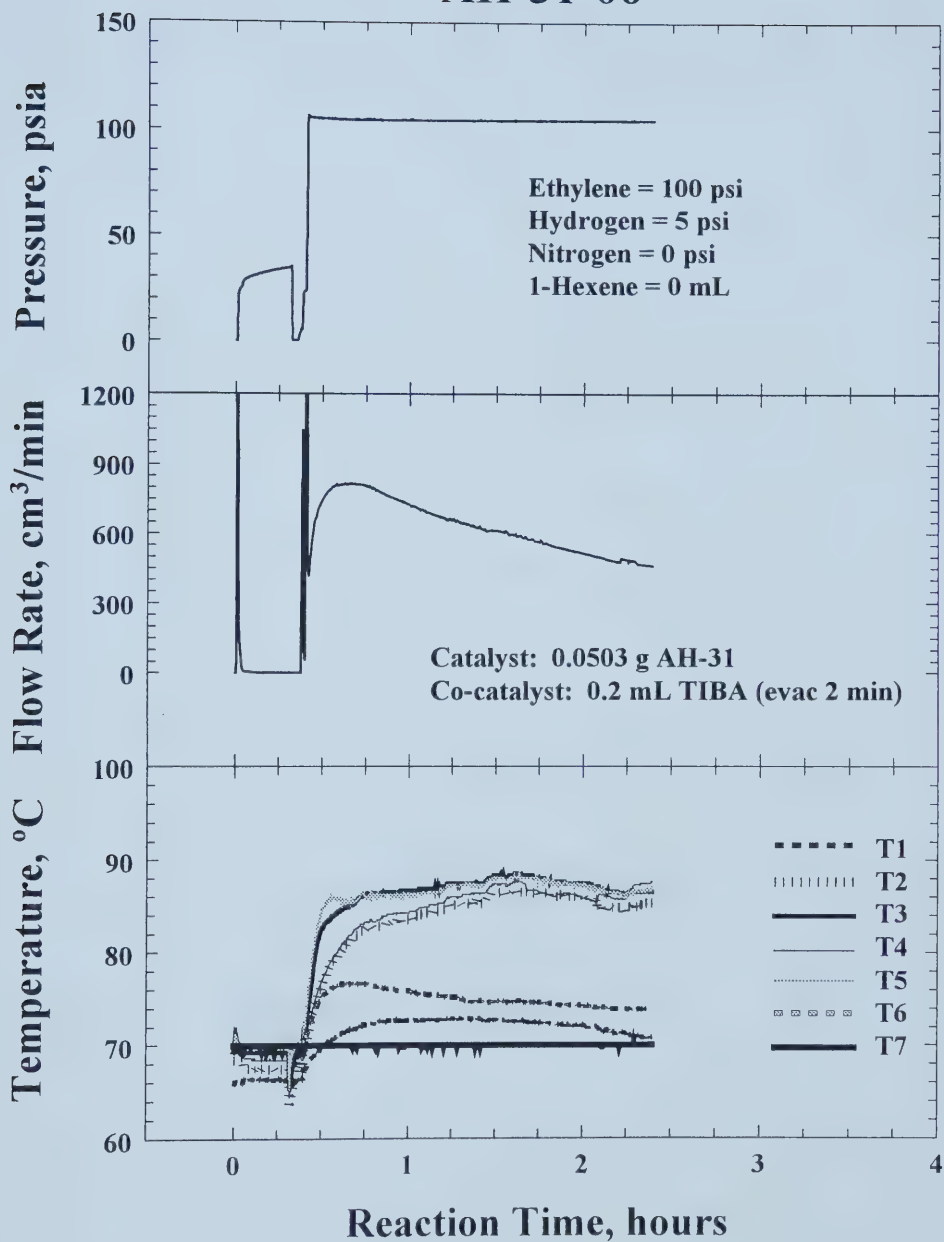
AH-31-04



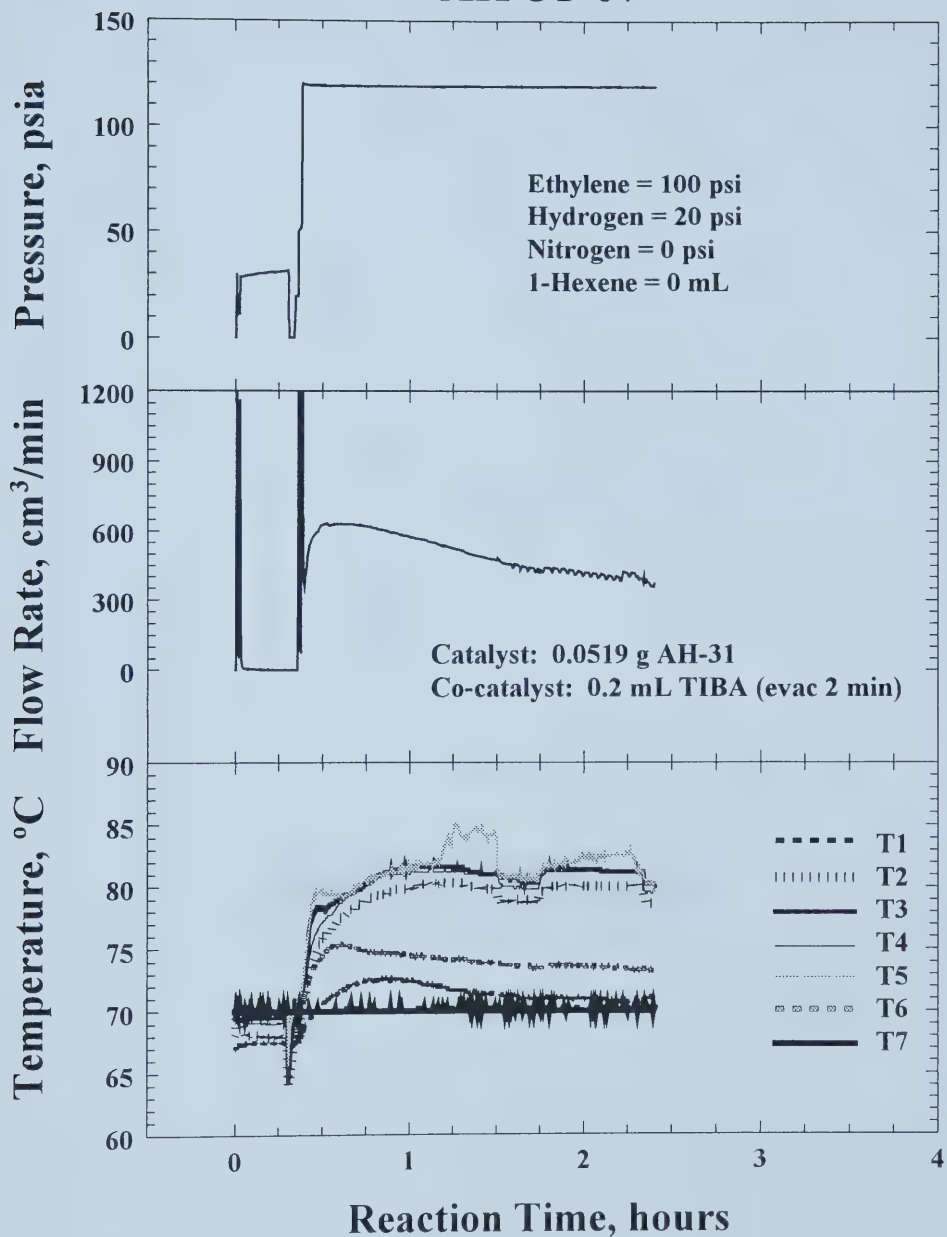
AH-31-05



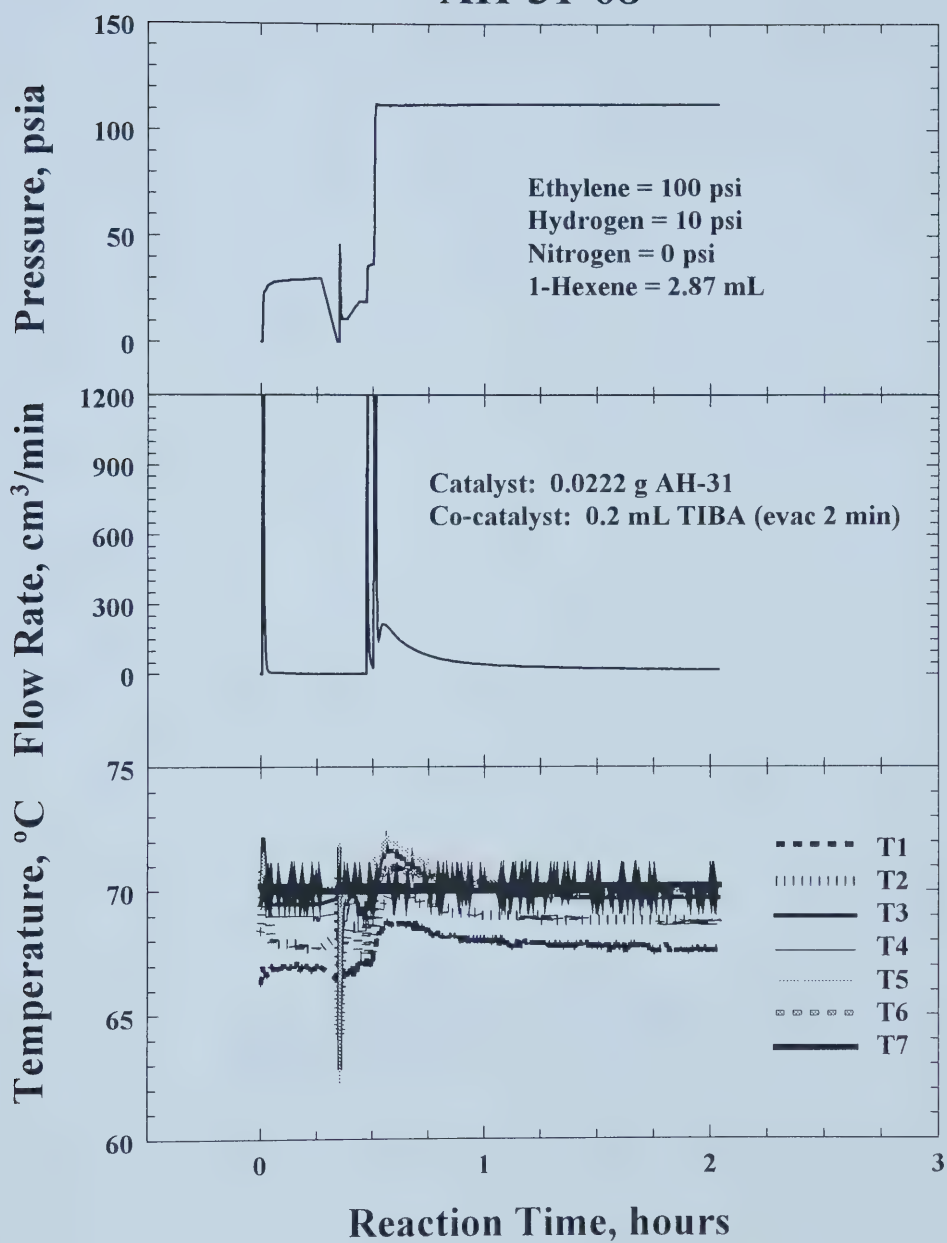
AH-31-06



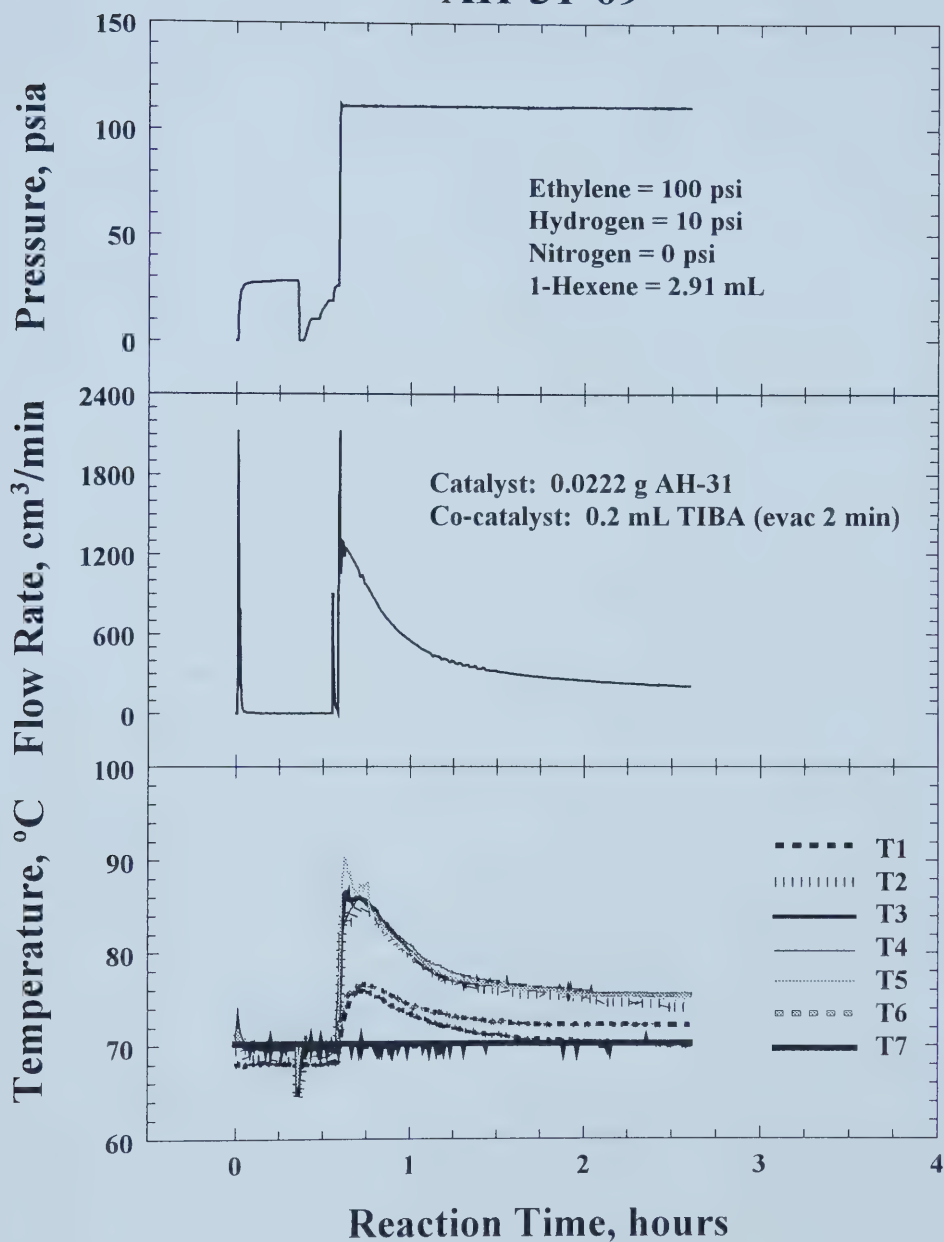
AH-31-07



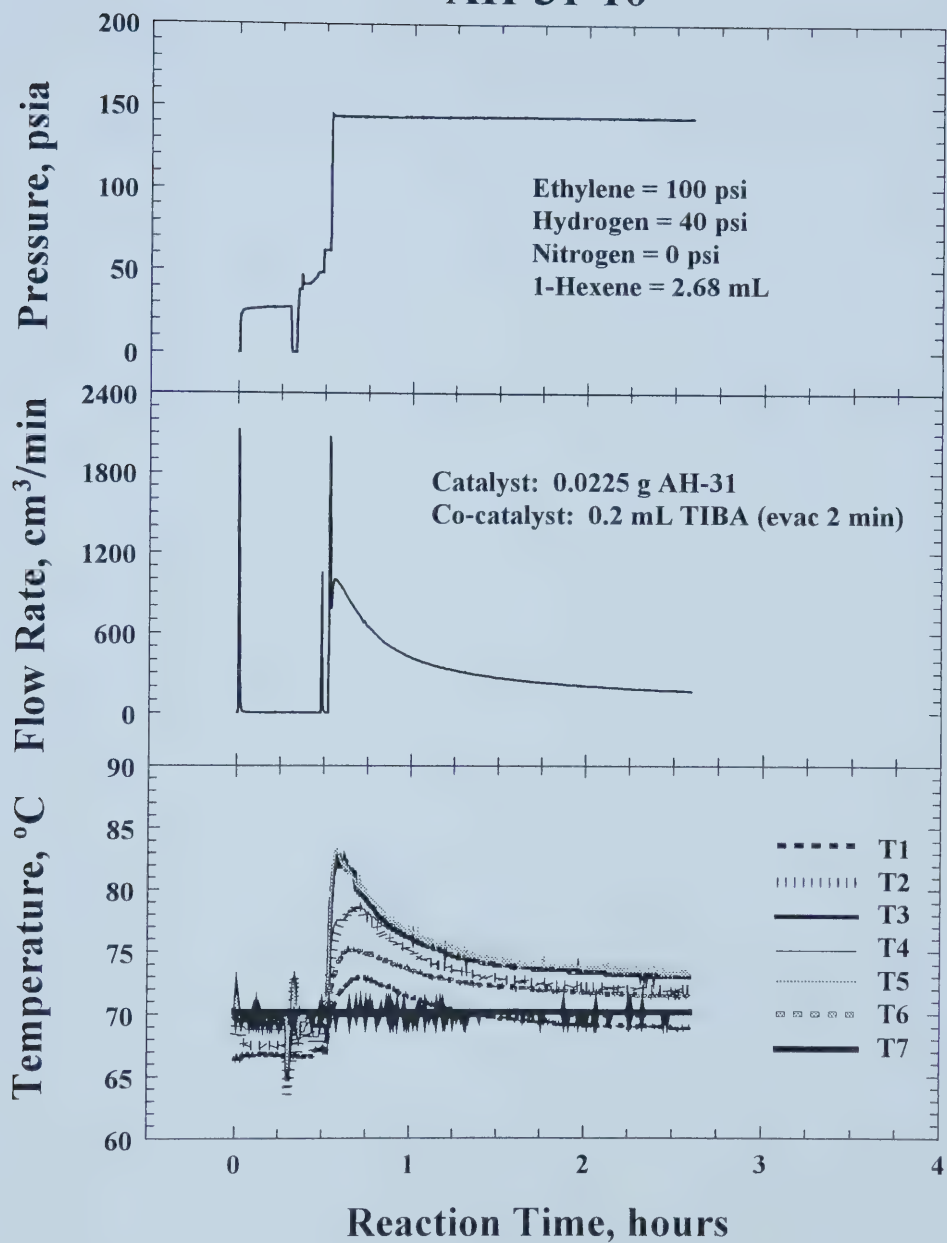
AH-31-08



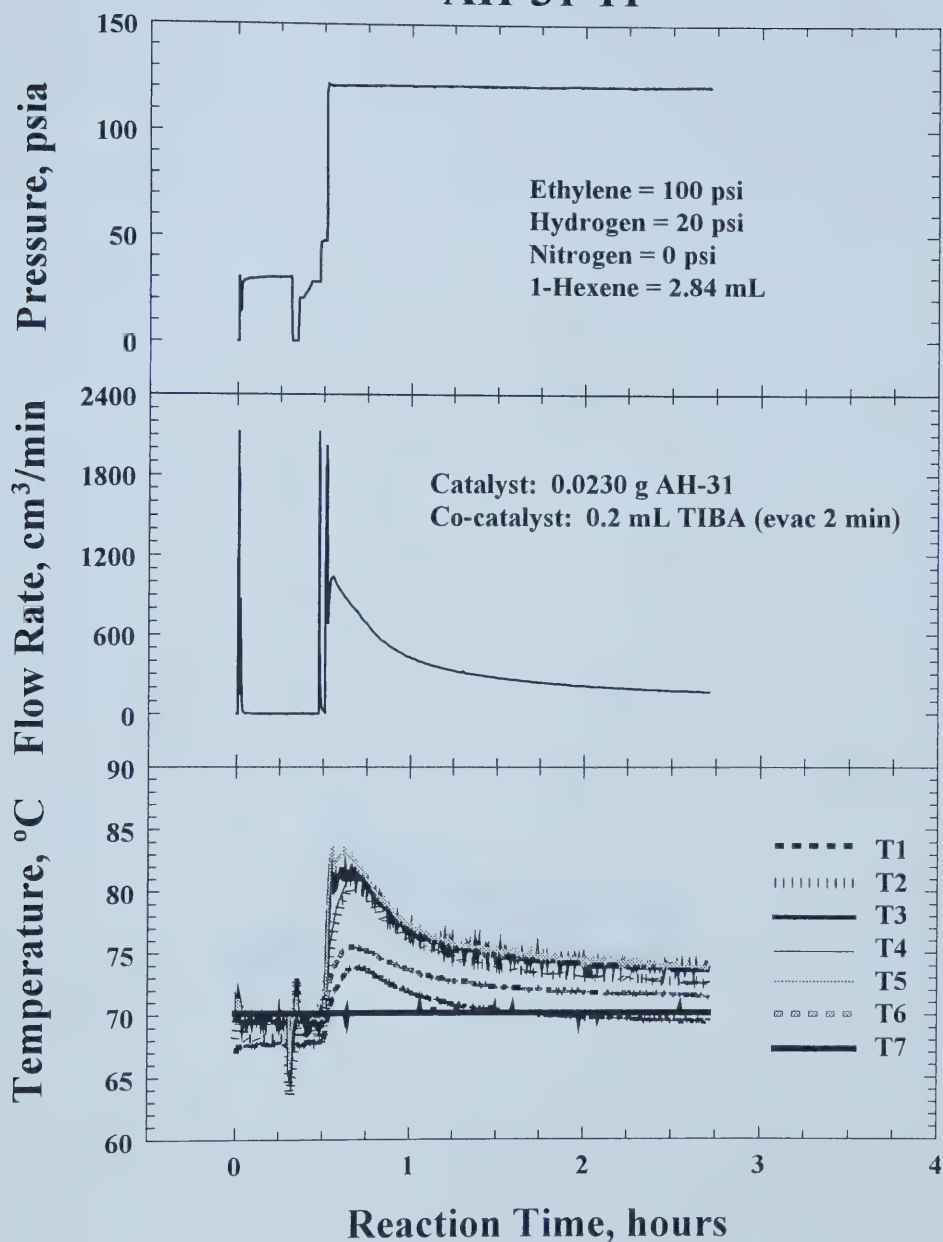
AH-31-09



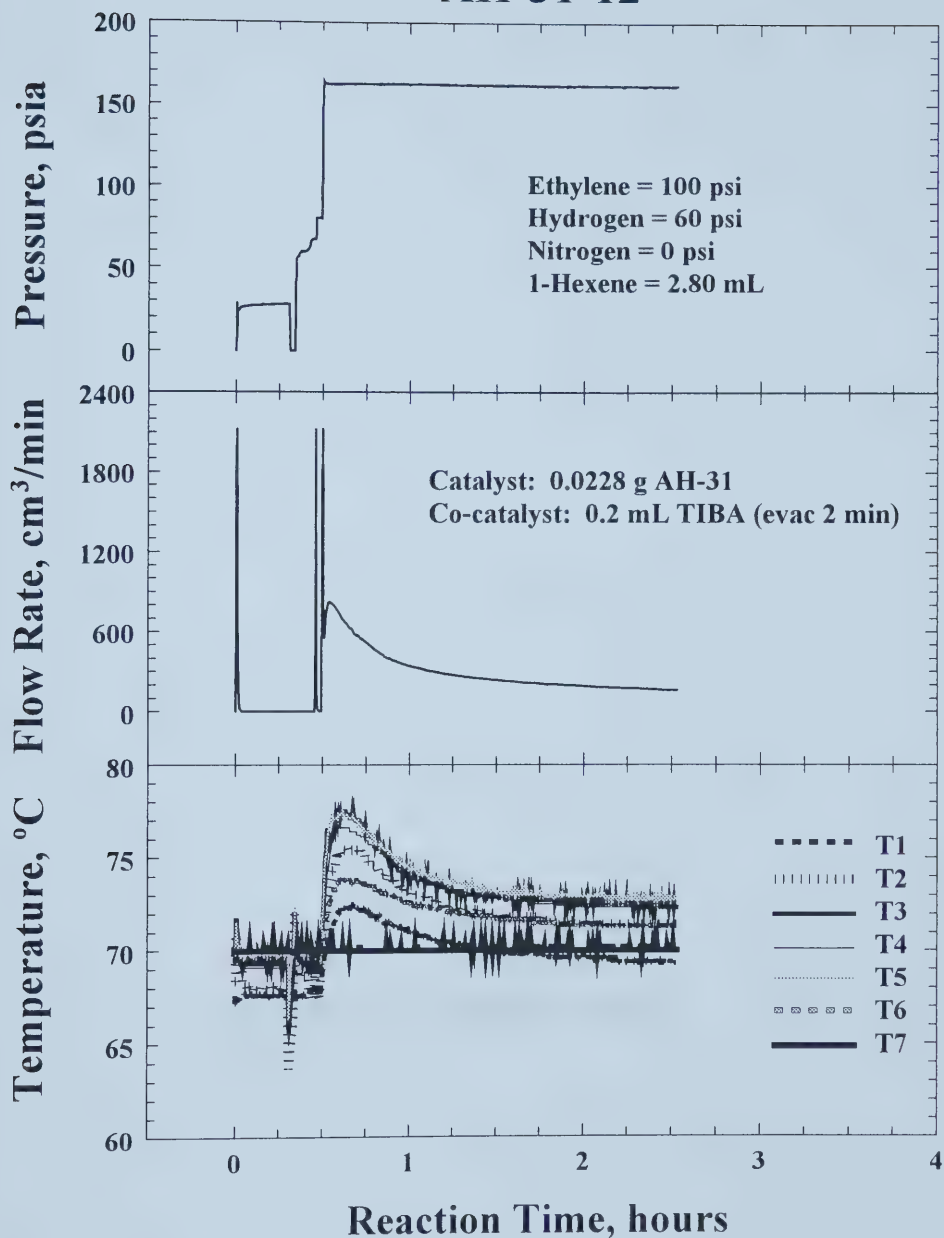
AH-31-10



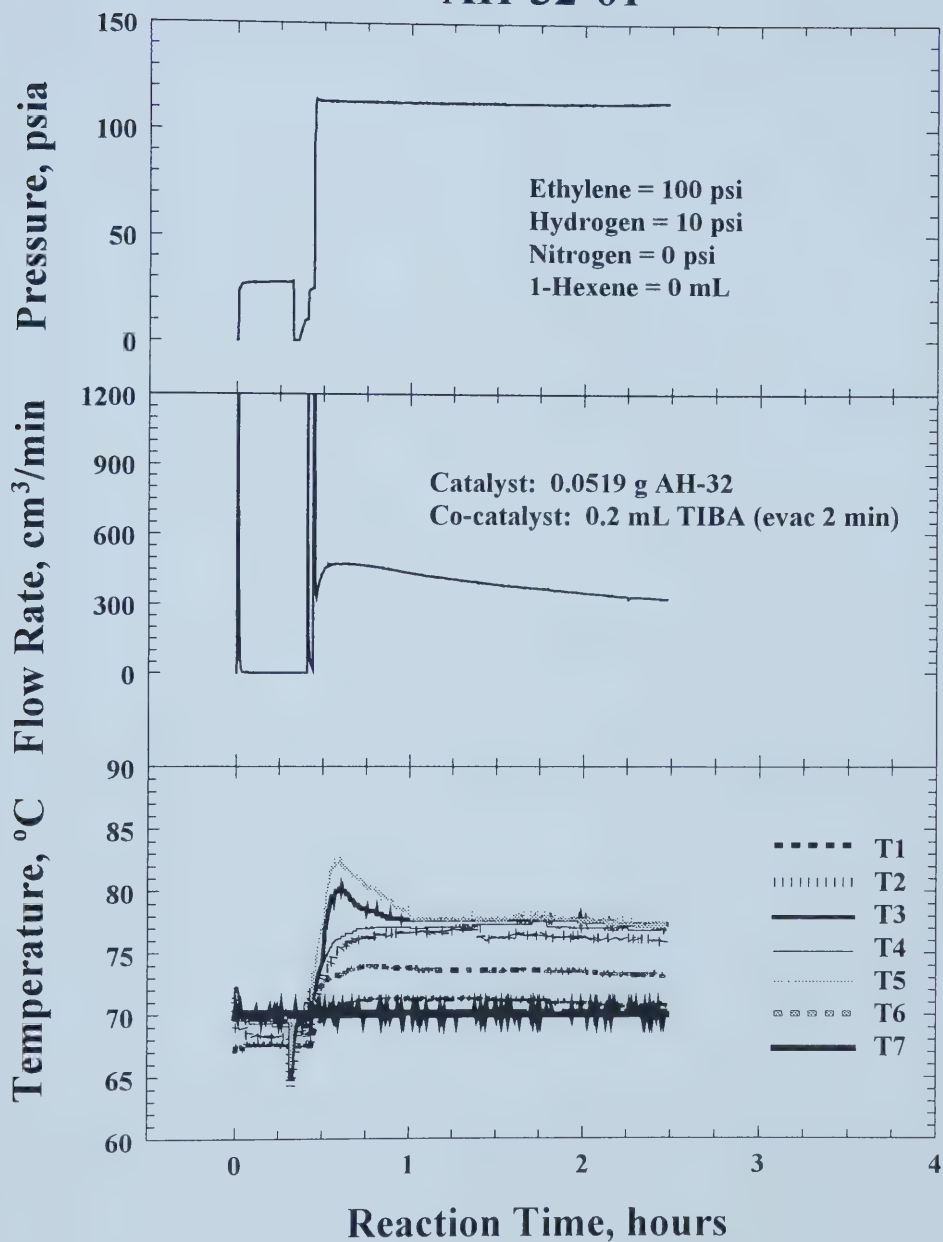
AH-31-11



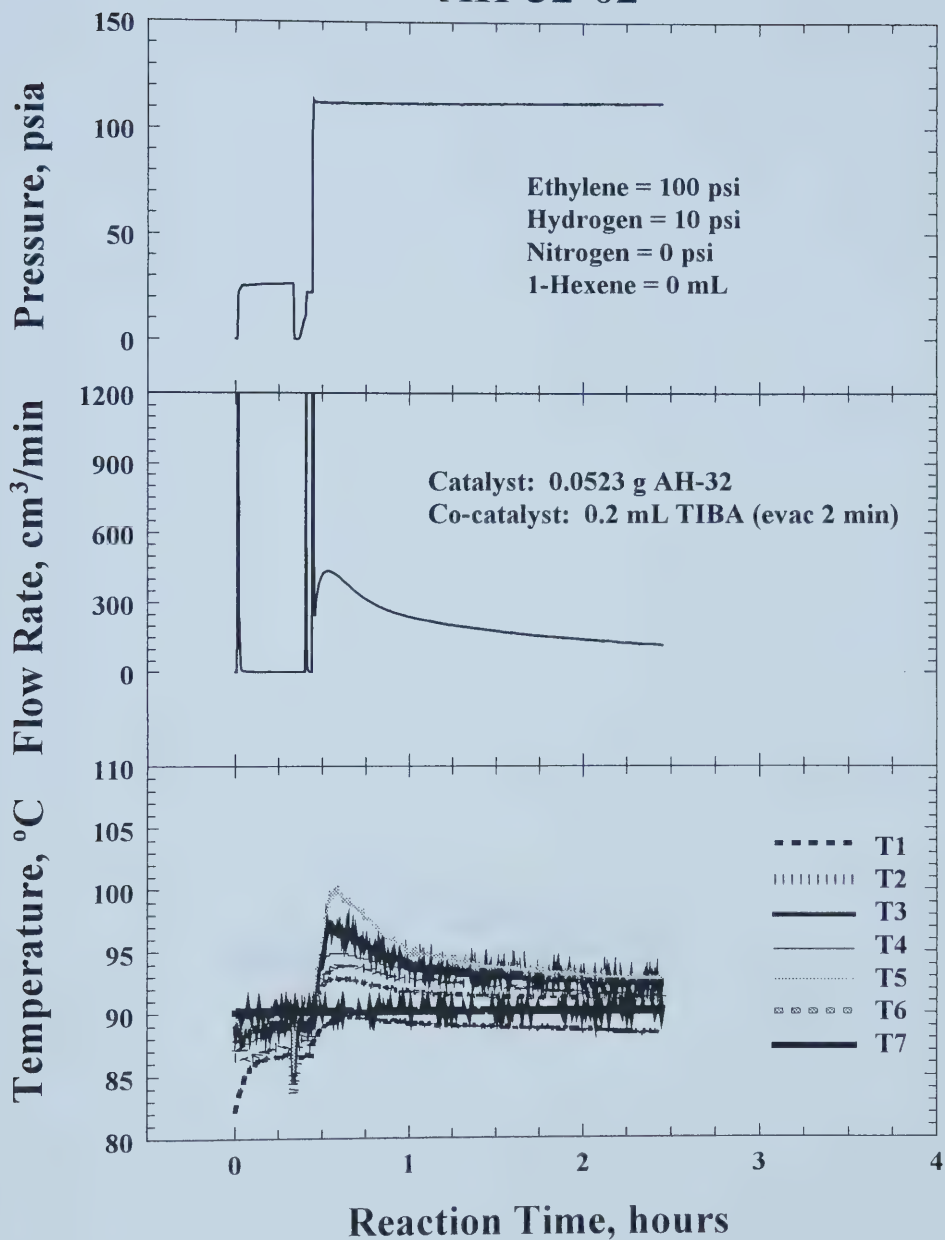
AH-31-12



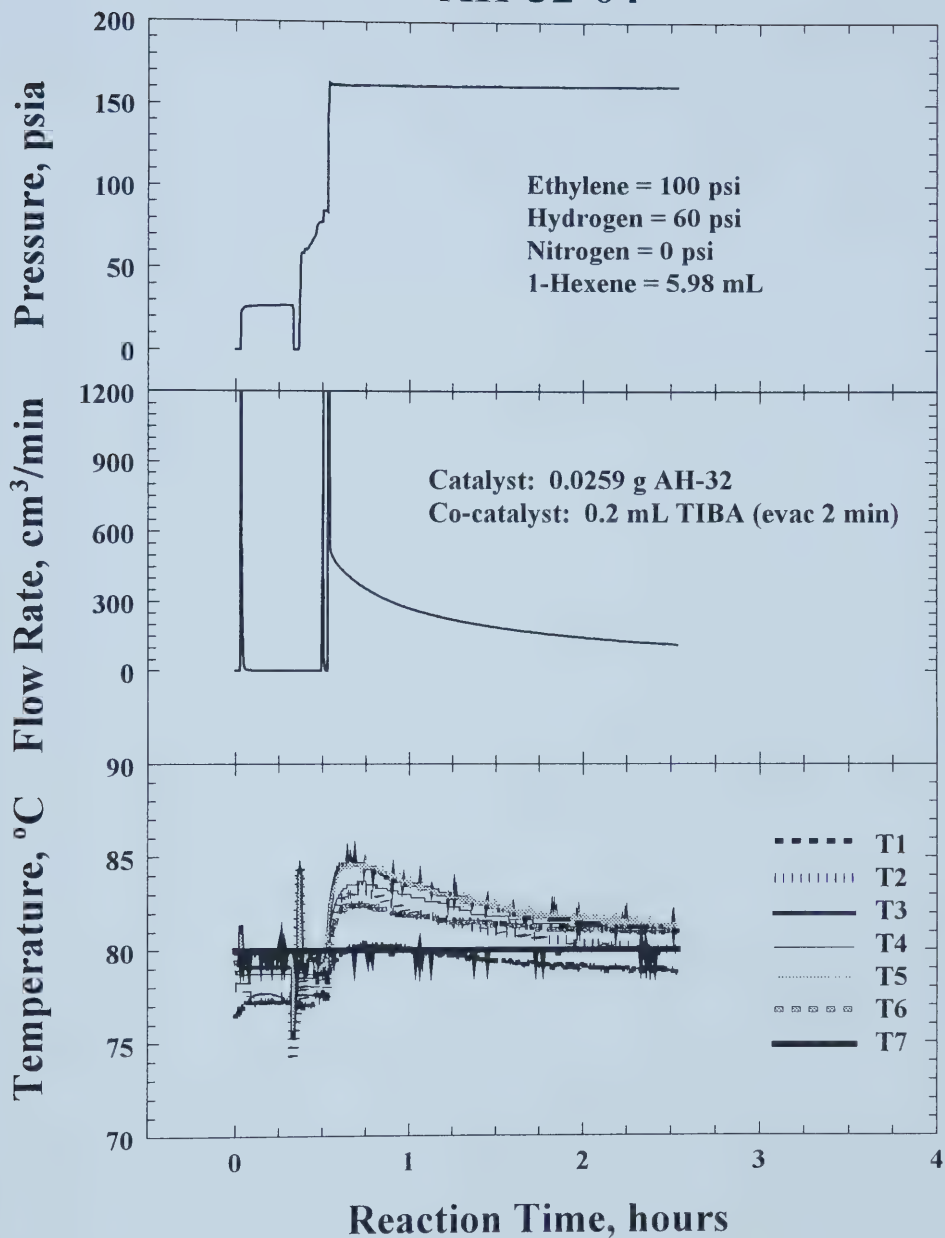
AH-32-01



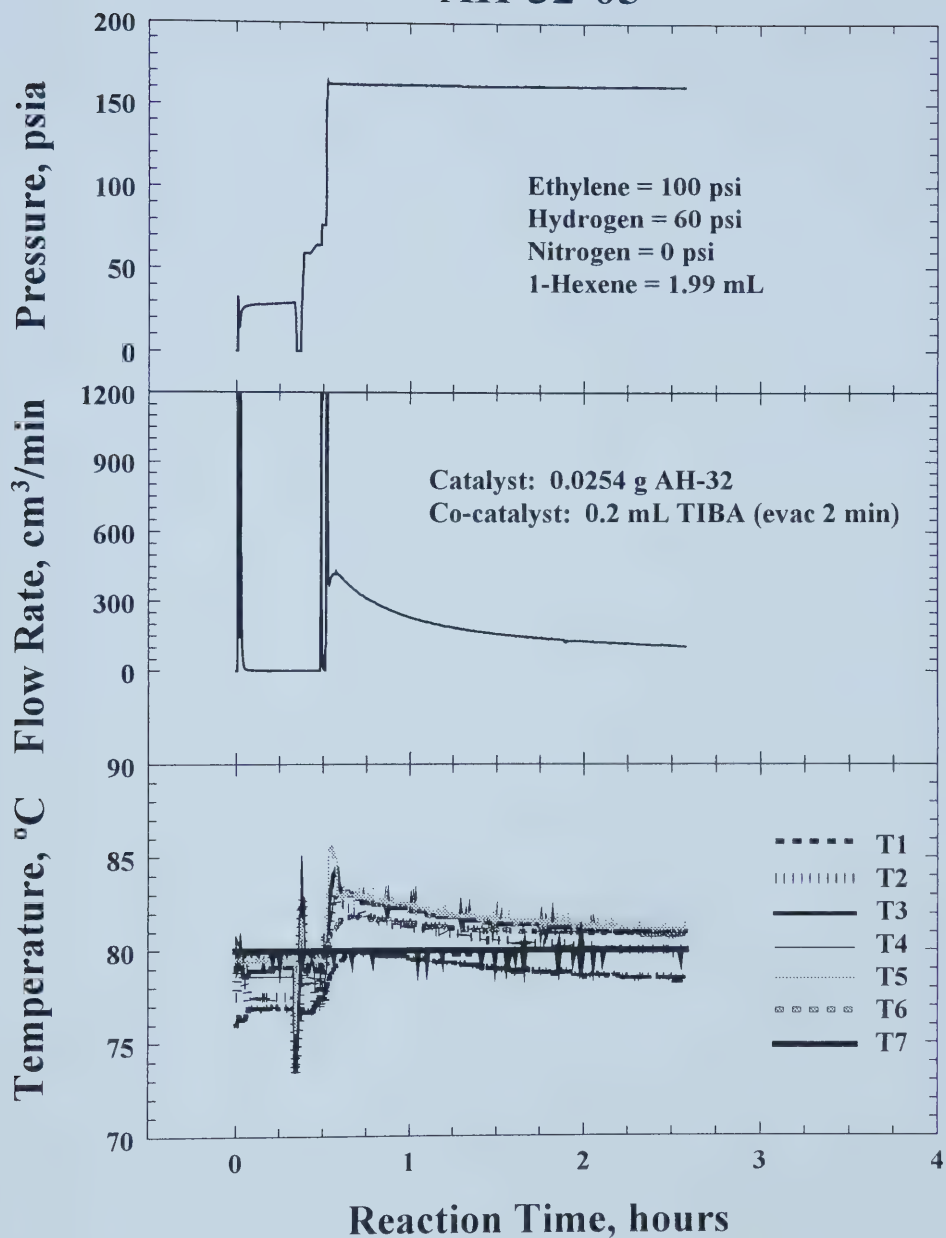
AH-32-02



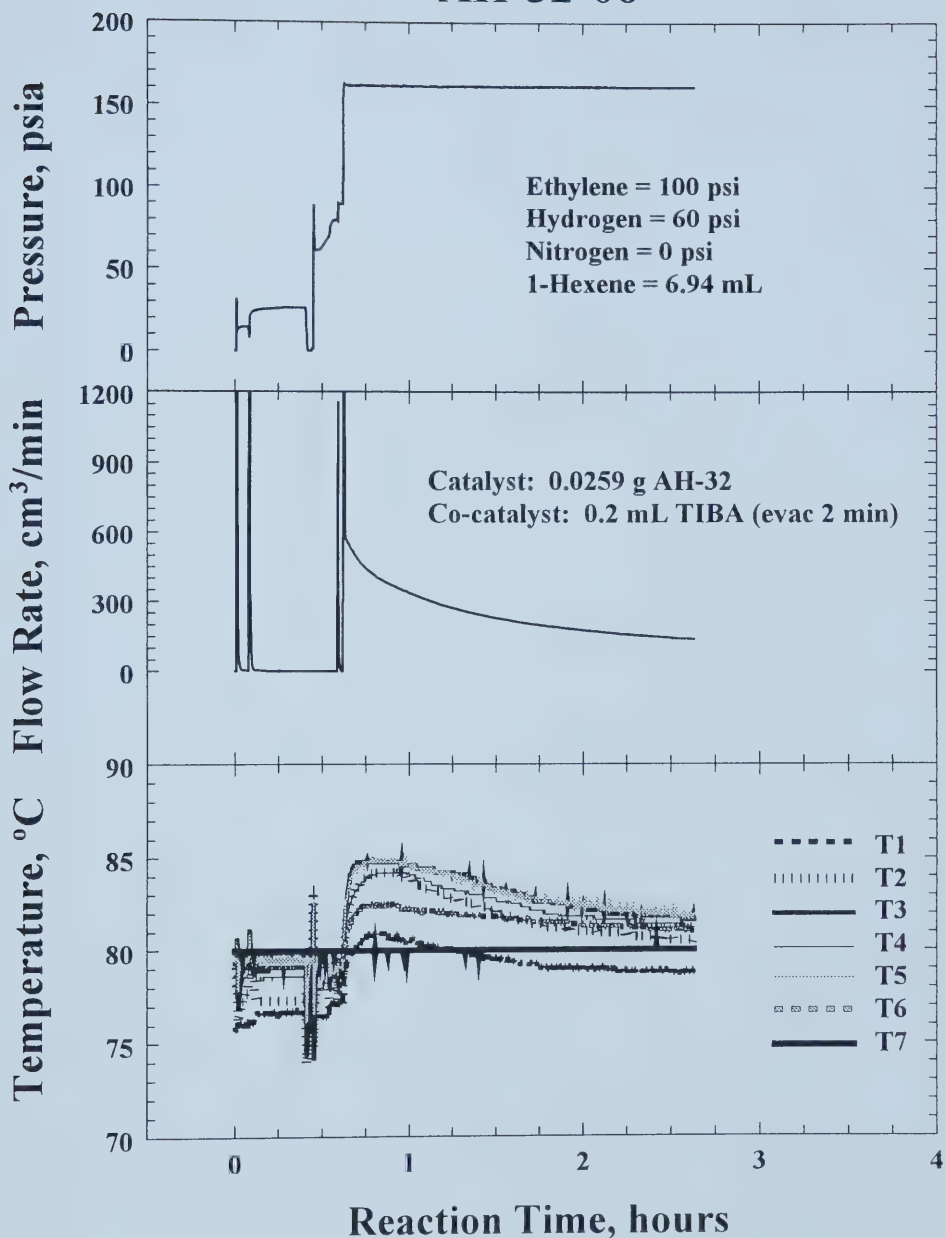
AH-32-04



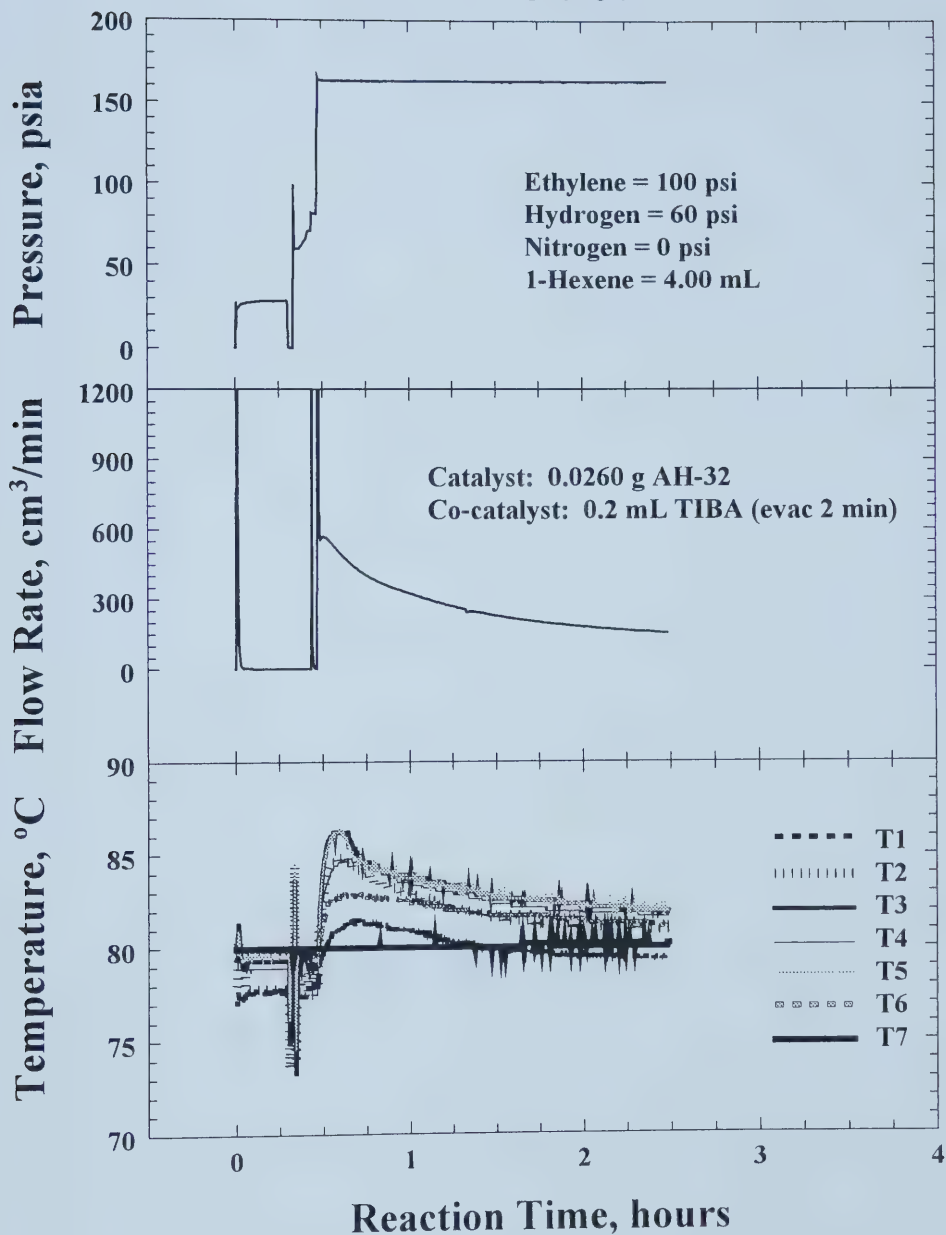
AH-32-05



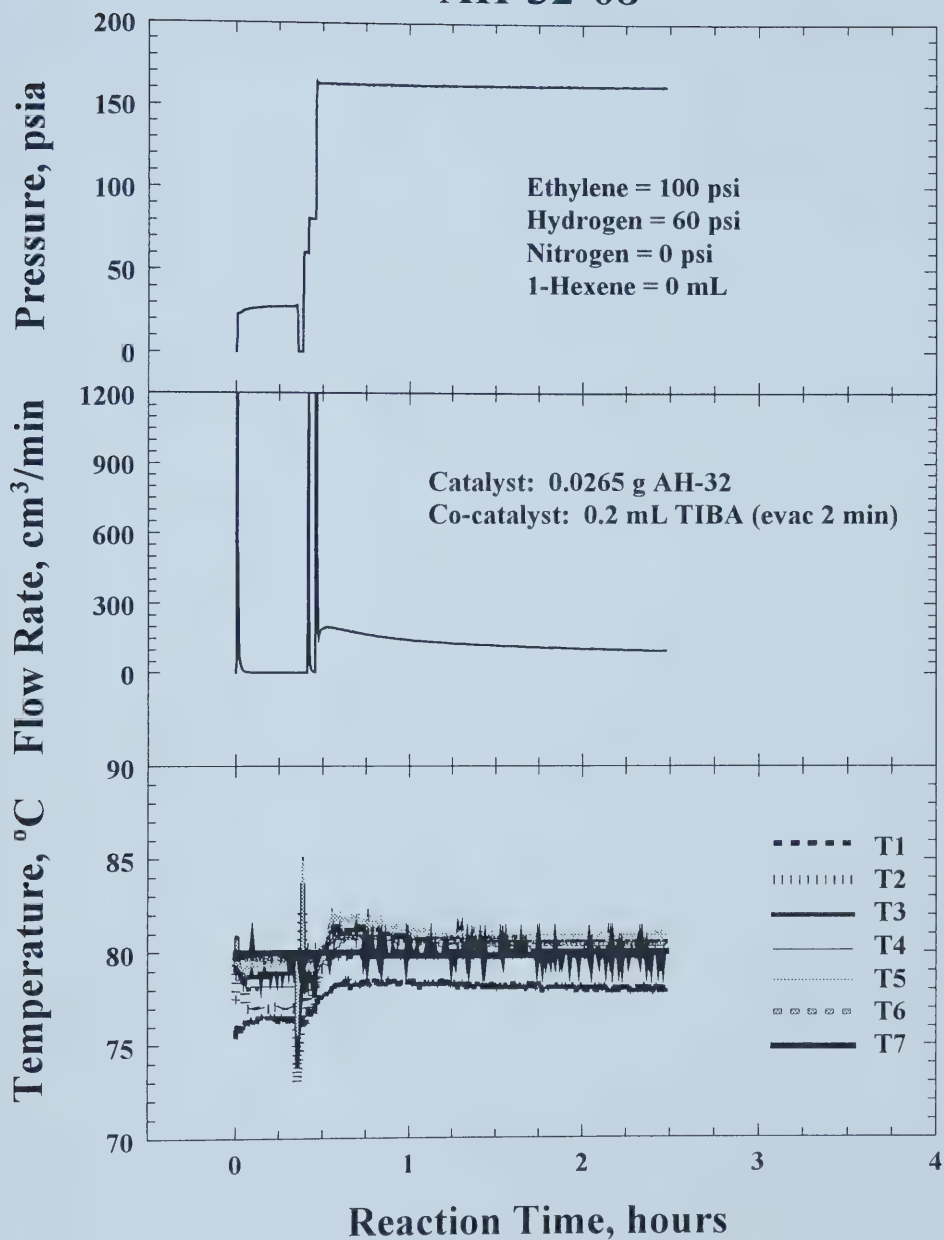
AH-32-06



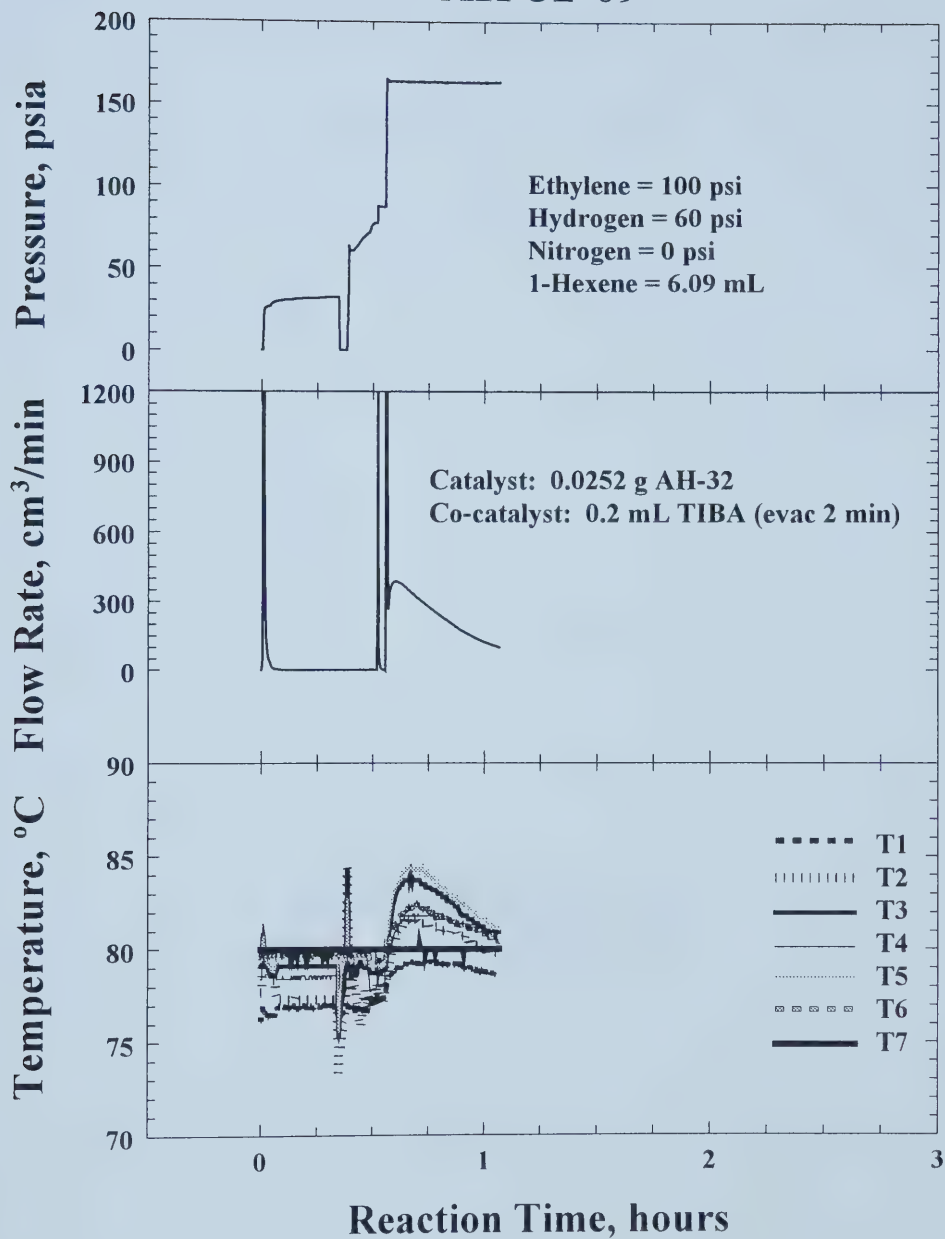
AH-32-07



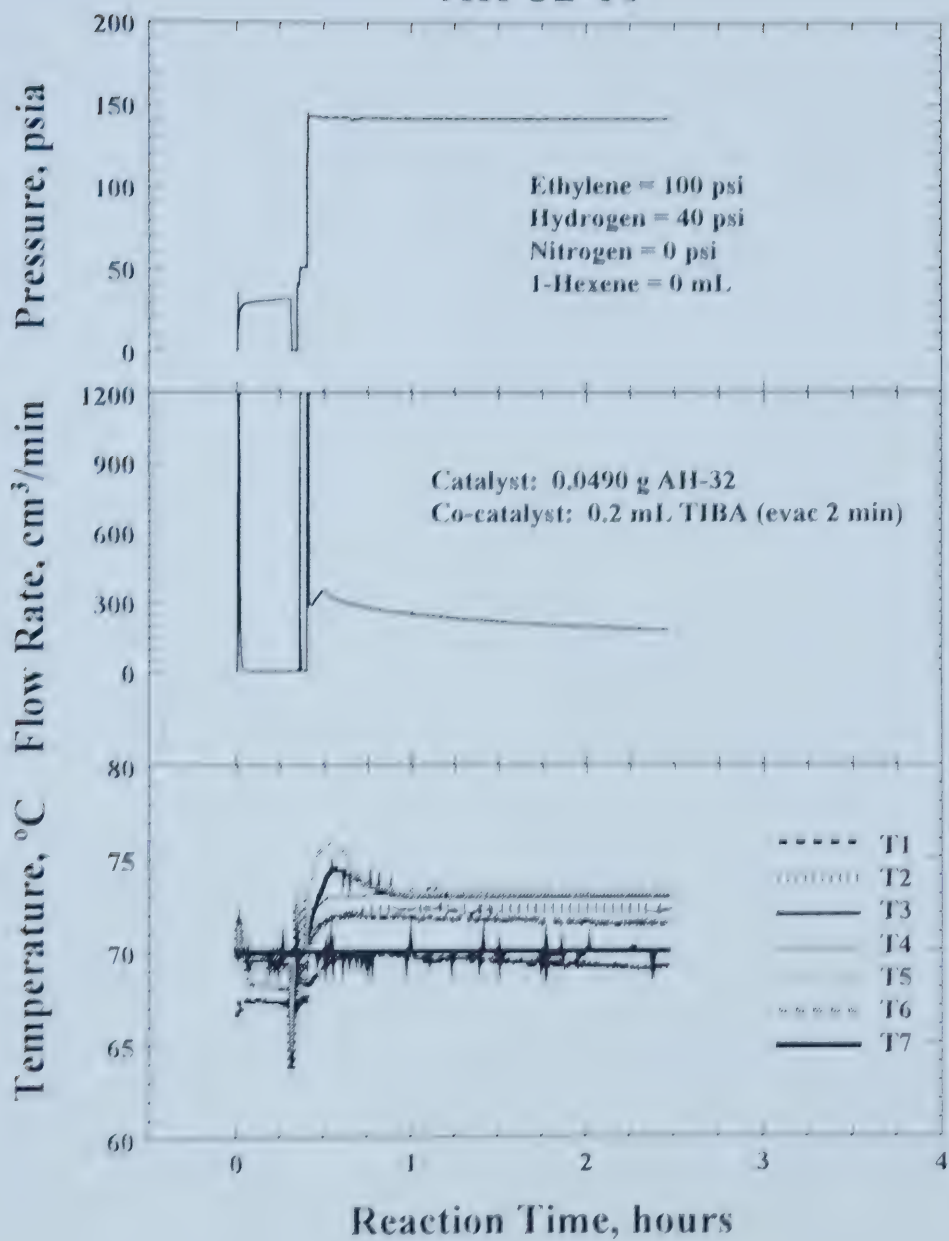
AH-32-08



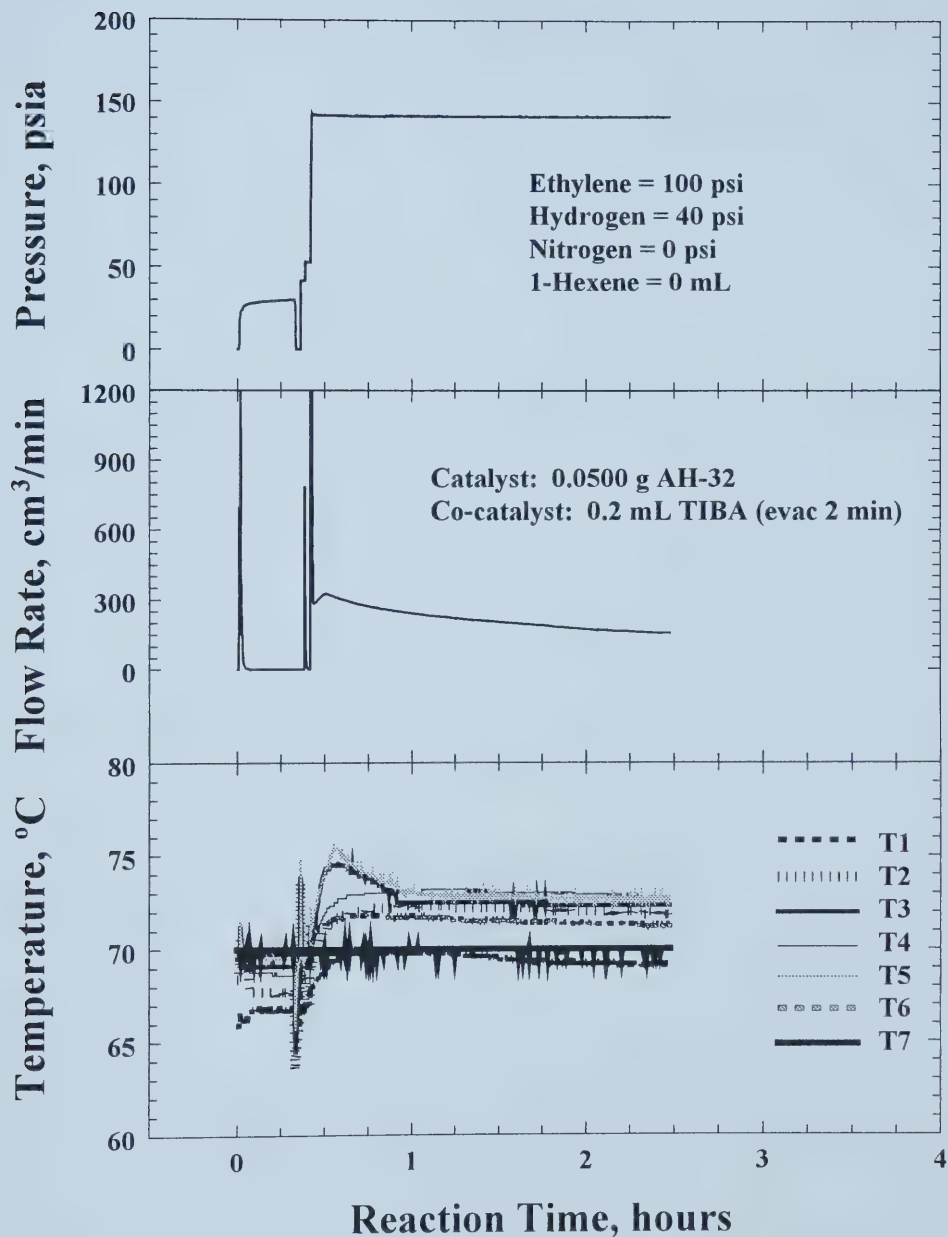
AH-32-09



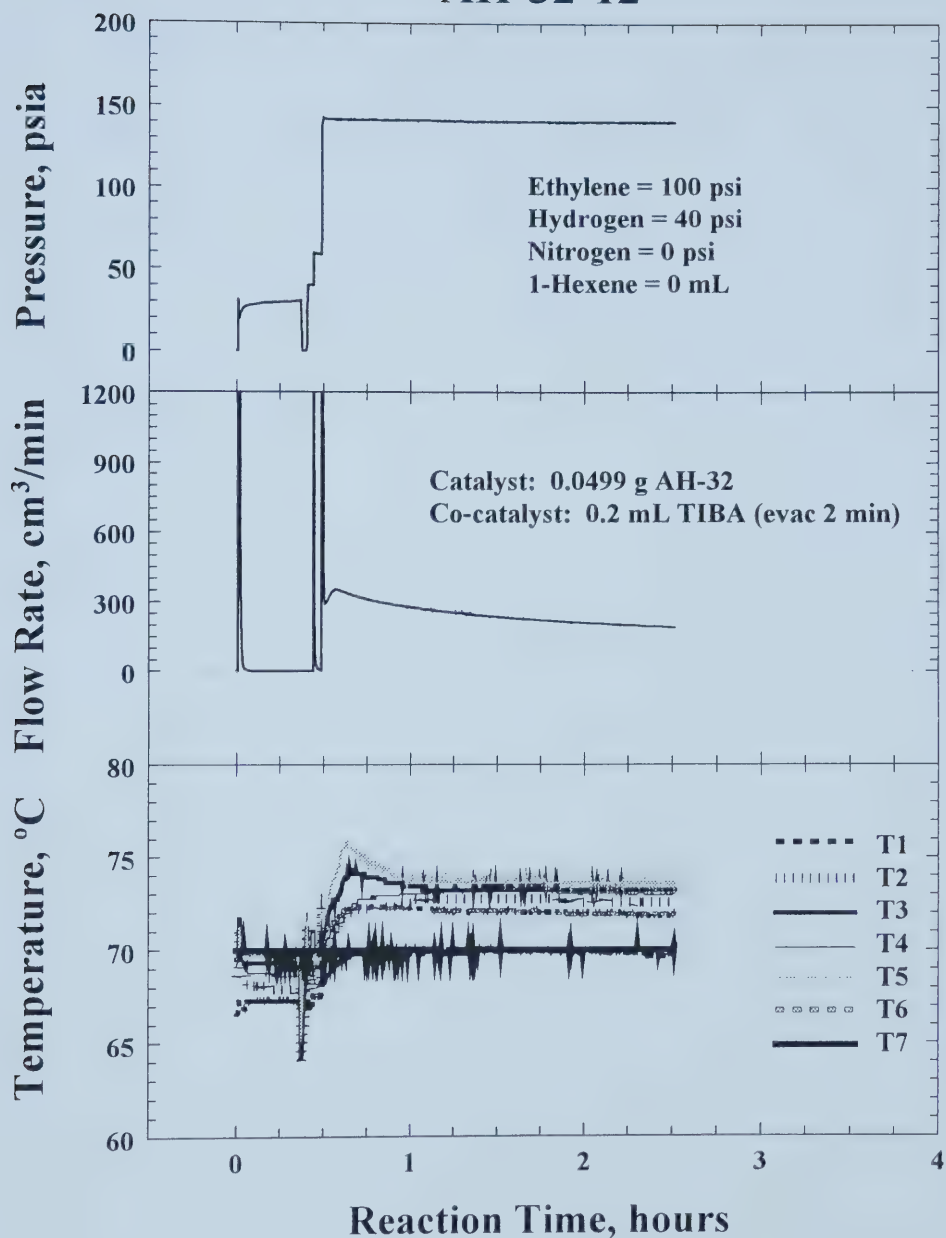
AH-32-10



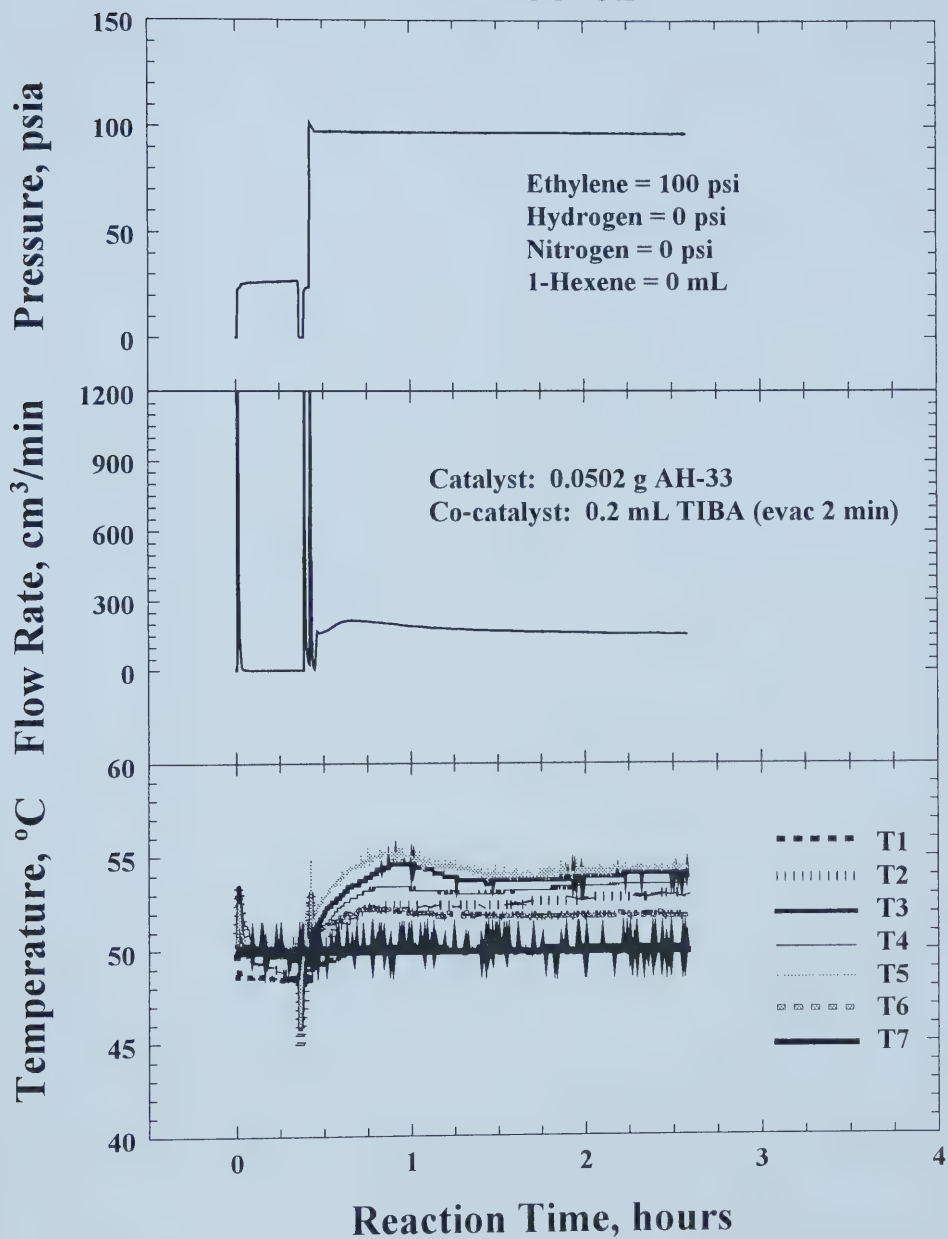
AH-32-11



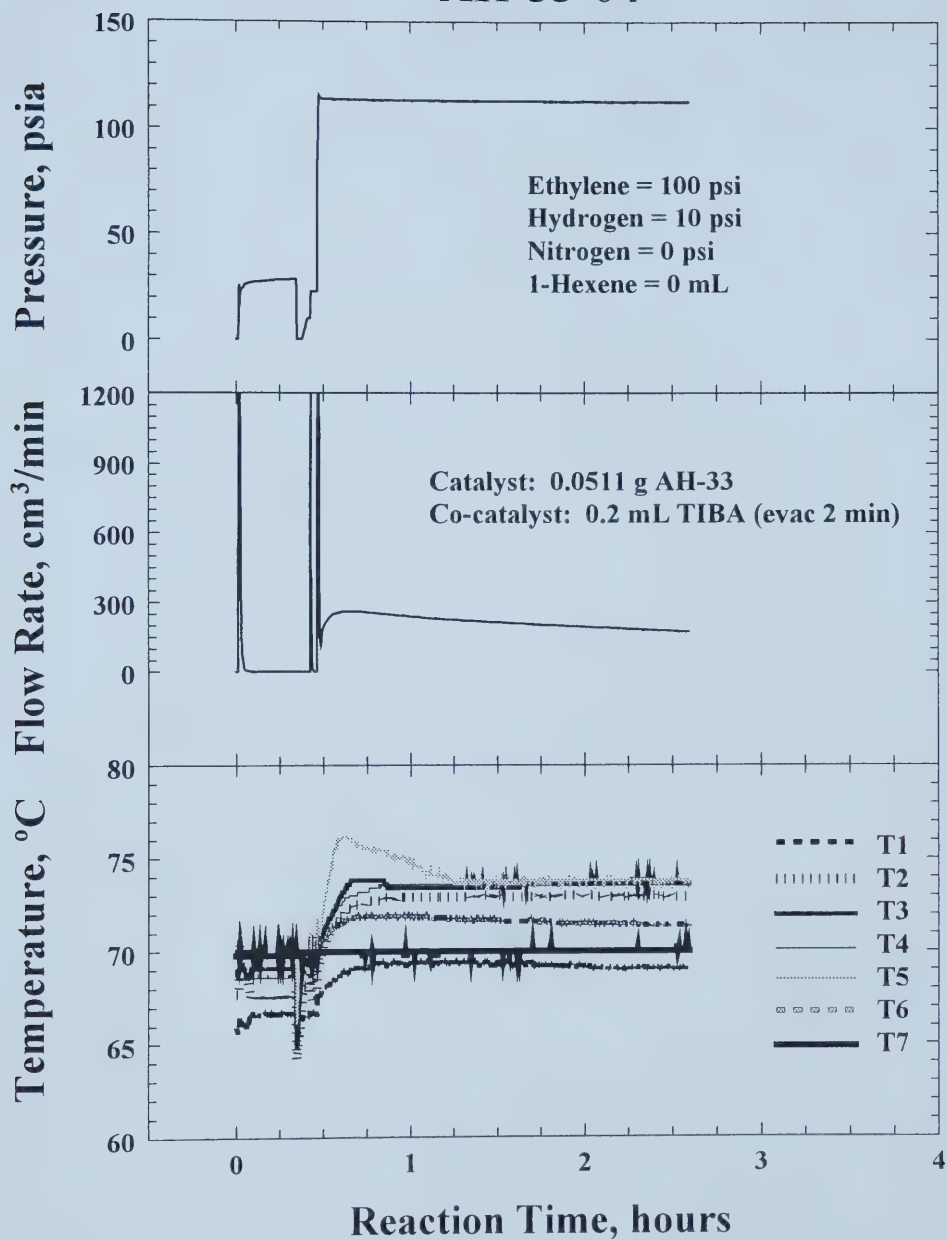
AH-32-12



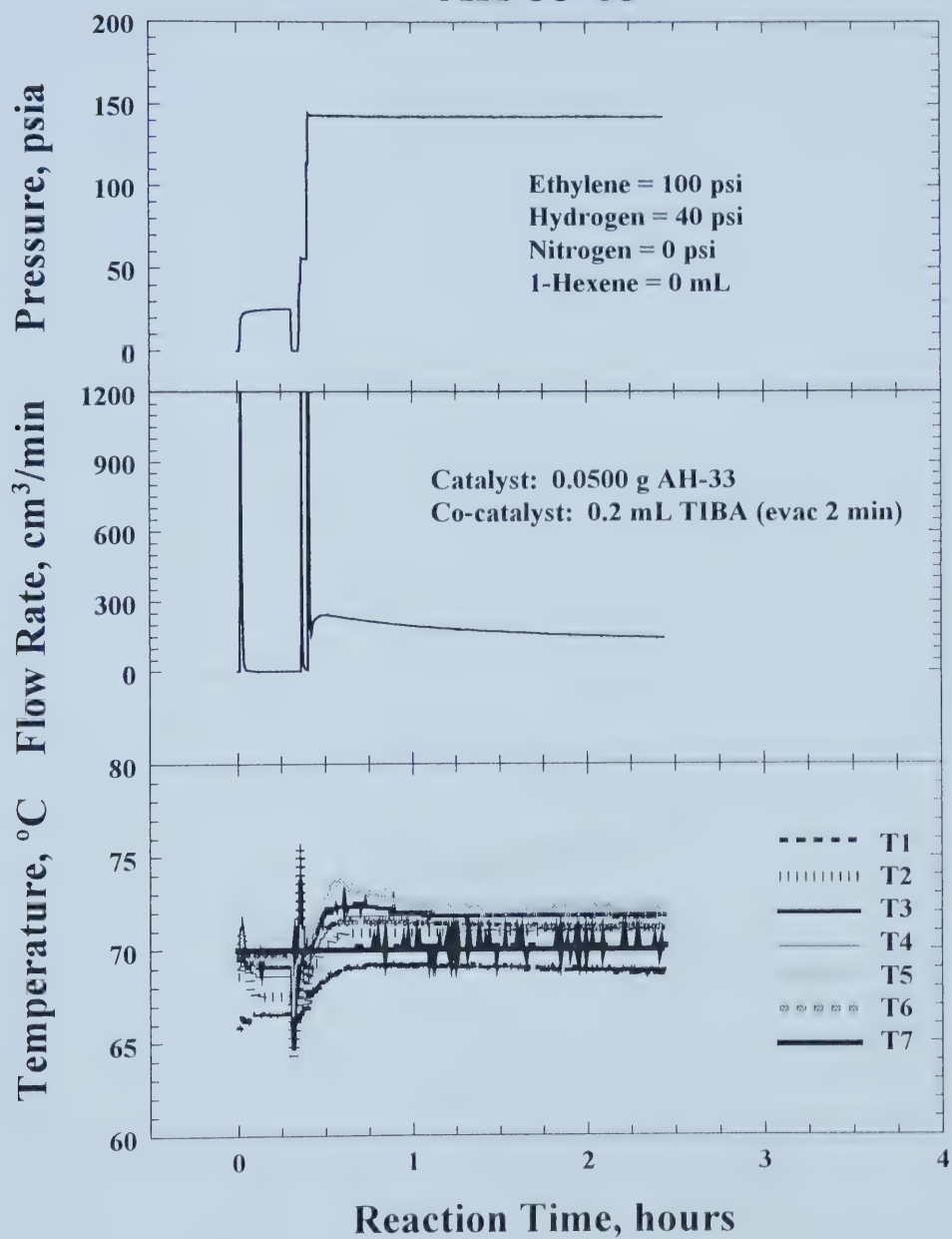
AH-33-02



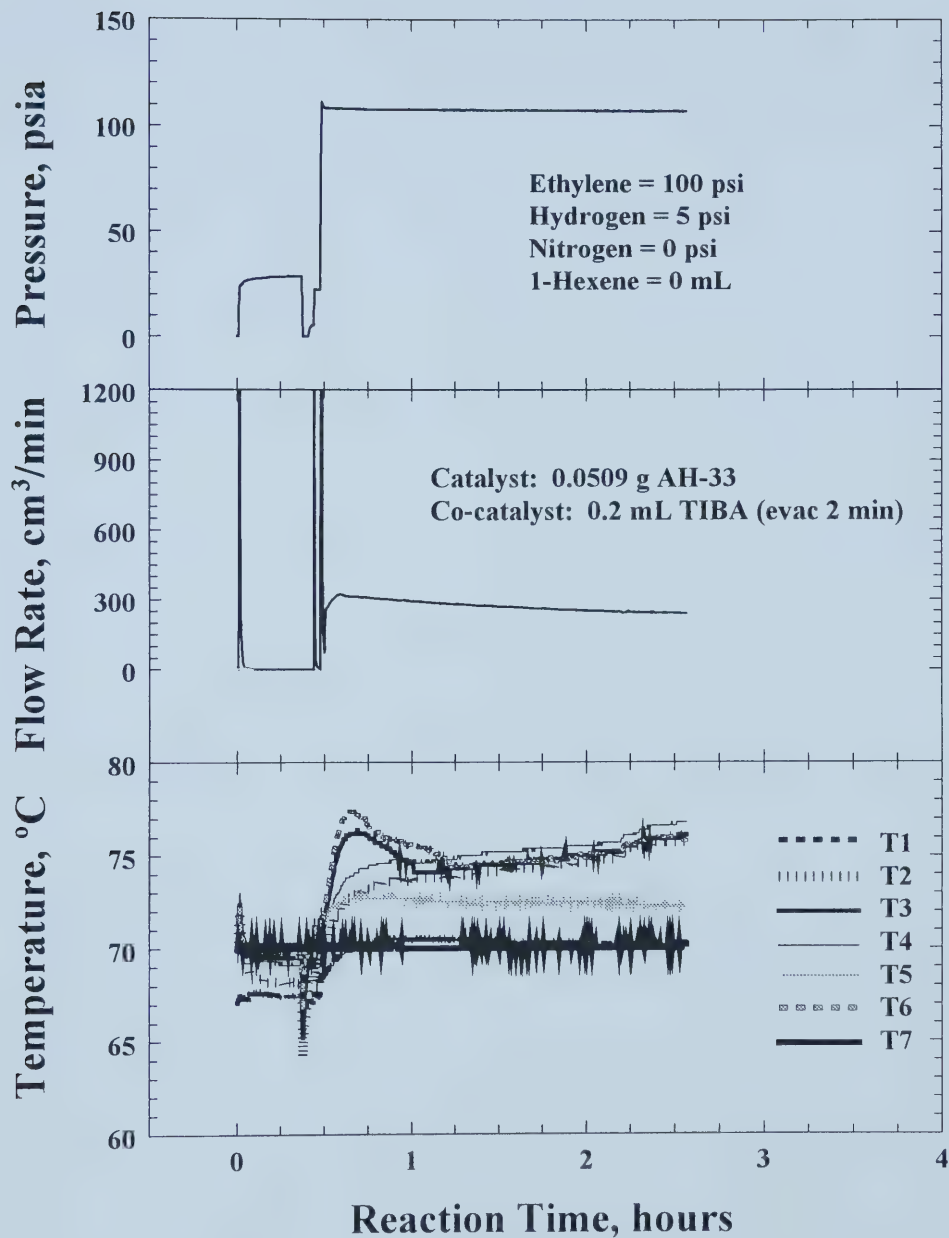
AH-33-04



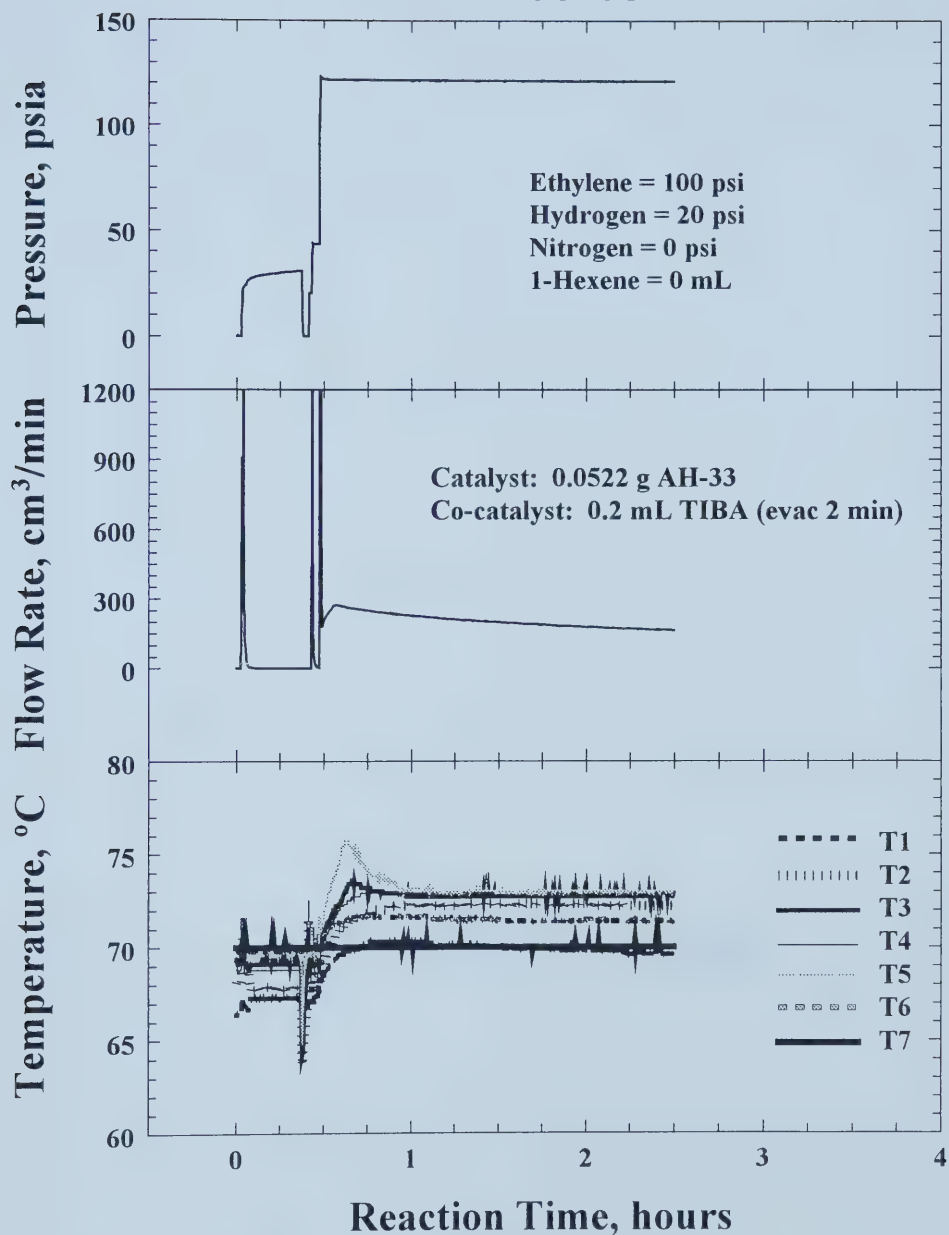
AH-33-05



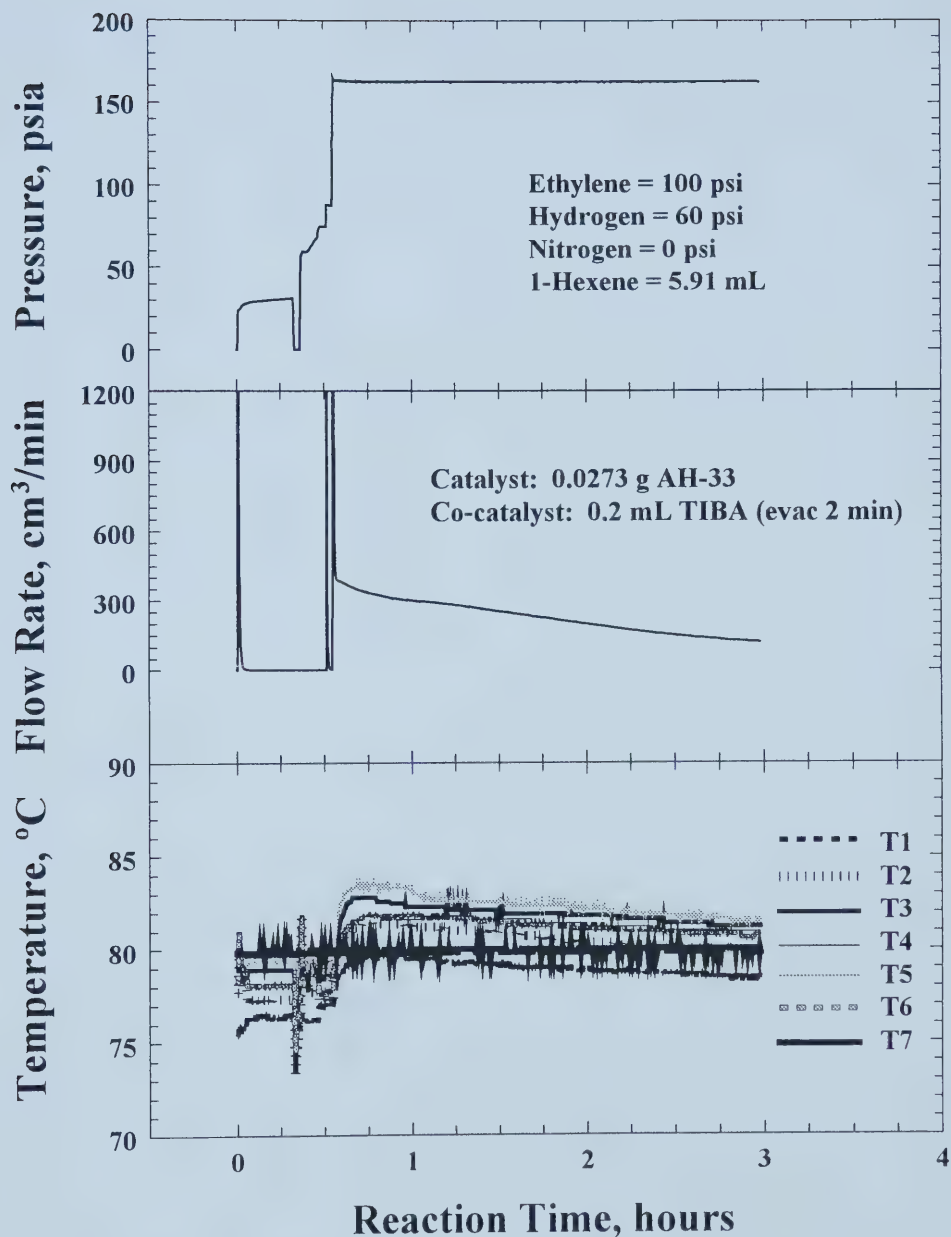
AH-33-06



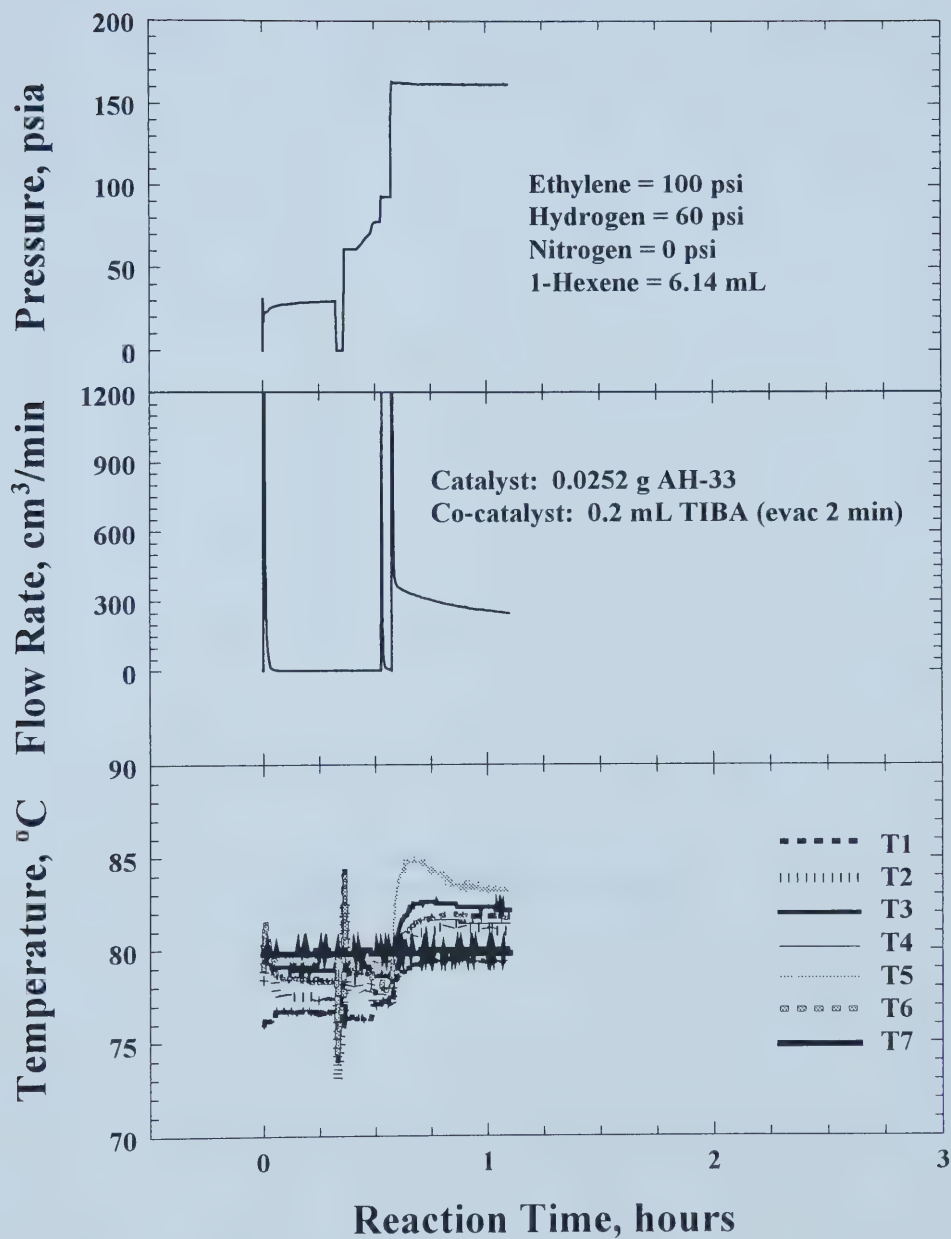
AH-33-08



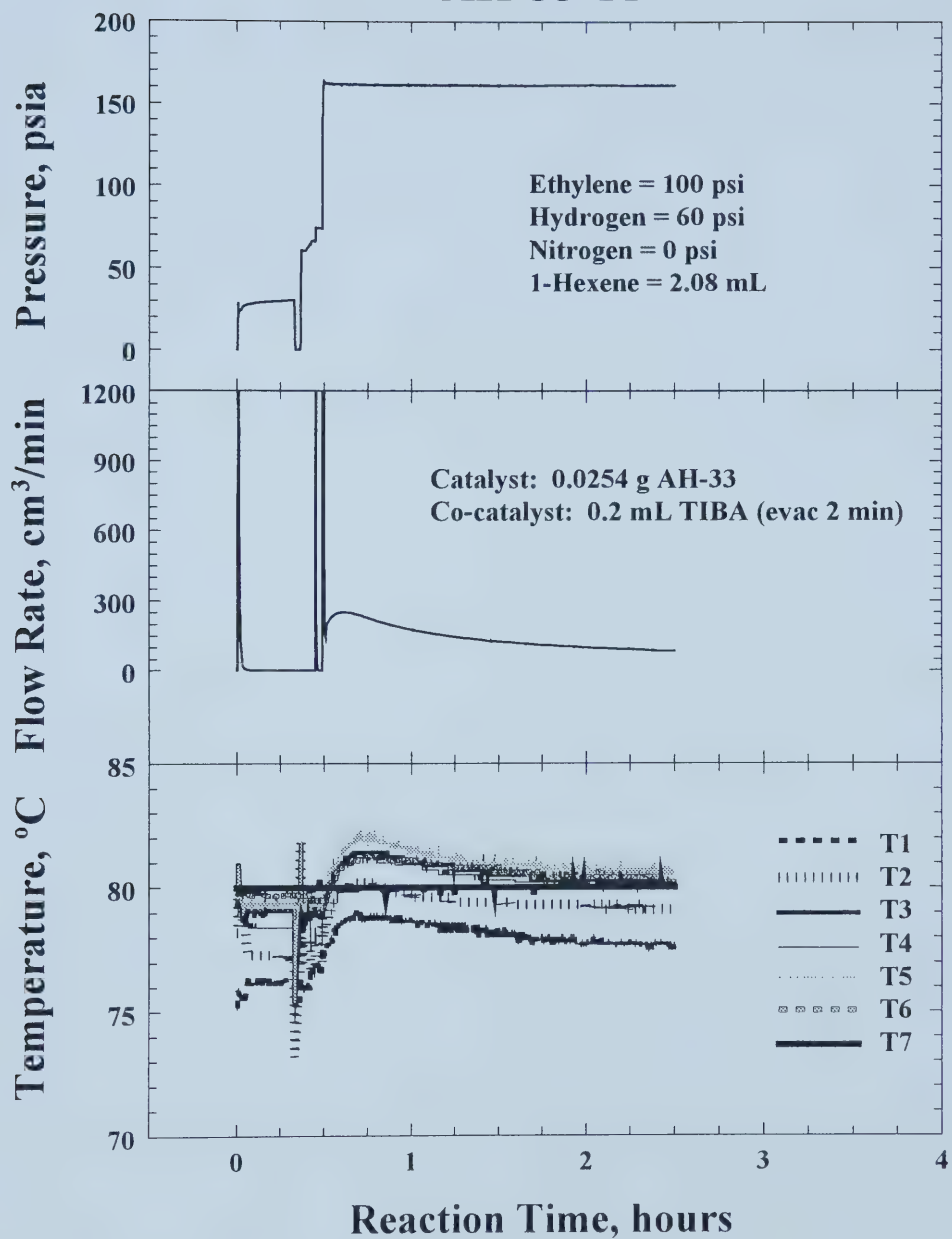
AH-33-09



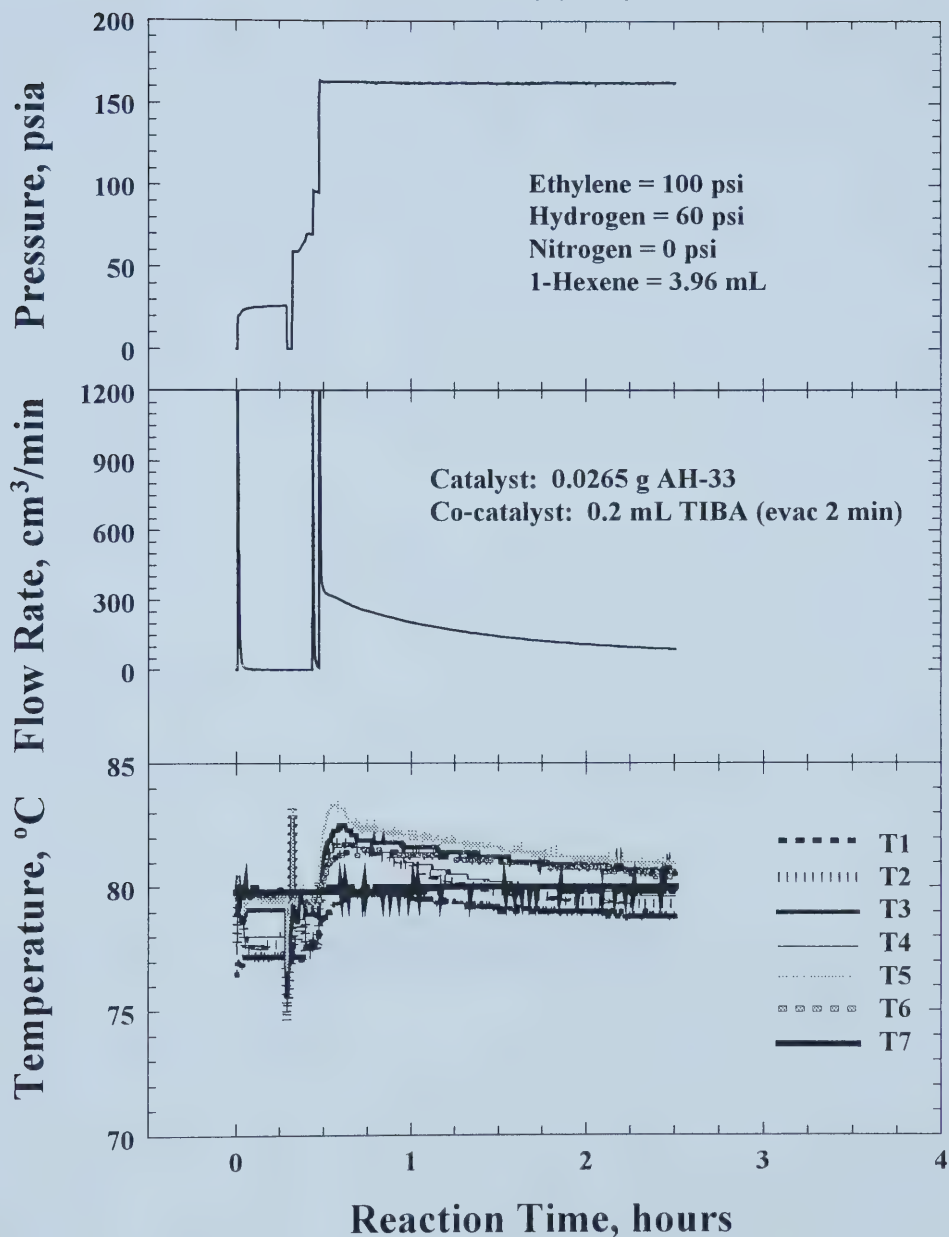
AH-33-10



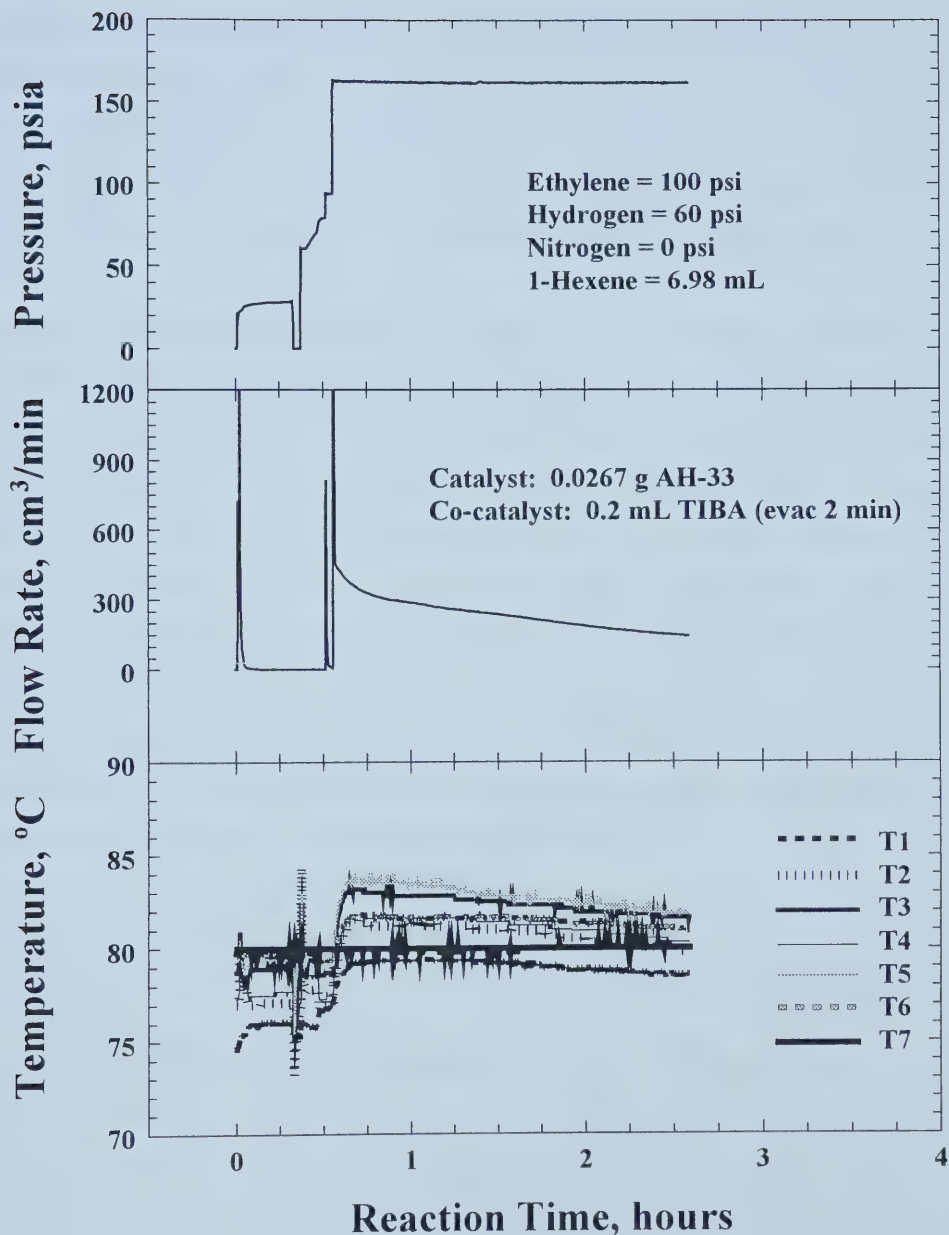
AH-33-11



AH-33-13



AH-33-14



APPENDIX C: Hydrogen Consumption Calculations

Hydrogen consumption due to chain termination can be determined using gas chromatographic and molar mass data as well as polymerization results such as polymer yields, hydrogen partial pressures (P_{H_2}), and initial gas-phase temperatures (T_i). These measurements were collected for four experiments (AH-29-06, AH-31-05, AH-31-06 and AH-31-07) and are summarized in Tables C.1 and C.2.

In principle, one hydrogen molecule is consumed in the termination mechanism for one polymer chain. The ideal gas law is used to determine the number of moles of hydrogen initially present in the reactor (n_{i,H_2}). The number moles of hydrogen consumed (n_{c,H_2}) is related to the yield and number average molar mass (M_n) for the polymer sample, and the final hydrogen fraction (X_{F,H_2}) can be calculated and compared to the measured value. Gas chromatographic measurements are used to construct calibration plots relating the hydrogen peak area % to the final hydrogen concentration (Figure C.1). Tables C.1 through C.4 give the calculations for hydrogen consumption due to chain termination. Comparing the calculated and measured area for the final hydrogen concentration shows that small quantities of hydrogen are consumed in chain termination (see Table C.4).

Table C.1: Polymerization Data for Hydrogen Consumption.

Run ID	P_{H_2} (psi)	P_T (psi)	T_i (K)	Yield (g)	M_n
AH-29-06	11	111	323	69.0	63746
AH-31-05	40	140	343	53.2	32793
AH-31-06	5	105	343	121.8	97188
AH-31-07	20	120	343	84.6	49449

Table C.2: GC Data for Hydrogen Consumption.

Run ID	H ₂ Concentration (mol %)	% H ₂ Peak Area at Start		% H ₂ Peak Area at End	
		Sample 1	Sample 2	Sample 1	Sample 2
AH-29-06	9.91	18.46	18.87	18.85	18.62
AH-30-05	9.09	17.29	17.01	17.02	16.60
AH-31-05	28.57	43.79	43.88	43.15	43.27
AH-31-06	4.76	10.87	10.18	8.27	7.93
AH-31-07	16.67	28.37	28.10	24.79	24.82

Table C.3: Calculated Values for Hydrogen Mole Fractions.

Run ID	Initial H ₂	Initial Fraction	Moles H ₂	Max. Fraction H ₂	Total
	Moles, n _{i,H2}	of H ₂ , X _{i,H2}	Consumed, n _{c,H2}	Consumed, X _{c,H2}	Moles, N _T
AH-29-06	0.026830	0.0991	0.001082	0.040344	0.270740
AH-31-05	0.091875	0.2857	0.001622	0.017658	0.321563
AH-31-06	0.011484	0.0476	0.001253	0.109126	0.241172
AH-31-07	0.045938	0.1667	0.001711	0.037243	0.275626

$$n_{i,H2} = (P_{H2}V)/RT_i = (6894.757P_{H2})(0.95/1000)/(8.314T_i)$$

$$X_{i,H2} = \text{initial fraction of hydrogen} = P_{H2}/P_T$$

$$n_{c,H2} = \text{hydrogen consumption if all termination due to hydrogen} = \text{Yield}/Mn$$

$$X_{c,H2} = \text{maximum fraction of hydrogen consumed} = n_{c,H2}/n_{i,H2}$$

$$N_T = \text{total moles of hydrogen in the reactor} = n_{i,H2}/X_{i,H2}$$

Table C.4: Comparison of Hydrogen Peak Areas.

Run ID	Calculated Final Fraction of H ₂ , X_{F,H_2}	Calculated Area % Final H ₂ Peak (Note 1)	Measured Area % H ₂ Peak (Note 2)		Calculated Area % Initial H ₂ Peak (Note 1)
			Final	Initial	
AH-29-06	0.095101	17.84	18.73	18.67	18.52
AH-31-05	0.280669	43.10	43.21	43.84	43.61
AH-31-06	0.042423	8.37	8.10	10.53	9.35
AH-31-07	0.160459	28.17	24.80	28.23	29.07

X_{F,H_2} = final fraction of hydrogen = $X_{i,H_2} - n_c/N_T$

Note 1: Used calibration equation determined from plotting Area % for final hydrogen concentration (see Figure C.1)

$$\text{Area \% Final H}_2 \text{ Peak} = 2.050013 (\text{mol \% H}_2) - 0.018332 (\text{mol \% H}_2)^2$$

Note 2: Average Area % H₂ Peak from gas chromatograms in Table C.2

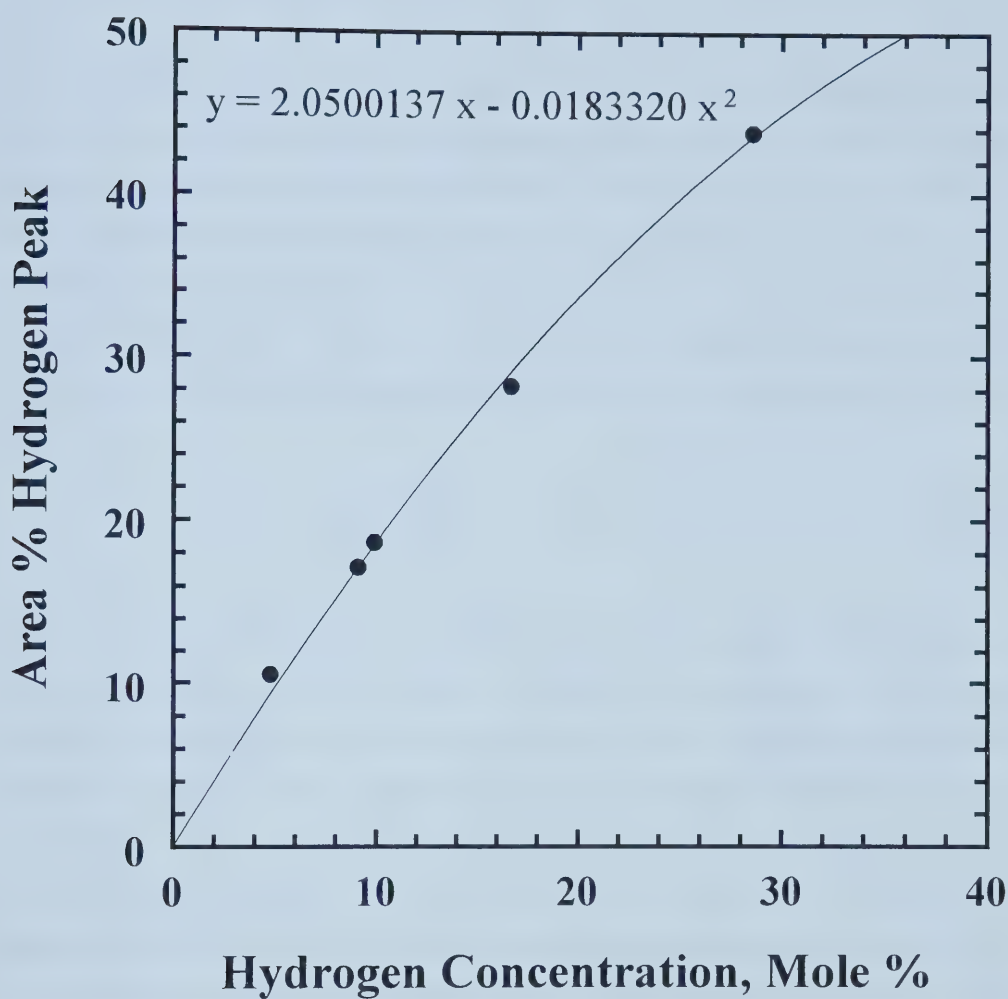


Figure C.1. Calibration plot for final hydrogen concentration.

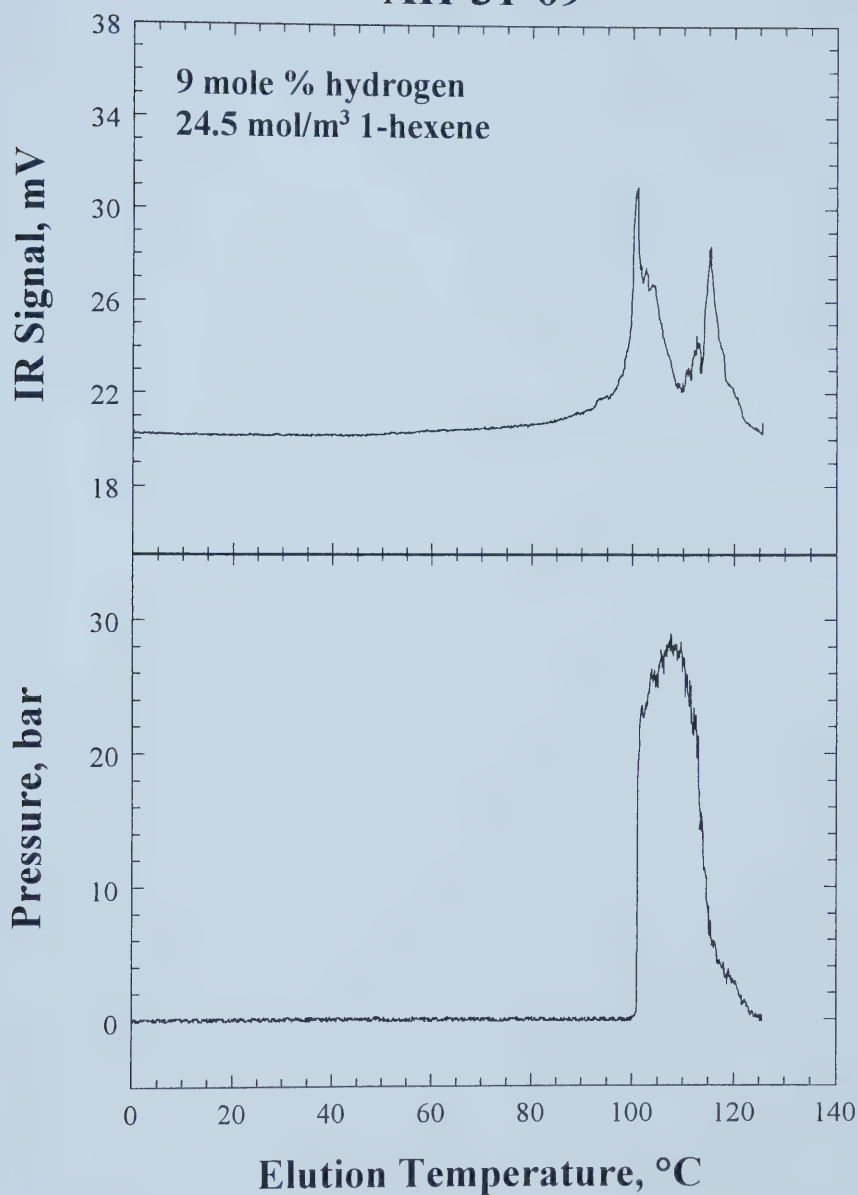
APPENDIX D: TREF Profiles

The correlation between TREF elution temperature (T) and methyl group concentration ($[\text{CH}_3]_T$) was constructed using linear paraffins (C_{40} and C_{60} from Fluka), polyethylene calibration standards (1475, 1482, 1483, and 1484 from NIST), and 17 linear polyethylene samples prepared in our laboratory. The polyethylene samples had number average molar masses of 1000 to 10,000 with narrow polydispersities (<1.3). Equation (D1) gives the correlation between elution temperature and methyl group concentration for the calibration samples, with T in $^{\circ}\text{C}$.

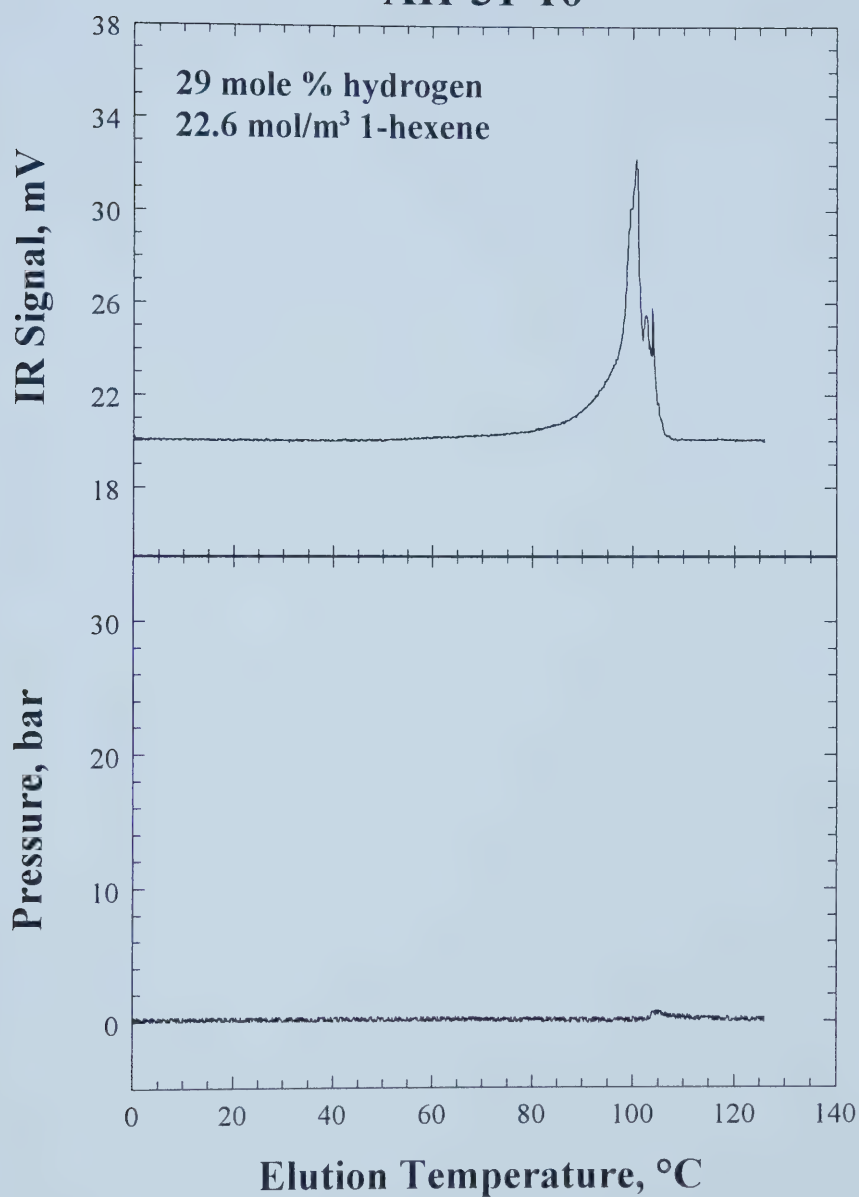
$$[\text{CH}_3]_T = \frac{\text{CH}_3 \text{ groups}}{1000 \text{ Carbons}} = 76.37 - 1.20T + 0.044T^2 \quad (\text{D1})$$

The TREF data acquisition program collected elution temperatures and IR voltages every 4 seconds, but five-point averages were used in the calculations. As well, the IR signal was shifted to zero by selecting one point in the low and high temperature regions, 40°C and 120°C , respectively. In the numerical integration for the determination of the average CH_3 concentrations, summations for number average (C_n) and weight average (C_w) methylene group concentrations were computed for temperatures of 40°C to 101.72°C , which corresponds to the temperature range for all the polyethylene to elute from the column during the calibration. The ratio C_w/C_n can be considered similar to the polydispersity index in SEC analysis; C_w/C_n gives an indication of the distribution of methyl groups in the polymer chains. The fraction of homopolymer in the sample was calculated as the amount of polymer eluted between 90.5 - 120°C relative to the total amount of polymer eluted for the temperature range of 40°C to 120°C .

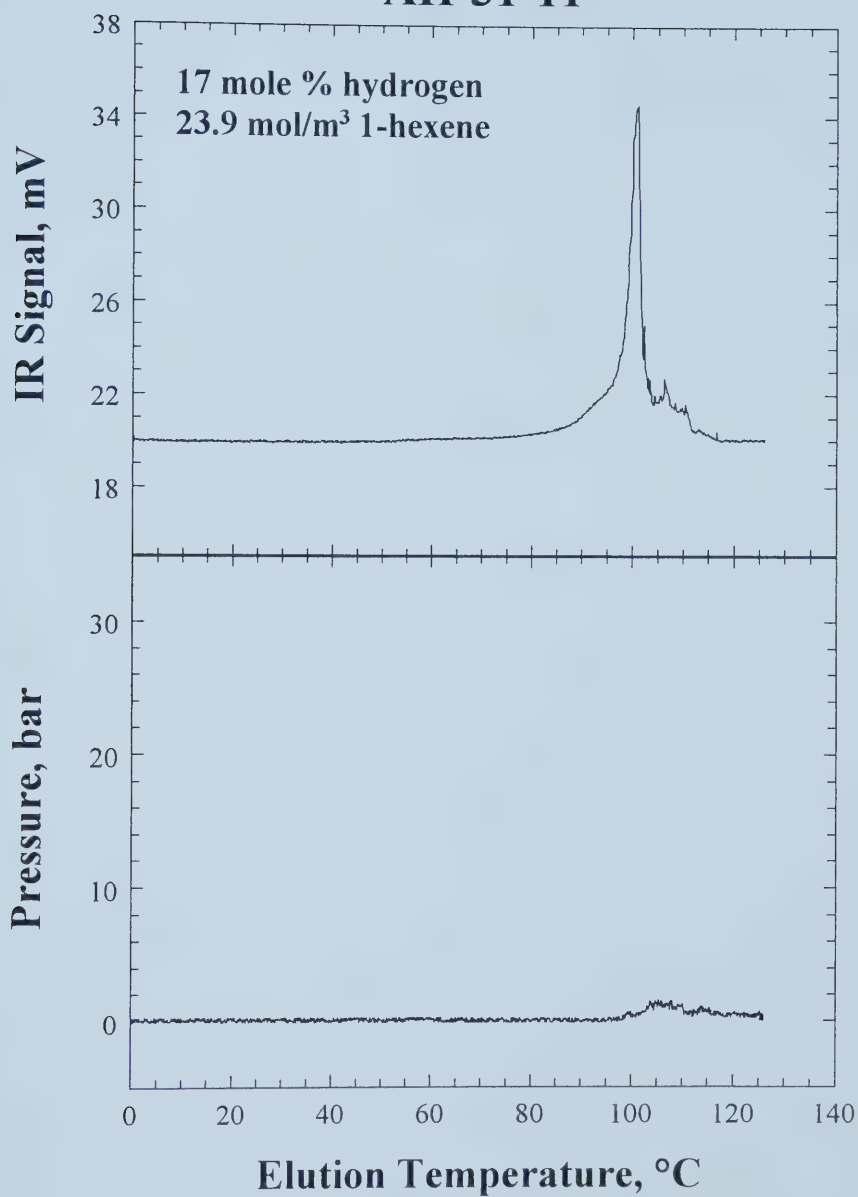
AH-31-09



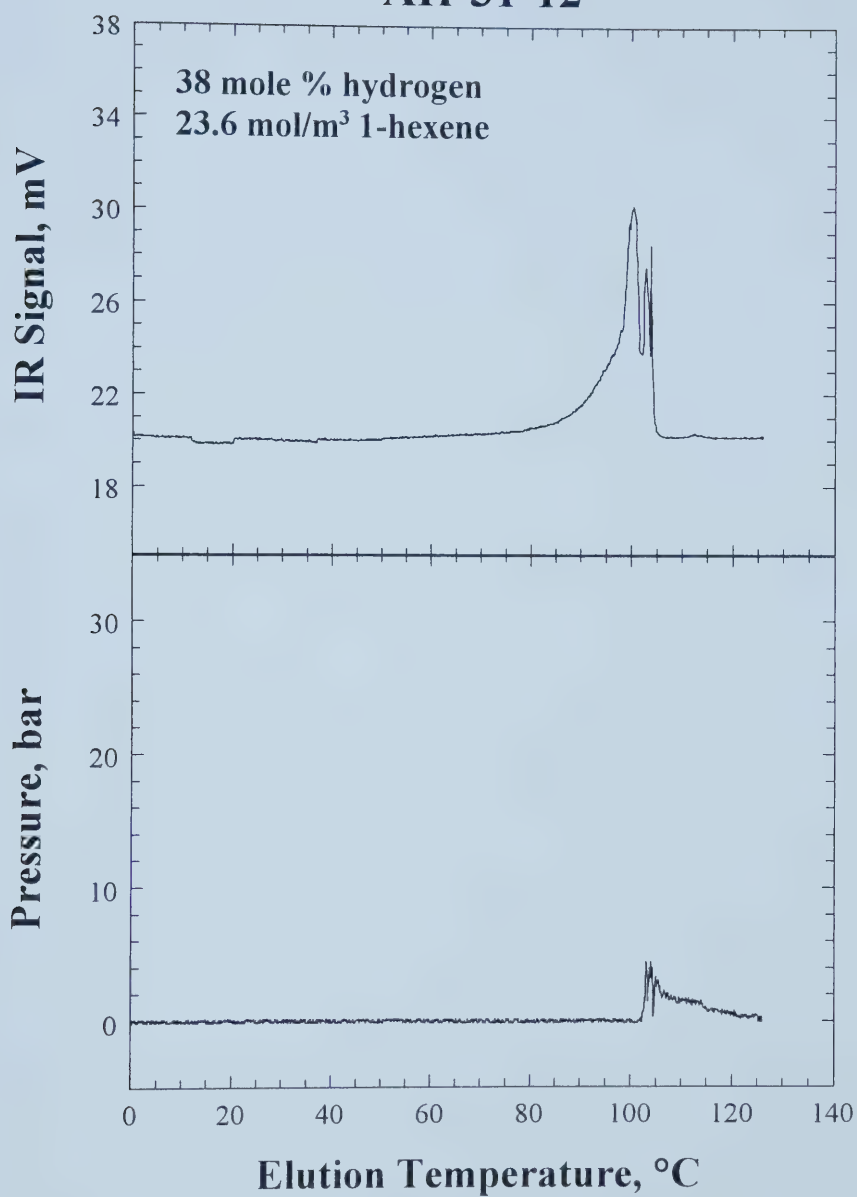
AH-31-10



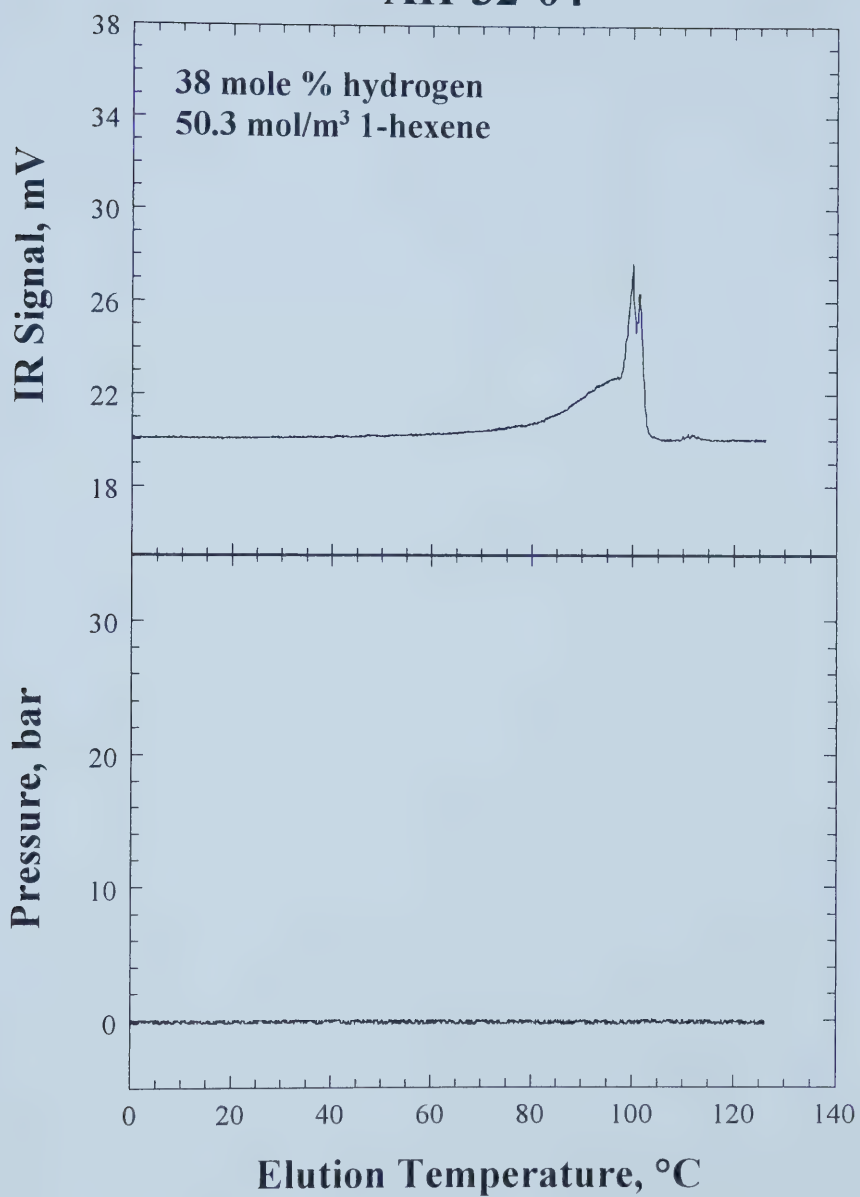
AH-31-11



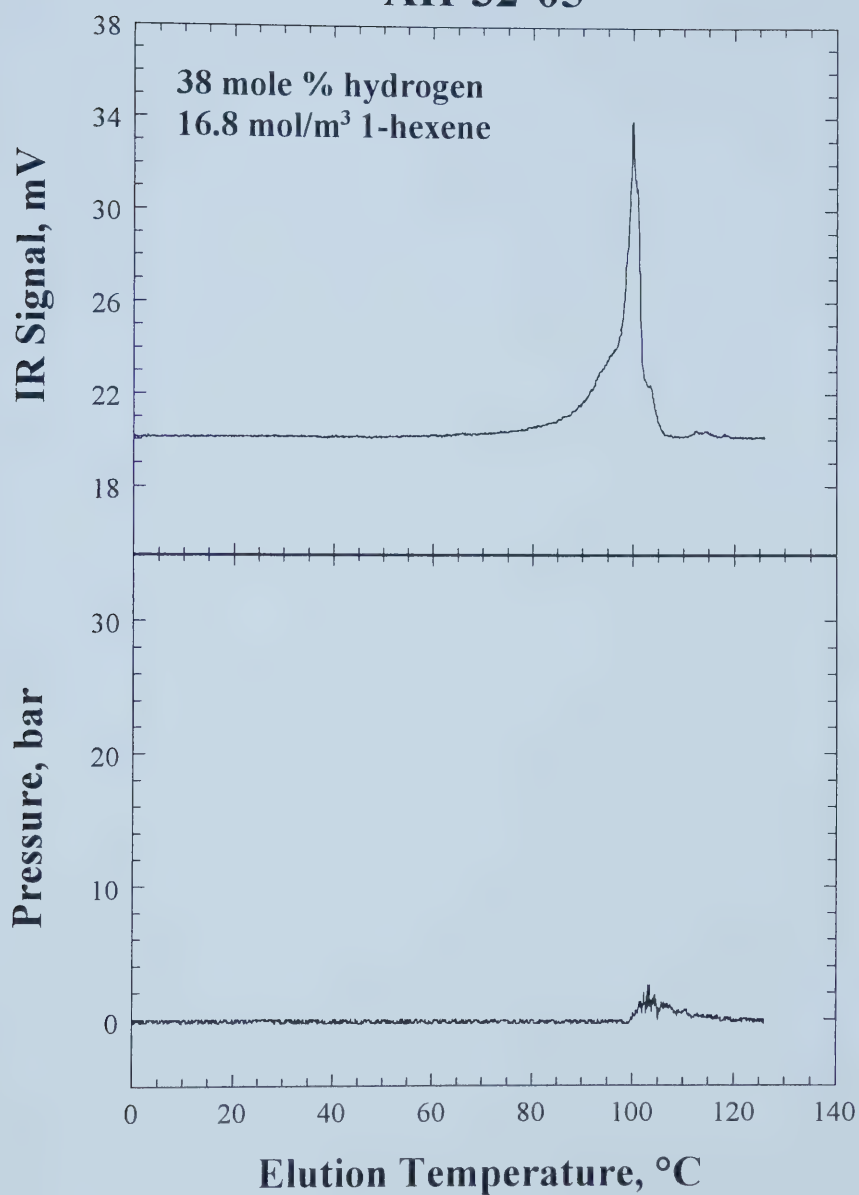
AH-31-12



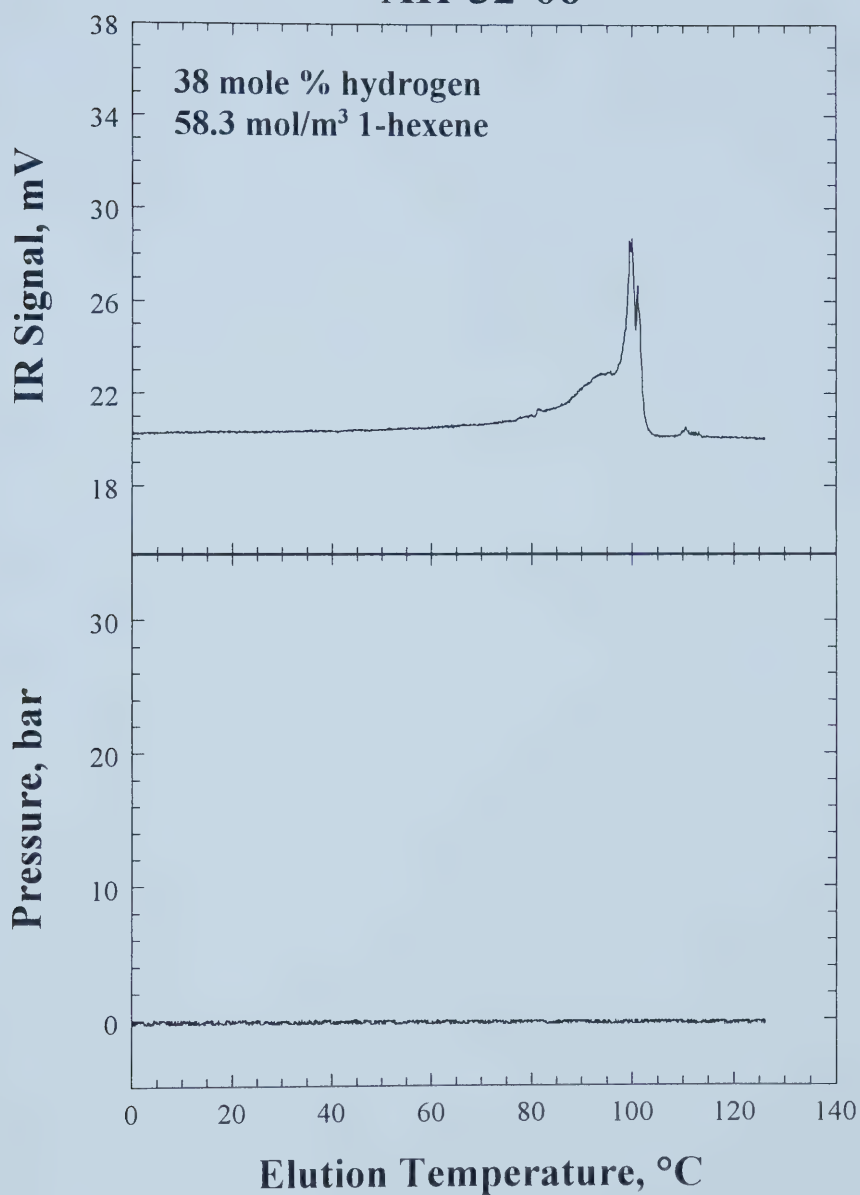
AH-32-04



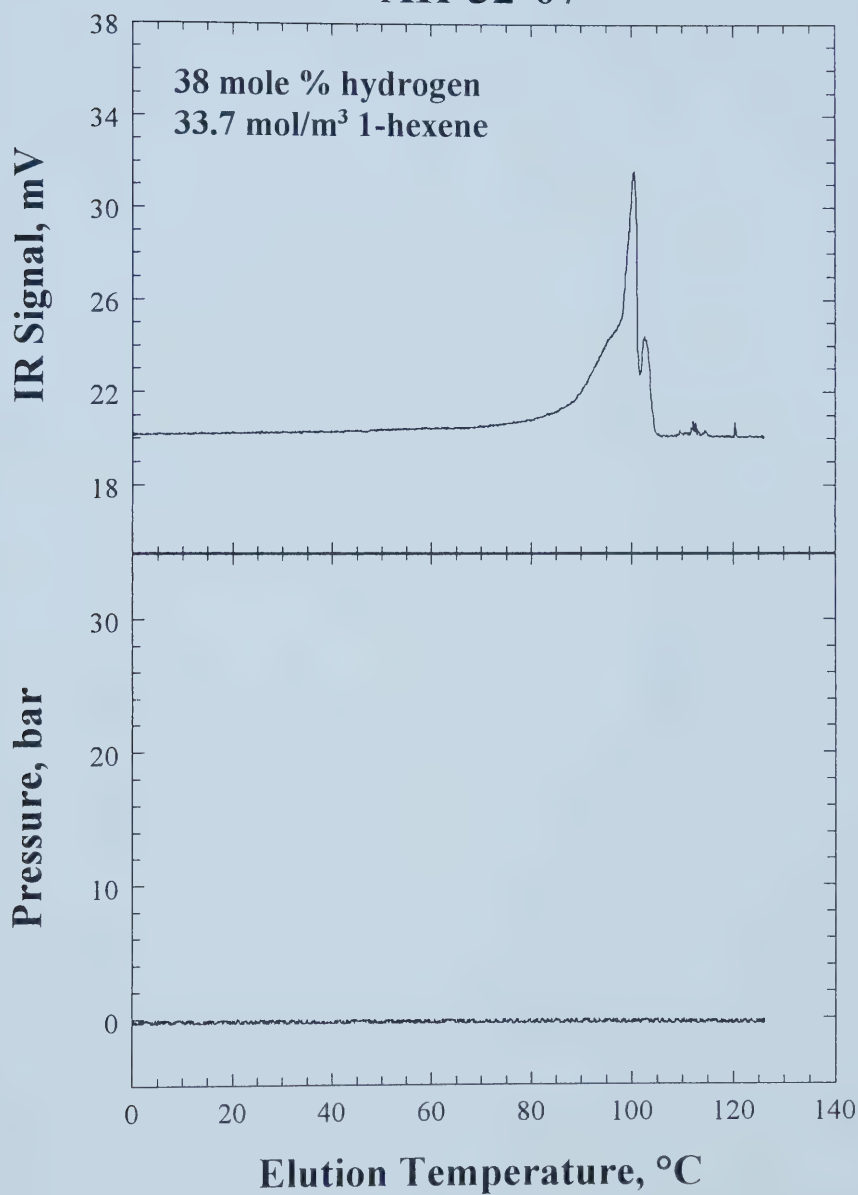
AH-32-05



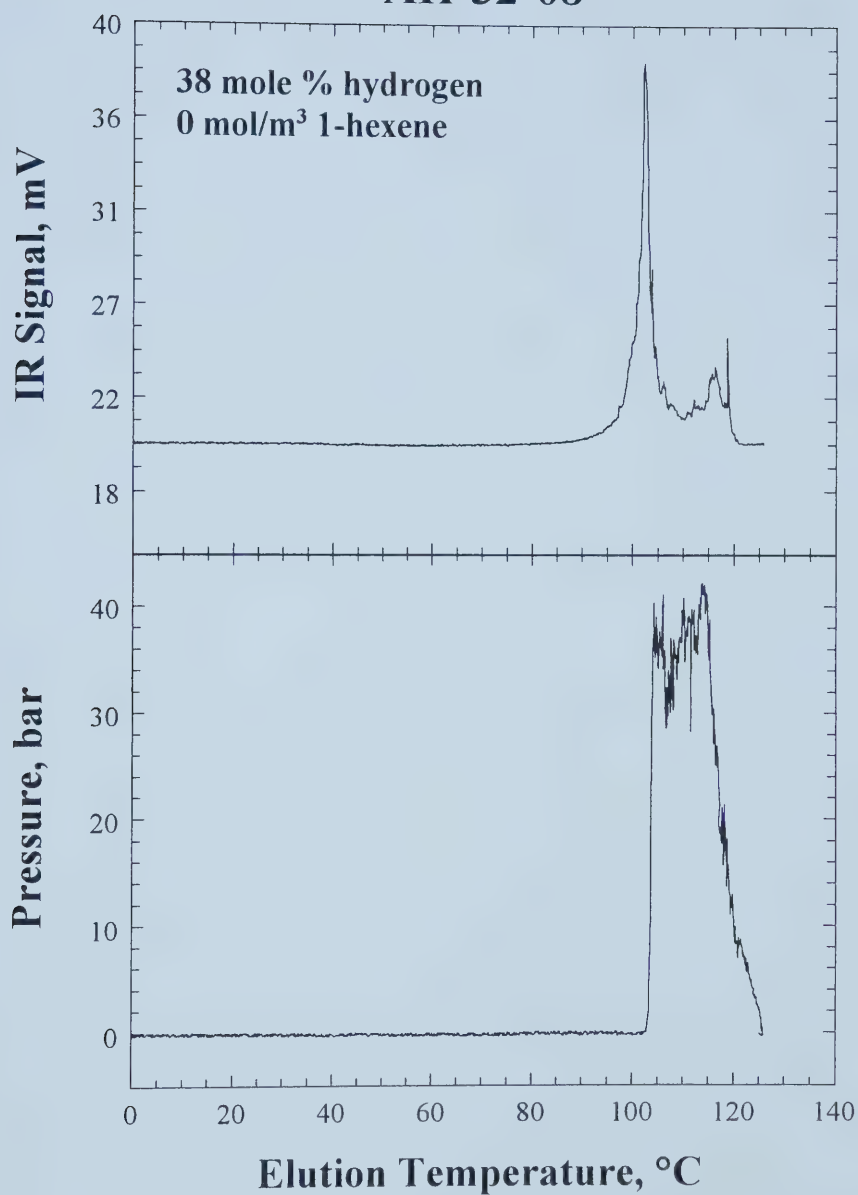
AH-32-06



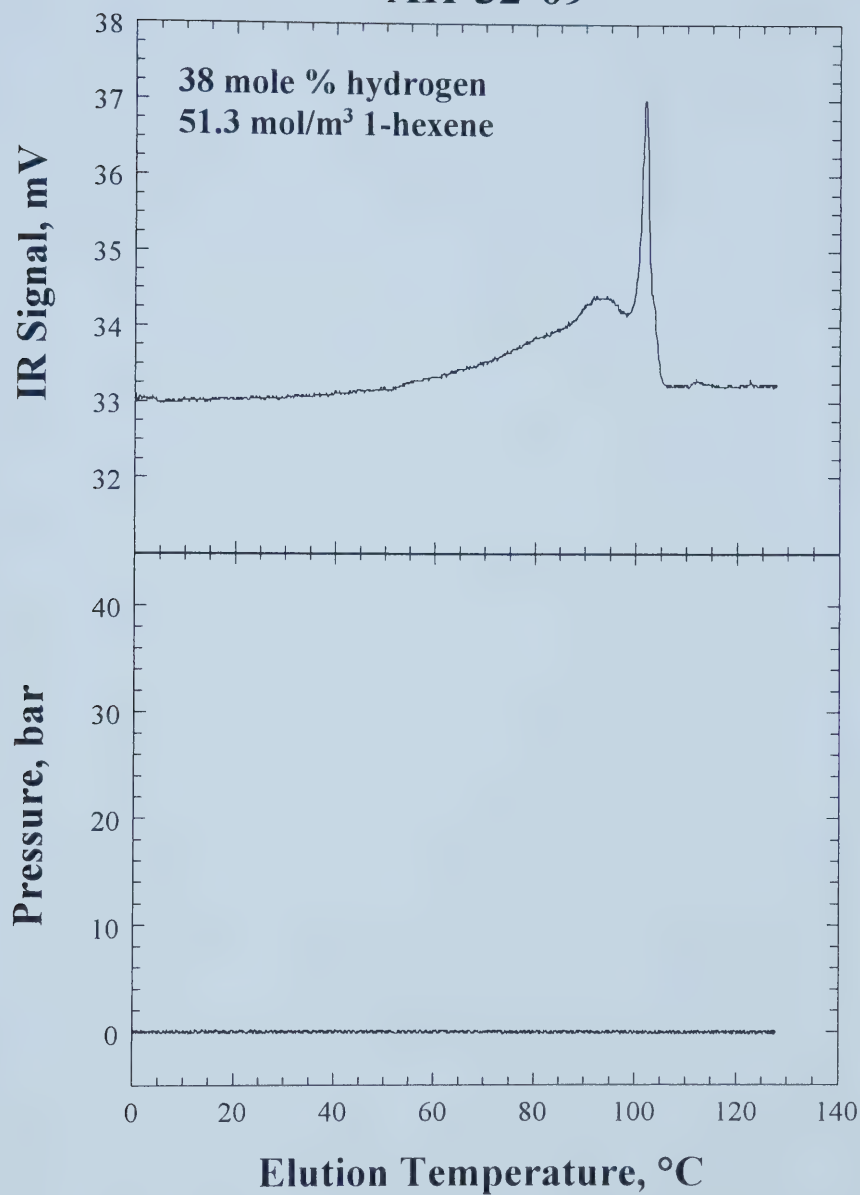
AH-32-07



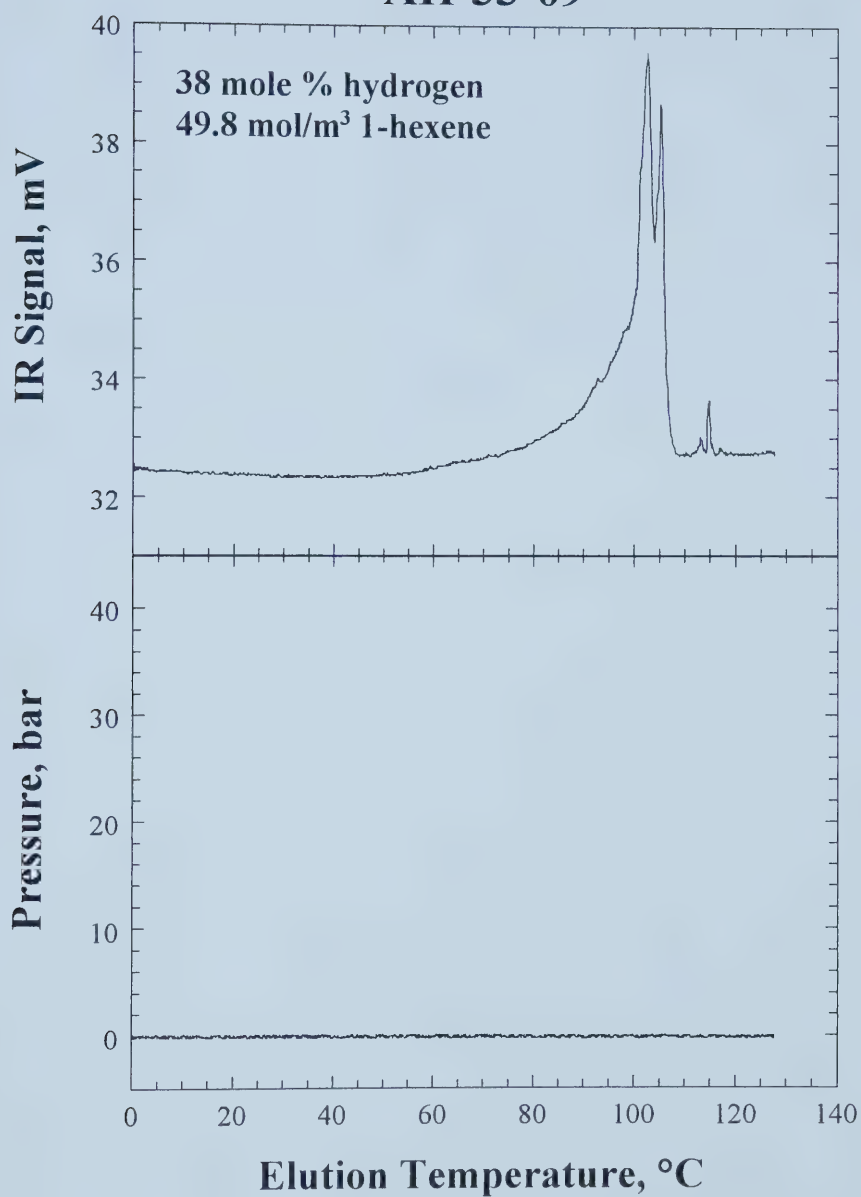
AH-32-08



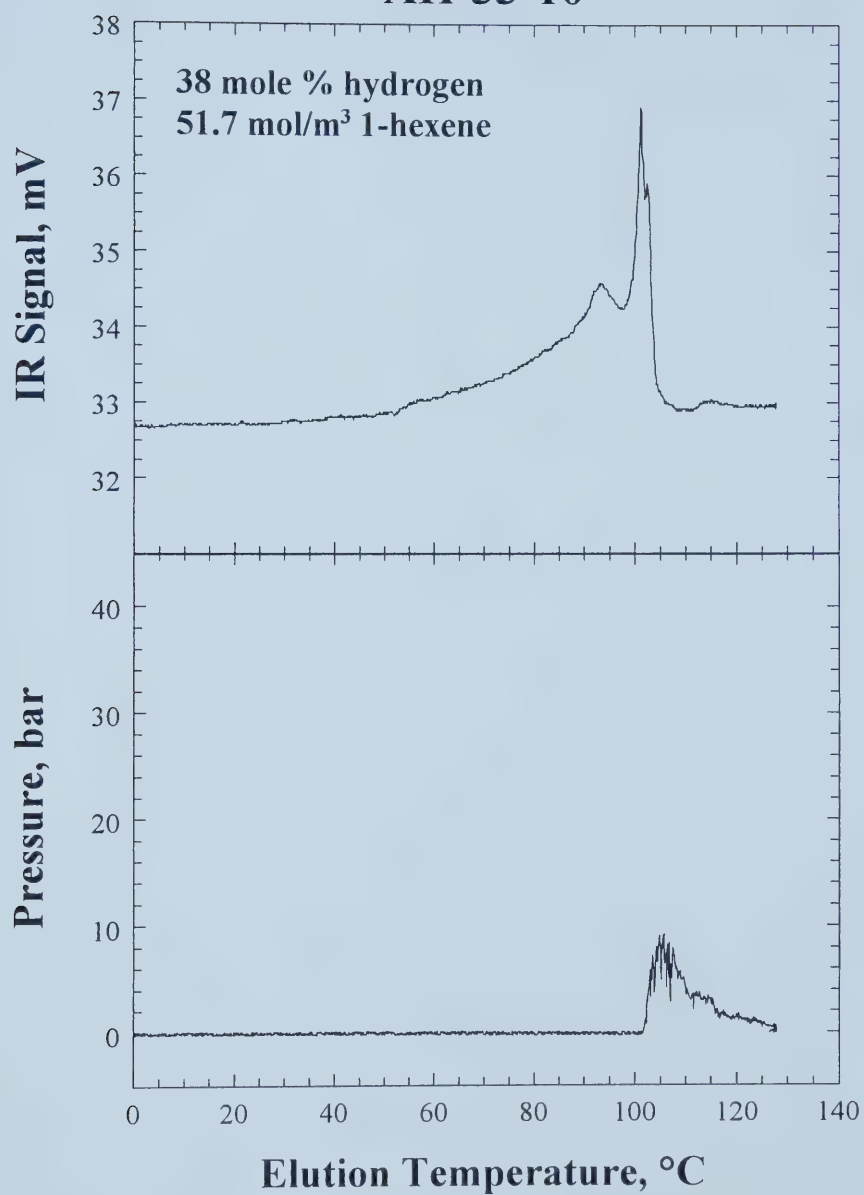
AH-32-09



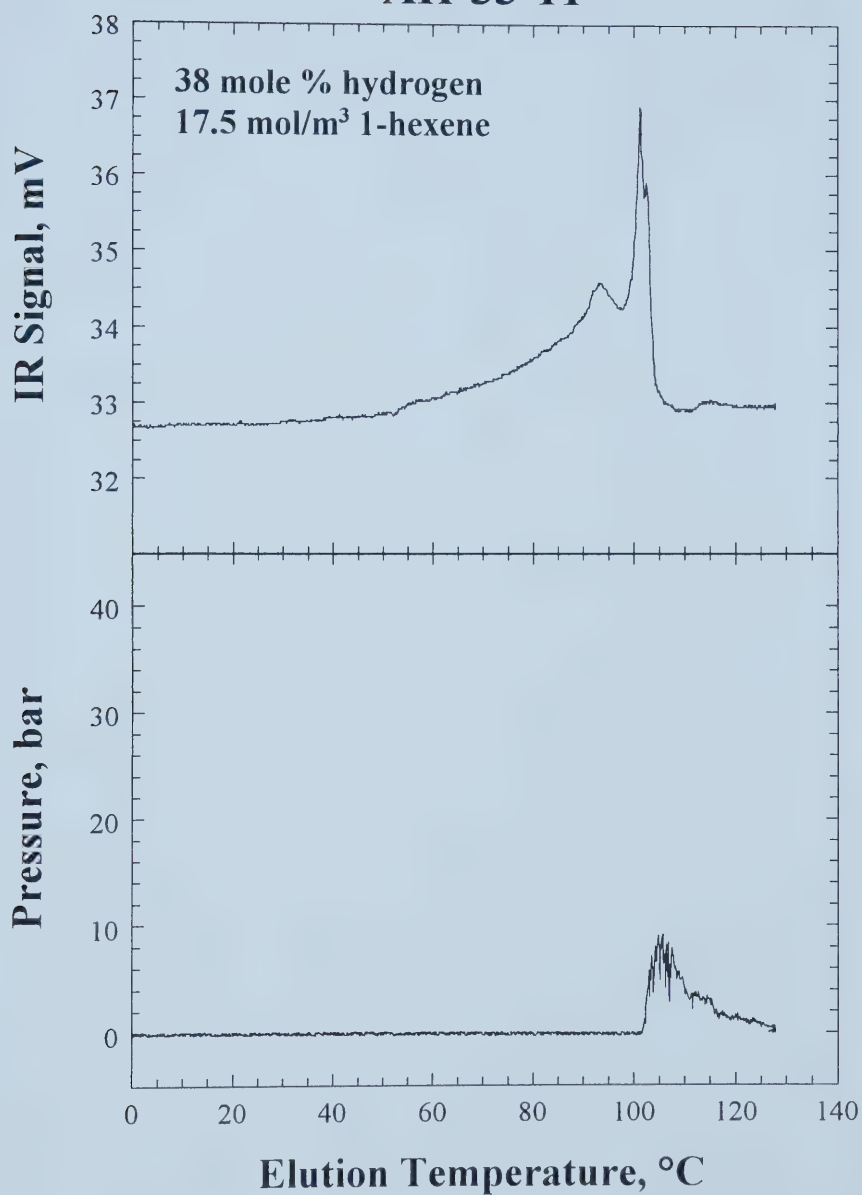
AH-33-09



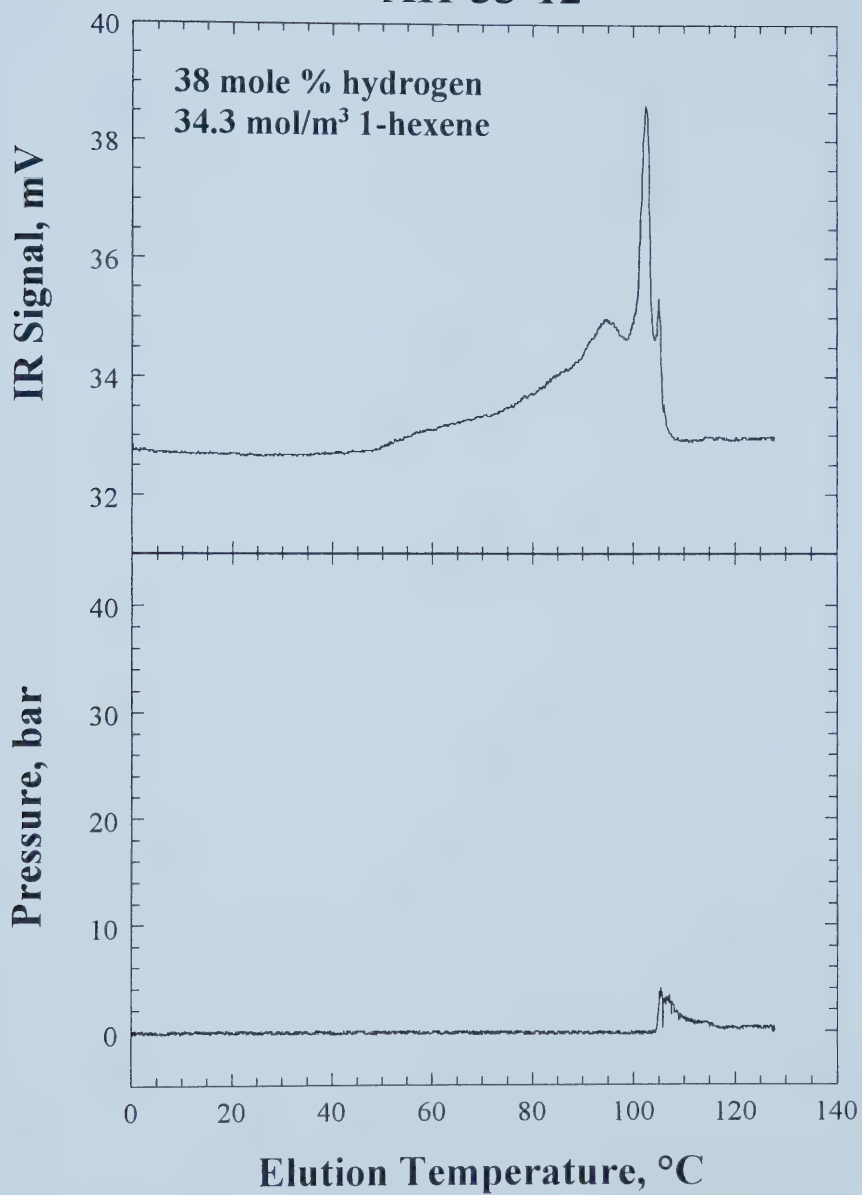
AH-33-10



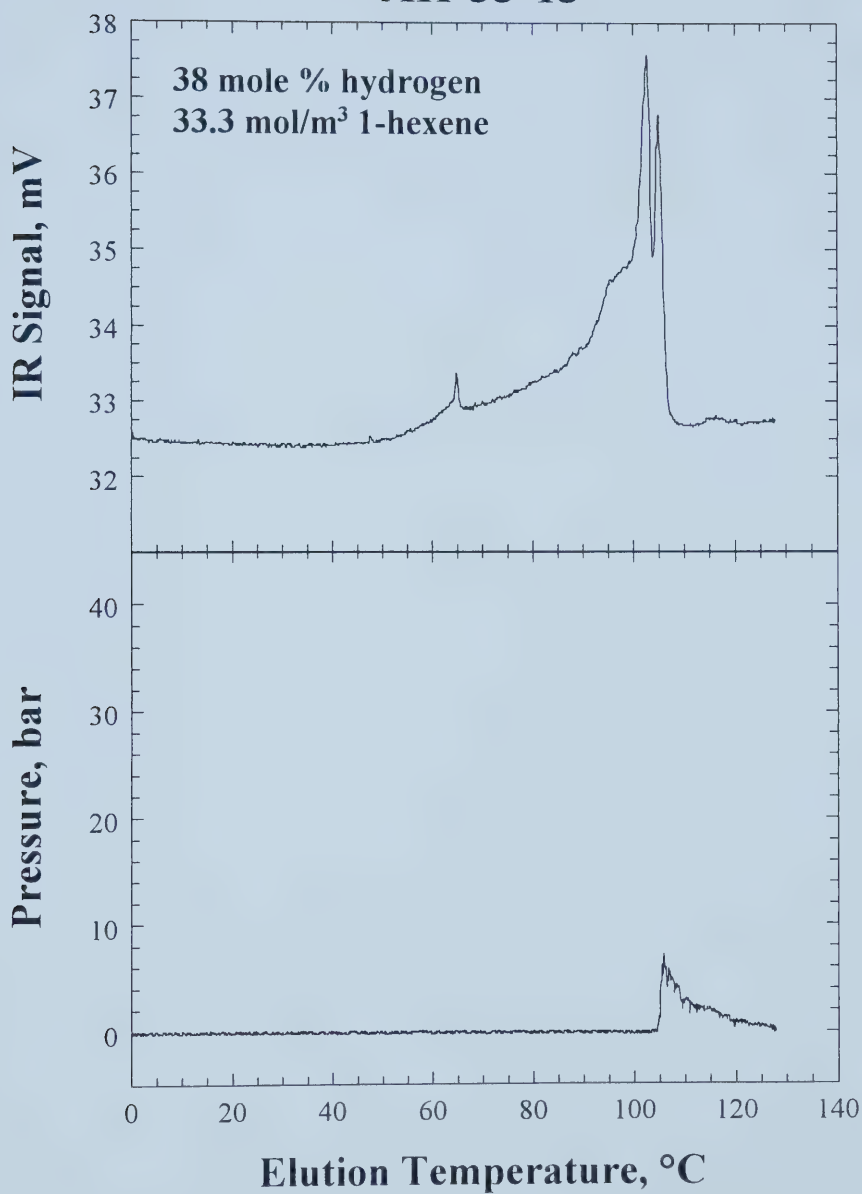
AH-33-11



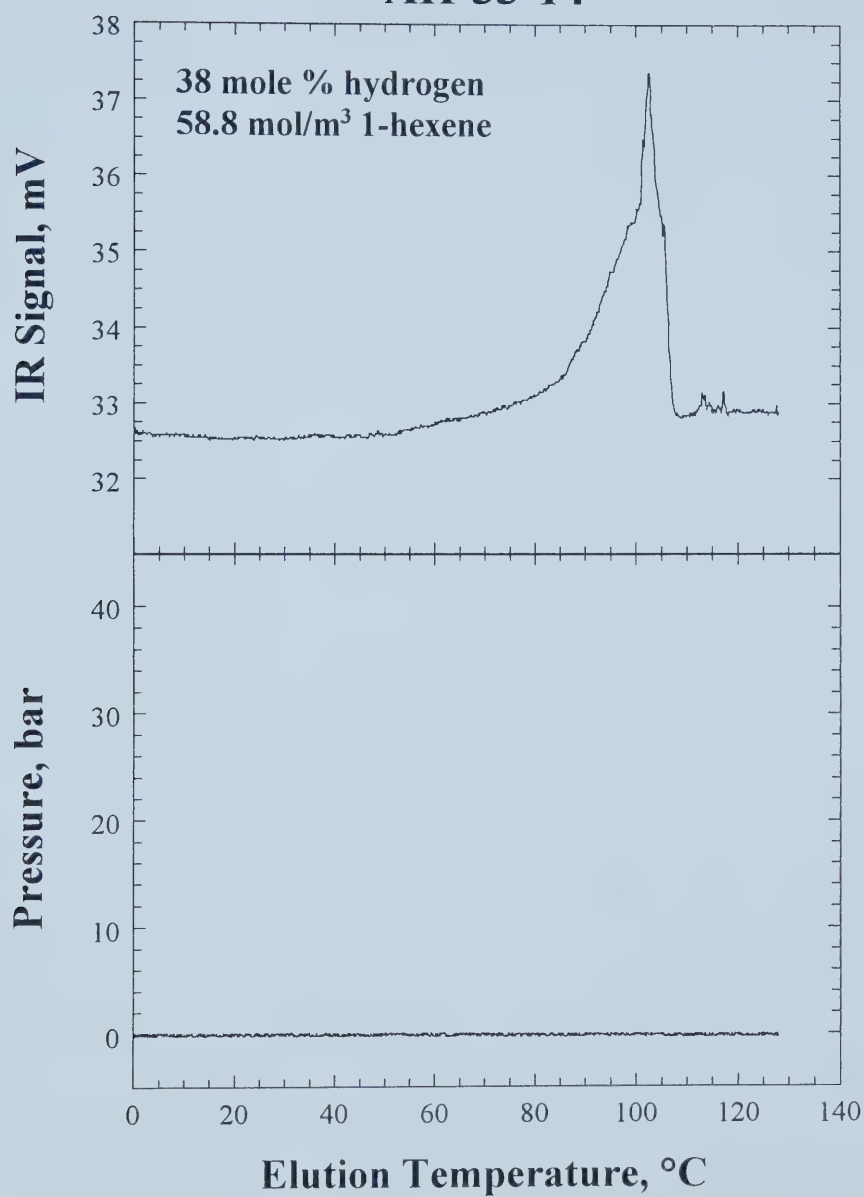
AH-33-12



AH-33-13



AH-33-14



University of Alberta Library



0 1620 1829 9592

B45837